Haemophilus influenzae Outer Membrane Proteins-Structure, Function and Virulence Mechanisms

Tamim, Al-Jubair

2016

Document Version:
Publisher's PDF, also known as Version of record

Haemophilus influenzae Outer Membrane Proteins

Structure, Function and Virulence Mechanisms

MD TAMIM AL JUBAIR
TRANSLATIONAL MEDICINE | FACULTY OF MEDICINE | LUND UNIVERSITY

Printed by Media-Tryck, Lund University 2016
Nordic Ecolabel 341903

Md Tamim Al Jubair was born and brought up in the town Tarail, in Kishoreganj, Bangladesh. He received his Bachelor of Science degree in Biotechnology and Genetic Engineering from Khulna University, Bangladesh in 2007. He moved to Sweden in 2008 for higher education and received his Master of Science degree in Protein Science from Lund University, Sweden by 2010. During his master study he became interested in protein structure and function. He was a project student for one year at the Dept. of Biochemistry and Structural Biology before he began his PhD at the Dept. of Translational Medicine in 2012.

His PhD thesis focuses on the outer membrane proteins of the human respiratory pathogen *Haemophilus influenzae*. Outside to the lab, Tamim loves to spend time with family and friends, and very much interested in fishing, gardening, playing cricket, music and films.

LUND UNIVERSITY
Faculty of Medicine

Lund University, Faculty of Medicine
Doctoral Dissertation Series 2016:58
ISBN 978-91-7619-284-9
ISSN 1652-8220

Haemophilus influenzae Outer Membrane Proteins

Structure, Function and Virulence Mechanisms

Haemophilus influenzae Outer Membrane Proteins

Structure, Function and Virulence Mechanisms

Md Tamim Al Jubair

LUND
UNIVERSITY

DOCTORAL DISSERTATION
by due permission of the Faculty of Medicine, Lund University, Sweden.
To be defended at the main lecture hall of the Pathology building.

Date: 10th June 2016 and time13:00.

Faculty opponent

Associate professor Junkal Garmendia

CSIC, Instituto Agrobiotecnología, Pamplona, Navarra, Spain.

Organization LUND UNIVERSITY	Document name: Doctoral Dissertation
	Date of issue: 10th of June 2016
Author(s): Md Tamim Al Jubair	Sponsoring organization

Title and subtitle: *Haemophilus influenzae* Outer Membrane Proteins - Structure, Function and Virulence Mechanisms

Abstract

Haemophilus influenzae is a Gram-negative bacterium that is classified by the presence or absence of a polysaccharide capsule, termed "typeable" and "non-typeable" *H. influenzae* (NTHi), respectively. Depending on the capsular polysaccharide composition and antigenicity, typeable isolates are further subdivided into six serotypes designated a–f. *H. influenzae* type b (Hib) has been the most common serotype causing invasive disease, for example, meningitis, epiglottitis, septicaemia, and osteomyelitis in former decades. Since the introduction of a Hib vaccine, the incidence of invasive Hib disease has significantly decreased. In contrast, the levels of invasive disease caused by other *H. influenzae* types, that is, NTHi and *H. influenzae* serotype f (Hif), is increasing, suggesting that NTHi and Hif are emerging pathogens. The mechanisms behind this emergence are not fully understood. To circumvent the bactericidal activities of the host antimicrobial peptides, complement system and nutritional immunity, many bacterial species, including *H. influenzae*, have evolved with several outer membrane proteins (OMPs) that play a role in subverting the host defense systems.

This study covers the structural and functional analysis of three *H. influenzae* OMPs; Protein E (PE) from NTHi, *Haemophilus* Surface Fibril (Hsf) from Hib and, finally, Protein H (PH) from Hif, to understand the molecular pathogenicity of *H. influenzae*. We successfully crystallized and solved the atomic structure of the ubiquitous multifunctional surface protein PE at 1.8 Å resolution. The detailed structure of PE highlights how this important virulence factor of *H. influenzae* has the capacity to simultaneously interact with host Vitronectin (Vn), Laminin (Ln), or Plasminogen (PLG), promoting bacterial pathogenesis. We also showed that *H. influenzae* acquired hemin on the surface via PE, and shared it with hemin-depleted co-cultured bacteria, that is, PE worked as a hemin storage reservoir for *H. influenzae*. The trimeric autotransporter Hsf interacts with Vn, contributing to Hib serum resistance, better adherence and internalization into host cells. *In silico* analysis and experimental results demonstrated that the architecture of the trimeric autotransporter Hsf is not straight but rather a twisted, doubled over "hairpin-like" structure. We characterized PH as Vn-binding protein of Hif and discovered that it recognized the C-terminal part of Vn (aa 352–362). We found that PH-dependent Vn binding resulted in better survival of Hif in human serum and increased bacterial adherence to alveolar epithelial cells. Structural information of these OMPs will increase knowledge of *H. influenzae* virulence mechanisms. In addition, to develop vaccines or drugs against *H. influenzae*, targeting of OMPs are a potential key to provide protection against infectious *Haemophilus* spp. disease. Hence, functional studies on OMPs of *H. influenzae* in combination with the structural data provide a deeper understanding of host-pathogen interactions.

Key words: Complement system, *Haemophilus influenzae*, *Haemophilus* surface fibril, Outer membrane proteins, Protein E, Protein H and Vitronectin.

Classification system and/or index terms (if any)

Supplementary bibliographical information	Language
ISSN and key title: 1652-8220	ISBN: 978-91-7619-284-9
Recipient's notes / Number of pages 162	Price
	Security classification

Signature 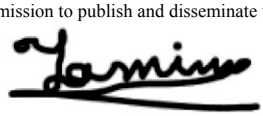 Date 2016-05-10

Haemophilus influenzae Outer Membrane Proteins

Structure, Function and Virulence Mechanisms

Md Tamim Al Jubair

LUND
UNIVERSITY

Cover photo by

Md Tamim Al Jubair

Medical Faculty | Department of Translational Medicine | Lund University

Lund University, Faculty of Medicine Doctoral Dissertation Series 2016:58
ISBN 978-91-7619-284-9
ISSN 1652-8220

Printed in Sweden by Media-Tryck, Lund University, Lund 2016

To my mother- Mina Jabbar,
father- Mohammad Abdul Jabbar
and my wife- Najnin Ahmed Khuki

Content

List of Papers

1. Singh B, **Al-Jubair T,** Förnvik K, Thunnissen MM and Riesbeck K. Crystallization and X-ray diffraction analysis of a novel surface-adhesin protein: protein E from *Haemophilus Influenzae,* **(2012)** *Acta Crystallographica Section F*, 68: 222-226.

2. Singh B, **Al-Jubair T,** Thunnissen MM and Riesbeck K. The unique structure of *Haemophilus influenzae* protein E reveals multiple binding sites for host factors, **(2013)** *Infection and Immunity*, 81 (3): 801-814.

3. **Al-Jubair T,** Singh B, Fleury C, Blom AM, Mörgelin M, Thunnissen MM, and Riesbeck K. *Haemophilus influenzae* stores and distributes hemin by using protein E, **(2014)** *International Journal of Medical Microbiology*, 304 (5-6): 662-668.

4. Singh B, Su YC, **Al-Jubair T,** Mukherjee O, Hallström T, Mörgelin M, Blom AM, and Riesbeck K. A fine-tuned interaction between the trimeric autotransporter *Haemophilus* surface fibrils and vitronectin leads to serum resistance and adherence to respiratory epithelial cells, **(2014)** *Infection and Immunity*, 82 (6): 2378-2389.

5. Singh B, **Al-Jubair T,** Mörgelin M, Sundin A, Linse S, Nilsson U J and Riesbeck K. *Haemophilus influenzae* surface fibril (Hsf) is a unique twisted hairpin-like trimeric autotransporter. **(2015)** *International Journal of Medical Microbiology*, 305 (1): 27-37.

6. **Al-Jubair T,** Mukherjee O, Oosterhuis S, Singh B, Su Y C, Fleury C, Horsefield T S and Riesbeck K. *Haemophilus influenzae* type f hijacks vitronectin using protein H to resist host innate immunity and adhere to pulmonary epithelial cells. **(2015)** *Journal of Immunology*, 195 (12): 5688-5695.

List of Other Papers not Included in the Thesis

1. Singh B, **Al-Jubair T**, Voraganti C, Andersson T, Mukherjee O, Su YC, Zipfel P and Riesbeck K. *Moraxella catarrhalis* binds plasminogen to evade host innate immunity, **(2015)** *Infection and Immunity*, 83 (9): 3458-3469.

2. Paulsson M, Singh B, **Al-Jubair T,** Su YC, Høiby N, Riesbeck K. Identification of outer membrane porin D as a vitronectin-binding factor in cystic fibrosis clinical isolates of *Pseudomonas aeruginosa*, **(2015)** *Journal of Cystic Fibrosis*, 14 (5): 600-607.

3. **Al-Jubair T**, Singh B, Su YC, Riesbeck K. Assays for studying the role of bacterial acquisition of vitronectin in adhesion and serum resistance, **(2016)** *Journal of Visualized Experiments,* (Accepted).

4. Singh B, Mukherjee O, **Al-Jubair T,** Marcin O, Blom AM, and Riesbeck K. A rapid protocol (MF-III) for purification of vitronectin from human serum or plasma*,* **(2016)** (Submitted).

Abbreviations

ABC Transporter	Adenosine triphosphate (ATP)-binding cassette transporter
AOM	Acute otitis media
COPD	Chronic obstructive pulmonary disease
ECM	Extracellular Matrix
ECL	Enhanced chemoluminescence
Fur	Ferric uptake regulator protein
Hib	*Haemophilus influenzae* serotype b
Hif	*Haemophilus influenzae* serotype f
Hap	*H. influenzae* adhesin protein
Ln	Laminin
LOS	Lipooligosaccharide
LPS	Lipopolysaccharide
MAC	Membrane attack complex
MMP-9	Metalloproteinase-9
MIR	Multiple isothermal replacement
MAD	Multi-wavelength anomalous diffraction
NTHi	Non-typeable *Haemophilus influenzae*
NAD	Nicotinamide adenine dinucleotide
NLR	Nucleotide-binding oligomerization domain (NOD)-like receptor
NTHi	Non-typeable *Haemophilus influenzae*
OM	Otitis media
OMV	Outer membrane vesicle
OMPs	Outer membrane proteins

ORF	Open reading frame
PAMP	Pathogen-associated molecular pattern
PF	*Haemophilus* Protein F
PRR	Pathogen pattern recognition receptor
PLG	Plasminogen
TCC	Terminal complement complex
TIMP-1	Tissue inhibitor of metalloproteinase-1
TLR	Toll-like receptor
Vn	Vitronectin

Populärvetenskaplig Sammanfattning

Bakterien *Haemophilus influenzae* är en vanlig orsak till infektioner i övre luftvägarna och mellanörat hos små barn. Den är också en vanlig orsak till infektioner i nedre luftvägarna samt orsakar stort lidande hos patienter med KOL (kronisk obstruktiv lungsjukdom). Dessa infektioner är vanliga och totalt sett ett omfattande kliniskt problem, vilket kompliceras av en ökande antibiotikaresistens. *H. influenzae* är en stavformad bakterie och delas in i typningsbara och icke-typningsbara *H. influenzae* (NTHi). De typningsbara *H. influenzae* stammarna är generellt farligare än NTHi. De typningsbara stammarna delas in i sex serotyper, a-f, där typ b (Hib) tidigare har varit den vanligaste serotypen vid invasiv sjukdom, till exempel meningit, epiglottit, septikemi, och osteomyelit. Ett effektivt Hib vaccin infördes i barnvaccinationsprogrammet 1992 och sedan dess har förekomsten av invasiva infektioner med Hib minskat drastiskt. Däremot har frekvensen av invasiva infektioner orsakade av andra *H. influenzae* typer ökat. I de flesta fall orsakas dessa nu av NTHi och *H. influenzae* serotyp f (Hif).

H. influenzae använder flera yttermembranproteiner (OMP) som hjälper dem att överleva attacken från det mänskliga immunförsvaret. För att förstå de sjukdomsframkallande egenskaperna hos *H. influenzae* har vi studerat tre OMP: Protein E (PE) från NTHi, Haemophilus surface fibril (Hsf) från Hib och Protein H (PH) från Hif. Vi har studerat den tredimensionella strukturen av PE och fann också att *H. influenzae* binder in hemin på ytan med hjälp av PE samt använder detta som järnreservoar. Genom bioinformatiska och experimentella analyser fann vi att Hsf är en mycket stor molekyl på ytan av bakterien och har en vriden "hårnålsliknande" struktur. Vi har sett att Hsf binder till vitronektin (Vn) och att denna interaktion både hjälper Hib att avvärja attacken från immunförsvaret och dessutom gör så att bakterien fastnar och går in i luftvägarnas epitelceller. Likaså har vi sett att PH från Hif binder Vn och att detta resulterade i bättre överlevnad av Hif i serum och ökad bindning av bakterier till epitelceller.

Upptäckten av nya OMP i kombination med strukturell och funktionell kunskap är viktig för en djupare förståelse av samspelet mellan bakterier och den mänskliga värden. Bakteriell inbindning till epitelceller och överlevnad i värden är beroende av bakteriens OMP. Inbindningen är en del av koloniseringen av luftvägen och en viktig del av processen som leder fram till senare sjukdomutveckling. Således är

bakteriens virulens beroende av dess OMP. Ett vaccin eller antibiotika som riktas mot dessa OMP är en potentiell nyckel till skydd mot smittsamma *H. influenzae*.

Introduction

Humans as a Bacterial Host

Bacteria are prokaryotic microorganisms that were the properly first life forms to appear on earth (1-3). Its habitats are almost everywhere; soil, water, acidic hot springs, radioactive waste and deep in the Earth's crust (4, 5). Around 40 million of bacterial cells can be found in a gram of soil and a million bacterial cells in a milliliter of fresh natural water (6). Globally, the total bacterial biomass which exceeds that of all plants and animals, which is estimated to consist of approximately 5×10^{30} cells (5). Bacteria can also be found in plants and animals with a symbiotic or parasitic relationships (7). The human body contains more bacterial cells than human cells, with the largest number of bacteria found in the gut, and the next largest number on the skin (8). Due to the protective effects of the human immune system, amongst other things, the majority of the bacteria are totally harmless, some are beneficial and some are only commensal. However, several species of bacteria are pathogenic and cause infectious diseases. Among all those types, commensal bacteria are the most interesting group of bacteria, usually living without affecting the host. Some can cause disease if there are any opportunities created by viral infection, inflammation or reduced immunity. That is why these types of bacteria are called opportunistic pathogens (9). The commensal bacteria colonize niches in the host and protect the host from invading pathogens by making a colonization barrier (10). This commensal community of bacteria is composed of 500–1000 species with a concentration of 10^{11} bacteria per gram of colon content (11).

The community of the commensal bacteria in the host may be influenced by various factors, including genetics, age, sex, stress, nutrition and diet (12). Normal flora first colonizes human at the moment of birth while passing through the birth canal. The fetus is sterile in utero but when the mother's water breaks and the birth process begins, bacterial colonization on the body surfaces start (13). Within approximately 48 hours, normal flora establishes on the skin, oral cavity and the intestine by handling and feeding of the infant after birth (14). The developmental stages of weaning, the eruption of the teeth, the onset and cessation (14) of ovarian functions, invariably affect the composition of the normal flora in the intestinal tract, the oral cavity, and the vagina, respectively (15, 16). However, during these

changes, the bacterial flora of humans is sufficiently constant and gives a general description of the situation.

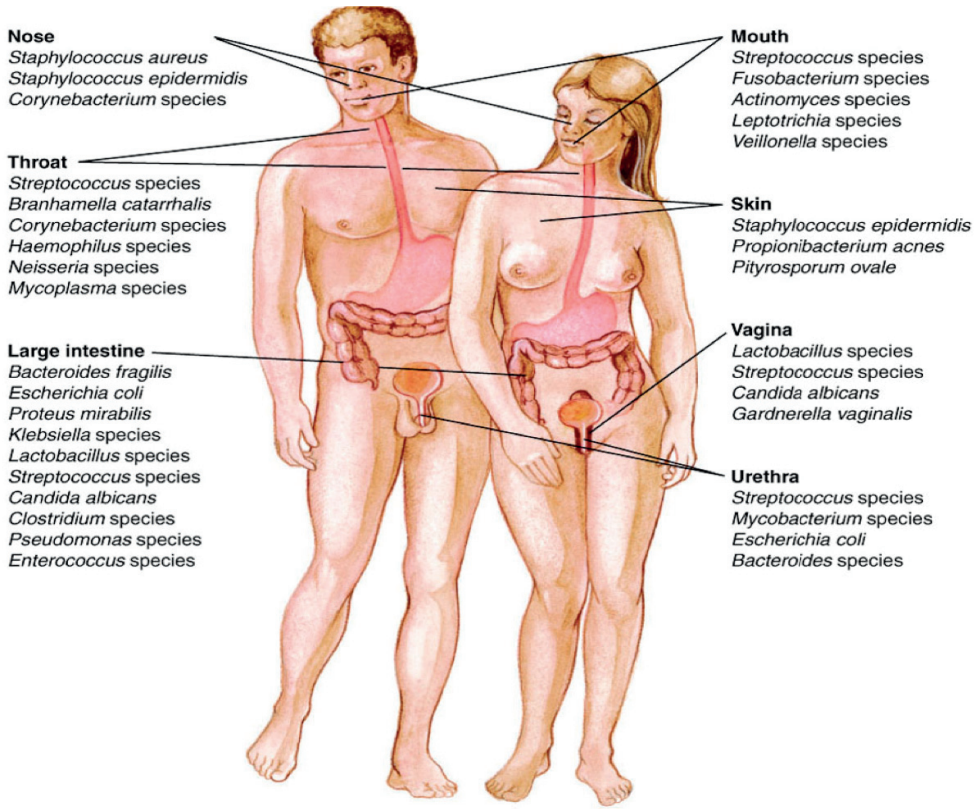

Figure 1: Bacterial species living in the human body. The main commensal bacterial species occupying different niches in the human body (McGraw-Hill education).

Commensal bacteria are present on all body surfaces and are exposed to the external environment such as gastrointestinal and respiratory tract, vagina, skin, etc. (Fig. 1) (17).

Human Bacterial Flora (Microbiome)

The normal bacterial flora influences the physiology, susceptibility to pathogens, and morbidity of the host. Different areas of the human skin can be compared to the geographic regions of Earth: the desert is the forearm, the cool woods region is the scalp and the tropical forest is the armpit (18). Depending on the character of

the microenvironment, the composition of the dermal micro-flora varies from site to site accordingly (18, 19). Skin colonizing bacteria mostly come from the four phyla: Actinobacteria (51.8%), Firmicutes (24.4%), Proteobacteria (16.5%), and Bacteroidetes (6.3%) (20). Bacterial flora in the digestive tract is essential for the development and function of the mucosal immune system at an early stage of life and is important for improvement of overall immunity in adults. The absence of digestive tract bacteria is associated with digestive enzyme activity, reductions in mucosal cell turnover, vascularity, muscle wall thickness, motility, baseline cytokine production, and with defective cell-mediated immunity (21). In addition, the intestinal bacterial flora makes important metabolic contributions to Vitamin K, folate, short-chain fatty acids and mediates the breakdown of dietary carcinogens (22, 23). In the urinary tract that is normally believe to be sterile and bacteria have problems gaining access and becoming established there (24). Studies suggest that the anterior urethra inhabited by a relatively consistent normal flora consisting of *Staphylococcus epidermidis*, *Enterococcus faecalis* and some alpha-hemolytic streptococci, however, their numbers are not plentiful (25). The acidic pH in the vaginal epithelium prevents establishment of most other bacteria as well as prevent from potentially pathogenic yeast, *Candida albicans*. This is a very good example of the protective effect of the normal bacterial flora for the human host (26-28).

Microbiome in the Respiratory Tract

The human respiratory tract is subdivided into two areas, the upper and lower respiratory tract, and consists of the nose, mouth, sinuses, throat, trachea, bronchial tubes, and lungs (Fig. 2).

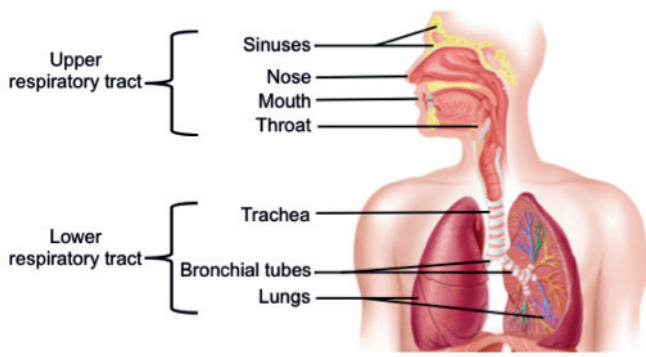

Figure 2: Human respiratory system. The depiction shows different parts of the upper and lower human respiratory tract.

The nose, mouth, sinuses, and throat (pharynx and larynx) belong to the upper respiratory tract, while the trachea, bronchial tubes, and lungs are included in the lower respiratory tract. A significant proportion of the normal bacterial microbiota in the upper and lower respiratory tract belongs to 9 major bacterial genera: *Prevotella, Sphingomonas, Pseudomonas, Acinetobacter, Fusobacterium, Haemophilus, Veillonella*, *Staphylococcus,* and *Streptococcus* (29). Most importantly some bacteria, namely, *Haemophilus influenzae, Streptococcus pyogenes, Streptococcus pneumoniae, Neisseria meningitidis,* and *Staphylococcus aureus,* are considered as normal bacterial flora in the respiratory tract but can cause serious diseases, especially in immunocompromised individuals (30-32). Bacterial flora of the respiratory system changes in relation to age, and unusual flora can be detrimental, which has been seen in patients with cystic fibrosis (29, 33). A large number of bacterial species colonize the nasopharynx and nostrils, predominantly *Staphylococcus epidermidis, Corynebacteria* spp., and *Staphylococcus aureus* (20% of the population). This part of the body is also the main carriage site of important pathogens. The healthy sinuses, in contrast, are sterile (34). The throat is normally colonized by *Streptococci* and various Gram-negative cocci. Sometimes pathogens such as *S. pneumoniae*, *S. pyogenes*, *H. influenzae* and *N. meningitidis* colonize the throat (35). Parts of the lower respiratory tract, such as the trachea, bronchi, and pulmonary tissues are nearly free of microorganisms, mainly because of the efficient cleansing action of the ciliated epithelium, which lines the tract. Any bacteria reaching the lower respiratory tract trapped in the mucus layer and are swept upward by the action of the mucociliary blanket that lines the bronchi and removed subsequently by coughing, sneezing, swallowing, etc. If the respiratory tract epithelium becomes damaged, as in bronchitis or viral pneumonia, the person may become susceptible to infection by pathogens such as *H. influenzae* or *S. pneumoniae* descending from the nasopharynx (36, 37).

Haemophilus influenzae

The history of Gram-negative *H. influenzae,* that was previously identified and known as Pfeiffer's bacillus or *Bacillus influenzae* (*B. influenzae*), has several interesting chapters. Before 1876, in the pre-microbiological era there was much confusion about the causes of great epidemic diseases like cholera and plague and also for the common communicable diseases like colds, smallpox, and measles. The idea of carriers or intermediate vectors was not easily anticipated, which was preventing many observers to accept an integrated concept of infectious diseases. Some of the diseases were directly transmissible from person to person, for example smallpox and others of which were acquired from intermediate vector hosts such as animals, as in the case with the plague. Others were acquired from contaminated environmental sources, *i.e*., cholera or were acquired by more than one of the mechanisms just noted, for example, smallpox and cholera. Influenza had been the more confusing of the pandemic diseases in the pre-microbial era; one of the reasons was that the signs and symptoms of influenza were non-specific, leading to confusion with other conditions (38).

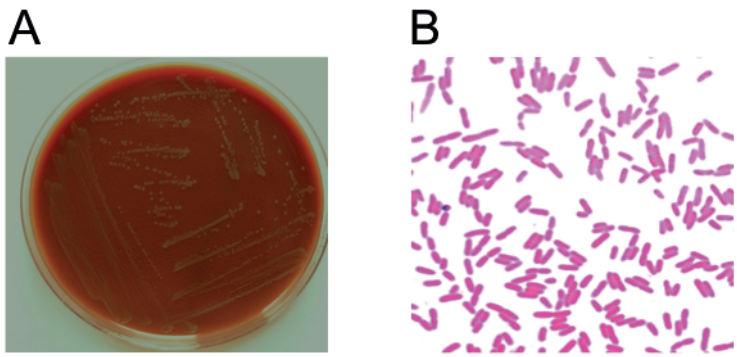

Figure 3: Photographs of *Haemophilus influenzae* (A) grown over night on chocolate agar plate and (B) after Gram-staining, visualized at 1000X magnification.

In 1892, the bacteriologist Richard Friedrich Johannes Pfeiffer (1858–1945) reported the discovery of a new bacterium (39). Richard Pfeiffer claimed that bacterium to be the cause of the pandemic influenza as he was frequently isolating those Gram-negative coccobacilli from the sputum of the patients of influenza pandemic in the late 1800's. When his initial, brief report in 1892 was followed up by more extensive data in 1893, *Bacillus influenzae*, as he called it was established as the true etiological agent of influenza in the scientific world (40).

B. influenzae was usually referred to as 'Pfeiffer's bacillus' in the literature of the late 19th and early 20th centuries, and is now known as *H. influenzae*. It was

clearly a pathogenic organism and was often cultured from fatal cases of influenza but other investigators were unable to confirm Pfeiffer's strong association (38, 41). The thought of *H. influenzae* as the true cause of influenza persisted up to the time of the next pandemic in 1918-1920, on that time the bacterium got its current name *Haemophilus influenzae* (42). Reflecting, "Blood" (from the Greek haemophilus, meaning "blood-loving") as the fastidious growth requirement of the organism, as well as its apparent association with influenza the organism was named *Haemophilus influenzae* (Fig. 3). But that doctrine about *B. influenzae*/*H. influenzae* described by Richard Pfeiffer was abandoned by Peter Kosciusko Olitsky (1886–1964) and Frederick L Gates (1886–1933) providing strong evidence against the causal association of *H. influenzae*, reporting that the infective influenza agent survived while passage through filters that excluded *H. influenzae* (43).

Despite the misleading initial ideas about *H. influenzae*, credit should be given to Pfeiffer, because with the recorded deaths during 1918–1919 influenza pandemic were associated with secondary bacterial invaders, among them *H. influenzae* (44). Moreover, Pfeiffer, a 38-year-old promising researcher at his time went on to have a long and distinguished career as an inventor of the typhoid vaccine, the discoverer of bacteriolysis named as 'Pfeiffer's phenomenon'. He was the first to discover the pathogenic organism Micrococcus now *Moraxella catarrhalis* and an identifier of the first endotoxin from bacteria (45). The discovery of the influenza virus as the etiology of the disease in 1933 eventually disproven the bacterial association with the influenza as suggested by Pfeiffer (46). However, studies revealed that *H. influenzae* was responsible for a wide spectrum of clinical diseases.

In the 1930s, Margaret Pittman a 30-year old microbiologist defined two major categories of *H. influenzae*: (i) S (smooth) strain and (ii) R (rough) strain on the basis of there appearance on the agar plate (47). She separated the S strains that causes invasive diseases and precipitated with the antisera from the normal R strains that did not precipitated (47). Pittman´s S strains and R strains are now known as encapsulated and non-encapculated *H. influenzae*. The encapsulated strains are then furthered serotyped from a to f on the basis of capsular polysaccharide composition and antigenicity.

H. influenzae Bacteriology

H. influenzae is a member of the *Pasteurellaceae* family. It is a non-motile, Gram-negative, rod-shaped bacterium. Generally it is aerobic but can also grow as a facultative anaerobe (48). *H. influenzae* is fastidious that requires X-factor (hemin) and V-factor (nicotinamide adenine dinucleotide) for growth. *H. influenzae* strains

are divided into two major groups, the encapsulated and the un-encapsulated strains, depending upon the presence or absence of a polysaccharide capsule. In humans, *H. influenzae* colonizes nasopharynx at the early stage of life and there is significant turnover of different strains particularly in young children. Although the role of this bacterium in the microbiome of upper respiratory tract are not fully understood, different isolates and colonization density can be correlated with middle ear infection (49). *H. influenzae* has several mechanisms to survive in the human host and its presence as a commensal in the nasopharynx serves as an ongoing source of potential infection for the respiratory tract.

There is an ambiguity in identifying clearly and separating *H. influenzae* from *H. haemolyticus*, which is also a species of Gram-negative bacteria. It is related to *H. influenzae* but is nonpathogenic. Recent observations suggest that the widely utilized and accepted methods do not reliably distinguish *H. influenzae* from *H. haemolyticus* (50). This obscurity has important implications for medical microbiology laboratories and also in the interpretation of reported studies about colonization of the human nasopharynx (51). *H. haemolyticus'* ability to produce a clear hemolytic zone on blood agar is the only characteristic used to differentiate it from *H. influenzae* (52), but recent observations showed that a substantial proportion of *H. haemolyticus* strains are non-hemolytic (53). Thus, many non-hemolytic strains of *H. haemolyticus* could have been misidentified and studied as *H. influenzae*. So, it is important to interpret the literature on respiratory tract colonization and infection by *H. influenzae* with the limitation in mind that some of strains recovered from respiratory tract and identified as *H. influenzae* may in fact be commensal *H. haemolyticus* (50).

Typeable *H. influenzae*

Encapsulated *H. influenzae* produce a polysaccharide capsule and are further subdivided into six serotypes designated as a, b, c, d, e, and f depending on the capsular polysaccharide composition and antigenicity (54). Among all types of *H. influenzae*, serotype type b (Hib) has been the most known to cause significant invasive disease (55-57).

In the late 1980's the effective Hib vaccines, polysaccharide vaccine in 1985 and conjugate vaccines during 1987–1990 were produced (58). In countries where Hib conjugate vaccines have been introduced, a dramatic reduction in Hib disease has been observed (59). In contrast, the number of cases with invasive disease caused by non-Hib, *i.e.*, NTHi and type f (Hif) seems to increase, suggesting a replacement phenomenon (60-62). In recent study it has been shown that even the distribution of capsular Hib in invasive disease has shifted to non-Hib, but that it is mainly towards non-typeable *H. influenzae* rather than non-serotype b strains of *H.*

influenzae (50). In the time before the Hib vaccines, it was far less common to recover the isolates of serotype a, c, d, e, and f from patients with invasive disease (63). Currently, of these non-Hib serotypes, serotype f has most commonly been associated with invasive diseases. It has been reported that in some vaccinated populations, the incidence of serotype f disease may have increased (64).

Non-typeable *H. influenzae*

Un-encapsulated strains are termed non-typeable *H. influenzae* (NTHi) because they lack a capsule. Genetically, and also through the expression of outer membrane proteins, un-encapsulated strains are enormously diversified (65). NTHi strains are found to be more diverse than encapsulated strains, one important reason for that may be that their population structures are more influenced by recombination (66, 67). NTHi are responsible for the majority of mucosal infections (68). It is very common in healthy adults that they have upper airway colonization of *H. influenzae*, in a process that very dynamic of which NTHi is the predominant strain (69). In the post vaccination era, invasive non-Hib disease in children is more common due to non-capsulated strains than to encapsulated isolates of the non-Hib serotypes (70). There has been an increase in adult non-Hib isolate invasive disease in some countries, where the Hib conjugate vaccines are used, most of which is due to non-capsulated isolates (71).

Bio-typing

As mentioned before, in-vitro growth of *H. influenzae* requires two growth factors found in blood. One is hemin, and the other one is nicotinamide adenine dinucleotide (NAD). Possible identification of *H. influenzae* is based on the following three criteria (i) growth requirement for both hemin and NAD (ii) characteristic colony morphology on a chocolate blood agar plate and (iii) Gram-stain morphology. Bio-typing of *H. influenzae* was done on the basis of their reactions in biochemical tests and production of indole, urease, and ornithine decarboxylase (72) with the Minitek Differentiation System (BBL Microbiology Systems) (73, 74) and proposed to be divided into eight biotypes. Absolute identification of *H. influenzae,* especially with non-typeable strains, needs 16S rRNA sequencing or other genetical methods (75). Using a molecular biology technique such as multilocus enzyme electrophoresis (MLEE), *H. influenzae* serotype a (Hia) and Hib can be classified as two different genetic lineages, whereas serotypes c, d, e, and f, form the monophyletic groups (76, 77). By contrast, non-encapsulated *H. influenzae* is distinct from the encapsulated strains,

appearing to be non-clonal in comparison with the serotypes and are genetically diverse (63).

Host Defense System in the Airways

Humans are in continuous contact with bacteria, including the normal bacterial flora that human live with (78). On relatively rare occasion, the bacteria from the normal flora cause damage to their host (79, 80). In part, this is due to the effectiveness of the host defense mechanisms, which restrict invasion by the bacteria from normal flora, some of which are potential pathogens and some of which defend against non-indigenous microorganisms that are overt pathogens (81, 82). The resultant infections caused either by a component of the normal flora or an exogenous pathogen depends on specific properties inherent to both the host and the microbe (83, 84). In some instances, the human host tolerates bacterial colonization by restricting it to regions of the body where it cannot do harm, *e.g*., *S. aureus* on the nasal membranes (85) or *H. influenzae*, *S. pneumoniae* in the upper respiratory tract (86-89). Sometimes commensal bacteria breach an anatomical barrier or reach beyond the point of colonization, causing infection (90).

A healthy person defends against pathogens at different stages. For most of the time, the host defenses are of such a degree that infection can be prevented or infection does occur but the defenses stop the process before disease is apparent (91). At the other times, the defenses may not be effective until infectious disease becomes symptomatic (92, 93). The immune system is composed of two major subdivisions; innate or nonspecific immunity, and adaptive or specific immunity. Innate immunity works as a primary defense against pathogens (94, 95), while adaptive immunity serves as a second line of defense (96). Although there is interplay between these two immune systems and both have cellular and humoral components by which they carry out their protective functions, these also differ in several ways (97, 98).

To understand the pathogenesis of *H. influenzae*, it is important to know the relevant host defense mechanism in our respiratory tract.

Innate Immunity

Mechanical Barrier

The upper respiratory airway is lined by ciliated pseudostratified columnar epithelium, multiple cell types comprising the respiratory epithelium. The three major cell types of the columnar epithelium are ciliated cells, goblet cells, and basal cells (99, 100). The respiratory system possesses mechanical measures to remove bacteria using cilia (101) on the epithelial cell surface and mucus produced by goblet cells (Fig. 4). Bacteria become trapped in the mucus produced by the goblet cells and moved by the "mucociliary escalator" of the respiratory system (102).

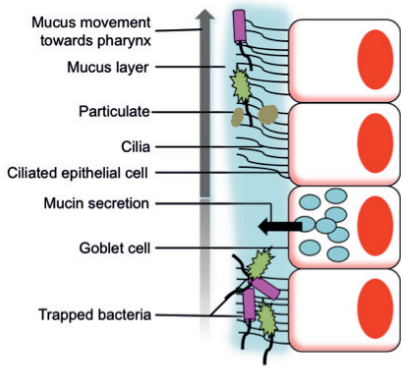

Figure 4: Mechanical removal of bacteria. Ciliated epithelial cells move mucus and removed dirt and trapped pathogens out of the airways, protecting the lungs from damage and disease.

Over 50% of all epithelial cells in the conducting airway are ciliated (103) with approximately 200 to 300 cilia per cell (104). While inhaled pathogens and other particulate matter are trapped in the mucus, the coordinated beating of cilia shifts the trapped material upwards toward the pharynx (Fig. 4) (105, 106).

Airway Epithelial Permeability

The apico-lateral border of the airway epithelial cells forms tight and adherens junctions that contribute to the paracellular permeability of airway epithelium, and also as a barrier to pathogens (107). Tight junctions regulate the transport of solutes and ions across epithelia and adherens junctions mediate cell-cell adhesion and promote formation of tight networks (108-110).

These intercellular junctions of the airway epithelium not only prevent inhaled pathogens and other environmental particles from injuring the airways, but also serve as signaling platforms to regulate cell proliferation and differentiation (111, 112). It is apparent that dissociation of the junction-complexes will disrupt the barrier function, interfere with normal repair and differentiation of airway epithelium. This epithelium is leaky, hyper-proliferative, and compared with healthy smokers, airway epithelium abnormally differentiate in smokers with asthma and COPD (113-115). Transient disruption of the tight or adherens junctions can be caused by viruses or bacterial infection (116, 117). Adherens junctions are located just below the tight junctions and mechanically connect adjacent cells and initiate the formation and maturation of cell-cell contacts. It is likely that excessive smoking decreases barrier function and facilitates invasion of airway epithelium by environmental allergens, pollutants, and pathogens.

Biochemical Barrier

In addition to being a physical barrier, airway epithelium also contributes in killing inhaled pathogens by producing enzymes, protease inhibitors, oxidants, and antimicrobial peptides (AMPs). Lysozyme enzyme that is found in airway epithelial secretions, has antimicrobial activities against a wide range of Gram-positive bacteria by degrading their peptidoglycan layer (118). In concert with lactoferrin, produced by airway epithelium lysozyme can disrupt the outer membrane and gain access to the peptidoglycan layer of Gram-negative bacteria (119). Lactoferrin levels increase in response to bacterial and viral infections in the host (120). While occupying a role in killing Gram-negative bacteria combined with lysozyme, lactoferrin itself is an iron-chelator and inhibits microbial growth by sequestering iron, which is also essential for microbial respiration (121). Lactoferrin stimulates an immune response against both RNA and DNA viruses by either inhibiting binding of the virus to host cells or by binding to the virus itself (122, 123).

Airway epithelial cells produce protease inhibitors, such as secretory leukoprotease inhibitor (SLPI), elastase inhibitor, α1-antiprotease, and antichymotrypsin. These protease inhibitors diminish the activities of the proteases secreted by pathogens and recruited immune cells (124, 125). The balance between anti-proteases and proteases in the airway lumen during infection is the key to prevent lung inflammation and maintenance of tissue homeostasis (126).

The respiratory epithelial cells also contribute to the immune response by producing antimicrobial peptides (AMPs). Human β-defensins (hBD) are the most abundant antimicrobial peptides expressed on the surface of airway epithelium and are effective against a wide range of bacteria (127). While hBD1 is constitutively expressed, hBD2 to hBD4 expressions are induced by LPS via nuclear factor kappa-beta (NF-κB) and by Interleukin-1 (IL-1) (128, 129). Cathelicidins are

another class of antimicrobial peptides and LL-37 is the only human version identified to date (130). Cathelicidin LL-37 binds to lipopolysaccharides, permeabilizes the bacterial membrane and inactivates its biological function (131). Extracellular hydrogen, produced by dual oxidase 1 and 2 peroxide belong to a family of Nicotinamide Adenine Dinucleotide Phosphate (NADPH) oxidases and are secreted to the extracellular milieu (132). The dual oxidase-generated hydrogen peroxide in combination with thiocyanate and lactoperoxidase, generate the microbicidal oxidant hypothiocyanite, which effectively kills both Gram positive and Gram-negative bacteria (133).

Inflammation

Inflammation is the body's natural response to infections and injuries; it is either the stimulation of epithelial cells or phagocytic cells (134). Inflammation can be described as the protective response that involves immune cells, blood vessels, and molecular mediators (135). The inflammatory response may be the most important for dealing with microbial infections. Inflammation is necessary for the proper functioning of all the host defenses, because it focuses all circulating antimicrobial factors on the site of infection (134). Stimulated cells activated the immune response through the cytokines and chemokines. Neutrophils are recruited from the bloodstream to the site of infection by an interleukin-8 (IL-8) gradient (134). When microbes are presented to a macrophage, it ingests the microbe through specific macrophage receptors and traps in a phagosome (136). Then, the phagosome fuses with a lysosome and within the phagolysosome created, enzymes and toxic peroxides digest the pathogen (137). Reactive oxygen intermediate and proteolytic enzyme released by stimulated macrophage and neutrophils, lead to recruitment of more inflammatory factors; these include phagocytes, lymphocytes, antibodies, complement and other antimicrobial components of plasma. Yet, inflammation is also an important aspect of bacterial pathogenesis, because the inflammatory response induced by a microbe can result in considerable damage to the host tissue, therefore, is part of the pathology of microbial disease.

The Complement System

The complement system consists of a tightly regulated network of proteins that play an important role in host defense. Complement activation results in opsonization of bacterial pathogens and their removal by phagocytes and cell lysis (138). The complement system is a part of serum. During airway inflammation, complement factors reach to the site through plasma effusion (139). This part of innate immunity works against foreign microbes in three steps: firstly, recognition of the microbial non-self; secondly, opsonization of the microbe and thirdly, for Gram-negative bacteria; lysis of the bacterial cell via the pore-forming membrane attack complex (MAC), also designated terminal complement complex (TCC).

Complement activation is triggered by one of three pathways– classical, alternative and lectin, depending on the nature of the foreign cell and therefore the activating surface (135). A central component of the complement system is Complement factor 3 (C3) protein, in all three pathways; C3-convertase cleaves and activates the C3 (140). A cascade of reactions starts by cleaving C3, yielding C3a and C3b. This C3b then binds to the surface of pathogens, leading opsonization by neutrophils and macrophages, and starts the terminal pathway (141). All of the above mentioned pathways can be activated in ways that lead to the terminal pathway (Fig. 5). The classical pathway is activated primarily by the interaction of C1q with immune complexes of antibody bound to microbes, but can also be achieved after interaction of C1q with non-immune molecules (138). The alternative pathway does not depend upon the presence of immune complexes; it starts with the spontaneous hydrolysis of C3 and subsequent deposition of C3b to the cell surface. The lectin pathway shares several factors with the classical pathway and is activated by the binding of mannose binding lectin (MBL) to the carbohydrates expressed on the bacterial surface (140). The result of all three pathways is induction of the terminal pathway of the complement system for destruction of the targeted bacteria forming the lytic molecules C5b-9 (142, 143).

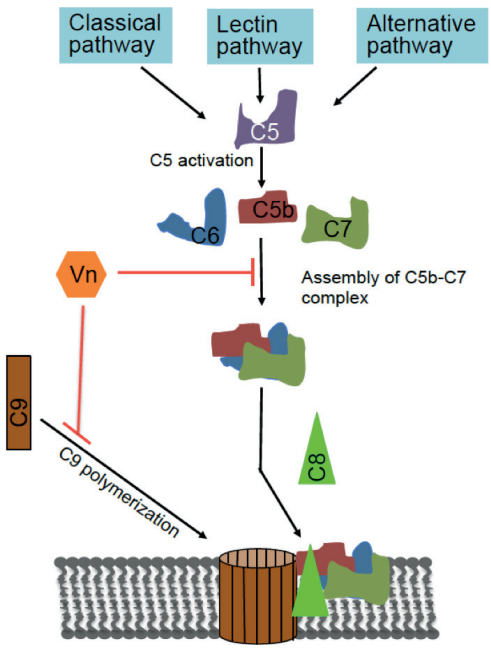

Figure 5: The common terminal pathway of the complement system. Vitronectin inhibits the terminal pathway by interacting with the C5b-7 complex assembly and also inhibits C9 polymerization during formation of a lytic pore.

Inappropriate activation of the complement system and complement deficiencies are the underlying cause of pathophysiology in many diseases (144). Therefore, the system is tightly regulated on almost every level. Complement down-regulating proteins include C1-inhibitor (C1-INH), C4b-binding protein (C4BP). Clusterin, Factor H (FH), Factor H-like protein 1 (FHL-1), Factor I (FI), Properdin and Vn (141).

Plasma exudation results in Vn exposure on the apical side of the airway epithelial cells (145, 146). Vn is a well-known complement regulator that inhibits the terminal complement pathway by interacting with the C5b-7 complex formation and C9 polymerization to form the membrane attack complex (MAC) (Fig. 5) (147). Vn is an effective regulator that inhibits the terminal lytic pathway regardless of which complement pathway is activated. *H. influenzae*, along with several other respiratory tract pathogens, *M. catarrhalis*, *P. aeruginosa*, *S. pneumoniae*, *S. pyogenes* and *S. aureus* have been shown to interact with Vn (147). Thus, Vn plays important role in the host and pathogen interaction.

Nutritional Immunity

Transition metals such as Iron (Fe), Manganese (Mn), Zink (Zn), Copper (Cu) and others are required by all living organisms to survive, because these are involved in many crucial biological processes including incorporation with metalloenzymes, storage proteins and transcription factors (148). Their reactivity is necessary for catalysis and their electrostatic properties stabilize substrates or reaction intermediates in the active sites of enzymes (149). The human body is a rich reservoir of essential nutrients for those bacteria that have evolved to exploit this resource. The catalytic activity of these metals potentiates their toxicity, and the levels of transition metals therefore must be controlled carefully. The mechanisms used to withhold the availability of free transition metals serve as a countermeasure against invading bacteria. The process that human cells and other mammalian cells use to restrict the access of essential metals to pathogenic bacteria is termed as “nutritional immunity” (150).

The functional roles of transition metals in biological systems can be divided broadly into non-catalytic functions, redox catalysis and non-redox catalysis. Of the redox-active metals, Fe is the most common, followed by Cu and Mo (Molybdenum) (151). Virtually all bacterial pathogens require Fe for diverse physiological processes such as DNA replication, transcription and central metabolism; therefore, bacteria must elaborate Fe acquisition systems in order to successfully colonize the host (152). *H. influenzae* has an absolute requirement for heme, because it lacks 6 of 7 enzymes in the heme synthetic pathway that consequently leads to an inability to produce Protoporphyrin IX (PPIX) (153). On

the other hand, vertebrates limit access to Fe to exploit this requirement as a potent defence mechanism against infection (154, 155).

To prevent bacterial access to Fe, the host uses a number of proteins to withhold this valuable nutrient and make largely inaccessible to pathogens that lack sophisticated Fe-capturing systems. In human, the majority of Fe is complexed to heme, a tetrapyrrole ring encircling a singular Fe atom and the cofactor of the oxygen transport protein hemoglobin (148). Furthermore, hemoglobin is contained within circulating erythrocytes, representing an additional barrier to access by pathogens. If free haemoglobin or heme is released from erythrocytes, these molecules are rapidly bound by haptoglobin and hemopexin, respectively (156). Intracellular Fe is stored in the Fe storage protein Ferritin in the host and is therefore only reachable to intracellular pathogens following host cell lysis (157). Moreover, Natural Resistance-Associated Macrophage Protein 1 (NRAMP1) that localizes to the phagosomal membrane, pumps Fe and Mn out of the phagosomal compartment, thereby reducing accessibility of these metals to the pathogens that reside within a phagosome (158).

Extracellular Fe^{2+} is oxidized to the insoluble Fe^{3+} at physiological pH and captured by the serum protein Transferrin with exceptionally high affinity (159). Free Fe^{3+} is also bound by Lactoferrin, a globular glycoprotein of the Transferrin family that is present in secretions such as breast milk, tears, and saliva (160). Even though, bacterial pathogens rely on additional nutrients such as carbon, nitrogen and sulphur in the host, most of the work in nutritional immunity has focused on transition metals (161, 162). Studies suggest that successful adaptation to the host environment by pathogens depend on the ability to take the advantage of the available carbon sources (163, 164). Therefore, with the nutrient metal restriction by the host, it is remained to be determined whether specific mechanisms are also involved in limiting the non-metal nutrient components as a part of the nutritional immunity.

Adaptive Immunity

Sercretory IgA

The amount of IgA produced in mucosal linings is greater than all other types of antibody combined in this location, and exists in two isotypes, IgA1 and IgA2 (165). The respiratory epithelium is dominated by the IgA1 isotype. These IgAs are poor activator of the complement system (166). IgAs are produced by the near plasma cells, and bind to the polymeric Ig-Receptor (pIgR) on the epithelial cells, through which they are passaged and secreted into the airway (167). IgAs agglutinate bacteria and prevent effective epithelial adherence and colonization (165). In *H. influenzae*, two genes of IgA1 protease have been identified and the

isolates carrying both genes in the genome believe to be more pathogenic than other isolates (168).

Specific Antibodies

Antigen specific antibodies, also known as an immunoglobulins (Ig), mainly produced by plasma cells that are used by the immune system to identify and neutralize pathogens such as bacteria. In short, the antigen is presented by antigen-presenting cells (APCs), T-cells and B-cells that mature into plasma cells (169). After primary challenge by the antigen, it takes weeks to produce antibodies with high avidity (170). However, the T- and B-cells can be differentiated into memory cells, which upon secondary stimulation with the same antigen, respond very rapidly. Antibodies are found in five different varieties, known as IgA, IgD, IgE, IgG, and IgM (171). Each immunoglobulin has two main parts; the highly variable Fab region that binds to the antigen, and the Fc region that mediates effector functions like phagocytosis or complement activation (172). IgA and IgG can be further divided into two and four subclasses, respectively. IgG1 and IgG2 are shown to be protective against infection causes by encapsulated *H. influenzae* type b (173). Deficiency of IgG2 has been reported to be the reason of high incidence and poor vaccination protection in the ethnic groups with unusual higher incidence of invasive Hib diseases (174). Antibody protection against NTHi does not occur equally depending on IgG2 and it has been reported that antibody produced by stimulation with one NTHi isolate offers substantial cross-protection against other NTHi isolates (175).

Haemophilus influenzae Pathogenicity

Several events take place before an infection is established by *H. influenzae*. Bacteria first need to reach and breakout from the mucociliary elevator, adhere to cells, evade host immunity, adapt to the host in a nutrient limited environment, and finally cause infection.

***H. influenzae*: An Opportunistic Pathogen**

Approximately 10% of the total bacterial flora in the human upper respiratory tract is consisted of *Haemophilus* species (176). The rate of *H. influenzae* carriage increases from infancy to early childhood, and is recoverable from the upper airways of approximately 20 to 80% of healthy children (176). Colonization of the respiratory surface is a dynamic process; bacteria are acquired, replaced, and reacquired many times in a lifetime. Previous studies have demonstrated a 62%

weekly turnover rate of *H. influenzae* isolated from healthy children (177). In addition to colonizing as a commensal in the respiratory tract and occasionally in the genital mucosa, *H. influenzae* also cause symptomatic infections specially in children and immuno-compromised people (178). *Haemophilus* spp. usually live in their host without causing disease, but cause problems only when other factors, such as a viral infection, compromised immune function or chronically inflamed tissues, *e.g*., from allergies, create an opportunity (9), further showing evidence that *H. influenzae* is recognized as an opportunistic pathogen.

Genetic Heterogeneity of *H. influenzae*

H. influenzae is a genetically divergent species with the core-genome consisting of 1485 genes present in all strains, close to 75% of the genomic content of any given isolate (179). The *H. influenzae* genome is predicted to contain approximately 4500 unique genes (180). However, since many strains of *H. influenzae* are naturally occurring competent for DNA uptake, it is likely that a constant and spontaneous genetic exchange occurs via uptake and recombination with in the intra-species bacterial population (181). It has been reported that individual strains find contemporary access to various parts of the genome of other strains during concomitant colonization of the same host (182). This mechanism of acquiring a wide variety of genes while still keeping their individual genome small, give them a fitness advantage. Although, the theory of specific genetic elements associated disease, antagonistic to asymptomatic colonization factors, have long remained mysterious but some genes have been found to be more prevalent among virulent strains (183). As a case example, when 210 geographically and clinically diverse NTHi strains were compared for total gene content, 149 genes were identified to be significantly associated with either virulence or commensalism. Interestingly, 28 genes of those were found in most of the virulent strains, none of the genes were in the group of well-characterized virulence factors those involved in adherence, lipooligosaccharide (LOS) biosynthesis or immune evasion (179). It would be interesting to study the disease-associated genes in *Haemophilus* spp. further more.

Host Colonization

Colonization and subsequent infection of the host is primarily dependent upon successful adherence to the host tissue. *H. influenzae* can escape the mucociliary escalator of the airway by decreasing the ciliary beating and detaching ciliated epithelial cells activating host protein kinase C epsilon (184). The cilial damage is reported to be mediated by LOS, injury to the ciliated cells and the detachment of

cilia is the first step in the series of events, ending in extensive epithelial damage (185). However, according to other reports, disintegration of the ciliated cells is not always observed and bacteria appeared to take refuge in para-cellular foci to evade the mucociliary elevator (68). Another obstacle for successful adherence is secretory IgA1, which is the main element of adaptive immunity in the human airway mucosa (166). Interestingly, *Haemophilus* species are found to be equipped with IgA1 protease to degrade secretory IgA1 (168). Both these strategies for escaping the mucociliary escalator and adaptive immunity in the airway can plausibly be implemented during host colonization by *H. influenzae*.

Subsequently, an important step towards disease is the effective attachment to the epithelium. *H. influenzae* is specialized in attaching to the airway epithelial cells, preferably to damaged epithelium (186). Epithelial cells are connected to the underlying extracellular matrix (ECM) proteins via a range of basal surface structures including integrins (187). The epithelium can be damaged by viral infections or chronic inflammation, whereby ECM proteins become exposed and targets for adherence by pathogens (188). A range of different factors from *H. influenzae* have been identified as adhesins and shown to involve in bacterial attachment to different components of the airway epithelium. Pili are present in nearly all Hib isolates and only in a subset of NTHi (189). Pili agglutinate erythrocytes and are important in the early phase of infection establishing binding to host epithelial cells and mucin (186, 190). The major non-pilus *H. influenzae* adhesins are High Molecular Weight proteins (HMW-1 and HMW-2) and are present in approximately 75% of NTHi (191). Despite significant homology, they have different ligands, with the HMW-1 known ligand to bind sialylated glycoproteins, while the ligand of HMW-2 is still unknown (192). Hsf are a non-pilus *H. influenzae* OMP that binds to Chang epithelial cells, found in most encapsulated *H. influenzae* (193). Two homologs of Hsf, *H. influenzae* Adhesin (Hia) and Cryptic *Haemophilus* Adhesion (cha) are found in NTHi isolates (194). Most NTHi isolates that do not express HMWs express hia. Hia can bind respiratory epithelial cells, and isolates expressing the cha adhesin can bind to genital cells as well as respiratory epithelial cells, but the exact ligands are not defined (191, 195).

Another non-pilus protein, *Haemophilus* Adhesion and Penetration Protein (Hap) helps *H. influenzae* to adhere to the ECM (196). Hap binding domain is normally released from the cell surface but can remain cell-associated through the help of host antimicrobial peptides, and this interaction increases bacterial adhesion capacity (196). P2 and P5 are the outer membrane lipoproteins expressed on almost all known isolates of *H. influenzae*, and both bind to respiratory mucin (197). P2 (198) is a porin with adhesive properties while P5 (199) is mainly adhesin that binds to multiple ligands. Protein D, another lipoprotein that promotes adherence to and internalization into epithelial cells, is highly conserved and

expressed on all tested isolates of *H. influenzae* (200). PE and Protein F (PF) are two well-studied lipoproteins found to promote adherence to alveolar epithelial cells, and interact with ECM proteins Vn and Laminin (Ln) (201).

Host Immune Evasion

In order to survive and successfully colonize the host, *H. influenzae* has developed a number of strategies to evade the host defense. It has been reported that *H. influenzae* avoids innate immune effectors such as AMPs, Transferrin and Nitric Oxide (202, 203) very effectively. *H. influenzae* evolved to produce an IgA-protease that hydrolyses the main effector of acquired immunity in the respiratory tract and facilitates the colonization in the niche (204). IgA proteases of *H. influenzae* are highly specific endopeptidases that cleave the hinge region of human IgA1 and mediate invasion in human respiratory epithelial cells (205). Typeable *H. influenzae* avoid phagocytosis by the use of capsular polysaccharide (206). Remarkably, NTHi can produce a "pseudo-capsule" via extensive branching of the LOS that blocks IgM from binding to bacterial surface epitopes (207). Therefore, neutrophil-mediated phagocytotic killing of *H. influenzae* is significantly impeded, providing one mechanistic explanation as to why the recruited neutrophils at sites of inflammation cannot clear *Haemophilus sp*. infections. In parallel with all Gram-negative bacteria, *H. influenzae* has the capacity to release outer membrane vesicles (OMV) (208). The host humoral response has been shown to be non-specifically activated via NTHi OMVs, specifically, the proliferating lymphocytes would produce antibodies that may not recognize NTHi, resulting in deviation of the human adaptive immunity (209).

Complement activity of human serum is crucial in controlling invasive infections. Polysaccharide capsule of typeable *H. influenzae* have been shown to be resistant to complement-mediated killing, which is regarded as one of its central virulence determinants. In contrast, NTHi devoid of capsular polysaccharide employs distinct strategies to block antibodies and complement components from reaching the surface via LOS modification. NTHi incorporates host-derived sialic acid and phosphorylcholine into its LOS as a mean of camouflage (210, 211), and alternates the surface glycans to prevent bactericidal antibodies from opsonizing, thereby preventing complement activation via the classical pathway (212). Furthermore, LgtC-mediated LOS modification has been shown to delay C4b deposition on the bacterial surface via an unclear mechanism (213). The complement system in humans is tightly regulated by C4b-binding protein, Factor H and Vn, regulators of the common final pathway (214) (Figure 5). Several species of bacteria including *H. influenzae* use outer membrane proteins to acquire complement regulatory factors and consequently increase their resistance to complement mediated killing (215, 216). Different isolates of *H. influenzae* can bind to all of

these regulators at varying degrees (217-220). Through these interactions, *in vitro* bacterial survival in human serum is increased.

Persistence in the Host

Bacteria and humans have co-evolved over thousands of years. After entering in the host, to survive and further colonize, adapting with host environment is important. The human nasopharyngeal tract is a nutrient-poor milieu for bacteria and *H. influenzae* DNA transformation machinery believe to be evolved with a nutrient uptake system in this desolate niche rather than for genetic recombination purposes (221). *H. influenzae* has an absolute growth requirement of heme and NAD and it has lost the genes for *de novo* biosynthesis of these two elements (222). Outer membrane lipoprotein P4 and the P2 porin reported as external NAD uptaking proteins of *H. influenzae* (223, 224). Porin P2 is the most abundant protein on the outer membrane, contributing to a steady uptake of exogenous NAD (225). The transport systems involved in the uptake of heme and iron, are tightly regulated. A recent study showed that the Ferric Uptake Regulator (Fur) in NTHi contains 73 genes, in which many of these genes were involved in iron-utilization (226). This study showed 55 core and 200 non-core ORFs are up- or down regulated in the absence of iron/heme, demonstrating how bacteria can save energy by tightly regulating the expression of iron/heme-utilization genes (227). The mechanisms for heme acquisition have not yet been fully elucidated for this bacterial species, but several heme-binding proteins of *Haemophilus* spp. have been studied for their interaction with heme (228). Most of these proteins are transporters or transport-associated proteins described as hemophores (227). Recently, we reported that PE, which is conserved in all typeable and non-typeable *H. influenzae*, is a heme-binding outer membrane protein. PE also serves as a reservoir of hemin for *H. influenzae* to overcome the nutritional immunity and assist the cells to survive in conditions related to heme paucity (229). Additionally, investigators have reported on a urease operon in *H. influenzae*. The importance of the enzyme urease is, raising the pH in the human respiratory tract microenvironment to facilitate bacterial growth (230).

One efficient way to avoid host immunity and adapt within the niche is to vary surface exposed molecules, a “moving target” strategy. While surface-exposed factors are necessary for adhesion and colonization, they are often immunogenic and make the bacteria to be recognized and killed by the host adaptive immune defense. When required, surface expression of such factors can be turned on and off, this process is called phase variation, and it is generally reversible (231). Exclusive human host species like *H. influenzae* can vary the surface expression of the LOS (232), hemagglutinating pili (233) and the High-Molecular Weight adhesins (234). Even though almost all Hib isolates carry the pili gene cluster, and

use the pili to attach to the human airway, Hib strains isolated from blood have lost their pili expression to avoid antibody detection in serum, and as a consequence survive better in the bloodstream (179).

Bacterial biofilm formation is a feature suggested to promote bacterial population survival. Biofilms are highly structured microbial communities consisting of bacterial cells embedded in a matrix consisting of extracellular protein, DNA and polysaccharide (235). The adhesin Hap in *H. influenzae* is known to promote bacterial aggregation (236). Most studies suggest that NTHi can form biofilms, biofilm-associated bacteria display increased resistance to biological, chemical and physical environmental stresses (including antibiotics and the host immune system) as compared to planktonic microbes, and are believed to be the cause of persistent NTHi infections (237). The expression of a range of adhesins is necessary for biofilm formation [100]. In NTHi, biofilm-formation includes double-stranded DNA, type IV pili and LOS (238, 239). When the entire protein content of the extracellular material of the NTHi biofilm was mapped, eighteen proteins, including P2 and P5, bacterial DNA as well as proteins from the cytoplasm, periplasm and the outer membrane were all reported to be present in the biofilm (240). NTHi in biofilms have demonstrated the ability to resist neutrophil killing (241). These data collectively put a spotlight on *H. influenzae* adaptation in various niches of the human body.

Diseases Caused by *H. influenzae*

Colonization with *H. influenzae* begins in infancy, mainly in the upper respiratory tract. Approximately 20% of newborns are colonized in the first year of life and the colonization increases over time (69). More than 50% of children by the age of 5–6 years old and at least 75% of the healthy adults will be colonized by this bacterium (65). Typically, adults are colonized with only one strain, while children carry multiple strains simultaneously and tend more so to become infected with this pathogen (242).

Since Margaret Pittman's original description of typeable *H. influenzae* isolates in 1931 (47), Hib had been the most clinically significant strain causing invasive disease. Hib causes meningitis, epiglottitis, septicemia and osteomyelitis (55, 56, 243). However, the incidence of invasive Hib disease has greatly reduced worldwide because of routine immunization with Hib conjugate vaccines (59). Hia and Hif are also found to cause invasive disease such as meningitis, especially in children (244, 245).

Non-typeable *H. influenzae* is the cause of otitis media in infants and children, sinusitis in children and adults, pneumonia in adults, and exacerbation in patients with chronic obstructive pulmonary disease (COPD) (246).

Vaccines Against *Haemophilus influenzae*

A series of vaccines were developed in the USA during the Spanish flu pandemic of 1918-1919 when *H. influenzae* was believed to be the etiological agent of influenza (247). A polysaccharide vaccine directed against *H. influenzae* type b was tested in the 1970's (248). The limitation was that small children did not develop protective antibodies using only polysaccharide antigens (249). In the 1980's, peptide conjugates were added to the polysaccharide vaccine, and this method was later emulated in vaccine development for other encapsulated bacteria (250). Peptide conjugated polysaccharide vaccines led to protection even in small children, and even better protection following booster doses, regardless of what conjugate was used (251). Large-scale public heath measures adoption of the protein-conjugated capsular-polysaccharide Hib vaccine starting in the late 1980's has been very successful (252). With the introduction of the efficient vaccine, Hib-mediated infections were practically eliminated (253). However, Hib-disease is still a major problem in areas that have not yet employed the vaccine on a large scale (254). Since the success with Hib-vaccine, the focus of *H. influenzae* vaccinology has moved to non-capsulated strains that provide a greater scientific challenge than Hib due the absence of a singular main surface antigen, which in the case of Hib was the capsule (9, 255).

Emerging Pathogenicity of *Haemophilus influenzae*

Since the introduction of a vaccine against Hib, the incidence of invasive Hib disease has significantly been decreased. The reduced carriage of Hib strains also led to herd immunity with a benefit added to non-vaccinated subjects (256). In the early 2000's there was a re-emergence of invasive Hib disease, primarily in England (257). Apart from this slight divergence, vaccination campaigns have been very successful and invasive Hib disease is now rare (59). A few reports in the mid 1990's have suggested increasing incidences of invasive disease by non-Hib isolates of *H. influenzae*. Most of these reports suggest that increased incidence occurs among individuals with underlying medical conditions (61, 70, 258-260). Recent studies suggesting an increased concern about Hif invasive disease (64, 219) show antibiotic resistance, which resembles NTHi rather than Hib in epidemiology (261). There are at least two reports of invasive disease by *H. influenzae* type a (262, 263), suggesting a virulence capacity that mimics Hib. In contrast to Hib, the number of cases with invasive diseases caused by NTHi and type f (Hif) seems to increase suggesting the emerging pathogenicity of the non-Hib members of the species *Haemophilus* (60-62).

The Present Investigation

The overall aim of this thesis was to learn more about the virulence mechanisms of *H. influenzae*. Hence we studied three OMPs; protein E, *Haemophilus* surface fibril and protein H respectively from non-typeable *H. influenzae*, *H. influenzae* type b and *H. influenzae* type f. Molecular and structural details of those OMPs are essential to have depth knowledge about the mechanism of *H. influenzae* pathogenicity. Targeting these OMPs for developing vaccines or antibacterial drugs against *H. influenzae* is much rational and that was the reason we focused on structural and functional studies of *H. influenzae* OMPs.

Aims of the Study

1. To solve the crystal structure, study biophysical properties and visualize the pathogenic regions on the Protein E involved in NTHi virulence mechanism.
2. To define the characteristic of Protein E as a hemin binding and storage protein that assists *H. influenzae* in persistence in the host.
3. To determine the molecular mechanisms and study the structural attributes of the trimetric autotransporter protein *Haemophilus* surface fibrils from Hib that leads to serum resistance and adherence to respiratory epithelial cells.
4. To characterize the involvement of Protein H as a Vitronectin-binding protein on the surface of Hif, that results in increased serum resistance and optimal adherence to pulmonary epithelial cells.

Results and Discussion

Papers I & II: Crystal Structure, Elucidation of the Multiple Binding Sites for the Host Factors and Immunogenic Mapping of Protein E

Adhesins are the surface proteins of pathogens not only use for adherence to the host cells but also to induce a pro-inflammatory response in the host (264). *Haemophilus* spp. adhesins are multifunctional, in addition to their role in adherence; some of them are transporters or trans-membrane proteins or are secreted during infection of the host (265). Some of the *H. influenzae* surface adhesins have been suggested as vaccine candidates in the recent years as they exhibit significant protective roles in experimental models (266). In general, structural information on the targeted protein has been useful in vaccine or drug development providing deeper insights into the host–pathogen relationship. There are several surface proteins that have been identified as adhesins (267), but the structural information of those adhesins are very limited. A few *H. influenzae* adhesins structures have partially been solved such as Hsf (268), its homologues Hia (268), HMW-1 and HMW-2 (269). Previously, the detailed crystal structure of the *H. influenzae* Adhesin Protein (Hap) was revealed and was shown to be involved in bacterial aggregation (236).

Earlier, our lab identified and described the role of the *H. influenzae* Protein E (PE) in interacting with host epithelial cells and its involvement in subverting the host innate immune system (270-272). PE is a ubiquitous adhesin of *Haemophilus* spp. and homologues of it are present in other bacterial pathogens of the *Pasteurellaceae* family (201). PE is a highly conserved (96.9%–100%) outer membrane lipoprotein, 16 kDa in size. Primarily, PE was identified in NTHi and described as an adhesin that bound to epithelial cells (270). Later, extensive studies found that PE was expressed in both encapsulated and un-encapsulated *H. influenzae* (219, 273). Moreover, PE simultaneously binds to extracellular matrix protein Ln, Vn and plasminogen (PLG), interactions that all contribute to bacterial virulence (217, 274-276).

In paper I, the expression, purification and optimization of protein crystallization techniques to collect the x-ray diffraction data of PE are described. For crystallization, PE was expressed in *Escherichia coli* BL21 and purified without any Histidine tag. Initial optimization for crystallization of the PE yielded crystals of good diffracting quality. To solve the phase problem using Multiple Isothermal Replacement (MIR) or Multi-wavelength anomalous diffraction (MAD) methods using heavy-atom derivative crystals of PE proved to be unsuccessful. Since the natural protein does not contain methionine residues, to overcome the phasing problem, two methionine residues were introduced into the Protein E by point

mutation (277). The positions of the possible point mutations were carefully analyzed to find two sites for methionine substitution without any constraint on the PE molecule. Thus, a choice was made both on the mutational ability and the position of the residues in possible secondary-structure elements. The idea was to label the protein with selenomethionine (SeMet) during protein production. To incorporate SeMet in PE, *E. coli* BL21 containing a modified construct of PE were cultured and expressed in the presence of L-selenomethionine in the culture medium. The purification of the SeMet labeled protein proceeded as described previously for native protein (277). The phase problem was solved using SeMet-labeled PE (SeMet-PE) crystals.

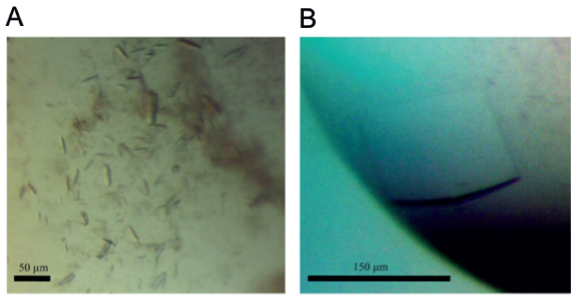

Figure 6: Photographs showing the native and SeMet-labeled PE crystals grown under different conditions. (A) Native PE (5 mg ml^{-1}) produced rod-shaped crystals of approximately 10×20×50 mm in size. (B) An SeMet-labeled PE crystal of 100×150×10 mm in size.

High-quality native PE crystals were produced at two different conditions; small rod-shaped crystals (Fig. 6A) and plate-like crystals, relatively larger in size compare to the rod-shaped crystals. Despite being smaller in size, the rod-shaped crystals that were approximately 10×20×50 mm in size (Fig. 6A) diffracted better then the plate shaped crystals. SeMet-PE crystals were produced under different conditions compared to the conditions when native PE crystals were produced. In the initial screening, the SeMet-PE was produced as microcrystals. The size of the crystals were improved reaching final dimensions of approximately 100×150×10 mm (Fig. 6B) using the microseeding technique. Finally, data were collected at 1.8Å resolution from native PE crystals and at 2.6Å resolution from SeMet-PE crystals.

In Paper II, the X-ray diffraction data collected at 1.8 Å resolution were used to obtain the structural model of the PE molecule. We studied structure-based selection of the exposed regions to verify their localizations and respective immunogenicities by producing antibodies in mice. The PE monomer consisted of a β-sheet formed by 6 antiparallel β-strands (Fig. 7A). In addition, a longer α-helix was found to be packed on the concave face of the sheet (Fig. 7B).

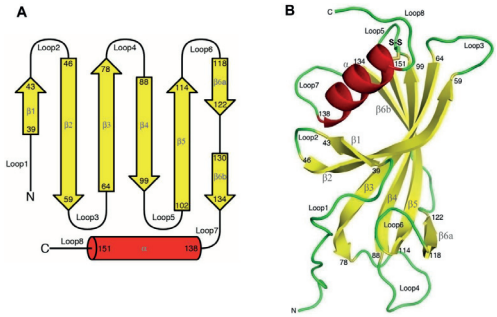

Figure 7: PE monomer and its secondary-structure elements. (A) PE 28 to 159 amino acids showing the secondary structure. In total, 6 β-strands, 8 loops, and 1 C-terminal helix exist. (B) In the monomer, 6 antiparallel β-strands form the β-sheet. A longer α-helix packs on the concave face of the sheet, where strands β1, β2, and β3 are curved around it.

PE was present as a dimer in the asymmetric unit explaining its multifunctional nature of interaction with several different host factors, including Vn, Ln, and PLG (201, 274, 275). During size exclusion purification of PE, the gel filtration profile showed that approximately 85% of recombinant PE molecules existed as dimers in solution and within the crystal structure, therefore the protein is present as a dimer (Fig. 8A).

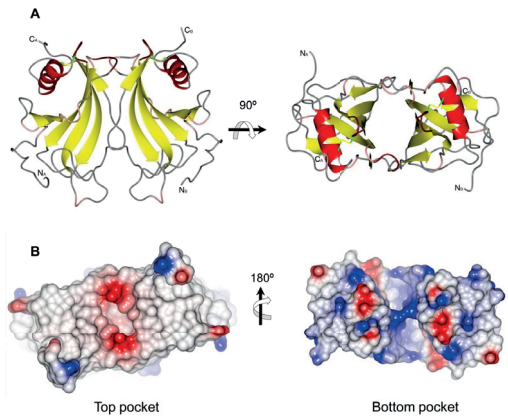

Figure 8: The PE dimer. (A) Cartoon representation of the PE dimer. (B) Surface of the PE dimer shown from the top and bottom cavities, in addition to the charge distribution of the molecule. The top surface of the molecule is neutral in charge, whereas the bottom side of the dimer is basic. The positive and negative charges are shown in blue and red, respectively.

Protein E is a lipoprotein (270) and on the basis of lipoprotein transport and lipidation mechanism (278, 279), the Cys16 residue on the N terminus of PE is thus predicted to be involved in anchoring of PE on the outer membrane in

bacteria. Thus, the N-terminus of the dimer faces toward the membrane side of the bacteria, whereas the C-terminus faces the outside. Additionally, presence of a well-formed pocket on the topside of the dimer (Fig. 8B), suggest the shape and accessibility of the pocket is very evocative of binding pockets in smaller ligand binding proteins. Consequently, a specific ligand-binding function for that pocket was analysed by bioinformatics tools, studied experimentally and was reported in the next paper.

Paper III: Nutrient Sharing: *Haemophilus influenzae* Stores and Distributes Hemin by Using Protein E

H. influenzae has an absolute requirement for hemin or heme. It is the source of iron and Protoporphyrin IX (PPIX) (280), an important precursor to essential prosthetic groups such as heme, cytochrome c, and chlorophylls (281, 282). *H. influenzae* lacks the enzymes in the synthetic pathway of the porhyrin ring and is therefore unable to synthesize PPIX, the immediate precursor of heme (153, 283, 284). Regardless, *H. influenzae* expresses fer-rochelatase, which mediates insertion of iron into PPIX to produce heme (153, 284). Free iron is relatively insoluble and toxic for living cells, so iron is present in complexes, bound to high-affinity iron-binding host proteins such as Transferrin, Lactoferrin, Ferritin, or incorporated into a protoporphyrin ring (285). Thus, *H. influenzae* utilizes hemin, hemoglobin, hemoglobin-haptoglobin, heme-hemopexin, as a source of PPIX and iron for growth (286). *H. influenzae* colonization and survival thus depends on the availability of heme in the host (287).

In paper III, we reported PE as an outer membrane hemin binding protein of NTHi and we showed that *H. influenzae* contains a PE-dependent resevoir of hemin, which resulted in a hemin supply to the *H. influenzae* population when there was a limitation of hemin in the environment.

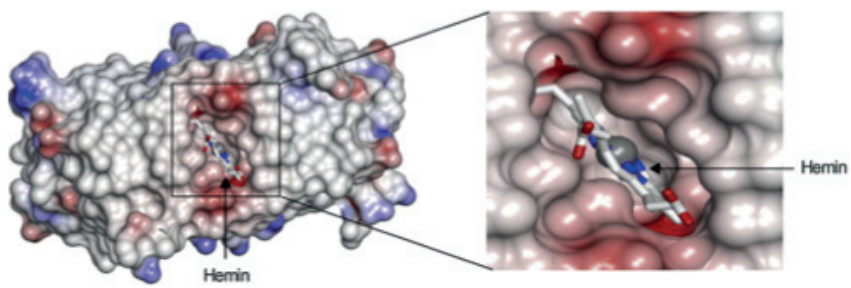

Figure 9: Putative docking of a hemin molecule in the binding pocket of the PE-dimer. Surface representation of the PE crystal structure with a hypothetical model of the PE-hemin complex. Insert: zoom in projection of a putative hemin-binding pocket in dimeric PE. Docking was performed manually using COOT (288-290). The figures were prepared with Pymol and CCP4MG.

When screening for specific ligands using the structural data of PE, it appeared as a dimer with a well-defined top pocket (201). The *in silico* modeling showed that the binding pocket can potentially accommodate a hemin molecule (Fig. 9).

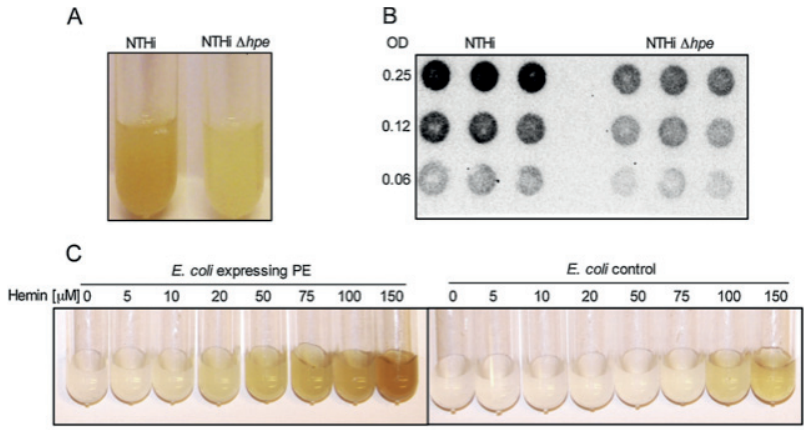

Figure 10: *Haemophilus influenzae* PE binds hemin at the bacterial surface. (A) Hemin binding to NTHi 3655 and NTHi 3655Δ*hpe*. Bacteria were grown overnight in BHI with hemin and NAD. After washing three times in PBS, 5 ml culture (OD=1.0) of each strain was suspended in 1 ml PBS. (B) Semi-quantitative measurement of PE-dependent hemin-binding on the surface of wild type NTHi 3655 as compared to the PE mutant NTHi3655Δhpe. Bacteria shown in panel A were serially diluted and spotted on a PVDF filter. Enhanced chemiluminescence (ECL) was used for detection of hemin on blots. (C) *E. coli* expressing PE with the surface bound hemin. *E. coli* expressing PE and control *E. coli* with an empty vector were incubated at room temperature with increasing concentrations of hemin. After 1h of incubation, bacteria were washed, resuspended in PBS and photographed.

To show that PE is a hemin binding outer membrane protein, we mutated the *hpe* gene encoding PE in NTHi 3655 strain and compared its hemin binding ability with the wild type NTHi 3655. We observed a difference in hemin binding between wild type NTHi 3655 and the PE mutant NTHi 3566Δ*hpe* as visually verified in test tubes (Fig. 10A). To compare hemin-binding difference in two strains (NTHi 3655 and NTHi 3566Δ*hpe*), bacteria from the cultures shown in Fig. 10A were also blotted on a nitrocellulose membrane and hemin was analyzed using enhanced chemiluminescence (ECL) (Fig. 10B). These visual observations indicated that NTHi3655 had acquired more hemin in comparison to the PE mutant NTHi 3655Δ*hpe*. Furthermore, to prove that PE binds hemin, recombinant PE was expressed at the surface of *E. coli* and incubated with different concentration of hemin. Similar to the results obtained with *H. influenzae* (Fig. 10A), addition of hemin to PE-expressing *E. coli* led to more hemin acquisition in comparison to a control *E. coli* carrying an empty vector (Fig. 10C). Additionally, growth analysis showed that PE plays a role as a reservoir for hemin that can be

used by the bacteria, and also shared with co-cultured hemin-starved bacteria (229).

Paper IV & V: Interactional Analysis with Human Vitronectin and Structure of the Trimeric Autotransporter *Haemophilus* Surface Fibrils (Hsf)

H. influenzae serotype b (Hib) has been the most virulent and well studied strain among all *H. influenzae* sub types. Successful colonization and subsequent infection by *Haemophilus* is dependent on bacterial adherence to host tissue achieved by the adhesins. Sometimes bacteria especially Hib, damage the epithelial barrier, by breaking and entering the basement membrane, penetrating deeper into tissue layers (50, 291, 292). Hib can cross the blood-brain barrier and cause meningitis (187). However, the invasive mechanisms of Hib are not yet fully elicited. Autotransporters are a specific group of proteins in Gram-negative pathogens, which are translocated to the cell surface by a type V secretion mechanism. Autotransporters are composed of an N-terminal signal peptide for secretion, followed by a passenger domain and a C-terminal translocator (membrane-anchoring) domain (293-296). These autotransporters are multifunctional proteins ranging from monomeric to multimeric arrangements (236). Recently, the biological role of few autotransporters of *H. influenzae* has been studied (297).

Hsf is a trimeric autotransporter adhesin of Hib and is a highly conserved protein among all typeable strains, with a monomeric size of approximately 243 kDa that forms into a trimer of approximately 750 kDa (268, 298). An Hsf homologue, Hia found in NTHi (299) and is present only in approximately 25% of clinical NTHi isolates. Hsf is comprised of various repetitive domains, which are also relatively similar in their secondary structures (297). Hsf acquires Vn on bacterial surface, and this phenomenon is very important for Hib survival in the host against formation of a lytic pore via the membrane attack complex (MAC) (216, 300).

In Paper IV, we defined the specific region of Vn involved in interaction with Hsf. We demonstrated that the Hsf-Vn interaction inhibited the assembly of the MAC on the bacterial surface, which protected *H. influenzae* from serum-mediated killing and increased the adherence and internalization of bacteria into the host cells. Most of the clinical Hib isolates had the capacity to acquire Vn. When the *hsf* gene encoding Hsf was deleted in RM804Δ*hsf*, Vn binding was significantly reduced when compared with the wild type. Analyzing Hsf with different recombinantly expressed Vn fragments (encompassing heparin-binding domain 3; HBD3) ($Vn\Delta^{352–362}$, $Vn\Delta^{362–374}$ and $Vn\Delta^{352–374}$) proved that Hsf bound to the amino acids 352 to 374 on C-terminal region of Vn. Serum resistance and adhesion to

epithelial cells were compared in Hib RM804 WT, RM804Δ*hsf*, *E. coli* WT and *E. coli* expressing Hsf. In both cases, Vn acquisition through Hsf was shown to be involved with increased serum resistance and better adherence to the epithelial cells.

In Paper V, we described the architecture of Hsf. We found that the N-terminal of Hsf is located near the C-terminal at the base of the fibril that resulted in a way that Hsf is not a straight molecule but is folded and doubled over (265).

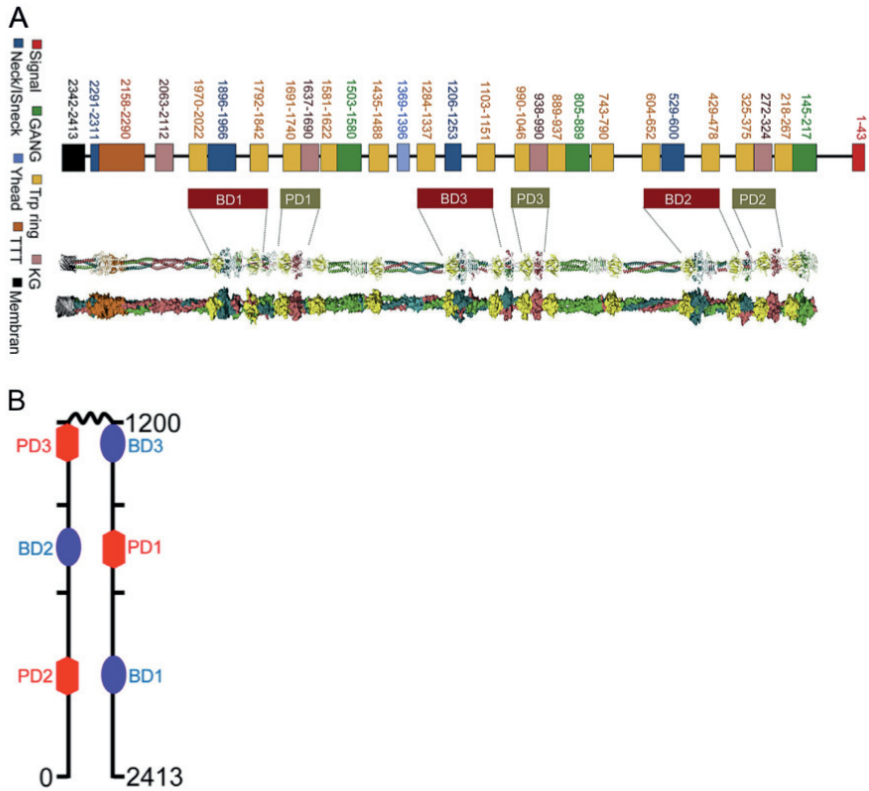

Figure 11: *In silico* modelling of the full length Hsf molecule. (A) The domain annotation of trimeric autotransporter adhesins (daTAA) server at Max Planck Institute for Developmental Biology, Tübingen, Germany (http://toolkit.tuebingen.mpg.de/dataa/search) was used to predict the repetitive motifs in the Hsf molecule. Domains are indicated according to their amino acid numbers, and the BD and PD are named according to the previously described nomenclature (268). (B) Representation of the architecture of double folded Hfs molecule. The distance of the small and large gold particles in several fibrils was measured and their relative frequency was plotted against the length of the fibril. The positions of sequences detected by antibodies (Abs) were delineated by illustration.

Hsf is large protein with 2413 amino acids, and has a repetitive domain structure (268) (Fig .11A).

Autotransporters are difficult to crystallize and being unsuccessful in crystalizing the Hsf, we modeled this protein by using an *in silico* approach. A computer model suggested that Hsf is a protein of approximate length 200 nm but the length observed by electron microscopy was only 100 nm. Size discrepancy of the Hsf found in our observations triggered us to analyze the structure of it. We directly examined the organization of Hsf on the bacterial surface by denaturing it using guanidinium chloride (GuHCl). Additionally, a set of specific anti-Hsf peptide antibodies was included in the analyses to locate the precise regions of the protein. In our analyses, we found that Hsf is not a straight fiber but rather consists of a "hairpin-like" twisted molecule (Fig.11B).

Three binding domains on the Hsf molecules named BD2 (529-652 aa), BD3 (1206−1337 aa) and BD1 (1896−2022 aa) were characterized on the basis of interactions with Chang conjunctival epithelial cells (268) (Fig. 11A). Each of the binding domains consist of an N-terminal Neck domain and a C-terminal Trp-ring domain "N-Neck: Trp ring-C" (Fig. 11A). The motifs' arrangements showed that within the N-terminus of the BDs, an additional Trp ring domain is present and assembled in an "N-Trp ring: Neck: Trp ring-C" triplet arrangement (Fig. 11A). Other structural Hsf motifs that are organized in a distinctive series without any known biological function were named as putative domains (PD) (55). There are three PDs on the Hsf, PD2 (272−375 aa), PD3 (938−1046 aa), and PD1 (1637−1740 aa), having 54.1–74.5% identity and 65.8–80.2% sequence similarity. Following the previous nomenclature, we named the adjacent PDs with a similar numbering (Fig. 11A), and the binding domain numbering of Hsf was assigned on the basis of the homology with Hia (268). We designatd the adjacent PDs with a similar numbering (Fig. 11A) and the PDs consist of a KG domain followed by a Trp-ring domain (N-KG: Trp ring-C). A KG domain is also present between amino acids 2063–2112 (Fig. 11A), which has a more variable sequence than the other 3 KG domains. Taken together, we demonstrated that Hsf is not straight but is folded and doubled over, and it is the first report providing the unique structural features of the Hsf (301).

Paper VI: *Haemophilus influenzae* Type f Acquires Vitronectin through Protein H to Evade Host Innate Immunity and Adhere to Pulmonary Epithelial Cells

In addition to NTHi, Hif has also been reported as an emerging pathogen causing invasive disease in humans (55, 60-62, 302). In Paper VI, we studied the outer membrane protein H as a human Vn-binding protein for Hif, and the roles of PH-

Vn interaction in Hif virulence. Previously, PH was identified and characterized as a human FH-binding protein, found in *H. influenzae* serotype b and f (303). This PH-Vn interaction has important role in Hif pathogenesis by increasing serum resistance and adhesion to alveolar epithelial cells.

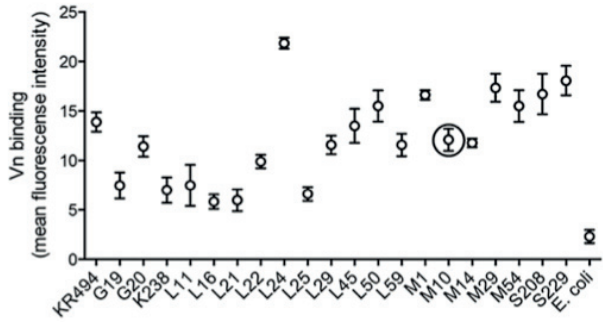

Figure 12: All *H. influenzae* serotype f clinical isolates show significant Vn binding at its surface. Vn-binding to clinical isolates of Hif was analyzed by flow cytometry. Equal numbers of bacteria of each isolate were incubated with 250 nM of Vn, and bound ligand was detected with sheep anti-Vn pAb and FITC-conjugated donkey anti-sheep pAb. Data are presented as the mean fluorescence intensity (mfi) after subtracting the background. *E. coli* was used as a negative control. Circled data indicates mfi of the strain Hif M10 used for the detailed study.

In light of the emergence of Hif invasive disease, we examined Hif blood and cerebrospinal fluid isolates (n=21) (180) for Vn binding in flow cytometry (Fig. 12). All clinical strains significantly bound Vn as compared with the negative control *E. coli*. Acquiring Vn is one of the many strategies in pathogenic bacteria to evade anti-bacterial activity of the human complement system, facilitating colonization and subsequent infection (147, 215, 276, 304, 305). Vn is an effective complement regulator that inhibits the terminal lytic pathway (Fig. 5) regardless of which complement pathway that is activated (147) (Fig. 5). Vn inhibits MAC assembly by blocking the membrane-binding site of the C5b–C7 complex and prevents polymerization of C9 (147, 217). In parallel to ELISA with recombinant PH and Vn that showed Vn binding ability of PH, we also tested the interaction on the bacterial surface. We deleted the PH encoding gene *lph* in Hif M10 strain, the resulting Hif M10Δ*lph* mutant bound significantly less Vn in comparison with the wild type, as revealed by flow cytometry experiments. We further analysed Vn binding-specificity of PH using recombinantly expressed PH at the surface of the heterologous host *E. coli*. This experimental system made it possible to evaluate the specificity of PH by excluding other surface proteins interfering with Vn. By implementing three different truncated fragments of Vn molecules encompassing deletions in Heparin Binding Domain-3 (HBD3) ($VnΔ^{352–362}$, $VnΔ^{362–374}$, and $VnΔ^{352–37}$), we further pinpointed the binding site for PH on the Vn molecule. Our

analyses confirmed that PH bound Vn at the amino acid sequence 352–362 within HBD3 at the C-terminal domain of Vn. We compared the Vn-binding affinity of PH with the well-defined Vn-binding NTHi outer membrane PE (201, 217). Our 1:1 protein-protein binding affinity (kD) calculation by Biolayer interferometry showed that PH interacted with Vn as efficiently as PE. The kD of 2.2 μM for the PH–Vn interaction was calculated and found to be similar to the kD for PE (0.4 μM) despite different methods being used (274). We also showed that the PH-Vn interaction resulted in an increased Hif adherence to epithelial cells. Hif binds to the C-terminal HBD3 domain via PH, leaving the N-terminal integrins bound to the RGD motif available on Vn. The binding of integrins to the RGD motifs on Vn is evolutionarily conserved (306, 307). Therefore bacterial binding to integrins, especially to alpha-v beta-3 (avb3) integrin on the host cells, is facilitated. Hence, a cross-link between bacteria and epithelial cells can occur using Vn as a bridging molecule to epithelial integrins (147, 308, 309). This study explores how the Hif utilizes the host protein Vn for evasion of the innate immunity, and invasion of the host. Further studies are required to fully understand the virulence factors related to Hif, to explain why there is an increased incidence of invasive Hif disease in the human population.

Concluding Remarks

This thesis was focused on outer membrane proteins (OMPs) from *Haemophilus influenzae* that represent important Gram-negative respiratory tract pathogens. Results of this study shed light on the structures, and functional role of *H. influenzae* OMPs protein E, *Haemophilus* surface fibril, and protein H.

We successfully determined the crystal structure of PE, which, together with other studies, allowed us to dissect the involvement of PE in the virulence mechanism of *H. influenzae*. Additionally, we elucidated that PE acquires hemin (an iron containing porphyrin) on the bacterial surface, acting as a reservoir of hemin that allows *H. influenzae* to survive in the scarcity of heme in the host.

Our data revealed the architecture of Hsf. Characterization of Vn and Hsf interactions, and immunological analyses, demonstrated how Hsf recruits the host factor Vn on bacterial surface, and thereby inhibiting the host innate immune response.

Finally, this study demonstrated that PH recognized the C-terminal part of Vn. PH-dependent Vn-acquisition increased bacterial survival during complement-mediated killing and also adhesion to the airways.

Collectively, this thesis on OMPs contributes to a deeper understanding of host-pathogen interactions and their significance during host infections.

Future Perspectives

Bacterial outer membrane proteins (OMPs) are targets of research to understand bacterial pathogenicity. These are the proteins use by the bacteria to adhere, settle, colonize and later invade the host. Molecular and structural details of such OMPs are essential to obtain an in depth understanding of the mechanism of host-bacterium interactions and *H. influenzae* pathogenicity. This knowledge can also be exploited for the development of novel vaccines or drugs against *H. influenzae* targeting these OMPs.

We solved the three dimensional structure of PE and it would be very interesting to crystallize PE in complex with any of the well-studied host factors Vn, Ln or PLG, and solve the crystal structure of the complex. This would help us to understand host pathogen interactions at an atomic level. The knowledge of a visual observation of the interaction will be helpful to manipulate the behavior of the pathogenic bacteria towards host. Moreover, PE has been found conserved in all types of *H. influenzae*, so this property makes it an excellent vaccine candidate against *H. influenzae*.

We reported that Hsf interaction with Vn inhibited assembly of the membrane attack complex (MAC) protecting *H. influenzae*, and also increased the adherence and internalization of bacteria into host cells. It would be interesting to search for other ligands from the host factors and elicit the functions and importance of those ligands binding properties of Hsf.

Using an *in silico* technique, we described the architecture of the protein Hsf, but what would be really striking is to see the Hsf in real-time using innovative methods such as crystallography, small-angle X-ray scattering (SAXS) or possibly using cryo-electron microscopy (cryo-EM). It is always advantageous to have structural data of the protein molecule, because structural detail of the molecule may be used to design specific inhibitors.

We demonstrated that PH-Vn synergy is important for Hif pathogenesis by increasing serum resistance and adhesion to the epithelial cells. At the present time, along with NTHi, Hif is one of the *H. influenzae* types showing potentiality to be a pathogen like Hib. Therefore, it is important to focus on Hif in order to develop novel therapeutic measurements. PH has been found to be a multifunctional protein, interacting with Vn, FH and recently we have found that, PH also interacts with other host proteins (unpublished data). We have generated

some data on the interactions of PH and other host factors. It would be intriguing to do further studies on bacteria and host interaction exploring PH functional and immunological importance in Hif virulence. It would also be a useful contribution to solve the three-dimensional crystal structure of PH. Detailed 3D images of the PH structure in complex with FH, Vn or any other host factors would also be worthwhile to understand part of the overall host pathogen interaction.

Acknowledgements

I would like to first thank my honorable supervisor **Professor Kristian Riesbeck** for his excellent guidance and support during my PhD studies. I started my master project at the **Department of Biochemistry and Structural Biology** at the Chemical Center, Lund. My Masters project was to crystallize and solve the three-dimensional structure of PE from *H. influenzae*. PE was discovered in your lab in Malmö, so to purify the protein I came to your lab and was introduced with you. During my MSc study, I used to work in a Pizza restaurant in Malmö to earn my living expenses. Dear Kristian, you provided me with a scholarship, so that I did not need to work in restaurant and rather concentrated on crystallizing the protein. I did that and then, you brought me the best opportunity of purusing my PhD study in your lab. It was a great journey of learning with you! You not only supported me in the lab with your knowledgeable mind, never-give-up attitude and generosity, you also supported me in other difficulties of my life as well. Thank you for keeping your faith on me!

I am very much grateful to **Assistant Professor Marjolein M G M Thunnissen** for giving me the opportunity to pursue by MSc project under your supervision, and your collaboration gave the chance to learn the beauty of the protein crystallography, I am thankful to **Associate Professor Susanna Törnroth Horsefield** and the people of the Department of Biochemistry and Structural Biology, Lund, for cordial collaboration with me and our group regarding protein structural research.

Doctor Birendra Singh, you are the person who welcomed me in the Riesbeck Lab at the very first moment and introduced me with Professor Kristian Riesbeck, and with that I got the chance to enter into the research world of scientific professionals. I have learnt almost all the techniques needed in my research from you. You are the best Finisher of the research projects. Your scientific mind in combination with your technical skill specially your **"Jogar Technology"** is one of the precious in the world. You are an excellent supervisor and very good friend. I am so much grateful to you that I do not have enough words to express it.

Marta Brant, you are like the **"God Father"** in our lab, you have the solution for every technical difficulty one can face with instruments and research methods. Your magical fingers can fix any broken equipment. Thanks for everything that you did for me and for all of us in the lab.

Doctor Yu Ching Su, my **"Lab Mother"** you teach me the experimental protocols, how very tiny thing in the procedure that could affect the research results, how any methodological problem can be solved in a scientific way. You helped me in my writing especially how to avoid critical comments from the reviewers. I am grateful to you for everything you did for me.

Doctor Farshid Jalalvand, former PhD student in the lab, I was fortunate to have you as my colleague, you helped me in every stage of my PhD study providing direct support with the academic materials and logistics. I have several points to thank you for, but my foremost gratitude to you for reading my PhD thesis. Through out my study you helped me with filling out all application forms those were in Swedish. Thanks for all the helps I am having from you, we will be in close contact!

Doctor Magnus Paulsson, you are a great colleague in the lab with a very curious mind and an excellent friend who is helping me a lot to adapt properly in the Swedish society. You are a true gentleman with a kind heart.

Doctor Ben Duell, you are a true gentlemen from Australia, excellent friend and colleague, your help in my PhD thesis proof reading is invaluable, thanks for reading my thesis and giving it a good shape. Tamim is very grateful to you!

To my former colleagues, **Doctor Christophe Fleury** and **Doctor Viveka Schaar**, thank you for keeping me in touch and continuing to help me out even though you left the lab quite long ago.

Sharon Oosterhuis, Thanks for your great contribution in the project that we published in the *Journal of Immunology*.

Emma Mattsson, you are an excellent colleague to share an office room with; your well-written lab-maintaining instructions were very helpful for all of us. **Kerstin Norrman**, a lady with very wise hand and experienced tips in flow cytometry experiments, your advices was very useful for me, I am very much grateful for that!

My most heartfelt thanks to all past and present colleagues at the division of **Medical Microbiology** that put up with me and made up the lab with a dynamic, funny and workable environment. In no particular order: **Dr. Fredrik Resman, Dr. Therese Nordström, Gisela, Klaudyna, Dr. Oindrilla Mukherjee, Dr. Tamara Ringwood, Dr. Corinna Richter, Dr. Viktor Månsson, Vera Alvardo, Selma Ramic, Mohammed Rizwan, Gladys Sergeon, Dr. Petra Halang, Dr. Florence Deknuydt, Dr. Nils Littorin, Dr. Alfonso Felipe-Lopez,** and anyone else that might have slipped my mind.

My warmest thanks to **Nasida, Anki** and **Margareta** at the substrate department. You ladies are integral part of our research group. Thanks you for going out of your way to help me.

To, past and present teachers, my teachers at the **Khulna University** back home country in Bangladesh.

Late Professor Cecilia Hägerhäll, the former coordinator of the master program "protein Science" at the Lund University, you helped me in different way providing information, sending official documents to come to Sweden from Bangladesh.

My gratefulness to my master program-mates and Lund University fellows, **Professor Lo Gorton, Rolf Eric Anithason, Subrata Paul, Shubhranshu Debnath**, **Dr. John Pettersson, Henry Ampah-Korsah, Dr. Kamrul Hasan, Badrul Arefin Russel, Ahibur Rahaman, Kazi Ashraful Alam, Mrinmoy Debnath, Mohammad Alif Arman, Saleh Khalil, Rumana Sharmin Labony, Zubaida Gulshan Ara, Martuza Sarwar Shawon, Mukul Hossain, Ahsan Uddin, Dr. Gazi Mohiuddin, Dr. Mahmudul Hasan,** my dearest "Vabigon", **Rupa Vabi, Mithun Vabi, Laila Vabi, Tania Vabi, Sumpi Vabi, Miftahul Vabi, Situ vabi, Shetu vabi,** Bangladeshi friends and very well-wishers in Lund and Malmö, **Azad vai, Shafi Vai, Arafat vai, Murad, Harun** and to all who made my foreign life livable and colorful here in Sweden.

Thanks to the Funding bodies that support my research work **Kungliga Fysiografen, Alfred Ö sterlund Foundation, the Anna and Edwin Berger Foundation, the Greta and Johan Kock Foundation**, **the Swedish**

Medical Research Counci and **Medical Faculty** of Lund University

My gratitude to my grand father **Hazi Sadat Ali**, grand mother **Elema Khatun**.

My acknowledgment to my siblings **Popy** (elder sister, boro Apu), **Topy** (elder sister, Meju Apu), **Happy** (elder sister, Choto Apu) and **Rony** (younger brother); Bothers in Law **Topu Vai, Tomal Vai** and **Tanim;** Sister in Law **Shathy** and **Bithy**, Father in Law **Nur Ahmed khakon** and Mother in Law **Fatema Akther** whithout your support it was not possible to reach here where I am now. Md. Tamim Al-Jubair is very thankful to you all people.

References

1. **Balch WE, Magrum LJ, Fox GE, Wolfe RS, & Woese CR** (1977) An ancient divergence among the bacteria. Journal of Molecular Evolution 9 (4): 305-311.
2. **Woese CR** (1977) Endosymbionts and mitochondrial origins. Journal of Molecular Evolution 10 (2): 93-96.
3. **Woese CR, Kandler O, & Wheelis ML** (1990) Towards a natural system of organisms: proposal for the domains Archaea, Bacteria, and Eucarya. Proceedings of the National Academy of Sciences of the United States of America 87 (12): 4576-4579.
4. **Fredrickson JK, *et al.*** (2004) Geomicrobiology of high-level nuclear waste-contaminated vadose sediments at the hanford site, washington state. Applied and Environmental Microbiology 70 (7): 4230-4241.
5. **Whitman WB, Coleman DC, & Wiebe WJ** (1998) Prokaryotes: the unseen majority. Proceedings of the National Academy of Sciences of the United States of America 95 (12): 6578-6583.
6. **Cabral JP** (2010) Water microbiology. Bacterial pathogens and water. International Journal of Environmental Research and Public Health 7 (10): 3657-3703.
7. **Morley NJ** (2016) Symbiotic bacteria of helminths: what role may they play in ecosystems under anthropogenic stress? Journal of Helminthology 12: 1-11.
8. **Sears CL** (2005) A dynamic partnership: celebrating our gut flora. Anaerobe 11 (5): 247-251.
9. **Jalalvand F & Riesbeck K** (2014) *Haemophilus influenzae*: recent advances in the understanding of molecular pathogenesis and polymicrobial infections. Current Opinion in Infectious Diseases 27 (3): 268-274.
10. **Stecher B & Hardt WD** (2008) The role of microbiota in infectious disease. Trends in Microbiology 16 (3): 107-114.
11. **Pedron T & Sansonetti P** (2008) Commensals, bacterial pathogens and intestinal inflammation: an intriguing menage a trois. Cell Host & Microbe 3 (6): 344-347.
12. **McFarland LV** (2000) Beneficial microbes: health or hazard? European Journal of Gastroenterology & Hepatology 12 (10): 1069-1071.
13. **Rodriguez JM, *et al.*** (2015) The composition of the gut microbiota throughout life, with an emphasis on early life. Microbial Ecology in Health and Disease 26: 26050.
14. **Neu J & Rushing J** (2011) Cesarean versus vaginal delivery: long-term infant outcomes and the hygiene hypothesis. Clinics in Perinatology 38 (2): 321-331.
15. **Bourlioux P, Koletzko B, Guarner F, & Braesco V** (2003) The intestine and its microflora are partners for the protection of the host: report on the Danone

Symposium "The Intelligent Intestine," held in Paris, June 14, 2002. The American Journal of Clinical Nutrition 78 (4): 675-683.

16. **Guarner F & Malagelada JR** (2003) Gut flora in health and disease. Lancet 361 (9356): 512-519.
17. **Tlaskalova-Hogenova H, *et al.*** (2004) Commensal bacteria (normal microflora), mucosal immunity and chronic inflammatory and autoimmune diseases. Immunology Letters 93 (2-3): 97-108.
18. **Marples MJ** (1969) Life on the human skin. Scientific American 220 (1): 108-115.
19. **Marples MJ** (1969) The normal flora of the human skin. The British Journal of Dermatology 81: Suppl 1:2-13.
20. **Grice EA, *et al.*** (2009) Topographical and temporal diversity of the human skin microbiome. Science 324 (5931): 1190-1192.
21. **Macdonald TT & Monteleone G** (2005) Immunity, inflammation, and allergy in the gut. Science 307 (5717): 1920-1925.
22. **Berg RD** (1996) The indigenous gastrointestinal microflora. Trends in Microbiology 4 (11): 430-435.
23. **Hooper LV, Midtvedt T, & Gordon JI** (2002) How host-microbial interactions shape the nutrient environment of the mammalian intestine. Annual Review of Nutrition 22:283-307.
24. **Zasloff M** (2007) Antimicrobial peptides, innate immunity, and the normally sterile urinary tract. Journal of the American Society of Nephrology 18 (11): 2810-2816.
25. **Davis CP** (1996) Normal Flora. Medical Microbiology, ed Baron S Galveston (TX), 4th Ed.
26. **Redondo-Lopez V, Cook RL, & Sobel JD** (1990) Emerging role of *lactobacilli* in the control and maintenance of the vaginal bacterial microflora. Reviews of Infectious Diseases 12 (5): 856-872.
27. **Redondo-Lopez V, Lynch M, Schmitt C, Cook R, & Sobel JD** (1990) Torulopsis glabrata vaginitis: clinical aspects and susceptibility to antifungal agents. Obstetrics and Gynecology 76 (4): 651-655.
28. **Redondo-Lopez V, *et al.*** (1990) Vulvovaginal candidiasis complicating recurrent bacterial vaginosis. Sexually Transmitted Diseases 17 (1): 51-53.
29. **Beringer PM & Appleman MD** (2000) Unusual respiratory bacterial flora in cystic fibrosis: microbiologic and clinical features. Current Opinion in Pulmonary Medicine 6 (6): 545-550.
30. **Schwartz B, *et al.*** (1994) Respiratory infections in day care. Pediatrics 94: 1018-1020.
31. **Fang GD, *et al.*** (1990) Community-acquired pneumonia caused by *Legionella dumoffii* in a patient with hairy cell leukemia. Infection 18 (6): 383-385.
32. **Fine MJ, *et al.*** (1990) Prognosis of patients hospitalized with community-acquired pneumonia. The American Journal of Medicine 88 (5N): 1N-8N.
33. **Beringer PM, Vinks AA, Jelliffe RW, & Shapiro BJ** (2000) Pharmacokinetics of tobramycin in adults with cystic fibrosis: implications for once-daily administration. Antimicrobial Agents and Chemotherapy 44 (4): 809-813.

34. **Albu S & Florian IS** (2013) Bacteriology of normal frontal sinuses. American Journal of Otolaryngology 34 (4): 327-330.

35. **Robinson J** (2004) Colonization and infection of the respiratory tract: What do we know? Paediatrics & Child Health 9 (1): 21-24.

36. **Varon E, *et al.*** (2000) Impact of antimicrobial therapy on nasopharyngeal carriage of *Streptococcus pneumoniae*, *Haemophilus influenzae*, and *Branhamella catarrhalis* in children with respiratory tract infections. Clinical Infectious Diseases 31(2): 477-481.

37. **Munier AL, *et al.*** (2013) Invasive pneumococcal disease in HIV-infected adults in France from 2000 to 2011: antimicrobial susceptibility and implication of serotypes for vaccination. Infection 41 (3): 663-668.

38. **Taubenberger JK, Hultin JV, & Morens DM** (2007) Discovery and characterization of the 1918 pandemic influenza virus in historical context. Antiviral Therapy 12(4 Pt B): 5 81-591.

39. **Pfeiffer R** (1892) I.-Preliminary communication on the exciting causes of influenza. British Medical Journal 1 (1620): 128.

40. **Pfeiffer R** (1893) Die aetiologie der influenza [The aetiology of influenza]. Zeitschrift Für Hygiene und Infektionskrankheiten; Medizinische Mikrobiologie,. Immunologie und Virologie (1893;13) : 357–385.

41. **Morens DM & Fauci AS** (2007) The 1918 influenza pandemic: insights for the 21st century. The Journal of Infectious Diseases 195 (7): 1018-1028.

42. **Winslow CE, *et al.*** (1920) The families and genera of the bacteria: Final report of the Committee of the Society of American Bacteriologists on Characterization and classification of bacterial types. Journal of Bacteriology 5 (3): 191-229.

43. **Olitsky PK & Gates FL** (1921) Experimental studies of the nasopharyngeal secretions from influenza patients: Iii. Studies of the concurrent infections. The Journal of Experimental Medicine 33 (3): 373-383.

44. **Taubenberger JK & Morens DM** (2006) 1918 Influenza: the mother of all pandemics. Emerging Infectious Diseases 12 (1): 15-22.

45. **Pfeiffer RK, W.** (1896) Ueber die specifische Immunitätsreaction der Typhusbacillen [On the specific immune reaction to the typhus bacillus]. Zeitschrift für Hygiene und Infektionskrankheiten 21: 203–246.

46. **Smith W, Andrewes CH, & Laidlaw PP,** (1933) A Virus Obtain from Influenza Patient. Lancent.

47. **Pittman M** (1931) Variation and Type Specificity in the Bacterial Species *Hemophilus influenzae*. The Journal of Experimental Medicine 53 (4): 471-492.

48. **Dousse F, *et al.*** (2008) Routine phenotypic identification of bacterial species of the family Pasteurellaceae isolated from animals. Journal of Veterinary Diagnostic Investigation 20 (6): 716-724.

49. **Long SS, Henretig FM, Teter MJ, & McGowan KL** (1983) Nasopharyngeal flora and acute otitis media. Infection and Immunity 41 (3): 987-991.

50. **Agrawal A & Murphy TF** (2011) *Haemophilus influenzae* infections in the *H. influenzae* type b conjugate vaccine era. Journal of Clinical Microbiology 49 (11): 3728-3732.
51. **Murphy TF, *et al.*** (2007) *Haemophilus haemolyticus*: a human respiratory tract commensal to be distinguished from *Haemophilus influenzae*. The Journal of Infectious Diseases 195 (1): 81-89.
52. **Marti S, *et al.*** (2015) Identification of *Haemophilus haemolyticus* in clinical samples and characterization of their mechanisms of antimicrobial resistance. The Journal of Antimicrobial Chemotherapy.
53. **McCrea KW, *et al.*** (2008) Relationships of nontypeable *Haemophilus influenzae* strains to hemolytic and nonhemolytic *Haemophilus haemolyticus* strains. Journal of Clinical Microbiology 46 (2): 406-416.
54. **Kirkman JB, Jr. & Crawford JJ** (1971) Serotyping of noncapsular *Haemophilus influenzae*. Applied Microbiology 22 (1): 133-134.
55. **Kutsuna S, *et al.*** (2015) [Analysis of Non-serotype b Encapsulated *Haemophilus influenzae* Isolated from Pediatric Patients]. Kansenshogaku Zasshi. The Journal of the Japanese Association for Infectious Diseases 89 (2): 237-243.
56. **Tudor-Williams G, *et al.*** (1989) *Haemophilus influenzae* type b disease in the Oxford region. Archives of Disease in Childhood 64 (4): 517-519.
57. **Murphy TF & Sethi S** (1992) Bacterial infection in chronic obstructive pulmonary disease. The American Review of Respiratory Disease 146 (4): 1067-1083.
58. **MacNeil JR, *et al.*** (2011) Current epidemiology and trends in invasive *Haemophilus influenzae* disease--United States, 1989-2008. Clinical infectious diseases: an official publication of the Infectious Diseases Society of America 53 (12): 1230-1236.
59. **Peltola H** (2000) Worldwide *Haemophilus influenzae* type b disease at the beginning of the 21st century: global analysis of the disease burden 25 years after the use of the polysaccharide vaccine and a decade after the advent of conjugates. Clinical Microbiology Reviews 13 (2): 302-317.
60. **Hoshino T, *et al.*** (2015) Analysis of *Haemophilus influenzae* serotype f isolated from three Japanese children with invasive *H. influenzae* infection. Journal of Medical Microbiology 64 (Pt 4): 355-358.
61. **Ladhani SN, *et al.*** (2012) Invasive *Haemophilus influenzae* serotype e and f disease, England and Wales. Emerging Infectious Diseases 18 (5): 725-732.
62. **Resman F, *et al.*** (2011) Necrotizing myositis and septic shock caused by *Haemophilus influenzae* type f in a previously healthy man diagnosed with an IgG3 and a mannose-binding lectin deficiency. Scandinavian Journal of Infectious Diseases 43 (11-12): 972-976.
63. **Meats E, *et al.*** (2003) Characterization of encapsulated and noncapsulated *Haemophilus influenzae* and determination of phylogenetic relationships by multilocus sequence typing. Journal of Clinical Microbiology 41 (4): 1623-1636.
64. **Urwin G, Krohn JA, Deaver-Robinson K, Wenger JD, & Farley MM** (1996) Invasive disease due to *Haemophilus influenzae* serotype f: clinical and epidemiologic characteristics in the *H. influenzae* serotype b vaccine era. The

Haemophilus influenzae Study Group. Clinical Infectious Diseases 22 (6): 1069-1076.

65. **St Geme JW, 3rd, Takala A, Esko E, & Falkow S** (1994) Evidence for capsule gene sequences among pharyngeal isolates of nontypeable *Haemophilus influenzae*. The Journal of Infectious Diseases 169 (2): 337-342.
66. **Musser JM, Barenkamp SJ, Granoff DM, & Selander RK** (1986) Genetic relationships of serologically nontypable and serotype b strains of *Haemophilus influenzae*. Infection and Immunity 52 (1): 183-191.
67. **Porras O, *et al.*** (1986) Difference in structure between type b and nontypable *Haemophilus influenzae* populations. Infection and Immunity 53 (1): 79-89.
68. **Ren D, *et al.*** (2012) Characterization of extended co-culture of non-typeable *Haemophilus influenzae* with primary human respiratory tissues. Experimental Biology and Medicine 237 (5): 540-547.
69. **Howard AJ, Dunkin KT, & Millar GW** (1988) Nasopharyngeal carriage and antibiotic resistance of *Haemophilus influenzae* in healthy children. Epidemiology and Infection 100 (2): 193-203.
70. **Heath PT, *et al.*** (2001) Non-type b *Haemophilus influenzae* disease: clinical and epidemiologic characteristics in the *Haemophilus influenzae* type b vaccine era. The Pediatric Infectious Disease Journal 20 (3): 300-305.
71. **Sarangi J, *et al.*** (2000) Invasive *Haemophilus influenzae* disease in adults. Epidemiology and Infection 124 (3): 441-447.
72. **Kilian M** (1976) A taxonomic study of the genus *Haemophilus*, with the proposal of a new species. Journal of General Microbiology 93 (1): 9-62.
73. **Back AE & Oberhofer TR** (1978) Use of the Minitek system for biotyping *Haemophilus* species. Journal of Clinical Microbiology 7 (3): 312-313.
74. **Kawakami Y, Okimura Y, & Kanai M** (1981) Biochemical characterization of *Haemophilus* species with the minitek differentiation system. Journal of Clinical Microbiology 14 (5): 579-581.
75. **Norskov-Lauritsen N, Overballe MD, & Kilian M** (2009) Delineation of the species *Haemophilus influenzae* by phenotype, multilocus sequence phylogeny, and detection of marker genes. Journal of Bacteriology 191 (3): 822-831.
76. **Musser JM, Kroll JS, Moxon ER, & Selander RK** (1988) Evolutionary genetics of the encapsulated strains of *Haemophilus influenzae*. Proceedings of the National Academy of Sciences of the United States of America 85 (20): 7758-7762.
77. **Musser JM, Kroll JS, Moxon ER, & Selander RK** (1988) Clonal population structure of encapsulated *Haemophilus influenzae*. Infection and Immunity 56 (8): 1837-1845.
78. **Floch MH** (2011) Intestinal microecology in health and wellness. Journal of Clinical Gastroenterology 45 Suppl: S108-110.
79. **Koboziev I, Reinoso Webb C, Furr KL, & Grisham MB** (2014) Role of the enteric microbiota in intestinal homeostasis and inflammation. Free Radical Biology & Medicine 68: 122-133.

80. **Venkatesh M, *et al.*** (2014) Symbiotic bacterial metabolites regulate gastrointestinal barrier function via the xenobiotic sensor PXR and Toll-like receptor 4. Immunity 41 (2): 296-310.

81. **Serban DE** (2011) The gut microbiota in the metagenomics era: sometimes a friend, sometimes a foe. Roumanian Archives of Microbiology and Immunology 70 (3): 134-140.

82. **Festi D, *et al.*** (2011) Gut microbiota and its pathophysiology in disease paradigms. Digestive Diseases 29 (6): 518-524.

83. **Nikoopour E & Singh B** (2014) Reciprocity in microbiome and immune system interactions and its implications in disease and health. Inflammation & Allergy Drug Targets 13 (2): 94-104.

84. **Lutay N, *et al.*** (2013) Bacterial control of host gene expression through RNA polymerase II. The Journal of Clinical Investigation 123 (6): 2366-2379.

85. **Libberton B, Coates RE, Brockhurst MA, & Horsburgh MJ** (2014) Evidence that intraspecific trait variation among nasal bacteria shapes the distribution of *Staphylococcus aureus*. Infection and Immunity 82 (9): 3811-3815.

86. ***Redinbo MR*** (2014) The microbiota, chemical symbiosis, and human disease. Journal of Molecular Biology 426 (23): 3877-3891.

87. **Tikhomirova A & Kidd SP** (2013) *Haemophilus influenzae* and *Streptococcus pneumoniae*: living together in a biofilm. Pathogens and Disease 69 (2): 114-126.

88. **Hong W, *et al.*** (2014) Nontypeable *Haemophilus influenzae* inhibits autolysis and fratricide of *Streptococcus pneumoniae* in vitro. Microbes and Infection 16 (3): 203-213.

89. **Cappelletty D** (1998) Microbiology of bacterial respiratory infections. The Pediatric Infectious Disease Journal 17 (8 Suppl): S55-61.

90. **Krishnamurthy A & Kyd J** (2014) The roles of epithelial cell contact, respiratory bacterial interactions and phosphorylcholine in promoting biofilm formation by *Streptococcus pneumoniae* and nontypeable *Haemophilus influenzae*. Microbes and Infection16 (8): 640-647.

91. **Cole AL, *et al*.** (2016) Host innate inflammatory factors and staphylococcal protein A influence the duration of human *Staphylococcus aureus* nasal carriage. Mucosal Immunology (ahead of print).

92. **Cohen S** (1976) Cell mediated immunity and the inflammatory system. Human Pathology 7 (3): 249-264.

93. **Shane SJ** (1959) Acquired immunity in tuberculosis. Canadian Medical Association Journal 81 (2): 113.

94. **Mackowiak PA** (1978) Microbial synergism in human infections (second of two parts). The New England Journal of Medicine 298 (2): 83-87.

95. **Mackowiak PA** (1978) Microbial synergism in human infections (first of two parts). The New England Journal of Medicine 298 (1): 21-26.

96. **Simon AK, Hollander GA, & McMichael A** (2015) Evolution of the immune system in humans from infancy to old age. Proceedings. Biological Sciences 282 (1821).

97. **Riera Romo M, Perez-Martinez D, & Castillo Ferrer C** (2016) Innate immunity in vertebrates: an overview. Immunology (ahead of print).
98. **Sirisinha S** (2014) Evolutionary insights into the origin of innate and adaptive immune systems: different shades of grey. Asian Pacific Journal of Allergy and Immunology 32 (1): 3-15.
99. **Green GM, Jakab GJ, Low RB, & Davis GS** (1977) Defense mechanisms of the respiratory membrane. The American Review of Respiratory Disease 115 (3): 479-514.
100. **Low ES, Low RB, & Green GM** (1977) Correlated effects of cigarette smoke components on alveolar macrophage adenosine triphosphatase activity and phagocytosis. The American Review of Respiratory Disease 115 (6): 963-970.
101. **Ganesan S, Comstock AT, & Sajjan US** (2013) Barrier function of airway tract epithelium. Tissue Barriers 1(4): e24997.
102. **Yamakawa I** (1981) [The mucociliary transport system of the respiratory tract]. Nihon Kyobu Shikkan Gakkai Zasshi 19 (12): 935-940.
103. **Spina D** (1998) Epithelium smooth muscle regulation and interactions. American Journal of Respiratory and Critical Care Medicine 158 (5 Pt 3): S141-145.
104. **Serafini SM & Michaelson ED** (1977) Length and distribution of cilia in human and canine airways. Bulletin Europeen de Physiopathologie Respiratoire 13 (4): 551-559.
105. **Kilburn KH** (1968) A hypothesis for pulmonary clearance and its implications. The American Review of respiratory Disease 98 (3): 449-463.
106. **Kilburn KH** (1968) Theory and models for cellular injury and clearance failure in the lung. The Yale Journal of Biology and Medicine 40 (5-6): 339-351.
107. **Pohl C, *et al.*** (2009) Barrier functions and paracellular integrity in human cell culture models of the proximal respiratory unit. European Journal of Pharmaceutics and Biopharmaceutics 72 (2): 339-349.
108. **Schneeberger EE & Lynch RD** (2004) The tight junction: a multifunctional complex. American journal of physiology. Cell Physiology 286 (6): 1213-1228.
109. **Hartsock A & Nelson WJ** (2008) Adherens and tight junctions: structure, function and connections to the actin cytoskeleton. Biochimica et Biophysica Acta 1778 (3): 660-669.
110. **Shin K, Fogg VC, & Margolis B** (2006) Tight junctions and cell polarity. Annual Review of Cell and Developmental Biology 22: 207-235.
111. **Balda MS & Matter K** (2009) Tight junctions and the regulation of gene expression. Biochimica et Biophysica Acta 1788 (4): 761-767.
112. **Koch S & Nusrat A** (2009) Dynamic regulation of epithelial cell fate and barrier function by intercellular junctions. Annals of the New York Academy of Sciences 1165: 220-227.
113. **Hogg JC & Timens W** (2009) The pathology of chronic obstructive pulmonary disease. Annual Review of Pathology 4: 435-459.

114. **Shaykhiev R, *et al.*** (2011) Cigarette smoking reprograms apical junctional complex molecular architecture in the human airway epithelium in vivo. Cellular and Molecular Life Sciences 68 (5): 877-892.

115. **Holgate ST** (2011) The sentinel role of the airway epithelium in asthma pathogenesis. Immunological Reviews 242 (1): 205-219.

116. **Sajjan U, Wang Q, Zhao Y, Gruenert DC, & Hershenson MB** (2008) Rhinovirus disrupts the barrier function of polarized airway epithelial cells. American Journal of Respiratory and Critical Care Medicine 178 (12): 1271-1281.

117. **Kim JY, Sajjan US, Krasan GP, & LiPuma JJ** (2005) Disruption of tight junctions during traversal of the respiratory epithelium by *Burkholderia cenocepacia*. Infection and Immunity 73 (11): 7107-7112.

118. **Ibrahim HR, Aoki T, & Pellegrini A** (2002) Strategies for new antimicrobial proteins and peptides: lysozyme and aprotinin as model molecules. Current Pharmaceutical Design 8 (9): 671-693.

119. **Ellison RT, 3rd & Giehl TJ** (1991) Killing of gram-negative bacteria by lactoferrin and lysozyme. The Journal of Clinical Investigation 88 (4): 1080-1091.

120. **Actor JK, Hwang SA, & Kruzel ML** (2009) Lactoferrin as a natural immune modulator. Current Pharmaceutical Design 15 (17): 1956-1973.

121. **Ganz T** (2002) Antimicrobial polypeptides in host defense of the respiratory tract. The Journal of Clinical Investigation 109 (6): 693-697.

122. **Van der Strate BW, Beljaars L, Molema G, Harmsen MC, & Meijer DK** (2001) Antiviral activities of lactoferrin. Antiviral Research 52 (3): 225-239.

123. **Laube DM, Yim S, Ryan LK, Kisich KO, & Diamond G** (2006) Antimicrobial peptides in the airway. Current Topics in Microbiology and Immunology 306:153-182.

124. **Taggart CC, *et al.*** (2001) Cathepsin B, L, and S cleave and inactivate secretory leucoprotease inhibitor. The Journal of Biological Chemistry 276 (36): 33345-33352.

125. **Walsh DE, *et al.*** (2001) Interleukin-8 up-regulation by neutrophil elastase is mediated by MyD88/IRAK/TRAF-6 in human bronchial epithelium. The Journal of Biological Chemistry 276 (38): 35494-35499.

126. **Parameswaran GI, Sethi S, & Murphy TF** (2011) Effects of bacterial infection on airway antimicrobial peptides and proteins in COPD. Chest 140 (3): 611-617.

127. **Ganz T** (2003) Defensins: antimicrobial peptides of innate immunity. Nature Reviews. Immunology 3 (9): 710-720.

128. **Becker MN, Diamond G, Verghese MW, & Randell SH** (2000) CD14-dependent lipopolysaccharide-induced beta-defensin-2 expression in human tracheobronchial epithelium. The Journal of Biological Chemistry 275 (38): 29731-29736.

129. **Singh PK, *et al.*** (1998) Production of beta-defensins by human airway epithelia. Proceedings of the National Academy of Sciences of the United States of America 95 (25): 14961-14966.

130. **Tjabringa GS, Rabe KF, & Hiemstra PS** (2005) The human cathelicidin LL-37: a multifunctional peptide involved in infection and inflammation in the lung. Pulmonary Pharmacology & Therapeutics 18 (5): 321-327.

131. **Bals R, Wang X, Zasloff M, & Wilson JM** (1998) The peptide antibiotic LL-37/hCAP-18 is expressed in epithelia of the human lung where it has broad antimicrobial activity at the airway surface. Proceedings of the National Academy of Sciences of the United States of America 95(16): 9541-9546.
132. **Yoshihara A, *et al.*** (2012) Regulation of dual oxidase expression and H2O2 production by thyroglobulin. Thyroid 22 (10): 1054-1062.
133. **Moskwa P, *et al.*** (2007) A novel host defense system of airways is defective in cystic fibrosis. American Journal of Respiratory and Critical care Medicine 175 (2): 174-183.
134. **Janeway CA, Jr.** (2001) How the immune system protects the host from infection. Microbes and Infection 3 (13): 1167-1171.
135. **Janeway CA, Jr.** (2001) How the immune system works to protect the host from infection: a personal view. Proceedings of the National Academy of Sciences of the United States of America 98 (13): 7461-7468.
136. **Weiss G & Schaible UE** (2015) Macrophage defense mechanisms against intracellular bacteria. Immunological Reviews 264 (1): 182-203.
137. **Aderem A & Underhill DM** (1999) Mechanisms of phagocytosis in macrophages. Annual Review of Immunology 17: 593-623.
138. **Sarma JV & Ward PA** (2011) The complement system. Cell and Tissue Research 343 (1): 227-235.
139. **Greiff L, Andersson M, Erjefalt JS, Persson CG, & Wollmer P** (2003) Airway microvascular extravasation and luminal entry of plasma. Clinical Physiology and Functional Imaging 23 (6): 301-306.
140. **Sjoberg AP, Trouw LA, & Blom AM** (2009) Complement activation and inhibition: a delicate balance. Trends in Immunology 30 (2): 83-90.
141. **Noris M & Remuzzi G** (2013) Overview of complement activation and regulation. Seminars in Nephrology 33 (6): 479-492.
142. **Walport MJ** (2001) Complement. Second of two parts. The New England Journal of Medicine 344 (15): 1140-1144.
143. **Walport MJ** (2001) Complement, first of two parts. The New England Journal of Medicine 344 (14): 1058-1066.
144. **Klein MA, *et al.*** (2001) Complement facilitates early prion pathogenesis. Nature Medicine 7(4): 488-492.
145. **Persson CG** (1991) Plasma exudation in the airways: mechanisms and function. The European Respiratory Journal 4 (10): 1268-1274.
146. **Persson CG, *et al.*** (1991) Plasma exudation as a first line respiratory mucosal defence. Clinical and Experimental Allergy 21 (1): 17-24.
147. **Singh B, Su YC, & Riesbeck K** (2010) Vitronectin in bacterial pathogenesis: a host protein used in complement escape and cellular invasion. Molecular Microbiology 78 (3): 545-560.
148. **Hood MI & Skaar EP** (2012) Nutritional immunity: transition metals at the pathogen-host interface. Nature Reviews. Microbiology 10 (8): 525-537.

149. **Porcheron G, Garenaux A, Proulx J, Sabri M, & Dozois CM** (2013) Iron, copper, zinc, and manganese transport and regulation in pathogenic *Enterobacteria*: correlations between strains, site of infection and the relative importance of the different metal transport systems for virulence. Frontiers in Cellular and Infection Microbiology 3: 90.

150. **Diaz-Ochoa VE, Jellbauer S, Klaus S, & Raffatellu M** (2014) Transition metal ions at the crossroads of mucosal immunity and microbial pathogenesis. Frontiers in Cellular and Infection Microbiology 4: 2.

151. **Andreini C, Bertini I, Cavallaro G, Holliday GL, & Thornton JM** (2008) Metal ions in biological catalysis: from enzyme databases to general principles. Journal of Biological Inorganic Chemistry 13 (8): 1205-1218.

152. **Braun V & Hantke K** (2011) Recent insights into iron import by bacteria. Current Opinion in Chemical Biology 15 (2): 328-334.

153. **Loeb MR** (1995) Ferrochelatase activity and protoporphyrin IX utilization in *Haemophilus influenzae*. Journal of Bacteriology 177 (12): 3613-3615.

154. **Weinberg ED** (2009) Iron availability and infection. Biochimica et Biophysica Acta 1790 (7): 600-605.

155. **Ong ST, Ho JZ, Ho B, & Ding JL** (2006) Iron-withholding strategy in innate immunity. Immunobiology 211 (4): 295-314.

156. **Schaer DJ, Vinchi F, Ingoglia G, Tolosano E, & Buehler PW** (2014) Haptoglobin, hemopexin, and related defense pathways-basic science, clinical perspectives, and drug development. Frontiers in Physiology 5: 415.

157. **Leon-Sicairos N, *et al.*** (2015) Strategies of Intracellular Pathogens for Obtaining Iron from the Environment. BioMed Research International 2015: 476534.

158. **Jabado N, *et al.*** (2000) Natural resistance to intracellular infections: natural resistance-associated macrophage protein 1 (Nramp1) functions as a pH-dependent manganese transporter at the phagosomal membrane. The Journal of Experimental Medicine 192 (9): 1237-1248.

159. **Khan AG, *et al.*** (2007) High-affinity binding by the periplasmic iron-binding protein from *Haemophilus influenzae* is required for acquiring iron from transferrin. The Biochemical Journal 404 (2): 217-225.

160. **Schaible UE, Collins HL, Priem F, & Kaufmann SH** (2002) Correction of the iron overload defect in beta-2-microglobulin knockout mice by lactoferrin abolishes their increased susceptibility to tuberculosis. The Journal of Experimental Medicine 196 (11): 1507-1513.

161. **Ponton F, Wilson K, Cotter SC, Raubenheimer D, & Simpson SJ** (2011) Nutritional immunology: a multi-dimensional approach. PLoS Pathogens 7 (12): e1002223.

162. **Rohmer L, Hocquet D, & Miller SI** (2011) Are pathogenic bacteria just looking for food? Metabolism and microbial pathogenesis. Trends in Microbiology 19 (7): 341-348.

163. **Eisenreich W, Dandekar T, Heesemann J, & Goebel W** (2010) Carbon metabolism of intracellular bacterial pathogens and possible links to virulence. Nature reviews. Microbiology 8 (6): 401-412.

164. **Price CT, Al-Quadan T, Santic M, Rosenshine I, & Abu Kwaik Y** (2011) Host proteasomal degradation generates amino acids essential for intracellular bacterial growth. Science 334 (6062): 1553-1557.

165. **Fagarasan S & Honjo T** (2003) Intestinal IgA synthesis: regulation of front-line body defences. Nature Reviews. Immunology 3 (1): 63-72.

166. **Holmgren J & Czerkinsky C** (2005) Mucosal immunity and vaccines. Nature Medicine 11 (4 Suppl): S45-53.

167. **Cerutti A & Rescigno M** (2008) The biology of intestinal immunoglobulin A responses. Immunity 28 (6): 740-750.

168. **Fernaays MM, Lesse AJ, Cai X, & Murphy TF** (2006) Characterization of igaB, a second immunoglobulin A1 protease gene in nontypeable *Haemophilus influenzae*. Infection and Immunity 74 (10): 5860-5870.

169. **Tolar P, Sohn HW, & Pierce SK** (2008) Viewing the antigen-induced initiation of B-cell activation in living cells. Immunological Reviews 221: 64-76.

170. **Arias-Bouda LM, *et al.*** (2003) Changes in avidity and level of immunoglobulin G antibodies to Mycobacterium tuberculosis in sera of patients undergoing treatment for pulmonary tuberculosis. Clinical and Diagnostic Laboratory Immunology 10 (4): 702-709.

171. **Smismans A, Goossens VJ, Nulens E, & Bruggeman CA** (2006) Comparison of five different immunoassays for the detection of Borrelia burgdorferi IgM and IgG antibodies. Clinical Microbiology and Infection 12 (7): 648-655.

172. **Moore GL, Chen H, Karki S, & Lazar GA** (2010) Engineered Fc variant antibodies with enhanced ability to recruit complement and mediate effector functions. MAbs 2 (2): 181-189.

173. **Shackelford PG, *et al.*** (1987) Subclass distribution of human antibodies to *Haemophilus influenzae* type b capsular polysaccharide. Journal of Immunology 138 (2): 587-592.

174. **Siber GR, *et al.*** (1990) Impaired antibody response to *Haemophilus influenzae* type b polysaccharide and low IgG2 and IgG4 concentrations in Apache children. The New England Journal of Medicine 323 (20): 1387-1392.

175. **King PT, *et al.*** (2008) Systemic humoral immunity to non-typeable *Haemophilus influenzae*. Clinical and Experimental Immunology 153 (3): 376-384.

176. **Mukundan D, Ecevit Z, Patel M, Marrs CF, & Gilsdorf JR** (2007) Pharyngeal colonization dynamics of *Haemophilus influenzae* and *Haemophilus haemolyticus* in healthy adult carriers. Journal of Clinical Microbiology 45 (10): 3207-3217.

177. **Farjo RS, *et al.*** (2004) Diversity and sharing of *Haemophilus influenzae* strains colonizing healthy children attending day-care centers. The Pediatric Infectious Disease Journal 23 (1): 41-46.

178. **Marrs CF, Krasan GP, McCrea KW, Clemans DL, & Gilsdorf JR** (2001) *Haemophilus influenzae* - human specific bacteria. Frontiers in Bioscience 6: E41-60.

179. **Eutsey RA, *et al.*** (2013) Design and validation of a supragenome array for determination of the genomic content of *Haemophilus influenzae* isolates. BMC Genomics 14: 484.

180. **Su YC, Resman F, Horhold F, & Riesbeck K** (2014) Comparative genomic analysis reveals distinct genotypic features of the emerging pathogen *Haemophilus influenzae* type f. BMC Genomics 15:38.

181. **Mell JC, Hall IM, & Redfield RJ** (2012) Defining the DNA uptake specificity of naturally competent *Haemophilus influenzae* cells. Nucleic Acids Research 40 (17): 8536-8549.

182. **Mell JC, Shumilina S, Hall IM, & Redfield RJ** (2011) Transformation of natural genetic variation into *Haemophilus influenzae* genomes. PLoS Pathogens 7 (7): e1002151.

183. **Garmendia J, Marti-Lliteras P, Moleres J, Puig C, & Bengoechea JA** (2012) Genotypic and phenotypic diversity of the noncapsulated *Haemophilus influenzae*: adaptation and pathogenesis in the human airways. International Microbiology 15 (4): 159-172.

184. **Bailey KL, *et al.*** (2012) Non-typeable *Haemophilus influenzae* decreases cilia beating via protein kinase Cepsilon. Respiratory Research 13: 49.

185. **Denny FW** (1974) Effect of a toxin produced by *Haemophilus influenzae* on ciliated respiratory epithelium. The Journal of Infectious Diseases 129 (2): 93-100.

186. **Wilson R, Read R, & Cole P** (1992) Interaction of *Haemophilus influenzae* with mucus, cilia, and respiratory epithelium. The Journal of Infectious Diseases 165 Suppl 1: S100-102.

187. **Singh B, Fleury C, Jalalvand F, & Riesbeck K** (2012) Human pathogens utilize host extracellular matrix proteins laminin and collagen for adhesion and invasion of the host. FEMS Microbiology Reviews 36 (6): 1122-1180.

188. **Alcock J, Maley CC, & Aktipis CA** (2014) Is eating behavior manipulated by the gastrointestinal microbiota? Evolutionary pressures and potential mechanisms. Bioessays 36 (10): 940-949.

189. **St Geme JW, *et al.*** (1996) *Haemophilus influenzae* pili are composite structures assembled via the HifB chaperone. Proceedings of the National Academy of Sciences of the United States of America 93 (21): 11913-11918.

190. **Gilsdorf JR, McCrea KW, & Marrs CF** (1997) Role of pili in *Haemophilus influenzae* adherence and colonization. Infection and Immunity 65 (8): 2997-3002.

191. **Rodriguez CA, *et al.*** (2003) Prevalence and distribution of adhesins in invasive non-type b encapsulated *Haemophilus influenzae*. Infection and Immunity 71 (4): 1635-1642.

192. **St Geme JW, 3rd** (2002) Molecular and cellular determinants of non-typeable *Haemophilus influenzae* adherence and invasion. Cellular Microbiology 4 (4): 191-200.

193. **Geme JW, 3rd & Cutter D** (1995) Evidence that surface fibrils expressed by *Haemophilus influenzae* type b promote attachment to human epithelial cells. Molecular Microbiology 15 (1): 77-85.

194. **Strouts FR, *et al.*** (2012) Lineage-specific virulence determinants of *Haemophilus influenzae* biogroup aegyptius. Emerging Infectious Diseases 18 (3): 449-457.

195. **Sheets AJ, Grass SA, Miller SE, & St Geme JW, 3rd** (2008) Identification of a novel trimeric autotransporter adhesin in the cryptic genospecies of *Haemophilus*. Journal of Bacteriology 190 (12): 4313-4320.

196. **Fink DL, Green BA, & St Geme JW, 3rd** (2002) The *Haemophilus influenzae* Hap autotransporter binds to fibronectin, laminin, and collagen IV. Infection and Immunity 70 (9): 4902-4907.

197. **King P** (2012) *Haemophilus influenzae* and the lung (*Haemophilus* and the lung). Clinical and translational medicine 1 (1): 10.

198. **Hiltke TJ, Sethi S, & Murphy TF** (2002) Sequence stability of the gene encoding outer membrane protein P2 of nontypeable *Haemophilus influenzae* in the human respiratory tract. The Journal of Infectious Diseases 185 (5): 627-631.

199. **Kyd JM, Cripps AW, Novotny LA, & Bakaletz LO** (2003) Efficacy of the 26-kilodalton outer membrane protein and two P5 fimbrin-derived immunogens to induce clearance of nontypeable *Haemophilus influenzae* from the rat middle ear and lungs as well as from the chinchilla middle ear and nasopharynx. Infection and Immunity 71 (8): 4691-4699.

200. **Janson H, Ruan M, & Forsgren A** (1993) Limited diversity of the protein D gene (hpd) among encapsulated and nonencapsulated *Haemophilus influenzae* strains. Infection and Immunity 61 (11): 4546-4552.

201. **Singh B, Al-Jubair T, Morgelin M, Thunnissen MM, & Riesbeck K** (2013) The unique structure of *Haemophilus influenzae* protein E reveals multiple binding sites for host factors. Infection and Immunity 81 (3): 801-814.

202. **Shelton CL, Raffel FK, Beatty WL, Johnson SM, & Mason KM** (2011) Sap transporter mediated import and subsequent degradation of antimicrobial peptides in *Haemophilus*. PLoS Pathogens 7 (11): e1002360.

203. **Harrington JC, *et al.*** (2009) Resistance of *Haemophilus influenzae* to reactive nitrogen donors and gamma interferon-stimulated macrophages requires the formate-dependent nitrite reductase regulator-activated ytfE gene. Infection and Immunity 77 (5): 1945-1958.

204. **Tsuji T, Alborno RM, Ehara M, Honda T, & Miwatani T** (1989) Detection of IgA protease from *Haemophilus influenzae* by immunoblotting. European Journal of Epidemiology 5 (2): 199-201.

205. **Murphy TF, et al.** (2015) Expression of IgA proteases by *Haemophilus influenzae* in the respiratory tract of adults with chronic obstructive pulmonary disease. The Journal of Infectious Diseases 212 (11): 1798-1805.

206. **Noel GJ, Hoiseth SK, & Edelson PJ** (1992) Type b capsule inhibits ingestion of *Haemophilus influenzae* by murine macrophages: studies with isogenic encapsulated and unencapsulated strains. The Journal of Infectious Diseases 166 (1): 178-182.

207. **Langereis JD & Weiser JN** (2014) Shielding of a lipooligosaccharide IgM epitope allows evasion of neutrophil-mediated killing of an invasive strain of nontypeable *Haemophilus influenzae*. mBio 5 (4): e01478-01414.

208. **Wispelwey B, Hansen EJ, & Scheld WM** (1989) *Haemophilus influenzae* outer membrane vesicle-induced blood-brain barrier permeability during experimental meningitis. Infection and Immunity 57 (8): 2559-2562.

209. **Deknuydt F, Nordstrom T, & Riesbeck K** (2014) Diversion of the host humoral response: a novel virulence mechanism of *Haemophilus influenzae* mediated via outer membrane vesicles. Journal of Leukocyte Biology 95 (6): 983-991.

210. **Apicella MA** (2012) Nontypeable *Haemophilus influenzae*: the role of N-acetyl-5-neuraminic acid in biology. Frontiers in Cellular and Infection Microbiology 2: 19.

211. **Clark SE, Snow J, Li J, Zola TA, & Weiser JN** (2012) Phosphorylcholine allows for evasion of bactericidal antibody by *Haemophilus influenzae*. PLoS Pathogens 8 (3): e1002521.

212. **Nakamura S, *et al.*** (2011) Molecular basis of increased serum resistance among pulmonary isolates of non-typeable *Haemophilus influenzae*. PLoS Pathogens 7 (1): e1001247.

213. **Ho DK, Ram S, Nelson KL, Bonthuis PJ, & Smith AL** (2007) lgtC expression modulates resistance to C4b deposition on an invasive nontypeable *Haemophilus influenzae*. Journal of Immunology 178 (2): 1002-1012.

214. **Hallstrom T, *et al.*** (2016) Conserved patterns of microbial immune escape: pathogenic microbes of diverse origin target the human terminal complement inhibitor vitronectin via a single common motif. PloS One 11 (1): e0147709.

215. **Blom AM, Hallstrom T, & Riesbeck K** (2009) Complement evasion strategies of pathogens-acquisition of inhibitors and beyond. Molecular Immunology 46 (14): 2808-2817.

216. **Hallstrom T & Riesbeck K** (2010) *Haemophilus influenzae* and the complement system. Trends in Microbiology 18 (6): 258-265.

217. **Singh B, *et al.*** (2011) *Haemophilus influenzae* protein E recognizes the C-terminal domain of vitronectin and modulates the membrane attack complex. Molecular Microbiology 81 (1): 80-98.

218. **Fleury C, *et al.*** (2014) Identification of a *Haemophilus influenzae* factor H-Binding lipoprotein involved in serum resistance. Journal of Immunology 192 (12): 5913-5923.

219. **Al-Jubair T, *et al.*** (2015) *Haemophilus influenzae* type f hijacks vitronectin using protein H to resist host innate immunity and adhere to pulmonary epithelial cells. Journal of Immunology 195 (12): 5688-5695.

220. **Su YC, *et al.*** (2013) *Haemophilus influenzae* acquires vitronectin via the ubiquitous Protein F to subvert host innate immunity. Molecular Microbiology 87 (6): 1245-1266.

221. **Redfield RJ** (1993) Genes for breakfast: the have-your-cake-and-eat-it-too of bacterial transformation. The Journal of Heredity 84 (5): 400-404.

222. **Gazzaniga F, Stebbins R, Chang SZ, McPeek MA, & Brenner C** (2009) Microbial NAD metabolism: lessons from comparative genomics. Microbiology and Molecular Biology Reviews 73 (3): 529-541.

223. **Kemmer G, *et al*.** (2001) NadN and e (P4) are essential for utilization of NAD and nicotinamide mononucleotide but not nicotinamide riboside in *Haemophilus influenzae*. Journal of Bacteriology 183 (13): 3974-3981.

224. **Andersen C, *et al.*** (2003) Porin OmpP2 of *Haemophilus influenzae* shows specificity for nicotinamide-derived nucleotide substrates. The Journal of Biological Chemistry 278 (27): 24269-24276.

225. **Murphy TF & Bartos LC** (1988) Human bactericidal antibody response to outer membrane protein P2 of nontypeable *Haemophilus influenzae*. Infection and Immunity 56 (10): 2673-2679.

226. **Tian GZ, *et al.*** (2012) Rapid detection of *Haemophilus influenzae* and *Haemophilus parainfluenzae* in nasopharyngeal swabs by multiplex PCR. Biomedical and Environmental Sciences 25 (3): 367-371.

227. **Whitby PW, Seale TW, VanWagoner TM, Morton DJ, & Stull TL (**2009) The iron/heme regulated genes *of Haemophilus influenzae*: comparative transcriptional profiling as a tool to define the species core modulon. BMC Genomics 10: 6.

228. **Mason KM, Raffel FK, Ray WC, & Bakaletz LO** (2011) Heme utilization by nontypeable *Haemophilus influenzae* is essential and dependent on Sap transporter function. Journal of Bacteriology 193 (10): 2527-2535.

229. **Al Jubair T, *et al.*** (2014) *Haemophilus influenzae* stores and distributes hemin by using protein E. International Journal of Medical Microbiology 304 (5-6): 662-668.

230. **Murphy TF & Brauer AL** (2011) Expression of urease by *Haemophilus influenzae* during human respiratory tract infection and role in survival in an acid environment. BMC Microbiology 11: 183.

231. **Van Ham SM, Van Alphen L, Mooi FR, & Van Putten JP** (1993) Phase variation of *H. influenzae* fimbriae: transcriptional control of two divergent genes through a variable combined promoter region. Cell 73 (6): 1187-1196.

232. **Weiser JN, Williams A, & Moxon ER** (1990) Phase-variable lipopolysaccharide structures enhance the invasive capacity of *Haemophilus influenzae*. Infection and Immunity 58 (10): 3455-3457.

233. **Farley MM, Stephens DS, Kaplan SL, & Mason EO, Jr.** (1990) Pilus- and non-pilus-mediated interactions of *Haemophilus influenzae* type b with human erythrocytes and human nasopharyngeal mucosa. The Journal of Infectious Diseases 161 (2): 274-280.

234. **Barenkamp SJ** (1996) Immunization with high-molecular-weight adhesion proteins of nontypeable *Haemophilus influenzae* modifies experimental otitis media in chinchillas. Infection and Immunity 64 (4): 1246-1251.

235. **Hall-Stoodley L, Costerton JW, & Stoodley P** (2004) Bacterial biofilms: from the natural environment to infectious diseases. Nature Reviews. Microbiology 2 (2): 95-108.

236. **Meng G, Spahich N, Kenjale R, Waksman G, & St Geme JW, 3rd** (2011) Crystal structure of the *Haemophilus influenzae* Hap adhesin reveals an intercellular oligomerization mechanism for bacterial aggregation. The EMBO Journal 30 (18): 3864-3874.

237. **Swords WE** (2012) Quorum signaling and sensing by nontypeable *Haemophilus influenzae.* Frontiers in Cellular and Infection Microbiology 2: 100.

238. **Murphy TF & Kirkham C** (2002) Biofilm formation by nontypeable *Haemophilus influenzae*: strain variability, outer membrane antigen expression and role of pili. BMC Microbiology 2:7.

239. **Jurcisek JA & Bakaletz LO** (2007) Biofilms formed by nontypeable *Haemophilus influenzae* in vivo contain both double-stranded DNA and type IV pilin protein. Journal of Bacteriology 189 (10): 3868-3875.

240. **Wu S, *et al.*** (2014) Biofilm-specific extracellular matrix proteins of nontypeable *Haemophilus influenzae*. Pathogens and Disease 72 (3): 143-160.

241. **Hong W, Juneau RA, Pang B, & Swords WE** (2009) Survival of bacterial biofilms within neutrophil extracellular traps promotes nontypeable *Haemophilus influenzae* persistence in the chinchilla model for otitis media. Journal of Innate Immunity 1 (3): 215-224.

242. **Murphy TF, Sethi S, Klingman KL, Brueggemann AB, & Doern GV** (1999) Simultaneous respiratory tract colonization by multiple strains of nontypeable *Haemophilus influenzae* in chronic obstructive pulmonary disease: implications for antibiotic therapy. The Journal of Infectious Diseases 180 (2): 404-409.

243. **Murphy TV, *et al.*** (1992) Invasive *Haemophilus influenzae* type b disease in children less than 5 years of age in Minnesota and in Dallas County, Texas, 1983-1984. The Journal of Infectious Diseases 165 Suppl 1: S7-10.

244. **Sadeghi-Aval P, Tsang RS, Jamieson FB, & Ulanova M** (2013) Emergence of non-serotype b encapsulated *Haemophilus influenzae* as a cause of pediatric meningitis in northwestern Ontario. The Canadian Journal of Infectious Diseases & Medical Microbiology 24 (1): 13-16.

245. **Ulanova M & Tsang RS** (2014) *Haemophilus influenzae* serotype a as a cause of serious invasive infections. The Lancet. Infectious Diseases 14 (1): 70-82.

246. **Murphy TF** (2003) Respiratory infections caused by non-typeable *Haemophilus influenzae*. Current Opinion in Infectious Diseases 16 (2): 129-134.

247. **Leary T** (1918) The use of influenza vaccine in the present epidemic. American Journal of Public Health 8 (10): 754-768.

248. **McCullers JA & Dunn JD** (2008) Advances in vaccine technology and their impact on managed care. P & T 33 (1): 35-41.

249. **Peltola H, Kayhty H, Virtanen M, & Makela PH** (1984) Prevention of *Hemophilus influenzae* type b bacteremic infections with the capsular polysaccharide vaccine. The New England Journal of Medicine 310 (24): 1561-1566.

250. **Schneerson R, Barrera O, Sutton A, & Robbins JB** (1980) Preparation, characterization, and immunogenicity of *Haemophilus influenzae* type b polysaccharide-protein conjugates. The Journal of Experimental Medicine 152 (2): 361-376.

251. **Kelly DF, Moxon ER, & Pollard AJ** (2004) *Haemophilus influenzae* type b conjugate vaccines. Immunology 113 (2): 163-174.

252. **Adams WG, *et al.*** (1993) Decline of childhood *Haemophilus influenzae* type b (Hib) disease in the Hib vaccine era. JAMA 269 (2): 221-226.

253. **Maiden MC** (2013) The impact of protein-conjugate polysaccharide vaccines: an endgame for meningitis? Philosophical Transactions of the Royal Society of London. Series B, Biological Sciences 368 (1623): 20120147.

254. **Morris SK, Moss WJ, & Halsey N** (2008) *Haemophilus influenzae* type b conjugate vaccine use and effectiveness. The Lancet. Infectious Diseases 8 (7): 435-443.

255. **Van Eldere J, Slack MP, Ladhani S, & Cripps AW** (2014) Non-typeable *Haemophilus influenzae*, an under-recognised pathogen. The Lancet. Infectious Diseases 14 (12): 1281-1292.

256. **Nix EB, *et al.*** (2012) Risk of invasive *Haemophilus influenzae* type b (Hib) disease in adults with secondary immunodeficiency in the post-Hib vaccine era. Clinical and Vaccine Immunology 19(5): 766-771.

257. **Ladhani SN, Ramsay M, & Slack MP** (2011) The impact of *Haemophilus influenzae* serotype B resurgence on the epidemiology of childhood invasive *Haemophilus influenzae* disease in England and Wales. The Pediatric Infectious Disease Journal 30 (10): 893-895.

258. **Dworkin MS, Park L, & Borchardt SM** (2007) The changing epidemiology of invasive *Haemophilus influenzae* disease, especially in persons > or = 65 years old. Clinical Infectious Diseases 44 (6): 810-816.

259. **Tsang RS, *et al.*** (2007) Characterization of invasive *Haemophilus influenzae* disease in Manitoba, Canada, 2000-2006: invasive disease due to non-type b strains. Clinical Infectious Diseases 44 (12): 1611-1614.

260. **Bajanca P, Canica M, & Multicenter Study G** (2004) Emergence of nonencapsulated and encapsulated non-b-type invasive *Haemophilus influenzae* isolates in Portugal (1989-2001). Journal of Clinical Microbiology 42 (2): 807-810.

261. **Campos J, *et al.*** (2003) Antibiotic resistance and clinical significance of *Haemophilus influenzae* type f. The Journal of Antimicrobial Chemotherapy 52 (6): 961-966.

262. **Adderson EE, *et al.*** (2001) Invasive serotype a *Haemophilus influenzae* infections with a virulence genotype resembling *Haemophilus influenzae* type b: emerging pathogen in the vaccine era? Pediatrics 108 (1): E18.

263. **Tsang RS, *et al.*** (2006) Invasive *Haemophilus influenzae* in Manitoba, Canada, in the postvaccination era. Journal of Clinical Microbiology 44 (4): 1530-1535.

264. **Kline KA, Falker S, Dahlberg S, Normark S, & Henriques-Normark B** (2009) Bacterial adhesins in host-microbe interactions. Cell Host & Microbe 5 (6): 580-592.

265. **Singh B, *et al.*** (2014) A fine-tuned interaction between trimeric autotransporter haemophilus surface fibrils and vitronectin leads to serum resistance and adherence to respiratory epithelial cells. Infection and Immunity 82 (6): 2378-2389.

266. **Murphy TF** (2009) Current and future prospects for a vaccine for nontypeable *Haemophilus influenzae*. Current Infectious Disease Reports 11(3): 177-182.

267. **Murphy TF, Bakaletz LO, & Smeesters PR** (2009) Microbial interactions in the respiratory tract. The Pediatric Infectious Disease Journal 28 (10 Suppl): S121-126.

268. **Cotter SE, Yeo HJ, Juehne T, & St Geme JW, 3rd** (2005) Architecture and adhesive activity of the *Haemophilus influenzae* Hsf adhesin. Journal of Bacteriology 187 (13): 4656-4664.

269. **Yeo HJ, *et al.*** (2007) The structure of the *Haemophilus influenzae* HMW1 pro-piece reveals a structural domain essential for bacterial two-partner secretion. The Journal of Biological Chemistry 282 (42): 31076-31084.

270. **Ronander E, *et al.*** (2009) Nontypeable *Haemophilus influenzae* adhesin protein E: characterization and biological activity. The Journal of Infectious Diseases 199 (4): 522-531.

271. **Ronander E, *et al.*** (2008) Identification of a novel *Haemophilus influenzae* protein important for adhesion to epithelial cells. Microbes and Infection 10 (1): 87-96.

272. **Barfod A, Singh B, Johanson U, Riesbeck K, & Kjellbom P** (2014) In vitro selection of RNA aptamers directed against protein E: a *Haemophilus influenzae* adhesin. Molecular Biotechnology 56 (8): 714-725.

273. **Singh B, Brant M, Kilian M, Hallstrom B, & Riesbeck K** (2010) Protein E of *Haemophilus influenzae* is a ubiquitous highly conserved adhesin. The Journal of Infectious Diseases 201 (3): 414-419.

274. **Hallstrom T, Blom AM, Zipfel PF, & Riesbeck K** (2009) Nontypeable *Haemophilus influenzae* protein E binds vitronectin and is important for serum resistance. Journal of Immunology 183 (4): 2593-2601.

275. **Barthel D, Singh B, Riesbeck K, & Zipfel PF** (2012) *Haemophilus influenzae* uses the surface protein E to acquire human plasminogen and to evade innate immunity. Journal of Immunology 188 (1): 379-385.

276. **Hallstrom T, *et al.*** (2011) *Haemophilus influenzae* protein E binds to the extracellular matrix by concurrently interacting with laminin and vitronectin. The Journal of Infectious Diseases 204 (7): 1065-1074.

277. **Singh B, Al Jubair T, Fornvik K, Thunnissen MM, & Riesbeck K** (2012) Crystallization and X-ray diffraction analysis of a novel surface-adhesin protein: protein E from *Haemophilus influenzae*. Acta Crystallographica. Section F 68 (Pt 2): 222-226.

278. **Hayashi S & Wu HC** (1990) Lipoproteins in bacteria. Journal of Bioenergetics and Biomembranes 22 (3): 451-471.

279. **Nakayama H, Kurokawa K, & Lee BL** (2012) Lipoproteins in bacteria: structures and biosynthetic pathways. The FEBS Journal 279 (23): 4247-4268.

280. **Wandersman C & Stojiljkovic I** (2000) Bacterial heme sources: the role of heme, hemoprotein receptors and hemophores. Current Opinion in Microbiology 3 (2): 215-220.

281. **Battersby AR, Fookes CJ, Matcham GW, & McDonald E** (1980) Biosynthesis of the pigments of life: formation of the macrocycle. Nature 285 (5759): 17-21.

282. **Lowe PN, Leeper FJ, & Perham RN** (1983) Stereoisomers of tetrahydrothiamin pyrophosphate, potent inhibitors of the pyruvate dehydrogenase multienzyme complex from Escherichia coli. Biochemistry 22 (1): 150-157.

283. **Evans NM, Smith DD, & Wicken AJ** (1974) Haemin and nicotinamide adenine dinucleotide requirements of *Haemophilus influenzae* and *Haemophilus parainfluenzae.* Journal of Medical Microbiology 7 (3): 359-365.

284. **Panek H & O'Brian MR** (2002) A whole genome view of prokaryotic haem biosynthesis. Microbiology 148 (Pt 8): 2273-2282.

285. **Ratledge C & Dover LG** (2000) Iron metabolism in pathogenic bacteria. Annual Review of Microbiology 54: 881-941.

286. **Fournier C, Smith A, & Delepelaire P** (2011) Haem release from haemopexin by HxuA allows *Haemophilus influenzae* to escape host nutritional immunity. Molecular Microbiology 80 (1): 133-148.

287. **Infante-Rivard C & Fernandez A** (1993) Otitis media in children: frequency, risk factors, and research avenues. Epidemiologic Reviews 15 (2): 444-465.

288. **Emsley P, Lohkamp B, Scott WG, & Cowtan K** (2010) Features and development of Coot. Acta Crystallographica. Section D 66 (Pt 4): 486-501.

289. **McNicholas S, Potterton E, Wilson KS, & Noble ME** (2011) Presenting your structures: the CCP4mg molecular-graphics software. Acta Crystallographica. Section D 67 (Pt 4): 386-394.

290. **Potterton E, McNicholas S, Krissinel E, Cowtan K, & Noble M** (2002) The CCP4 molecular-graphics project. Acta Crystallographica. Section D 58 (Pt 11): 1955-1957.

291. **Ulanova M & Tsang RS** (2009) Invasive *Haemophilus influenzae* disease: changing epidemiology and host-parasite interactions in the 21st century. Infection, Genetics and Evolution 9 (4): 594-605.

292. **Geme JW, 3rd** (1996) Molecular determinants of the interaction between Haemophilus influenzae and human cells. American Journal of Respiratory and Critical Care Medicine 154 (4 Pt 2): S192-196.

293. **Barnard TJ, Dautin N, Lukacik P, Bernstein HD, & Buchanan SK** (2007) Autotransporter structure reveals intra-barrel cleavage followed by conformational changes. Nature Structural & Molecular Biology 14 (12): 1214-1220.

294. **Dautin N & Bernstein HD** (2007) Protein secretion in gram-negative bacteria via the autotransporter pathway. Annual Review of Microbiology 61: 89-112.

295. **Leo JC, Grin I, & Linke D** (2012) Type V secretion: mechanism(s) of autotransport through the bacterial outer membrane. Philosophical Transactions of the Royal Society of London. Series B, Biological Sciences 367 (1592): 1088-1101.

296. **Mikula KM, *et al.*** (2012) The translocation domain in trimeric autotransporter adhesins is necessary and sufficient for trimerization and autotransportation. Journal of Bacteriology 194 (4): 827-838.

297. **Spahich NA & St Geme JW, 3rd** (2011) Structure and function of the *Haemophilus influenzae* autotransporters. Frontiers in Cellular and Infection Microbiology 1: 5.

298. **Cotter SE, Surana NK, & St Geme JW, 3rd** (2005) Trimeric autotransporters: a distinct subfamily of autotransporter proteins. Trends in Microbiology 13 (5): 199-205.

299. **St Geme JW, 3rd, Kumar VV, Cutter D, & Barenkamp SJ** (1998) Prevalence and distribution of the hmw and hia genes and the HMW and Hia adhesins among genetically diverse strains of nontypeable *Haemophilus influenzae*. Infection and Immunity 66 (1): 364-368.

300. **Winkelstein JA & Moxon ER** (1992) The role of complement in the host's defense against *Haemophilus influenzae*. The Journal of Infectious Diseases 165 Suppl 1: S62-65.

301. **Singh B, *et al.*** (2015) *Haemophilus influenzae* surface fibril (Hsf) is a unique twisted hairpin-like trimeric autotransporter. International Journal of Medical Microbiology 305 (1): 27-37.

302. **Resman F, *et al*.** (2011) Invasive disease caused by *Haemophilus influenzae* in Sweden 1997-2009; evidence of increasing incidence and clinical burden of non-type b strains. Clinical Microbiology and Infection 17 (11): 1638-1645.

303. **Fleury C, Resman F, Rau J, & Riesbeck K** (2014) Prevalence, distribution and transfer of small beta-lactamase-containing plasmids in Swedish *Haemophilus influenzae*. The Journal of Antimicrobial Chemotherapy 69 (5): 1238-1242.

304. **Singh B, *et al.*** (2010) Vitronectin binds to the head region of *Moraxella catarrhalis* ubiquitous surface protein A2 and confers complement-inhibitory activity. Molecular Microbiology 75 (6): 1426-1444.

305. **Su YC, Hallstrom BM, Bernhard S, Singh B, & Riesbeck K** (2013) Impact of sequence diversity in the *Moraxella catarrhalis* UspA2/UspA2H head domain on vitronectin binding and antigenic variation. Microbes and Infection 15 (5): 375-387.

306. **Ruoslahti E** (1996) RGD and other recognition sequences for integrins. Annual Review of Cell and Developmental Biology 12: 697-715.

307. **Ruoslahti E** (1996) Integrin signaling and matrix assembly. Tumour Biology 17 (2): 117-124.

308. **Leroy-Dudal J, Gagniere H, Cossard E, Carreiras F, & Di Martino P** (2004) Role of alphavbeta5 integrins and vitronectin in Pseudomonas aeruginosa PAK interaction with A549 respiratory cells. Microbes and Infection 6 (10): 875-881.

309. **Buommino E, *et al.*** (2014) Alpha(v)beta5 integrins mediates *Pseudomonas fluorescens* interaction with A549 cells. Frontiers in Bioscience 19: 408-415.

Paper I

Acta Crystallographica Section F
Structural Biology and Crystallization Communications
ISSN 1744-3091

Crystallization and X-ray diffraction analysis of a novel surface-adhesin protein: protein E from *Haemophilus influenzae*

Birendra Singh,[a] Tamim Al Jubair,[a] Karolina Förnvik,[b] Marjolein M. Thunnissen[b] and Kristian Riesbeck[a]*

[a]Medical Microbiology, Department of Laboratory Medicine Malmö, Lund University, Skåne University Hospital, SE-205 02 Malmö, Sweden, and [b]Centre of Molecular Protein Science, Lund University, Getingevägen 60, SE-221 00 Lund, Sweden

Correspondence e-mail: kristian.riesbeck@med.lu.se

Received 15 October 2011
Accepted 23 December 2011

Protein E (PE) is a ubiquitous multifunctional surface protein of *Haemophilus* spp. and other bacterial pathogens of the *Pasteurellaceae* family. *H. influenzae* utilizes PE for attachment to respiratory epithelial cells. In addition, PE interacts directly with plasminogen and the extracellular matrix (ECM) components vitronectin and laminin. Vitronectin is a complement regulator that inhibits the formation of the membrane-attack complex (MAC). PE-mediated vitronectin recruitment at the *H. influenzae* surface thus inhibits MAC and protects against serum bactericidal activity. Laminin is an abundant ECM protein and is present in the basement membrane that helps in adherence of *H. influenzae* during colonization. Here, the expression, purification and crystallization of and the collection of high-resolution data for this important *H. influenzae* adhesin are reported. To solve the phase problem for PE, Met residues were introduced and an SeMet variant was expressed and crystallized. Both native and SeMet-containing PE gave plate-like crystals in space group $P2_1$, with unit-cell parameters $a = 44$, $b = 57$, $c = 61$ Å, $\beta = 96^\circ$. Diffraction data collected from native and SeMet-derivative crystals extended to resolutions of 1.8 and 2.6 Å, respectively.

1. Introduction

Haemophilus influenzae is an important respiratory pathogen that causes acute otitis media in children and exacerbates chronic, obstructive pulmonary disease (COPD; Murphy *et al.*, 2009). Adhesins are surface proteins of pathogens that are used not only for adherence to host cells but also to induce a pro-inflammatory response and thus communication between the host and the pathogen in question (Kline *et al.*, 2009). In recent years, some surface adhesins from *H. influenzae* have been suggested as vaccine candidates as they exhibit protective roles in experimental models (Murphy, 2009). These *Haemophilus* adhesins are multifunctional; in addition to their role in adhesion, some of them are transporters or transmembrane proteins or are secreted during infection of the host. There are 8–10 different surface proteins that have been identified to be adhesins (Murphy, 2009), but only the structures of *Haemophilus* surface fibril and its homologues Hia (Cotter *et al.*, 2005) and high-molecular-weight protein (HMW; Yeo *et al.*, 2007) have partially been determined. Recently, the structure of the *H. influenzae* adhesin protein HAP was revealed (Meng *et al.*, 2011). In general, structural information on adhesins has been useful in providing insights into the host–pathogen relationship.

We recently described the role of the hitherto unknown *H. influenzae* protein E (PE) in interacting with host epithelial cells and its involvement in subverting the host innate immune system. Protein E is a 16 kDa surface lipoprotein from *H. influenzae* that functions as an adhesin and induces a pro-inflammatory response during infection, leading to IL-8 secretion and up-regulation of ICAM-1 (CD54) in both cell lines and primary epithelial cells originating from patients with COPD. Interestingly, immunization of mice with the PE peptide 84–108 showed a protective role in pulmonary clearance (Ronander *et al.*, 2009). By using a detailed peptide-mapping approach, we have described several host protein-binding

regions in PE (Hallström *et al.*, 2009, 2011; Singh *et al.*, 2011). PE was found to be highly conserved among *Haemophilus* spp. and other members of the *Pasteurellaceae* family, with a sequence identity of 34.1–98.8% and a similarity of 55.3–100% (Singh *et al.*, 2010), and thus is likely to also function as an adhesin in other species of this family.

In this paper, we describe the expression of PE in *Escherichia coli* and its purification using various chromatographic steps. The conditions for crystallization were found by using commercial kits and an automated robotic system. A fine grid optimization yielded crystals of good diffracting quality. Since the natural protein does not contain methionine residues, a heavy-atom derivative search to solve the phase problem using MIR or MAD methods was started. This proved to be unsuccessful. To overcome the phasing problem, two methionine residues were introduced into the protein and the phase problem was solved using SeMet-labelled PE. Finally, data were collected to 1.8 Å resolution from native PE crystals and to 2.6 Å resolution from SeMet-labelled PE crystals. These data will be used to solve the structure of PE and will be extremely useful in elucidating the mode of interaction with host proteins.

2. Materials and methods

2.1. Selection of Met positions for phasing

Guidance for the selection of the amino acids to be substituted by methionine residues was obtained from the Dayhoff matrix as well as a putative protein fold based on prediction (Fig. 1). A secondary-structure prediction based on *JPred*3 (Cole *et al.*, 2008) and *PredictProtein* (Rost & Liu, 2003) was used to select low-penalty substitutions placed within secondary-structure elements. The presence of a Met residue in related sequences in a multi-sequence alignment by *ClustalW* was also taken into account.

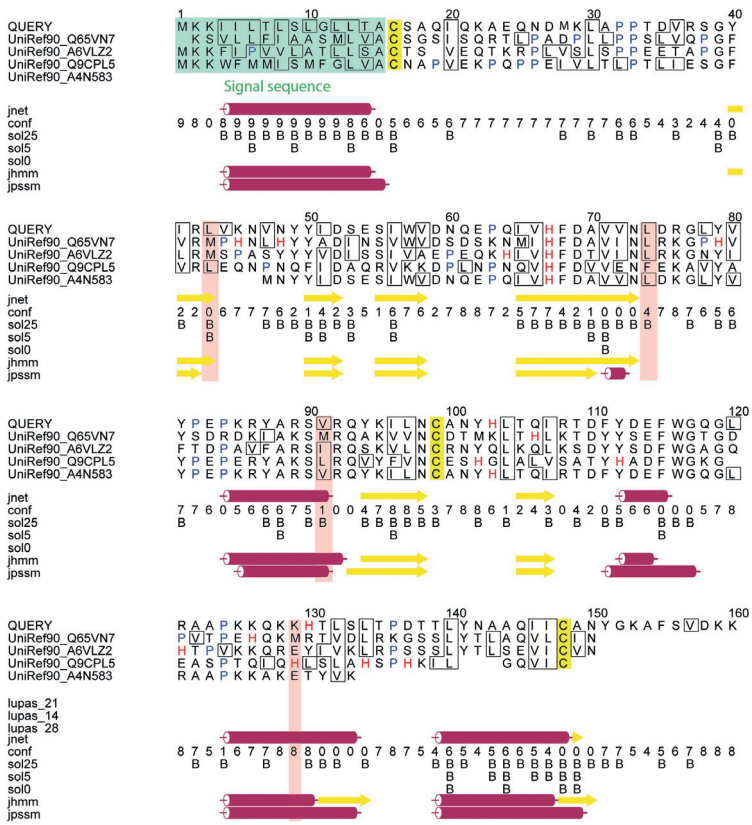

Figure 1
Plan of the site-directed mutagenesis of the PE molecule. The PE amino-acid sequence was analysed for secondary-structure-based alignment using the *JPred*3 software. PE homologues were compared to determine the availability of Met in their sequences. Possible mutations for the introduction of Met are highlighted in magenta at four positions. Leu43 is present as Met in other homologues of PE and thus was selected for mutation. Additionally, the conserved Leu74 residue was mutated to Met. In the alignment scheme, β-sheets are shown as yellow arrows and α-helices are shown as cylinders.

2.2. Construction of vectors, site-directed mutagenesis and expression of PE

The *H. influenzae* gene (HI0178) encoding PE has successfully been cloned and His-tagged PE has been expressed in our laboratory (Ronander *et al.*, 2009; Singh *et al.*, 2011). For crystallization, we produced PE without any tag. The *pe* gene encoding amino acids 17–158 (excluding the signal peptide) was amplified using PCR with the forward primer PE_For, 5′-GCCATGCATC**CATATG**TCTGCTCA-AATCCAAAAGGCTGAACAAAATGA-3′, and the reverse primer PE_Rev, 5′-CCC**GAATTC**TCAATCAACTGAAAATGCTTTACC-ATAATTTGCACA-3′ (*Nde*I and *Eco*RI restriction sites are shown in bold). The insert was ligated into pET26b that had been digested with *Nde*I and *Eco*RI followed by dephosphorylation. Finally, the sequenced and correct vector was transformed into *E. coli* BL21 (DE3). The purpose of this construct was to produce untagged PE in the cytoplasm, which resulted in the formation of inclusion bodies owing to protein misfolding. Purification of the inclusion bodies and protein refolding was performed to obtain optimally purified PE.

Residues Leu43 and Leu74 were mutated to methionine using a site-directed mutagenesis approach as described previously (Singh & Röhm, 2008; Singh *et al.*, 2011). The forward primer L43M_For, 5′-GCGGATATATACGT**A**TGGTAAAGAATGTG-3′, and the reverse primer L43M_Rev, 5′-CACATTCTTTACCA**T**ACGTATATATCC-GC-3′, were used to mutate Leu43 to Met; a subsequent second mutation was made in this template using the primers L74M_For, 5′-GCAGTGGTGAAT**A**T**G**GATAAGGGATTG-3′, and L74M_Rev, 5′-CAATCCCTTATC**CA**T**A**TTCACCACTGC-3′. The bases that were mutated are shown in bold. QuikChange site-directed mutagenesis was performed using high-fidelity *PfuTurbo* DNA polymerase (Stratagene, La Jolla, California, USA). Finally, the sequenced vector was transformed into *E. coli* 834 (DE3). For selenomethionine labelling of the PE^{L43M,L74M} variant, a SelenoMet Medium Base and SelenoMet Nutrient Mix expression-media kit (Molecular Dimensions, Athena Enzyme Systems, Baltimore, Maryland, USA) was used and solutions were prepared according to the manufacturer's instructions. For labelling, a single colony of *E. coli* 834 (DE3) containing pET26PE^{L43M,L74M} was grown overnight in 100 ml SelenoMet Medium supplemented with L-methionine containing 50 µg ml^{-1} kanamycin. Cells were spun down at 4000*g*, washed three times with 100 ml sterile water and resuspended in 5 ml sterile water. This culture was subsequently inoculated into 1 l pre-heated (310 K) SelenoMet Medium containing L-selenomethionine and grown for 2 h at 310 K with 200 rev min^{-1} shaking. The expression of protein was induced by the addition of 1 m*M* IPTG and further growth was performed for 6 h at 310 K with 200 rev min^{-1} shaking. Bacteria were harvested and resuspended in 25 ml PBS. The expression of unlabelled PE was performed using a routine laboratory protocol as described in Singh *et al.* (2011). In brief, a single colony of *E. coli* containing pET26bPE was inoculated into 5 ml LB containing 100 µg ml^{-1} kanamycin and incubated overnight at 310 K at 200 rev min^{-1}. Thereafter, the bacterial culture was transferred to 1 l fresh LB containing 50 µg ml^{-1} kanamycin and incubated at 310 K at 200 rev min^{-1} until the OD reached 1.0. Expression was induced by the addition of 1 m*M* IPTG followed by 6 h further incubation using the same conditions. Finally, the bacterial cells were harvested and resuspended in 25 ml PBS.

2.3. Inclusion-body preparation and refolding of PE

The bacterial cells were lysed mechanically by sonication (1 min cycle at 10×), keeping the samples in an ice bath. The DNA from the cell lysate was digested by the addition of 1 mg DNase I (Sigma, Missouri, USA) followed by incubation for 30 min at 310 K. The lysate was then centrifuged at 10 000*g* at 277 K for 20 min. The pellet, which consisted of inclusion bodies, was washed with 5 *M* urea and dissolved in 10 ml 8 *M* urea with constant stirring for 6 h at 277 K. The refolding of PE was performed by a dilution method, in which 10 ml PE (in 8 *M* urea) was added to 200 ml refolding buffer (50 m*M* Tris–HCl pH 7.8, 500 m*M* NaCl, 5 m*M* DTT, 0.005% Tween-20, 2 *M* urea) at 1 ml h^{-1} at room temperature. The refolded protein solution was centrifuged at 10 000*g* for 30 min at 277 K. The supernatant was dialysed against 50 m*M* Tris–HCl pH 7.8 containing 135 m*M* NaCl and 2 m*M* DTT. Finally, the dialysed PE solution was centrifuged at 10 000*g* for 30 min at 277 K to remove aggregated proteins. The supernatant containing folded PE was used in further purification steps.

2.4. Ion-exchange and gel filtration

Q-Sepharose Fast Flow anion-exchange resin (GE Healthcare Biosciences, Uppsala, Sweden) was packed into XK-16 glass columns (GE Healthcare Biosciences) attached to an ÄKTAprime plus FPLC system (GE Healthcare Biosciences). The column was washed with several volumes of degassed double-distilled H_2O and equilibrated with 50 m*M* Tris–HCl pH 7.8 buffer containing 135 m*M* NaCl and 2 m*M* DTT. The refolded PE solution was loaded onto the column at 0.5 ml min^{-1} using Superloop (GE Healthcare Biosciences). PE is a basic protein and did not interact with the anion-exchange resin, but other contaminant proteins bound to the resin. Therefore, the flow-through collected from the column was concentrated and used in the next purification step. The flowthrough was added to 500 m*M* NaCl and concentrated to 2–3 ml in volume using a 5000 Da molecular-weight cutoff Vivaspin concentrator (Sartorius Stedim Biotech, Göttingen, Germany). A Superdex 200 gel-filtration column (GE Healthcare Biosciences) was connected to the FPLC system and equilibrated with 50 m*M* Tris–HCl pH 7.5 buffer containing 500 m*M* NaCl and 2 m*M* DTT. Samples (250–300 µl) were injected and the proteins were separated at 0.5 ml min^{-1}. Fractions were collected at 1 ml and the purity of the proteins was assessed by SDS–PAGE stained with Coomassie Blue R250. Concentrations were measured using a Nanodrop spectrophotometer and the BCA method according to the manufacturer's recommendations (Pierce, Rockford, Illinois, USA).

2.5. Crystallization of proteins

For the production of native crystals, PE was finally concentrated to 10 mg ml^{-1} in gel-filtration buffer (50 m*M* Tris–HCl pH 7.5, 500 m*M* NaCl, 2 m*M* DTT). PACT Premier Screen, JCSG+, Structure Screens 1 and 2 (Molecular Dimensions, Newmarket, England), Crystal Screen and Crystal Screen 2 (Hampton Research, Aliso Viejo, California, USA) were used for initial screening. Drops consisting of 200 nl reservoir solution and 200 nl protein solution at a concentration of 5–10 mg ml^{-1} were produced using a Mosquito robot (TTP LabTech, Melbourn, England) in 96-well MRC plates at the MAX IV laboratory crystallization facility (Lund University, Sweden). The plates were stored at 298 K and photographed using a CrystalPro camera and the data were managed using *CrystalLims* software (both from TriTek Corporation, Sumerduck, Virginia, USA). PACT Premier kit condition A3, consisting of 100 m*M* SPG buffer pH 6.0, 25%(*w*/*v*) polyethylene glycol (PEG) 1500, produced small rod-shaped crystals. From the same kit, condition F3 [100 m*M* bis-tris propane pH 6.5, 200 m*M* NaI, 20%(*w*/*v*) PEG 3350] produced thin plate-like crystals. Additionally, Crystal Screen 2 condition No. 26 [100 m*M* MES pH 6.5, 200 m*M* ammonium sulfate, 30%(*w*/*v*) poly-

ethylene glycol monomethyl ether 5000] also produced thin plate-like crystals. Usually, all of these crystals appeared in drops after 3–4 d of setup. The conditions described above [100 m*M* SPG buffer and 25%(*w*/*v*) PEG 1500 or 100 m*M* bis-tris propane buffer, 200 m*M* NaI and 20%(*w*/*v*) PEG 3350] were used to reproduce crystals manually using the sitting-drop method. Single crystals were obtained that could be used for data collection.

SeMet PE^{L43M,L74M} did not produce crystals under the native PE crystallization conditions, so the four kits mentioned above were screened again to obtain initial conditions. PACT Premier condition B7 [100 m*M* MES pH 6, 200 m*M* NaCl, 20%(*w*/*v*) PEG 6000] and condition B8 [100 m*M* MES pH 6, 200 m*M* NH_4Cl, 20%(*w*/*v*) PEG 6000] produced microcrystals. The pH, salt and precipitant concentrations were optimized based on these conditions, but this did not improve the sizes of the crystals. Hence, microseeding was used to improve the crystal size. Microseeds were prepared using a Seed Bead kit (Hampton Research). In brief, 400 nl of a microcrystal-containing drop was mixed with 15 µl seed-crystal stabilizing solution [100 m*M* MES pH 6.0, 300 m*M* NaCl, 20%(*w*/*v*) PEG 6000], vortexed and dilutions were made according to the kit manual. Four different reservoir solutions, (i) 100 m*M* MES pH 6, 100 m*M* NH_4Cl, 20%(*w*/*v*) PEG 6000; (ii) 100 m*M* MES pH 6, 200 m*M* NH_4Cl, 20%(*w*/*v*) PEG 6000; (iii) 100 m*M* MES pH 6, 100 m*M* NaCl, 20%(*w*/*v*) PEG 6000 and (iv) 100 m*M* MES pH 6, 200 m*M* NaCl, 20%(*w*/*v*) PEG 6000, were pipetted into MRC 96-well plates in duplicate rows using a Freedom EVO 150 liquid-handling workstation (Tecan, Männedorf, Switzerland). Serial dilutions of seeds were made in up to eight steps. In each drop, 100 nl seed solution, 300 nl reservoir solution and 200 nl protein solution were pipetted using a Mosquito robot. Conditions (ii) and (iv) with seeds produced crystals of approximate dimensions 100 × 150 × 10 µm. These crystals were used to collect MAD data sets at the MAX IV Laboratory, Lund University, Sweden.

2.6. Data collection

Crystals were quickly cooled with a cryoprotectant solution in a mitotic loop using liquid nitrogen before exposing them to the X-ray beam. Several cryoprotectants such as glycerol, *m*-phenylenediamine (MPD) and PEG 400 were tried at different concentrations before a suitable one was identified. For native PE crystals, a universal cryosolution consisting of 32%(*w*/*v*) glycerol, 32%(*w*/*v*) ethylene, 36%(*w*/*v*) sucrose and 2%(*w*/*v*) glucose was used to flash-cool the crystals. This universal cryosolution was added in a 1:1 ratio to the protein drop before picking up crystals using a mitotic loop and placing them in a cryogenic N_2-gas stream. 15%(*w*/*v*) PEG 400 in the reservoir conditions acted as the best cryoprotectant for the SeMet PE crystals.

All crystal testing and data collection was performed at station I911-3 at the MAX IV Laboratory (Lund University, Sweden). The data were collected on a MAR 225 CCD detector (MAR Research, Germany) using an MD2 goniostat (Maatel, France). To obtain phase information to solve the structure of PE, three data sets, peak (PK), inflection point (IP) and remote (RM), were collected at the Se *K* edge (∼0.9795 Å) from the same SeMet-containing crystal (see Table 1 for data-collection details and statistics).

Data for PK and IP were collected first, with exposure times such that the influence of radiation damage on the phasing could be

Table 1
Data-processing and phasing statistics.

Values in parentheses are for the last shell.

	Native 1	SeMet PK	SeMet IP	SeMet RM
Space group	$P2_1$	$P2_1$	$P2_1$	$P2_1$
Unit-cell parameters				
a (Å)	44.2	44.1	44.1	44.1
b (Å)	57.3	56.9	56.9	56.9
c (Å)	61.4	61.4	61.4	61.4
β (°)	96.1	96.1	96.1	96.1
Wavelength (Å)	1.000	0.97918	0.97942	0.9700
Maximum resolution (Å)	1.8	2.6	2.7	2.3
Monomers in asymmetric unit	2	2	2	2
V_M (Å^3 Da^{-1})	2.28	2.26	2.26	2.26
Solvent content (%)	46.0	45.7	45.7	45.7
Total observations	115628	62016	60725	101090
Unique reflections	28219	17365	16137	26407
R_{merge} (%)	6.2 (45.7)	5.5 (20.2)	4.7 (15.7)	9.4 (50.4)
Completeness (%)	99.5 (98.6)	94.4 (68.2)	98.8 (94.3)	99.0 (95.1)
Average $I/\sigma(I)$	12.34 (2.64)	16.37 (4.19)	20.45 (6.76)	11.40 (2.85)
Phasing				
FOM	—			0.32
Phasing power (isomorphous)	—	—	0.713 (0.538)	0.331 (0.253)
Phasing power (anomalous)	—	1.079	1.050	0.416
Cullis *R* factor (isomorphous)	—	—	0.617 (0.642)	0.899 (0.976)
Cullis *R* factor (anomalous)	—	0.843	0.826	0.958

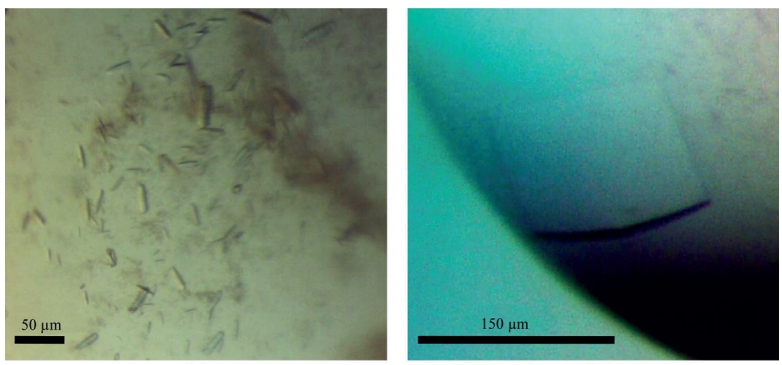

(*a*) (*b*)

Figure 2
Native and SeMet PE crystals grown under different conditions. (*a*) Native PE (5 mg ml^{-1}) produced rod-shaped crystals of approximately 10 × 20 × 50 µm in size using 100 m*M* SPG buffer pH 6.0, 25%(*w*/*v*) PEG 1500. (*b*) An SeMet PE crystal (100 × 150 × 10 µm) obtained after microseeding in a solution consisting of 100 m*M* MES pH 6, 200 m*M* NH_4Cl with 20%(*w*/*v*) PEG 6000.

minimized; however, the data for RM were collected with longer exposure times in order to obtain reliable data out to the diffraction limit of the crystals (see Table 1). All data were integrated and scaled using *XDS* (Kabsch, 2010). A first impression of the phasing power was obtained using *HKL2MAP* (Pape & Schneider, 2004), which provides a graphical interface to a set of programs from the *SHELX* suite (Sheldrick, 2008). Six of the eight possible Se positions could be identified using Patterson methods in *SHELXC*. Subsequent refinement and phasing of the structure was achieved with *autoSHARP* (Vonrhein *et al.*, 2007) using data from all three data sets.

3. Results and discussion

We expressed and purified native and SeMet PE 17–158 without any tag with a high purity suitable for crystallization. Approximately 1 l *E. coli* culture yielded 50–60 mg purified protein after ion-exchange and gel-filtration chromatography. The majority of PE was obtained in a dimeric form, while a minor fraction was oligomeric (data not shown). The protein purity was >98% pure as judged by SDS–PAGE. PE was stable at 253 K for more than a year and successfully produced crystals. Different expression, purification and storage batches did not alter the crystallization behaviour of the protein. The results obtained here were thus reproducible. The homogeneity and multimeric association of each protein-preparation batch was further confirmed by dynamic light-scattering (DLS) experiments before proceeding to crystallization experiments. The DLS data also suggested that >85% of PE was present as a dimer, while ∼15% was oligomeric (data not shown).

In order to solve the phase problem, Met residues were introduced (Fig. 1). For success, it was important that the point mutation in the PE molecule did not produce any constraint on the PE molecule and that the structures of the native and the SeMet variant were very similar. The positions of possible mutations were carefully analyzed. A Met residue favours a nonpolar environment in the core of the protein and thus a choice was made both on the mutability and the position of the residues in possible secondary-structure elements. The resulting SeMet PE behaved almost identically to native PE and existed with the majority in a dimeric form.

During screening, two different conditions produced high-quality native PE crystals: (i) 100 m*M* SPG buffer pH 6.0, 25%(*w*/*v*) PEG 1500 and (ii) 100 m*M* bis-tris propane pH 6.5, 200 m*M* NaI and 20%(*w*/*v*) PEG 3350. The first condition produced small rod-shaped crystals with approximately dimensions 10 × 20 × 50 µm (Fig. 2*a*) and after fine-tuning of the conditions produced plate-like crystals with approximate dimensions 100 × 150 × 10 µm. Data sets were collected from both crystal forms and despite their smaller size the rod-shaped crystals (Fig. 2*a*) diffracted as well as the larger plate-shaped crystals. The space groups and details of the data sets are described in Table 1. Finding a suitable cryosolution for the native PE crystals was critical and challenging, since the crystals were easily damaged and the diffraction pattern compromised. After a search for appropriate cryoconditions, the universal cryosolution 32%(*w*/*v*) glycerol, 32%(*w*/*v*) ethylene, 36%(*w*/*v*) sucrose and 2%(*w*/*v*) glucose gave the best results when applied in a 1:2 ratio to the protein drop in which the crystals appeared.

SeMet PE crystals were produced under different conditions and the size of the crystals was improved using the microseeding technique. Two conditions generated SeMet PE crystals: (i) 100 m*M* MES pH 6, 200 m*M* NH_4Cl, 20% PEG 6000 and (ii) 100 m*M* MES pH 6, 200 m*M* NaCl, 20% PEG 6000. These crystals were small in size and were not useful for diffraction. In order to proceed, these microcrystals were used for seed preparation; serially diluted seeds were added to new fresh drops of conditions (i) and (ii). Of these two conditions, 100 m*M* MES pH 6, 200 m*M* NH_4Cl with 20% PEG 6000 produced large plate-like crystals with final dimensions of approximately 100 × 150 × 10 µm (Fig. 2*b*). Before proceeding to X-ray exposure, SeMet PE crystals were soaked in reservoir-condition solution supplemented with 15%(*w*/*v*) PEG 400 as a cryoprotectant. We collected full data sets from a single SeMet PE crystal at the peak (PK), inflection-point (IP) and remote (RM) wavelengths of the Se *K* edge, with the RM data set extending to the diffraction limit of 2.3 Å, while taking care that no major radiation damage occurred during the collection of the first two data sets that could hinder the subsequent phase determination. Therefore, the first two data sets (PK and IP) extended to only 2.6–2.7 Å resolution, while the RM data set, which was collected last with longer exposure times, extended to 2.3 Å resolution. The three data sets collected for this MAD data set were used to obtain the positions of the Se atoms in the structure in Patterson functions and to subsequently solve the structure. During data processing and subsequent calculations for phasing, the PK data set was used as a reference set. Six out of eight positions were found using Patterson searches in *SHELXC*. Using the data set from the rod-shaped crystals (native 1), we managed to extend the PE atomic structure to 1.8 Å resolution, which allowed us to obtain a reliable model of the structure of PE.

The authors report no potential conflicts of interest. This work was supported by grants from the Alfred Österlund, the Anna and Edwin Berger, the Greta and Johan Kock, the Janne Elgqvist, the Gyllenstiernska Krapperup and the Lars Hierta Memorial Foundations, the Swedish Medical Research Council, the Cancer Foundation at the University Hospital in Malmö and Skåne County Council's research and development foundation. The personnel of the I911-3 beamline and the protein crystallization facility of the MAX IV Laboratory are thanked for their help and assistance.

References

Cole, C., Barber, J. D. & Barton, G. J. (2008). *Nucleic Acids Res.* **36**, W197–W201.
Cotter, S. E., Yeo, H.-J., Juehne, T. & St Geme, J. W. III (2005). *J. Bacteriol.* **187**, 4656–4664.
Hallström, T., Blom, A. M., Zipfel, P. F. & Riesbeck, K. (2009). *J. Immunol.* **183**, 2593–2601.
Hallström, T., Singh, B., Resman, F., Blom, A. M., Mörgelin, M. & Riesbeck, K. (2011). *J. Infect. Dis.* **204**, 1065–1074.
Kabsch, W. (2010). *Acta Cryst.* D**66**, 133–144.
Kline, K. A., Falker, S., Dahlberg, S., Normark, S. & Henriques-Normark, B. (2009). *Cell Host Microbe*, **5**, 580–592.
Meng, G., Spahich, N., Kenjale, R., Waksman, G. & St Geme, J. W. III (2011). *EMBO J.* **30**, 3864–3874.
Murphy, T. F. (2009). *Curr. Infect. Dis. Rep.* **11**, 177–182.
Murphy, T. F., Faden, H., Bakaletz, L. O., Kyd, J. M., Forsgren, A., Campos, J., Virji, M. & Pelton, S. I. (2009). *Pediatr. Infect. Dis. J.* **28**, 43–48.
Pape, T. & Schneider, T. R. (2004). *J. Appl. Cryst.* **37**, 843–844.
Ronander, E., Brant, M., Eriksson, E., Mörgelin, M., Hallgren, O., Westergren-Thorsson, G., Forsgren, A. & Riesbeck, K. (2009). *J. Infect. Dis.* **199**, 522–531.
Rost, B. & Liu, J. (2003). *Nucleic Acids Res.* **31**, 3300–3304.
Sheldrick, G. M. (2008). *Acta Cryst.* A**64**, 112–122.
Singh, B., Brant, M., Kilian, M., Hallström, B. & Riesbeck, K. (2010). *J. Infect. Dis.* **201**, 414–419.
Singh, B., Jalalvand, F., Mörgelin, M., Zipfel, P., Blom, A. M. & Riesbeck, K. (2011). *Mol. Microbiol.* **81**, 80–98.
Singh, B. & Röhm, K. H. (2008). *Biol. Chem.* **389**, 33–36.
Vonrhein, C., Blanc, E., Roversi, P. & Bricogne, G. (2007). *Methods Mol. Biol.* **364**, 215–230.
Yeo, H.-J., Yokoyama, T., Walkiewicz, K., Kim, Y., Grass, S. & St Geme, J. W. III (2007). *J. Biol. Chem.* **282**, 31076–31084.

Paper II

IAI
Journals.ASM.org

The Unique Structure of *Haemophilus influenzae* Protein E Reveals Multiple Binding Sites for Host Factors

Birendra Singh,[a] Tamim Al-Jubair,[a] Matthias Mörgelin,[b] Marjolein M. Thunnissen,[c] Kristian Riesbeck[a]

Medical Microbiology, Department of Laboratory Medicine Malmö, Lund University, Skåne University Hospital, Malmö, Sweden[a]; Section of Clinical and Experimental Infectious Medicine, Department of Clinical Sciences, Lund University, Lund, Sweden[b]; Centre of Molecular Protein Science, Lund University, Lund, Sweden[c]

***Haemophilus influenzae* protein E (PE) is a multifunctional adhesin involved in direct interactions with lung epithelial cells and host proteins, including plasminogen and the extracellular matrix proteins vitronectin and laminin. We recently crystallized PE and successfully collected X-ray diffraction data at 1.8 Å. Here, we solved the structure of a recombinant version of PE and analyzed different functional regions. It is a dimer in solution and in the asymmetric unit of the crystals. The dimer has a structure that resembles a flattened β-barrel. It is, however, not a true β-barrel, as there are differences in both the hydrogen-bonding pattern and the shape. Each monomer consisted of a 6-stranded antiparallel β-sheet with a rigid α-helix at the C terminus tethered to the concave side of the sheet by a disulfide bridge. The laminin/plasminogen binding region (residues 41 to 68) is exposed, while the vitronectin binding region (residues 84 to 108) is partially accessible in the dimer. The dimerized PE explains the simultaneous interaction with laminin and vitronectin. In addition, we found this unique adhesin to be present in many bacterial genera of the family *Pasteurellaceae* and also orthologues in other, unrelated species (*Enterobacter cloacae* and *Listeria monocytogenes*). Peptides corresponding to the surface-exposed regions PE 24 to 37, PE 74 to 89, and PE 134 to 156 were immunogenic in the mouse. Importantly, these peptide-based antibodies also recognized PE at the bacterial surface. Taken together, our detailed structure of PE explains how this important virulence factor of *H. influenzae* simultaneously interacts with host vitronectin, laminin, or plasminogen, promoting bacterial pathogenesis.**

Haemophilus influenzae is an important Gram-negative respiratory pathogen that causes, for example, acute otitis media in children and exacerbations in patients with chronic obstructive pulmonary disease (COPD), but also invasive diseases, such as meningitis and sepsis (1). Encapsulated *H. influenzae* is categorized into six different serotypes, a to f, whereas the remaining noncapsulated *H. influenzae* is designated nontypeable *H. influenzae* (NTHI) (2). *H. influenzae* resides in the mucosa, and NTHI is mainly associated with infections in the respiratory tract, whereas encapsulated *H. influenzae*, including *H. influenzae* type b (Hib), causes invasive disease. Until the 1990s, Hib was the most common serotype, but a dramatic reduction in Hib cases was observed after the introduction of a conjugate vaccine against Hib. However, an increasing incidence of invasive disease caused by nontype b *H. influenzae* has recently been reported from several countries (2–4).

In contrast to the very efficient vaccine against Hib, no suitable vaccine has been implemented for NTHI. Lipopolysaccharide (LPS) and surface-exposed antigenic proteins of Gram-negative pathogens are generally predicted to be putative starting points for screening of suitable vaccine candidates (5). However, not all surface proteins or LPS are suitable for eliciting protection in the host against a particular pathogen. In recent years, several surface adhesin proteins, including HMW-1 and -2 (6), PilA (7), P6 (8), and protein D (9), have been analyzed for their vaccine potential. Some of these NTHI surface proteins showed initial protection in experimental models, and protein D is now included in the vaccine Synflorix, giving partial protection against *H. influenzae* in humans (10, 11). Structural data are, however, available for only a few of these vaccine candidates.

We have described the role of a hitherto unknown *H. influenzae* protein E (PE) in interactions with host epithelial cells and in subversion of the host innate immune response (12). Protein E is a 16-kDa surface lipoprotein of *H. influenzae* that functions as an adhesin and induces a proinflammatory response during infection, leading to interleukin 8 (IL-8) secretion and upregulation of ICAM-1 (CD54) in both cell lines and primary epithelial cells originating from patients with COPD. An isogenic *pe* mutant showed defective adhesion and internalization of host epithelial cells. Furthermore, by using a peptide-mapping approach, we suggested that the amino acid region 84 to 108 is involved in binding to epithelial cells. Importantly, immunization with the PE amino acid (aa) 84 to 108 peptide showed significantly better pulmonary clearance in a mouse model than immunization with an unrelated control peptide (12). When the *pe* gene was sequenced in all *Haemophilus* spp., including Hib and NTHI clinical isolates, we found that PE is a ubiquitous *Haemophilus* outer membrane protein (13). The active vitronectin-binding region PE aa 84 to 106 was found to be 100% conserved. PE homologues were also present in other members of the family *Pasteurellaceae*, including *Aggregatibacter* spp., *Actinobacillus* spp., *Mannheimia succiniciproducens*, and *Pasteurella multocida* (13).

Vitronectin (Vn) and laminin (Ln) are among other proteins found in the extracellular matrix (ECM) (14, 15). In addition, Vn

Received 15 October 2012 **Returned for modification** 21 November 2012
Accepted 18 December 2012
Published ahead of print 28 December 2012
Editor: B. A. McCormick
Address correspondence to Kristian Riesbeck, kristian.riesbeck@med.lu.se.
Supplemental material for this article may be found at http://dx.doi.org/10.1128/IAI.01111-12.

doi:10.1128/IAI.01111-12

plays a crucial role in maintaining homeostasis in the regulation of the complement system, i.e., the innate immunity. We recently observed that NTHI binds Vn via surface-exposed PE and that this interaction leads to increased serum resistance. The peptide region covered by amino acids 84 to 108 is the Vn interaction domain (14–16), and further analysis revealed that in particular, the residues K85 and R86 are involved in Vn binding (17). In addition to the PE-dependent Vn binding, we observed that the region comprising PE amino acids 41 to 68 interacts with Ln, an abundant ECM protein in the basement membrane, and that this interaction leads to better adhesion of NTHI to host tissues (18). Interestingly, the Ln and Vn binding sites on the PE molecule are completely separate and do not interfere with each other during binding. The outer membrane PE thus both functions as an adhesin and concurrently protects bacteria from complement-mediated killing (18). More recently, we observed that PE also binds plasminogen, which is ultimately converted into plasmin, and this consequently leads to degradation of complement 3 (C3) and dampening of the host innate response (19).

We recently published a technical report on crystallization data for a recombinant variant PE and an Se-methionine-labeled PE (SeMet PE) (20). In the present study, the X-ray diffraction data at 1.8-Å resolution were analyzed in detail to obtain the structure of PE. Based upon the crystal, we show that the PE molecule is a dimer in the asymmetric unit. The structure of the monomer contained six antiparallel β-sheets connected with loops. At the C-terminal end, a rigid α-helix was found that was fixed in its position by a disulfide bond to the top of the β-sheet. The laminin and plasminogen binding regions of PE were exposed at the surface of the molecule, while the Vn binding region, previously defined by a peptide-mapping approach, was partially exposed. Furthermore, we used structure-based selection of the exposed regions to verify their localizations and respective immunogenicities by raising antibodies in mice. These structural findings provide insight into the regions that are involved in interactions with host proteins and a possible mode of PE-mediated host interaction by *H. influenzae*.

MATERIALS AND METHODS

Protein expression, purification, and crystallization. PE and SeMet PE were recombinantly expressed in *Escherichia coli* as inclusion bodies, and purification was performed as described previously (20). In brief, *E. coli* BL21(DE3) harboring plasmids encoding PE and SeMet PE were grown in 1 liter LB with 50 μg/ml kanamycin, and protein expression was induced by addition of 1 mM IPTG (isopropyl-β-D-thiogalactopyranoside). The cells were lysed by sonication, and inclusion bodies were collected by centrifugation. The inclusion bodies were washed with 5 M urea and dissolved in 10 ml of 8 M urea. Refolding of PE was performed by the dilution method in refolding buffer containing 50 mM Tris-HCl, pH 7.8, 500 mM NaCl, 5 mM dithiothreitol (DTT), 0.005% Tween 20, and 2 M urea. The refolded proteins were dialyzed against 50 mM Tris-HCl, pH 7.8, buffer containing 135 mM NaCl and loaded into a Q-Sepharose Fast Flow anion-exchange column (GE Healthcare Biosciences, Uppsala, Sweden) equilibrated with 50 mM Tris-HCl, pH 7.8, buffer containing 135 mM NaCl and 2 mM DTT. The flowthrough of the column that contained PE was collected and further purified with a Superdex 200 gel filtration column (GE Healthcare Biosciences) equilibrated with 50 mM Tris-HCl, pH 7.5, buffer containing 500 mM NaCl and 2 mM DTT (20). The protein purity was estimated by SDS-PAGE, and concentrations were measured with a Nano-Drop spectrophotometer.

The recombinant variant of PE and SeMet PE were concentrated up to 5 mg/ml. The crystallization conditions were screened by using commercial kits as described elsewhere (20). Crystals of the recombinant variant PE were obtained in 100 mM sucrose-phosphate-glutamic acid (SPG) buffer, pH 6.0, 25% (wt/vol) polyethylene glycol (PEG) 1500. The SeMet PE produced crystals in 100 mM MES (morpholineethanesulfonic acid), pH 6, 200 mM NaCl, and 20% PEG 6000. The size of the SeMet PE crystals was further improved by using the microseeding technique. Both PE proteins produced crystals within 4 to 5 days of incubation at 25°C. Details of the crystallization strategies were published previously (20).

Data collection and refinement. Crystals were quickly cooled in the presence of a cryoprotectant solution in a MiTeGen loop (Ithaca, NY) using a stream of nitrogen gas at 100 K before exposing them to the X-ray beam. The universal cryosolution, containing 32% (wt/vol) glycerol, 32% (wt/vol) ethylene, 36% (wt/vol) sucrose, and 2% glucose, was used for the recombinant variant PE crystals. Suitable crystals were incubated in drops of mother liquor to which an equal volume of the cryosolution was added. After about 30 s of incubation, they were mounted in loops and placed in a cryogenic N_2 gas stream at 100 K. In contrast to the cryoconditions for the recombinant variant PE crystals, 15% (wt/vol) PEG 400 in reservoir solution was used for SeMet PE crystals. All data collections were performed at station I911-3 at the MAX IV Laboratory (Lund University, Sweden). The station was equipped with an MD2 goniostat (Maatel, France) and a MAR225 charge-coupled-device (CCD) detector (Marresearch, Norderstedt, Germany).

To obtain reliable phase information, three data sets, peak (PK), point of inflection (PI), and remote (RM), were collected at the K edge of selenium (around 0.9795 Å) from the same SeMet-containing crystal (Table 1 shows data collection details and statistics). Data for PK and PI sets were collected first, with reduced exposure times, so that the influence of radiation damage on the phasing could be minimized. The data for RM, however, were collected with longer exposure times in order to obtain data to the diffraction limit of the crystals (Table 1). All data were integrated and scaled using the program XDS (21). The phasing power was monitored by using HKL2MAP (22), a graphical interface to a set of programs from the SHELX suite. Six of the 8 possible Se positions could be identified using Patterson methods in SHELXC (23). Subsequent refinement and phasing of the structure was achieved by using autoSHARP (24), using data from all 3 data sets.

autoSHARP built 246 residues out of 282 possible using ARP/wARP (25). The model was inspected using Coot (26), and subsequent rounds of refinement and model building were performed by using the PHENIX package (27) and Coot. In total, 130 residues for each chain could be traced, with 10 residues missing at the N terminus and 1 residue at the C-terminal end of each of the protein chains. During refinement, an additional 127 water molecules were added to the model. The final model had good stereochemistry (the root mean square deviation [RMSD] from ideal geometry in bonds was 0.017 Å and in angle was 1.65°), and 97.3% of the residues were in the most favored part of the Ramachandran plot.

Data for the two different crystal forms of the recombinant variant PE were also collected. XDS was used for data processing and scaling (Table 1). The solvent content of the 2nd type of crystals was relatively low (around 30%), which probably was the reason for the diffracting power of these crystals. Both crystal forms were monoclinic, and details of the different data sets are described in Table 1. The structure of the SeMet mutant form of PE was used as a starting model in molecular replacement using Phaser (28) for the first crystal form. For the 2nd crystal form of the recombinant variant PE protein, the first form was used as a search model and Phaser was used for the molecular replacement. Both structures were refined using TLS refinement within the Phenix suite, and model inspection was performed using Coot. During refinement, difference density indicated the presence of ethylene and glycerol molecules from the cryosolutions, and they were placed accordingly.

Immunization of mice. Based upon the crystal structure of the PE, peptides were designed for immunization and conjugated with keyhole limpet hemocyanin (KLH) (Innovagen AB, Lund, Sweden). Mice (BALB/c; 6 in each group) were immunized with KLH-conjugated peptides according to a standard immunization protocol (12). In brief, 50 μg

TABLE 1 Data processing, phasing, and refinement statistics

Parameter[a]	Value				
	PE 1	PE 2	SeMet peak	SeMet inf	SeMet rem
Space group	$P2_1$	$P2_1$	$P2_1$	$P2_1$	$P2_1$
a (Å)	44.2	54.7	44.1	44.1	44.1
b (Å)	57.3	42.5	56.9	56.9	56.9
c (Å)	61.4	56.8	61.4	61.4	61.4
β (°)	96.05	116.3	97.1	97.1	97.1
Wavelength (Å)	1.000	1.000	0.97918	0.97942	0.9700
Maximum resolution (Å)	1.8	2.1	2.6	2.7	2.3
$V_{Matthews}$ (Da/Å^3) dimer in asymmetric unit	2.28	1.75	2.26	2.26	2.26
Solvent content (%)	46.0	29.7	45.7	45.7	45.7
Total no. of observations	115,628	32,032	62,016	60,725	101,090
No. of unique reflections	28,219	12,867	17,365	16,137	26,407
R_{merge} (%)	6.2 (45.7)	5.6 (45.9)	5.5 (20.2)	4.7 (15.7)	9.4 (50.4)
Completeness (%)	99.5 (98.6)	91.4 (79.8)	94.4 (68.2)	98.8 (94.3)	99.0 (95.1)
Avg $(I)/(\Sigma I)$	12.34 (2.64)	11.94 (2.03)	16.37 (4.19)	20.45 (6.76)	11.40 (2.85)
Multiplicity	4.09	2.49	3.57	3.76	3.83
Phasing					
Figure of merit					0.32
Phasing power					
Isomorphous			0	0.713 (0.538)	0.331 (0.253)
Anomalous			1.079	1.050	0.416
Cullis R factor					
Isomorphous			0	0.617 (0.642)	0.899 (0.976)
Anomalous			0.843	0.826	0.958
Refinement					
Refinement range (Å)	29–1.8	28–2.1			29–2.3
R_{crys} (%)	20.07	18.17			18.68
R_{free} (%)	23.10	24.46			25.49
No. of water molecules	127	50			119
Other	3 GOL, 2 EDO	1 GOL, 2 EDO			
RMSD bond length (Å)	0.013	0.07			0.009
RMSD angle (°)	1.498	1.055			1.208
Favorable region	99.2	98.4			98.1
Additional allowed region	0.8	1.6			1.9
Disallowed	0	0			0

[a] RMSD, root mean square difference.

peptide with complete Freund's adjuvant was subcutaneously administered. After 4 weeks, booster doses of 50 μg peptide with aluminum hydroxide were injected over the following 3 weeks. Blood was drawn 1 week after the last booster dose, and specific antibodies (Abs) were immunopurified using the same peptide, followed by testing in sandwich enzyme-linked immunosorbent assays (ELISAs) against the various peptides or recombinant PE. The animal experiments were done according to the general rules established by the Swedish Government (Svensk författnings-samling 1988:534 and Ändringsförfattning 2012: 256; Riksdagen, Stockholm, Sweden). An ethics permit (no. M193-11) was obtained from Malmö/Lund District Court (Djurförsöksetiska nämnden, Tingsrätten, Lund, Sweden). This body approved the protocol used in the study.

ELISA. Ninety-six-well PolySorb microtiter plates (Nunc-Immuno, Roskilde, Denmark) were coated with PE peptides or recombinant PE 22 to 160 (100 ng) in 100 μl of 100 mM Tris-HCl, pH 9.0, for 15 h at 4°C. The coated plates were washed 3 times with phosphate-buffered saline (PBS) and blocked with 2.5% bovine serum albumin (BSA) in PBS containing 0.05% Tween 20 (PBST). Serum or purified antibodies in 2.5% BSA plus PBST were added to the wells and allowed to bind for 1 h at room temperature. After washes with PBST, horseradish peroxidase (HRP)-conjugated rabbit anti-mouse polyclonal Ab (PAb) (Dako, Denmark) were added in 2.5% BSA plus PBST. Finally, the plates were washed 4 times with PBST and developed with HRP substrate containing 20 mM tetramethylbenzidine and 0.1 M potassium citrate. After color development, the reactions were terminated with 1 M H_2SO_4, and finally, the plates were read at 450 nm in a microplate reader.

Flow cytometry. NTHI 3655 (12) from overnight cultures was grown in broth to an optical density at 600 nm (OD_{600}) of 0.8. Thereafter, the bacteria were washed twice with PBS containing 1% BSA and incubated with purified mouse anti-PE peptide antiserum according to a standard protocol. After washing, the bacteria were incubated with fluorescein isothiocyanate (FITC)-conjugated secondary rabbit-anti-mouse PAbs (Dako Sweden, Stockholm, Sweden) followed by two washes and then flow cytometry analysis (Epics XL-MCL; Coulter, Hialeah, FL).

Dynamic light scattering and electron microscopy. Dynamic-light-scattering (DLS) experiments were performed by using a Zetasizer Nano ZS (Malvern Instruments, Worcestershire, United Kingdom). Different concentrations of PE (1 mg/ml, 3 mg/ml, and 5 mg/ml) were used to collect data in triplicate, and mean values were plotted. We used negative staining and transmission electron microscopy (TEM) to visualize the PE molecules, as described elsewhere (29).

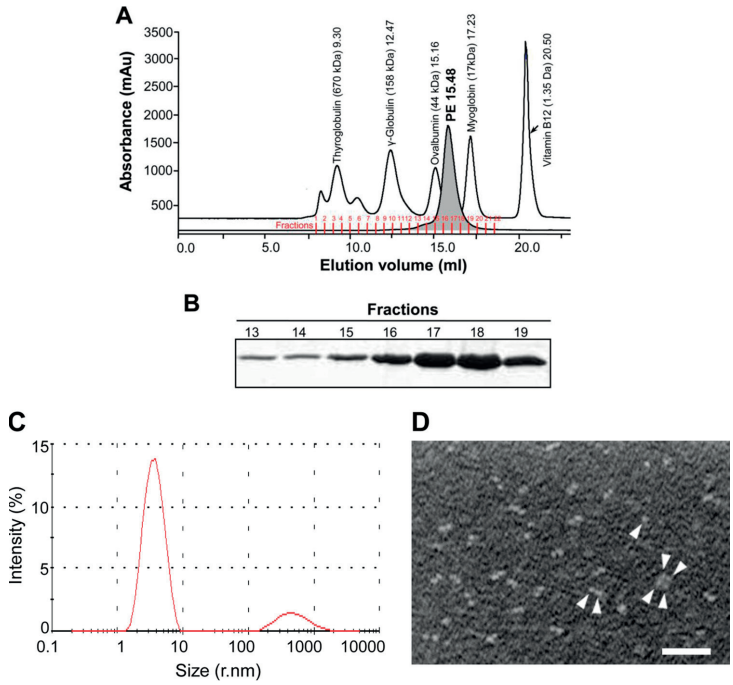

FIG 1 Purification of recombinant PE. (A) The gel filtration profile of the recombinant variant PE (approximately 2 mg protein purified by anion exchange as described in Materials and Methods) was injected into an equilibrated Superdex 200 column. The separation chromatogram of PE is shown, along with a standard molecular weight filtration marker. mAu, milliabsorbance unit. (B) Fractions collected from panel A were separated using 12% SDS-PAGE, followed by staining with Coomassie blue R250. A similar gel filtration profile and purity pattern were also observed with SeMet PE (data not shown). (C) DLS pattern of the recombinant variant PE purified by gel filtration. (D) Transmission electron microscopy showing PE molecules (arrowheads). Bar, 100 nM.

Protein structure accession numbers. All coordinates and structure factors for the different models were submitted to the Protein Data Bank (PDB) with codes 3zh6 for the SeMet mutant, 3zh5 for the recombinant PE variant PE 1, and 3zh7 for the recombinant PE variant PE 2.

RESULTS

Protein E is a dimer. The gel filtration profile showed that the majority (>85%) of recombinant PE molecules existed as dimers in solution, whereas only a minor fraction consisted of an oligomeric form under these conditions (Fig. 1A and B). The pooled fractions 13 to 18 in Fig. 1A were also analyzed by dynamic light scattering. These experiments confirmed that approximately 85% of PE that eluted as a single peak represented dimers, whereas the minor peak containing the remaining 10 to 15% represented tetramers (Fig. 1C). In addition, TEM (negative staining) of recombinant PE also verified that >85% of PE existed in dimers, with a minor fraction as tetramers and a few monomers (Fig. 1D). Taken together, these results clearly indicated that PE is a dimer.

When the crystal structure was determined, we found that PE is also present as a dimer in the asymmetric unit. Each PE monomer consists of a β-sheet formed by 6 antiparallel β-strands (β1, residues 39 to 43; β2, 46 to 59; β3, 64 to 78; β4, 88 to 99; β5, 102 to 114; β6a, 118 to 122; and β6b, 130 to 134) (Fig. 2A). In addition, a longer α-helix (residues 138 to 151) packs on the concave face of the sheet (Fig. 2B), and strands β1, β2, and β3 are curved around it. Strand β6 consists of two shorter strands, β6a and β6b, interrupted by a short loop from residues 123 to 129. After the loop, β2b lines up to strand β3, and proper hydrogen bond interactions for a sheet are formed. The edge of the sheet is formed by strand β1 and part of strand β2 at one side and strands β6a and β6b at the other side. The α-helix is tethered to the β-sheet through a conserved disulfide bond between cysteine residues 99 and 148. This disulfide bond connects the top of the central strand of the β-sheet and one end of the α-helix. The α-helix shields the upper half of the concave β-sheet, and in particular, the part formed by strands β1, β2, β3, and partly β4 is protected from solvent by the helix while the remaining part of the face is exposed.

The convex side of the sheet is not protected by other structural elements in the PE monomer. However, the two monomers in the asymmetric unit pack together through the convex side of each of their β-sheets to form a nearly continuous antiparallel β-sheet that resembles a flattened barrel-like dimer structure. The dimer formations are nearly identical in the different crystal forms presented. The resulting dimer is 55 Å by 44 Å by 25 Å in size (Fig. 3A and B). The barrel has a wedge-like shape, with the top narrower

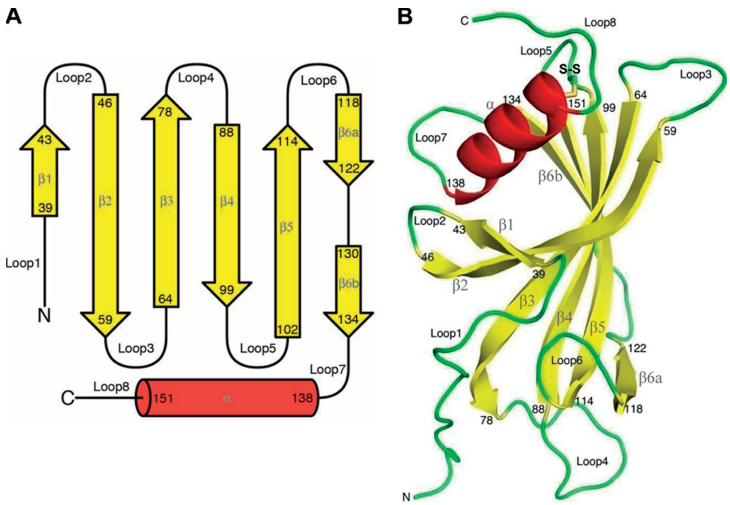

FIG 2 Secondary-structure elements and the PE monomer. (A) PE 28 to 159 amino acids showing the secondary structure. In total, 6 β-strands, 8 loops, and one C-terminal helix exist. (B) In the monomer, 6 antiparallel β-strands form the β-sheet. A longer α-helix packs on the concave face of the sheet, where strands β1, β2, and β3 are curved around it. It is tethered to the β-sheet through a conserved disulfide bond between cysteines 99 and 148.

than the bottom. Loops connecting the β-strands at the top of the barrel (Fig. 2, loops 3, 5, and 7) are smaller than the loops found at the bottom of the barrel (loops 1, 2, 4, and 6). No electron density for amino acids 17 to 27 (before loop 1) of PE could be observed in the crystal structure, and hence, they are not modeled. At each side of the barrel, strand β6b from one monomer and the end of strand β2 and loop 3 from another monomer lined up to close the barrel (Fig. 4A), with similar interactions between the two monomers at each side of the barrel. The interactions between these two segments are not through main-chain atom hydrogen bonding inter-

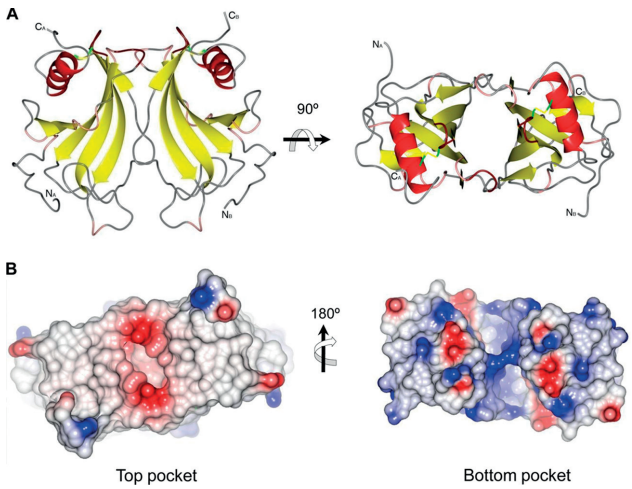

FIG 3 The PE dimer. (A) Cartoon representation of the PE dimer. (B) Surface of the PE dimer shown from the top and bottom cavities, in addition to the charge distribution of the molecule. The top surface of the molecule is neutral in charge, whereas the bottom side of the dimer is basic. The positive and negative charges are shown in blue and red, respectively.

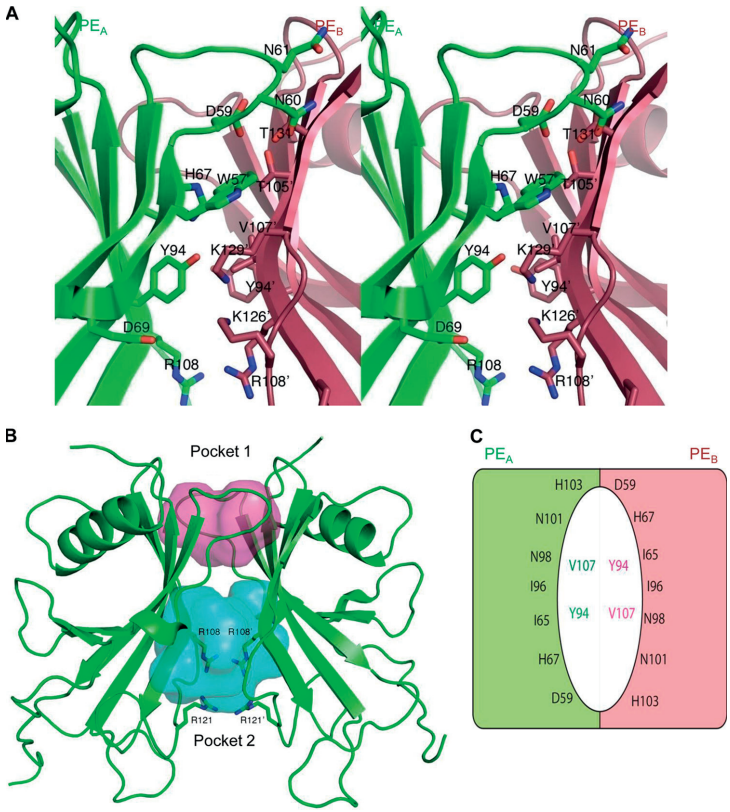

FIG 4 Dimer interface and PE internal cavities. (A) Stereoview showing side chains in the loop from residues 52 to 61 from one monomer (green A) to main-chain atoms in the strand β6b in the other monomer (red B). Two central residues are AsnA60 and TrpA57. The Nδ2 of AsnA60 forms a hydrogen bond with the backbone oxygen of ThrB131, and Oδ1 makes a hydrogen bond with the backbone nitrogen from the same ThrB131. The side chain of TrpA57 occupies a hydrophobic pocket formed by the aliphatic part of the side chain of Lys B129, the methyl moiety of Thr B105, and the side chain of His A67. The Nε1 of TrpA57 makes a hydrogen bond with the backbone oxygen of LysB129. Other interactions are formed between AspA59 and ThrB131, Gln A61, and Ser133. Tyr A94 from strand β4 completes the main interactions through a hydrogen bond to the Nz of Lys B129. (B) Top and bottom pockets of the dimer (red and blue, respectively). The side chains of Arg108 and Arg121 in each monomer are shown. (C) Schematic drawing of the residues lining the walls of the top pocket of the dimer. The colored halves represent the two monomers, and the colored residues inside the pocket are located at the bottom wall of the pocket.

actions, as seen in true β-barrels, but rather through interactions of atoms from side chains of residues in loop 52 to 61 from one monomer (named PE$_A$) with main-chain atoms in strand β6b in the other monomer (named PE$_B$). The central 2 residues are Asn60 and TrpA57. The Nδ2 of Asn60 forms a hydrogen bond with the backbone oxygen of Thr131, whereas the Oδ1 makes a hydrogen bond with the backbone nitrogen from the same Thr131. The side chain of Trp57 occupies a hydrophobic pocket formed by the aliphatic part of the side chain of Lys129, the methyl moiety of Thr105, and the side chain of His67. The Nε1 of Trp57 makes a hydrogen bond with the backbone oxygen of Lys129 (Fig. 4A). Other interactions are formed between Asp59 and Thr131, Gln61, and Ser133. Tyr94 from strand β4 completes the main interactions through a hydrogen bond to the Nz of Lys129 (Fig. 4A). The dimer interactions are not extensive, and only 625 Å^2 is buried in the interface, according to an analysis using Pisa (30).

Both the top and bottom sides of the barrel-like feature are hollow, and deep pockets are formed (Fig. 4B). The pocket at the wider bottom is larger and not well defined or well protected from solvent. The volume of the pocket is 857 Å^3 as calculated by Pocketfinder (http://www.modelling.leeds.ac.uk/pocketfinder/). This pocket is lined with a number of charged residues, most notably 4 arginines (Arg108 and Arg121 from each subunit), that come together in the center of the pocket to form a ring-like arrangement (Fig. 4B). Two Asp residues (Asp110 from each monomer) are

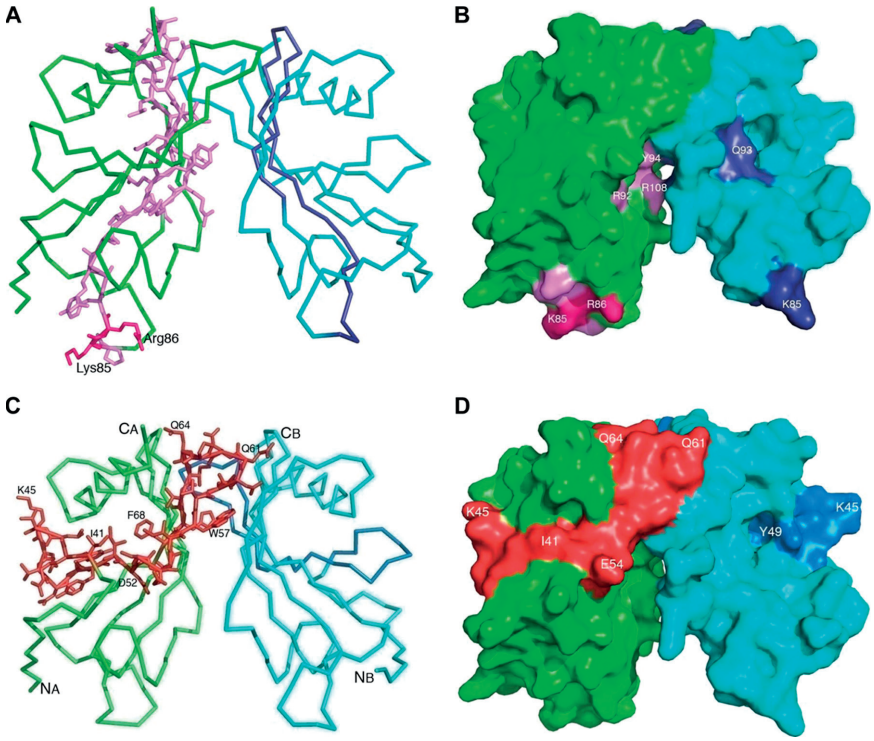

FIG 5 Binding sites of the various host factors on the PE dimer. (A) Ribbon diagram of a PE dimer that shows the Vn binding region. The two separate monomers are shown in green and light blue, whereas the amino acid region 84 to 108 (based on peptide mapping) is shown in dark magenta and dark blue in the two monomers. (B) Surface of the PE dimer with exposed K85 and R86 side chains, along with other residues. (C) The Ln/plasminogen binding region of PE. The ribbon model shows the Ln/plasminogen binding region in red. The amino acids of the binding region are shown as stick models. For ease of following the chain, several residues along this fragment are numbered. (D) Surface of PE with the Ln and plasminogen binding region indicated in red.

positioned between two of the Arg residues and provide some charge compensation (see Fig. S1 in the supplemental material). Further charged residues that line the inner pocket are Lys125 and Lys126 (see Fig. S1).

The second pocket at the top of the barrel is much more confined in space and better defined. It has a flattened shape, with dimensions of 14 Å by 8 Å and is about 10 Å deep, with a volume of 363 $Å^3$ (Fig. 4B). The central part of the pocket is lined with four Ile residues (Ile65 and Ile96 from each monomer), whereas at the inside walls of the pocket, more polar residues (His67, Asp59, and Thr105 from each monomer) are found (Fig. 4B and C). The rim of the pocket is also polar in character, and residues His103, Asn98, and Asn101 are located there. Since this pocket is very well defined in shape and protected from the solvent, it seems likely that it has a ligand binding feature. The residues that line the walls of both pockets, however, are not particularly conserved within a family of homologous proteins from different pathogens, as described below.

Functional host factor-binding regions of PE are exposed at the surface of the molecule. We previously used a peptide-mapping approach to identify the PE amino acid regions that were involved in binding to epithelial cells (12). A peptide consisting of the PE 84 to 108 amino acid region directly interacted with lung epithelial cells. More recently, a similar region was verified that bound Vn (16, 17). In the present crystal structure, the 84 to 108 amino acid region is located partly in loops 4 and 5 and in beta strands 4 and 5 (Fig. 5A). The structure shows that loop 4 plays a role at the base of the protein, where amino acids Asn73-Arg89 are well exposed (Fig. 5B). In contrast, the Ser90-Arg108 part is located in beta strands 4 and 5, which are positioned in the core of the PE dimer. Thus, the loop 4 region up to amino acid 84 seems more likely to be the real epithelial-cell-interacting domain (Fig. 5B). Recently, we showed that amino acids Lys85 and Arg86 are important for the PE-dependent interaction with vitronectin (17). Importantly, in loop 4, the side chains for Lys85 and Arg86 are well exposed (Fig. 5A and B). The linear sequence of loop 4 in all *Haemophilus* spp. is highly conserved, which suggests similar ligand specificities, while in other pathogens this loop is only partially conserved (Fig. 6A).

Since the multifunctional PE also interacts with laminin, we

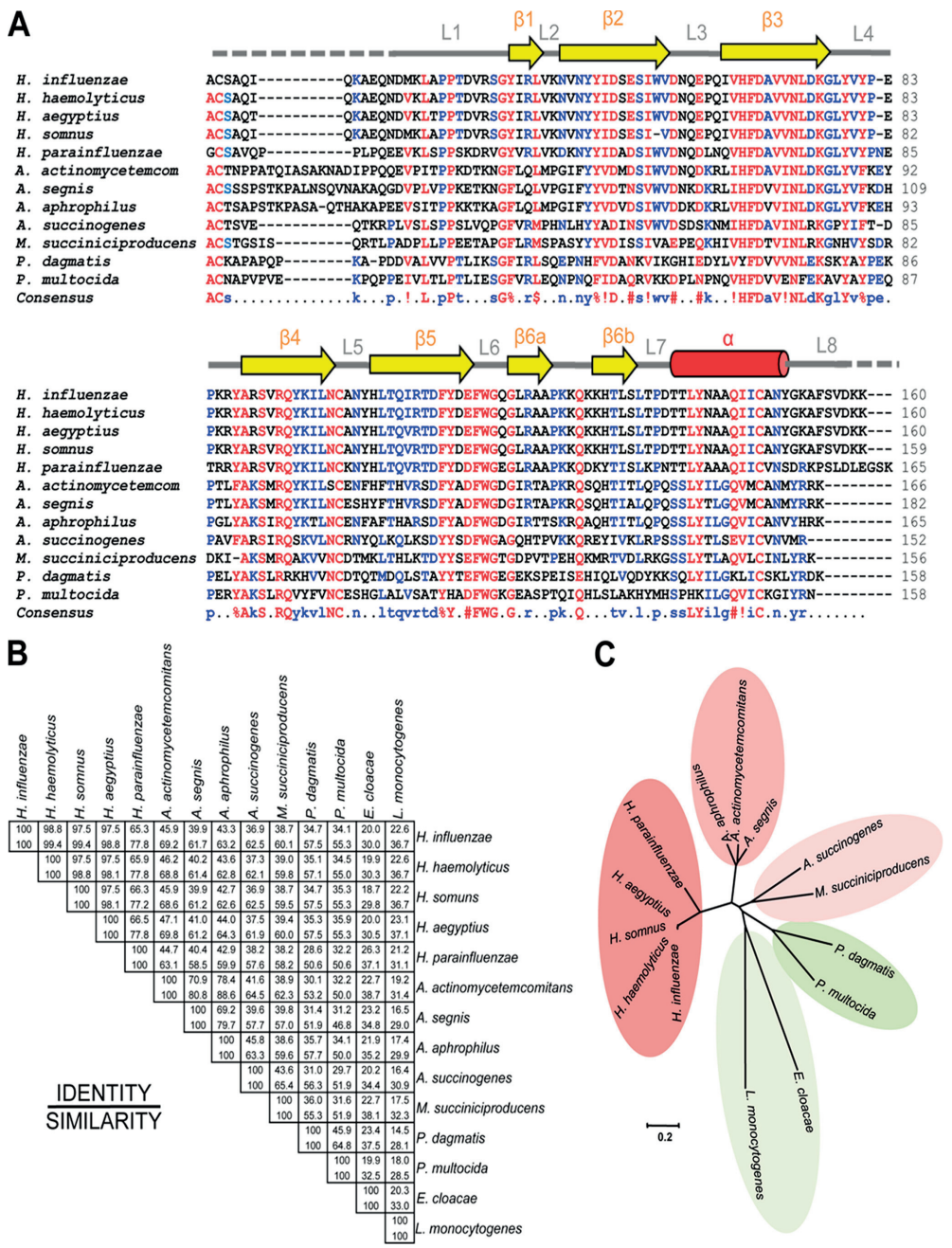
A
L1
β1
L2
β2
L3
β3
L4
H. influenzae ACSAQI----------QKAEQNDMKLAPPTDVRSGYIRLVKNVNYYIDSESIWVDNQEPQIVHFDAVVNLDKGLYVYP-E 83
H. haemolyticus ACSAQI----------QKAEQNDVKLAPPTDVRSGYIRLVKNVNYYIDSESIWVDNQEPQIVHFDAVVNLDKGLYVYP-E 83
H. aegyptius ACSAQT----------QKAEQNDVKLTPPTDVRSGYIRLVKNVNYYIDSESIWVDNQEPQIVHFDAVVNLDKGLYVYP-E 83
H. somnus ACSAQI----------QKAEQNDMKLAPPTDVRSGYIRLVKNVNYYIDSESI-VDNQEPQIVHFDAVVNLDKGLYVYP-E 82
H. parainfluenzae GCSAVQP----------PLPQEEVKLSPPSKDRVGYVRLVKDKNYYIDADSIWVDNQDLNQVHFDAVVNLDKGLYVYPNE 85
A. actinomycetemcom ACTNPPATQIASAKNADIPPQQEVPITPPKDTKNGFLQLMPGIFYYVDMDSIWVDNQDKRLIHFDAVINLDKGLYVFKEY 92
A. segnis ACSSSPSTKPALNSQVNAKAQGDVPLVPPKETKNGFLQLVPGIFYYVDTNSVWVDNKDKRLIHFDVVINLDKGLYVFKDH 109
A. aphrophilus ACTSAPSTKPASA-QTHAKAPEEVSITPPKKTKAGFLQLMPGIFYYVDVDSIWVDDKDKRLVHFDVVINLDKGLYVFKEH 93
A. succinogenes ACTSVE----------QTKRPLVSLSPPSLVQPGFVRMPHNLHYYADINSVWVDSDSKNMIHFDAVINLRKGPYIFT-D 85
M. succiniciproducens ACSTGSIS---------QRTLPADPLLPPEETAPGFLRMSPASYYYVDISSIVAEPEQKHIVHFDTVINLRKGNHVYSDR 82
P. dagmatis ACKAPAPQP--------KA-PDDVALVVPTLIKSGFIRLSQEPNHFVDANKVIKGHIEDYLVYFDVVVNLEKSKYAYPEK 86
P. multocida ACNAPVPVE--------KPQPPEIVLTLPTLIESGFVRLEQNPNQFIDAQRVKKDPLNPNQVHFDVVENFEKAVYAYPEQ 87
Consensus ACs.....k...p.!.L.pPt...sG%.r$..n.ny%!D.#s!wv#..#k..!HFDaV!NLdKglYv%pe.
β4
L5
β5
L6
β6a
β6b
L7
α
L8
H. influenzae PKRYARSVRQYKILNCANYHLTQIRTDFYDEFWGQGLRAAPKKQKKHTLSLTPDTTLYNAAQIICANYGKAFSVDKK--- 160
H. haemolyticus PKRYARSVRQYKILNCANYHLTQIRTDFYDEFWGQGLRAAPKKQKKHTLSLTPDTTLYNAAQIICANYGKAFSVDKK--- 160
H. aegyptius PKRYARSVRQYKILNCANYHLTQVRTDFYDEFWGQGLRAAPKKQKKHTLSLTPDTTLYNAAQIICANYGKAFSVDKK--- 160
H. somnus PKRYARSVRQYKILNCANYHLTQVRTDFYDEFWGQGLRAAPKKQKKHTLSLTPDTTLYNAAQIICANYGKAFSVDKK--- 159
H. parainfluenzae TRRYARSVRQYKILNCKNYHLTQVRTDFYDFWGEGLRAAPKKQDKYTISLKPNTTLYAAAQIICVNSDRKPSLDLEGSK 165
A. actinomycetemcom PTLFAKSMRQYKILSCENFHFTHVRSDFYADFWGDGIRTAPKRQSQHTITLQPQSSLYILGQVMCANMYRRK-------- 166
A. segnis PTLYAKSMRQYKILNCESHYFTHVRSDFYADFWGDGIRTAPKRQSQHTIALQPQSSLYTLGQVMCANMYRRK-------- 182
A. aphrophilus PGLYAKSIRQYKTLNCENFAFTHARSDFYADFWGDGIRTTSKRQAQHTITLQPQSSLYILGQVICANVYHRK-------- 165
A. succinogenes PAVFARSIRQSKVLNCRNYQLKQLKSDYYSDFWGAGQHTPVKKQREYIVKLRPSSSLYTLSEVICVNVMR---------- 152
M. succiniciproducens DKI-AKSMRQAKVVNCDTMKLTHLKTDYYSEFWGTGDPVTPEHQKMRTVDLRKGSSLYTLAQVLCINLYRK--------- 156
P. dagmatis PELYAKSLRRKHVVNCDTQTMDQLSTAYYTEFWGEGEKSPEISEHIQLVQDYKKSQLYILGKLICSKLYRDK-------- 158
P. multocida PERYAKSLRQVYFVNCESHGLALVSATYHADFWGKGEASPTQIQHLSLAKHYMHSPHKILGQVICKGIYRN--------- 158
Consensus p..%AkS.RQykvlNC.n..ltqvrtd%Y.#FWG.G.r..pk.Q...tv.l.p.ssLYilg#!iC.n.yr.....
B
H. influenzae
H. haemolyticus
H. somnus
H. aegyptius
H. parainfluenzae
A. actinomycetemcomitans
A. segnis
A. aphrophilus
A. succinogenes
M. succiniciproducens
P. dagmatis
P. multocida
E. cloacae
L. monocytogenes
100 98.8 97.5 97.5 65.3 45.9 39.9 43.3 36.9 38.7 34.7 34.1 20.0 22.6 H. influenzae
100 99.4 99.4 98.8 77.8 69.2 61.7 63.2 62.5 60.1 57.5 55.3 30.0 36.7 H. haemolyticus
100 97.5 97.5 65.9 46.2 40.2 43.6 37.3 39.0 35.1 34.5 19.9 22.6 H. somuns
100 98.8 98.1 77.8 68.8 61.4 62.8 62.1 59.8 57.1 55.0 30.3 36.7 H. aegyptius
100 97.5 66.3 45.9 39.9 42.7 36.9 38.7 34.7 35.3 18.7 22.2 H. parainfluenzae
100 98.1 77.2 68.6 61.2 62.6 62.5 59.5 57.5 55.3 29.8 36.7 A. actinomycetemcomitans
100 66.5 47.1 41.0 44.0 37.5 39.4 35.3 35.9 20.0 23.1 A. segnis
100 77.8 69.8 61.2 64.3 61.9 60.0 57.5 55.3 30.5 37.1 A. aphrophilus
100 44.7 40.4 42.9 38.2 38.2 28.6 32.2 26.3 21.2 A. succinogenes
100 63.1 58.5 59.9 57.6 58.2 50.6 50.6 37.1 31.1 M. succiniciproducens
100 70.9 78.4 41.6 38.9 30.1 32.2 22.7 19.2 P. dagmatis
100 80.8 88.6 64.5 62.3 53.2 50.0 38.7 31.4 P. multocida
100 69.2 39.6 39.8 31.4 31.2 23.2 16.5 E. cloacae
100 79.7 57.7 57.0 51.9 46.8 34.8 29.0 L. monocytogenes
100 45.8 38.6 35.7 34.1 21.9 17.4
100 63.3 59.6 57.7 50.0 35.2 29.9
100 43.6 31.0 29.7 20.2 16.4
100 65.4 56.3 51.9 34.4 30.9
100 36.0 31.6 22.7 17.5
100 55.3 51.9 38.1 32.3
100 45.9 23.4 14.5
100 64.8 37.5 28.1
100 19.9 18.0
100 32.5 28.5
100 20.3
100 33.0
100
100
IDENTITY
SIMILARITY
C
H. influenzae
H. haemolyticus
H. aegyptius
H. somnus
H. parainfluenzae
A. actinomycetemcomitans
A. aphrophilus
A. segnis
A. succinogenes
M. succiniciproducens
P. dagmatis
P. multocida
E. cloacae
L. monocytogenes
0.2

previously applied a peptide-mapping approach to determine the specific laminin binding amino acid region in PE. Interestingly, the region consisting of PE aa 41 to 68 was directly interacting with Ln (18). The same peptide also has affinity for plasminogen (19). This particular region is located in loop 1 between strands β1 and β2 and beta strand β2 and loop 2. The whole region is partly exposed at the surface and presents diagonally, along with the whole length of the dimer (Fig. 5C and D). In parallel with loop 4, the laminin/plasminogen binding region (loop 3) is also conserved among *Haemophilus* spp., but it is diverse in other pathogens. However, loop 3 has acidic amino acids that are highly conserved in most of the PE homologues for which sequence information is available (Fig. 6A).

PE is a unique adhesin of the family *Pasteurellaceae*. All pathogenic bacterial species are equipped with specific adhesins that very precisely recognize host tissues in particular anatomical niches. This group of proteins has numerous structurally diverse members. In general, adhesins may be fimbriae, pili, or other, nonpilus adhesins (31). There are only a limited number of adhesins for which structures have been determined, and that limits the categorization of this group of proteins (http://supfam.cs.bris.ac.uk). The structural classification of adhesins on the basis of domains involved in recognition of host proteins was performed in the database available at http://supfam.cs.bris.ac.uk/SUPERFAMILY/cgi-bin/scop.cgi?sunid=49401. The database includes a limited number of proteins, such as collagen-binding proteins, fibrinogen-binding proteins, pilus subunits, PapG adhesion receptor-binding proteins, F17-C type adhesin, and Dr family adhesins. However, a large number of other known bacterial adhesins are not yet categorized due to lack of structural information on the domain recognition.

Pasteurellaceae is a large and diverse family of Gram-negative proteobacteria (32). Recently, the family was classified into 17 different genera (http://www.pasteurellaceae.life.ku.dk/). The latest BLAST update in the ExPASy (NCBI BLAST2) database showed that there are 11 different bacterial pathogens that have a *pe* gene homologue (Fig. 6A). The similarity matrix showed that *H. influenzae* has 34.1 to 98.8% identity and 55.3 to 99.4% similarity with other members of *Pasteurellaceae* (Fig. 6B), and a primary amino acid sequence-based phylogenetic tree showed 5 separate clusters (Fig. 6C). *Haemophilus* spp. grouped into a single cluster with 65.3 to 98.8% identity and 77.0 to 99.4% similarity. *Actinobacillus actinomycetemcomitans* showed 70.9 to 78.4% sequence identity and 80.8 to 88.6% similarity with *Actinobacillus segnis* and *Actinobacillus aphrophilus*, respectively. In the third cluster, *Actinobacillus succinogenes* showed 43.6% identity and 65.4% similarity to *M. succiniciproducens* (Fig. 6B). *Pasteurella* spp. also have PE analogues that are approximately 34% similar to *H. influenzae* PE, whereas PE derived from *P. multocida* is only 45.9% identical and 64.8% similar to *Pasteurella dagmatis* PE. In addition to these *Pasteurellaceae* family members, *Enterobacter cloacae* and *Listeria monocytogenes* have PE orthologues (E3G4R8 and E1UDL7, respectively), albeit with lower homology (Fig. 6B and C). We suggest that PE belongs to a unique group of bacterial outer membrane proteins in the family *Pasteurellaceae*.

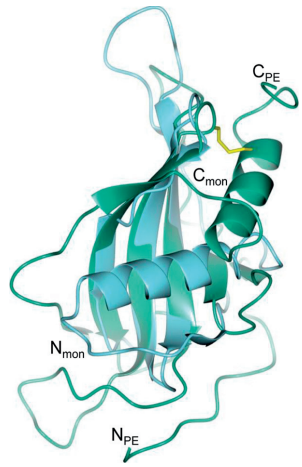

FIG 7 PE has a monellin-like fold. Shown are the superimposed structures of monellin (mon) (PDB code 2O9U) chain A (blue) and PE monomer (green). The beta sheet arrangements in the protein backbone are very similar. However, helices are present at the C terminus in PE and at the N terminus in monellin.

PE belongs to the cystatin family of proteins. To verify the folding pattern, the PE structure was matched with a fold database (33). The arrangement of a 6-stranded antiparallel β-sheet and α-helix packing at one face, as seen within the monomer, was observed in a number of different proteins. In these proteins, however, the other side of the sheet is normally shielded by other secondary-structure elements, and thus, the sheet and helix are part of larger fold arrangements that are not related to each other. The closest structures, which have the same minimal arrangement, can be seen in the monellin/cystatin family fold (34), which is also composed of a single antiparallel β-sheet with an α-helix protecting the concave face of the sheet. Proteins in this family are either cysteine protease inhibitors (cystatin-like) or sweet proteins from plants (monellin-like). The basic folds of, e.g., monellin and PE superimpose well (Fig. 7). However, the position of the helix within the secondary-structure topology of the monellin/cystatin family fold is different than it is within the PE structure. In the monellin/cystatin family, it is placed after the first strand of the sheet, whereas it is positioned at the C-terminal end of the PE molecule. The helix for the monellin/cystatin family is positioned

FIG 6 PE homologues also exist in other pathogens. (A) BLAST results revealed that several other pathogens have PE homologues. Retrieved sequences were aligned using the MultAlin online tool (42). Highly conserved amino acids are shown in red, and partially conserved amino acids are in blue. Secondary structures are shown at the top, with beta strands as arrows and helices as cylinders. (B) Identity and similarity matrix of protein sequences analyzed by using the pairwise alignment tool Needle (http://www.ebi.ac.uk). (C) Rooted phylogenetic tree showing 5 different clusters. *Haemophilus* spp. formed a single cluster, and distantly related sequences of *Pasteurella* spp. and *E. cloacae* and *L. monocytogenes* formed two separate clusters. The sequences were analyzed for phylogenetic relations by using MEGA5 software (43).

in the center of the beta-sheet face and protects the whole face of the protein. The helix in PE, however, is tethered to the top of the sheet by the disulfide bridge, and therefore, part of the sheet is more exposed. Thus, it seems that PE and monellin/cystatin probably are analogues of each other and probably are products of convergent evolution.

The most homologous regions for all the species are located in the secondary-structure elements, especially within the central-strand β3. Interestingly, one region with very high homology is not associated with a secondary-structure element, but instead, it is found in loop 6 and consists of the fingerprint (FY)111-(YH)-X-(DE)-F-W-G-X-G119. This loop between β5 and β6 folds back over the convex inner side of the sheet and forms a small hydrophobic core on the inside bottom of the β-barrel-like dimer. The aromatic residues in the fingerprint interact with residues from the different strands, as well as with the N-terminal loop 1. In particular, the residues Tyr/His112 and Trp116 are involved in multiple interactions with residues from different secondary-structure elements (Fig. 6A). Using the Prosite Web server (35) to scan the database for sequences with similar fingerprints, it seems that this fingerprint is unique, and thus, it might be an indicator of this particular fold family.

Structural approach for mapping immunogenic and surface-exposed regions of PE by raising peptide antibodies. Previously, we reported that immunization with PE 84 to 108 mediated protection in a mouse pulmonary clearance model (12). The ubiquitous presence of PE among NTHI clinical isolates further signified the importance of the protein as a vaccine candidate (13). To verify our crystal model, as well as to analyze the immunogenic capacities of various surface-exposed regions of PE, we designed a series of peptides, as outlined in Fig. 8A and B (PE 24 to 37, PE 74 to 89, PE 84 to 108, and PE 134 to 156). In addition, a peptide based upon the cryptic region PE 104 to 128 was used as a negative control. KLH-conjugated peptides were used for subcutaneous immunization of BALB/c mice. Sera from immunized mice ($n = 6$ in each group) were pooled, and peptide Abs were purified using affinity chromatography and finally tested in ELISA. All peptides produced specific Abs directed against their corresponding peptides (Fig. 8C). In contrast, the resulting antibodies showed different recognition patterns against recombinant full-length PE 22 to 160 in ELISA. Antibodies directed against PE 24 to 37, PE 74 to 89, and PE 134 to 156 recognized the PE 22 to 160 molecule, whereas the anti-PE 84 to 108 Ab recognized PE 22 to 160 with less efficiency (Fig. 8D). However, purified peptide antibodies directed against PE 24 to 37 and PE 84 to 108 displayed cross-reactivity against both peptides in ELISA. As expected, the negative-control Ab against PE 104 to 128 did not detect full-length PE.

We also wanted to test whether our peptide Abs recognized PE when the molecule was surface exposed in its native PE form on the clinical isolate NTHI 3655. Bacteria were incubated with Abs, followed by flow cytometry analysis. In parallel with the results obtained by ELISA, anti-PE 24 to 37, anti-PE 74 to 89, and anti-PE 134 to 156 Abs all detected PE at the bacterial surface, whereas the anti-84 to 108 Ab showed a minor shift compared to the negative control consisting of the secondary antibody only (Fig. 8E). Taken together, Abs directed against surface-exposed epitopes of the PE molecule that were defined by the designed peptides fit very well with the crystal structure.

DISCUSSION

Protein E is an outer membrane protein found in both encapsulated *H. influenzae* and NTHI. We have shown that NTHI equipped with the multifunctional adhesin PE binds to several different host proteins, including Vn, Ln, and plasminogen (13, 16, 17, 19). The majority of NTHI infections are in general noninvasive, although an increasing trend of invasive NTHI disease has been observed the last 5 years (3). Active degradation of host tissues and the ECM, however, is a property of typeable *H. influenzae*, such as Hib. Adherence mediated by the PE-Ln interaction thus could provide a firm anchorage for host basal lamina and tissues (Fig. 9). In contrast to Hib, NTHI may also use Ln as a ligand, particularly when the epithelial mucosa is destroyed by a prior viral infection or mixed bacterial infections. In parallel, plasminogen bound to PE degrades C3b and inhibits the complement-mediated innate immunity. The protease activity of plasmin also degrades the ECM (Fig. 9), which eventually increases the host damage. Experimental evidence suggests that Ln and plasminogen share similar binding domains in PE (16, 19). This might, of course, be conditional according to the abundance and affinity of ligands. An interesting finding is that recombinant PE simultaneously binds Ln and Vn (18). We have also observed that laminin LG1 to -5 domains of the alpha chain interact with PE and that this interaction can be inhibited by heparin (18). The PE loop 3 region has a few acidic residues (residues D59 and E62) that might be involved in binding to the LG4 and -5 domains of laminin. The present data on a dimerized PE molecule (Fig. 3A) explain these *in vitro* observations. However, it is at present unclear whether the dual-ligand-binding mode of the PE molecule also exists *in vivo*.

Protein E is a lipoprotein that has a signal peptide at the N terminus, followed by Cys16 (12). According to the general described mechanisms of lipoprotein transport and lipidation mechanisms, the protein is transported to the outer membrane, followed by addition of lipid chains and removal of the signal peptide (36, 37). The Cys16 residue is thus predicted to be involved in lipidation and functions as an anchor of PE on the outer membrane in bacteria. The N terminus of the dimer is supposed to face toward the membrane side of the bacteria, whereas the C terminus faces the outside.

The presence of a well-formed pocket on the top side of the dimer (Fig. 3B) is intriguing. The shape and accessibility of the pocket is very reminiscent of binding pockets in smaller ligand binding proteins. However, a clear function for this pocket cannot be deduced, and due to the variability of the residues lining the pocket, it does not seem to be associated with a conserved function within the family of PE-like proteins. It has been suggested, however, that a high level of diversity within interacting surfaces of adhesins when in contact with their host proteins stems from the need of the pathogen to change these recognition sites in order to avoid an immune response while retaining a common biological function (38). This possibility needs to be further investigated. Identification of a putative ligand to the smaller and well-defined pocket of PE would be an asset in these investigations.

Protein E is known as one of the *H. influenzae* Vn binding proteins with the highest affinity (dissociation constant $[K_d] = 4.0 \times 10^{-7}$ M), and most importantly, Vn bound to PE protects NTHI from the membrane attack complex (MAC). The vitronec-

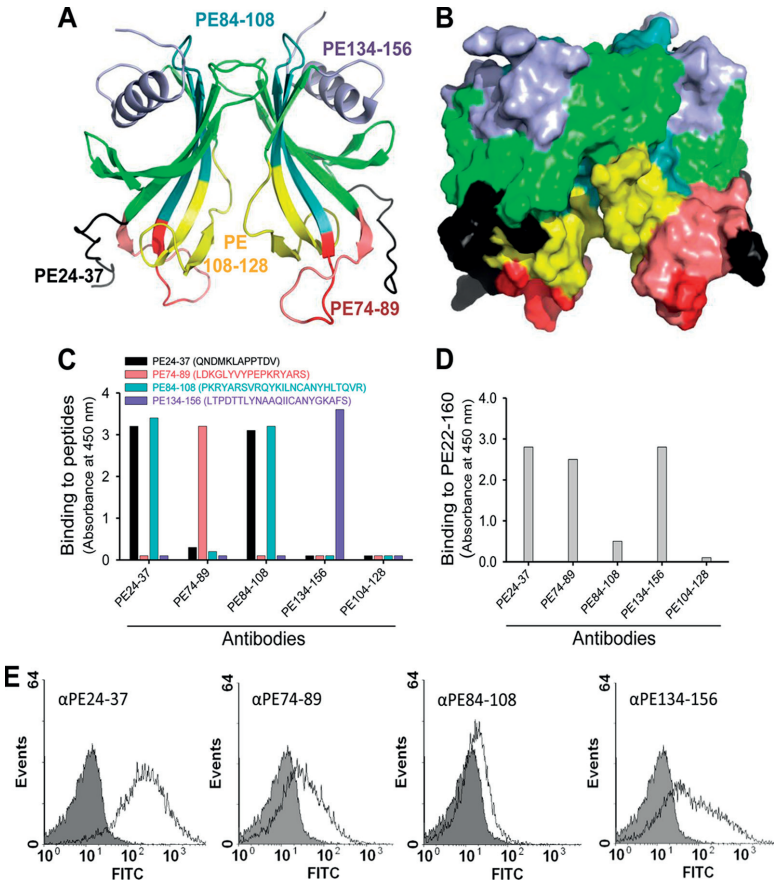

FIG 8 Mapping of surface-exposed immunogenic regions using mouse anti-PE peptide Abs. (A) Ribbon diagram showing PE amino acid regions (indicated with different colors) that were selected for immunization of a series of mice. (B) Surface structure of selected regions as shown in panel A. (C) Results from ELISA that demonstrate Ab recognition of peptides with which microtiter plates were coated. (D) Recognition of full-length recombinant PE 22 to 160 by peptide Abs shown in ELISA. (E) Flow cytometry profiles of NTHI showing surface recognition of PE at the surfaces of bacteria using anti-PE peptide Abs.

tin-binding region PE 84 to 108 that is embedded in the structure is mostly located in the dimer interface. Recently, we further suggested that Lys85 and Arg86 of PE are involved in binding to Vn (17). Lys85 and Arg86 are located in the end of the exposed loop 4. Thus, a probable region for Vn interactions may be mostly located between amino acids Leu78 and Ala88 of loop 4. Vn is also known to function as a bridge molecule that interacts with bacterial surface proteins and the host integrins via an RGD motif (14, 39). Similarly, the PE-mediated recruitment of Vn by *H. influenzae* might also be involved in adhesion to and internalization into epithelial cells.

Protein E meets the criteria to be suitable as a vaccine candidate, i.e., its ubiquitous presence, highly conserved nature, favored immunogenicity, and protective role in model animals (12). In our preliminary experiments, the structure-based approach for designing antibodies against the surface-exposed part of the PE molecule recognized recombinant PE, in addition to PE at the surfaces of bacteria (Fig. 8E). This indicated that these peptides may be appropriate for immunization against NTHI.

PE has a unique three-dimensional structure that is involved in adhesion of *H. influenzae* to epithelial cells and binds and/or recruits multiple host proteins. The PE structure is formed by β-sheets, with an α-helix covering one side. Within the crystal structure, the protein is present as a dimer, with the two monomers forming a β-barrel-like structure. The dimer of PE resembles a flattened β-barrel-like structure, as it seems to form a continuous up and down antiparallel β-sheet, resulting in the formation of large pockets inside the molecule. However, in a number of

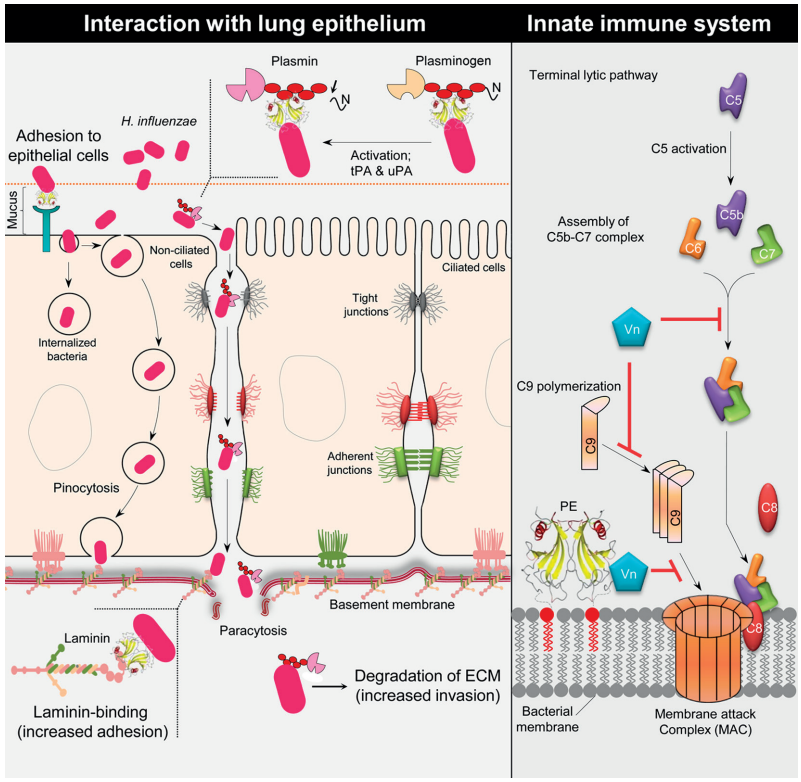

FIG 9 Schematic representation of the multiple functions of PE. (Left) *H. influenzae* PE interacts with the host epithelium. The PE molecule mediates binding to the epithelial surface utilizing a hitherto unknown receptor. This interaction contributes to bacterial adhesion and induction of a proinflammatory response by the epithelial cells. PE binds to Ln, which contributes to adhesion of *H. influenzae* to the basement membrane and the host ECM. In addition to Ln, *H. influenzae* binds plasminogen by using PE. When plasminogen is bound to PE, it is converted into active plasmin by host urokinase plasminogen activator (uPA) or tissue plasminogen activator (tPA). Active plasmin may help in bacterial invasion and degradation of the ECM. (Right) PE inhibits the MAC at the surface of *H. influenzae*, which is accomplished by the binding of Vn. Vitronectin is a well-known complement regulator that inhibits the terminal complement pathway by interacting with the C5b-7 complex assembly and also inhibits C9 polymerization during formation of a lytic pore. PE is able to bind both Ln and Vn at the same time, and the two ligands do not interfere with each other; thus, adhesion and MAC inhibition can be carried out simultaneously.

aspects, it differs from true β-barrel structure. The first is that at the sides of the monomers interacting with each other, the contact surfaces are not made through β-strands, but instead, loops are used in an extended conformation. The hydrogen-bonding system is not like that observed in a β-sheet; here, instead, hydrogen bonds are built up through side chain interactions. Although the interaction area is limited, the presence of dimers is also seen in gel filtration, DLS, and TEM experiments, indicating that this is not likely to be an artifact of crystallization. The other unusual aspect of this "barrel-like" structure is the way the barrel fans out at the bottom. This is mainly achieved by the high twist in the separate sheets of each monomer. Only the top part of the barrel is intact and continuous, while the bottom part is sheared and open at the sides. This is an unusual arrangement and is not observed in other proteins, as judged by fold recognition searches using Dali (33).

The protein-folding pattern has a partial match with that of the monellin/cystatin family. However, cystatins are in general monomeric, whereas monellin is a heterodimer formed by an A chain of 42 aa and a B chain of 50 aa. A higher oligomeric variant of monellin has been observed in crystal structures (40). The dimer arrangement of PE, however, is different from that of monellin, and in PE, a more side-to-side barrel-like dimer is found. Proteins in the monellin/cystatin family have been studied extensively for their capacity to aggregate (41). However, the aggregation of PE has not yet been fully investigated. Besides this similarity to monellin/cystatin, there are no other bacterial adhesins that have this kind of structural appearance. However, orthologues belonging to the PE adhesin subfamily are also present in *E. cloacae* and *L. monocytogenes*. We conclude from sequence comparisons within this set of proteins that the residues that are important for the

specific features of the fold are very well conserved. These conserved patches at the surface of PE that might be important for the structure of the common fold are shown in Fig. S2 in the supplemental material. The specific roles of these proteins in the various bacterial species are not yet elucidated. In fact, the best-characterized member of this family is PE, which is described in this paper. We would therefore propose that PE and its homologues belong to a new group of adhesins that in particular present in the family of *Pasteurellaceae*.

ACKNOWLEDGMENTS

This work was supported by Alfred Österlund, Åke-Wiberg, Anna and Edwin Berger, Greta and Johan Kock, Lars Hierta, FLÄK, the Gyllenstiernska Krapperup, the Marianne and Marcus Wallenberg Foundation, the Physiographical Society, the Swedish Medical Research Council (grant number 521-2010-4221; http://www.vr.se), the Cancer Foundation at the University Hospital in Malmö, the Skåne County Council's research and development foundation, and GlaxoSmithKline-Rixensart, Belgium.

We thank the staff at the MAX IV laboratories and the crystallization facility for their valuable help.

REFERENCES

1. **Murphy TF, Faden H, Bakaletz LO, Kyd JM, Forsgren A, Campos J, Virji M, Pelton SI.** 2009. Nontypeable *Haemophilus influenzae* as a pathogen in children. Pediatr. Infect. Dis. J. **28**:43–48.
2. **van Wessel K, Rodenburg GD, Veenhoven RH, Spanjaard L, van der Ende A, Sanders EA.** 2011. Nontypeable *Haemophilus influenzae* invasive disease in The Netherlands: a retrospective surveillance study 2001–2008. Clin. Infect. Dis. **53**:e1–e7. doi:10.1093/cid/cir268.
3. **Resman F, Ristovski M, Ahl J, Forsgren A, Gilsdorf JR, Jasir A, Kaijser B, Kronvall G, Riesbeck K.** 2011. Invasive disease caused by *Haemophilus influenzae* in Sweden 1997–2009; evidence of increasing incidence and clinical burden of non-type b strains. Clin. Microbiol. Infect. **17**:1638–1645.
4. **Rubach MP, Bender JM, Mottice S, Hanson K, Weng HY, Korgenski K, Daly JA, Pavia AT.** 2011. Increasing incidence of invasive *Haemophilus influenzae* disease in adults, Utah, USA. Emerg. Infect. Dis. **17**:1645–1650.
5. **Grandi G.** 2001. Antibacterial vaccine design using genomics and proteomics. Trends Biotechnol. **19**:181–188.
6. **Giufre M, Carattoli A, Cardines R, Mastrantonio P, Cerquetti M.** 2008. Variation in expression of HMW1 and HMW2 adhesins in invasive nontypeable *Haemophilus influenzae* isolates. BMC Microbiol. **8**:83.
7. **Jurcisek JA, Bookwalter JE, Baker BD, Fernandez S, Novotny LA, Munson RS, Jr, Bakaletz LO.** 2007. The PilA protein of non-typeable *Haemophilus influenzae* plays a role in biofilm formation, adherence to epithelial cells and colonization of the mammalian upper respiratory tract. Mol. Microbiol. **65**:1288–1299.
8. **Chang A, Kaur R, Michel LV, Casey JR, Pichichero M.** 2011. *Haemophilus influenzae* vaccine candidate outer membrane protein P6 is not conserved in all strains. Hum. Vaccin. **7**:102–105.
9. **Dicko A, Odusanya OO, Diallo AI, Santara G, Barry A, Dolo A, Diallo A, Kuyinu YA, Kehinde OA, Francois N, Borys D, Yarzabal JP, Moreira M, Schuerman L.** 2011. Primary vaccination with the 10-valent pneumococcal non-typeable *Haemophilus influenzae* protein D conjugate vaccine (PHiD-CV) in infants in Mali and Nigeria: a randomized controlled trial. BMC Public Health **11**:882.
10. **Prymula R, Kriz P, Kaliskova E, Pascal T, Poolman J, Schuerman L.** 2009. Effect of vaccination with pneumococcal capsular polysaccharides conjugated to *Haemophilus influenzae*-derived protein D on nasopharyngeal carriage of *Streptococcus pneumoniae* and *H. influenzae* in children under 2 years of age. Vaccine **28**:71–78.
11. **Murphy TF.** 2009. Current and future prospects for a vaccine for nontypeable *Haemophilus influenzae*. Curr. Infect. Dis. Rep. **11**:177–182.
12. **Ronander E, Brant M, Eriksson E, Morgelin M, Hallgren O, Westergren-Thorsson G, Forsgren A, Riesbeck K.** 2009. Nontypeable *Haemophilus influenzae* adhesin protein E: characterization and biological activity. J. Infect. Dis. **199**:522–531.
13. **Singh B, Brant M, Kilian M, Hallstrom B, Riesbeck K.** 2010. Protein E of *Haemophilus influenzae* is a ubiquitous highly conserved adhesin. J. Infect. Dis. **201**:414–419.
14. **Singh B, Su YC, Riesbeck K.** 2010. Vitronectin in bacterial pathogenesis: a host protein used in complement escape and cellular invasion. Mol. Microbiol. **78**:545–560.
15. **Singh B, Fleury C, Jalalvand F, Riesbeck K.** 2012. Human pathogens utilize host extracellular matrix proteins laminin and collagen for adhesion and invasion of the host. FEMS Microbiol. Rev. **36**:1122–1180.
16. **Hallstrom T, Blom AM, Zipfel PF, Riesbeck K.** 2009. Nontypeable *Haemophilus influenzae* protein E binds vitronectin and is important for serum resistance. J. Immunol. **183**:2593–2601.
17. **Singh B, Jalalvand F, Morgelin M, Zipfel P, Blom AM, Riesbeck K.** 2011. *Haemophilus influenzae* protein E recognizes the C-terminal domain of vitronectin and modulates the membrane attack complex. Mol. Microbiol. **81**:80–98.
18. **Hallstrom T, Singh B, Resman F, Blom AM, Morgelin M, Riesbeck K.** 2011. *Haemophilus influenzae* protein E binds to the extracellular matrix by concurrently interacting with laminin and vitronectin. J. Infect. Dis. **204**:1065–1074.
19. **Barthel D, Singh B, Riesbeck K, Zipfel PF.** 2012. *Haemophilus influenzae* uses the surface protein E to acquire human plasminogen and to evade innate immunity. J. Immunol. **188**:379–385.
20. **Singh B, Al Jubair T, Fornvik K, Thunnissen MM, Riesbeck K.** 2012. Crystallization and X-ray diffraction analysis of a novel surface-adhesin protein: protein E from *Haemophilus influenzae*. Acta Crystallogr. Sect. F Struct. Biol. Cryst. Commun. **68**:222–226.
21. **Kabsch W.** 2010. XDS. Acta Crystallogr. D Biol. Crystallogr. **66**:125–132.
22. **Pape T, Schneider TR.** 2004. HKL2MAP: a graphical user interface for phasing with SHELX programs. J. Appl. Crystallogr. **37**:843–844.
23. **Sheldrick GM.** 2008. A short history of SHELX. Acta Crystallogr. A **64**:112–122.
24. **Vonrhein C, Blanc E, Roversi P, Bricogne G.** 2007. Automated structure solution with autoSHARP. Methods Mol. Biol. **364**:215–230.
25. **Langer G, Cohen SX, Lamzin VS, Perrakis A.** 2008. Automated macromolecular model building for X-ray crystallography using ARP/wARP version 7. Nat. Protoc. **3**:1171–1179.
26. **Emsley P, Lohkamp B, Scott WG, Cowtan K.** 2010. Features and development of Coot. Acta Crystallogr. D Biol. Crystallogr. **66**:486–501.
27. **Adams PD, Afonine PV, Bunkoczi G, Chen VB, Davis IW, Echols N, Headd JJ, Hung LW, Kapral GJ, Grosse-Kunstleve RW, McCoy AJ, Moriarty NW, Oeffner R, Read RJ, Richardson DC, Richardson JS, Terwilliger TC, Zwart PH.** 2010. PHENIX: a comprehensive Python-based system for macromolecular structure solution. Acta Crystallogr. D Biol. Crystallogr. **66**:213–221.
28. **McCoy AJ, Grosse-Kunstleve RW, Adams PD, Winn MD, Storoni LC, Read RJ.** 2007. Phaser crystallographic software. J. Appl. Crystallogr. **40**:658–674.
29. **Engel J, Furthmayr H.** 1987. Electron microscopy and other physical methods for the characterization of extracellular matrix components: laminin, fibronectin, collagen IV, collagen VI, and proteoglycans. Methods Enzymol. **145**:3–78.
30. **Krissinel E, Henrick K.** 2007. Inference of macromolecular assemblies from crystalline state. J. Mol. Biol. **372**:774–797.
31. **Soto GE, Hultgren SJ.** 1999. Bacterial adhesins: common themes and variations in architecture and assembly. J. Bacteriol. **181**:1059–1071.
32. Kuhnert P, Christensen H. (ed). 2008. *Pasteurellaceae*: biology, genomics and molecular aspects. Caister Academic Press, Norfolk, United Kingdom.
33. **Holm L, Rosenstrom P.** 2010. Dali server: conservation mapping in 3D. Nucleic Acids Res. **38**:W545–W549.
34. **Esposito V, Temussi PA.** 2011. Cystatins: a versatile family. BioMol. Concepts **2**:95–102.
35. **de Castro E, Sigrist CJ, Gattiker A, Bulliard V, Langendijk-Genevaux PS, Gasteiger E, Bairoch A, Hulo N.** 2006. ScanProsite: detection of PROSITE signature matches and ProRule-associated functional and structural residues in proteins. Nucleic Acids Res. **34**:W362–W365.
36. **Hayashi S, Wu HC.** 1990. Lipoproteins in bacteria. J. Bioenerg. Biomembr. **22**:451–471.
37. **Nakayama H, Kurokawa K, Lee BL.** 2012. Lipoproteins in bacteria: structures and biosynthetic pathways. FEBS. J. **279**:4247–4268.
38. **Johnson S, Tan L, van der Veen S, Caesar J, Goicoechea De Jorge E,**

Harding RJ, Bai X, Exley RM, Ward PN, Ruivo N, Trivedi K, Cumber E, Jones R, Newham L, Staunton D, Ufret-Vincenty R, Borrow R, Pickering MC, Lea SM, Tang CM. 2012. Design and evaluation of meningococcal vaccines through structure-based modification of host and pathogen molecules. PLoS Pathog. **8**:e1002981. doi:10.1371/journal.ppat.1002981.

39. **Bergmann S, Lang A, Rohde M, Agarwal V, Rennemeier C, Grashoff C, Preissner KT, Hammerschmidt S.** 2009. Integrin-linked kinase is required for vitronectin-mediated internalization of *Streptococcus pneumoniae* by host cells. J. Cell Sci. **122**:256–267.
40. **Bujacz G, Miller M, Harrison R, Thanki N, Gilliland GL, Ogata CM, Kim SH, Wlodawer A.** 1997. Structure of monellin refined to 2.3 A resolution in the orthorhombic crystal form. Acta Crystallogr. D Biol. Crystallogr. **53**:713–719.
41. **Esposito V, Guglielmi F, Martin SR, Pauwels K, Pastore A, Piccoli R, Temussi PA.** 2010. Aggregation mechanisms of cystatins: a comparative study of monellin and oryzacystatin. Biochemistry **49**:2805–2810.
42. **Corpet F.** 1988. Multiple sequence alignment with hierarchical clustering. Nucleic Acids Res. **16**:10881–10890.
43. **Tamura K, Peterson D, Peterson N, Stecher G, Nei M, Kumar S.** 2011. MEGA5: molecular evolutionary genetics analysis using maximum likelihood, evolutionary distance, and maximum parsimony methods. Mol. Biol. Evol. **28**:2731–2739.

Figure S1, Singh *et al*

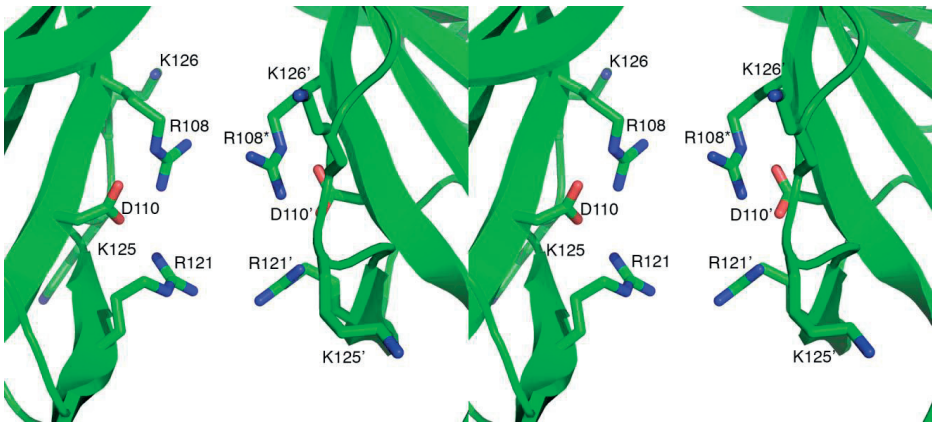

FIG. S1. Stereoview showing the side chains of the charged residues that line the bigger pocket (pocket 2) at the bottom of the PE dimer.

Figure S2, Singh *et al*

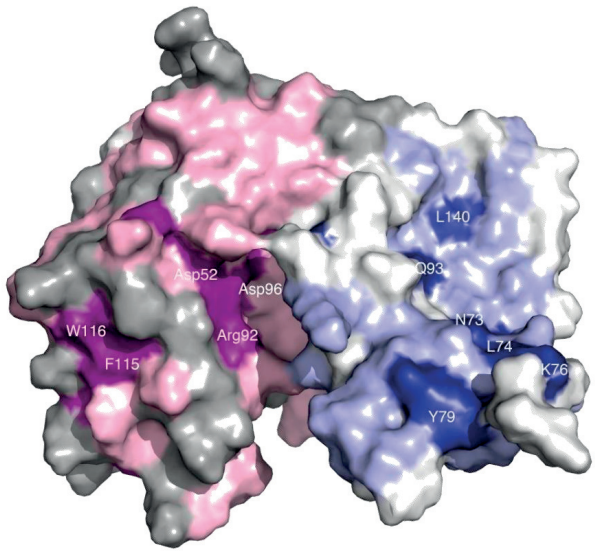

FIG. S2. Conserved residues at the surface of PE. Identical residues in the whole family of PE like proteins are shown in dark purple, homologous residues in pink, and finally non-conserved residues in white. Most of the conserved patches seem to be associated with regions that are important for the structure of the fold and are located in the core of the proteins. The two pockets that are found within the dimer of the protein are not themselves lined with conserved residues. However, in the wide funnel opening leading to the pocket at the bottom of the dimer there is a very conserved highly polar patch with central residues Asp52, Asp96 and Arg92. Some of these residues reside in the peptide 41 - 69 which has been implicated in Ln binding as described above.

Paper III

International Journal of Medical Microbiology 304 (2014) 662–668

Contents lists available at ScienceDirect

International Journal of Medical Microbiology

journal homepage: www.elsevier.com/locate/ijmm

Haemophilus influenzae stores and distributes hemin by using Protein E

Tamim Al Jubair[a], Birendra Singh[a], Christophe Fleury[a], Anna M. Blom[b], Matthias Mörgelin[c], Marjolein M. Thunnissen[d], Kristian Riesbeck[a,*]

[a] Medical Microbiology, Department of Laboratory Medicine Malmö, Lund University, SE-205 02 Malmö, Sweden
[b] Protein Chemistry, Department of Laboratory Medicine Malmö, Lund University, SE-205 02 Malmö, Sweden
[c] Section of Clinical and Experimental Infectious Medicine, Department of Clinical Sciences, Lund University, SE-221 84 Lund, Sweden
[d] Department of Biochemistry and Structural Biology, Lund University, SE-221 00 Lund, Sweden

ARTICLE INFO

Article history:
Received 13 March 2014
Received in revised form 23 April 2014
Accepted 27 April 2014

Keywords:
Haemophilus influenzae
Hemin
Protein E

ABSTRACT

The human pathogen *Haemophilus influenzae* causes mainly respiratory tract infections such as acute otitis media in children and exacerbations in patients with chronic obstructive pulmonary disease. We recently revealed the crystal structure of *H. influenzeae* protein E (PE), a multifunctional adhesin that is involved in direct interactions with lung epithelial cells and host proteins. Based upon the PE structure we here suggest a hypothetical binding pocket that is compatible in size with a hemin molecule. An *H. influenzae* mutant devoid of PE bound significantly less hemin in comparison to the PE-expressing wild type counterpart. In addition, *E. coli* expressing PE at the surface resulted in a hemin-binding phenotype. An interaction between hemin and recombinant soluble PE was also demonstrated by native-PAGE and UV-visible spectrophotometry. Surface plasmon resonance revealed an affinity (K_d) of 1.6×10^{-6} M for the hemin-PE interaction. Importantly, hemin that was bound to PE at the *H. influenzae* surface, was donated to co-cultured luciferase-expressing *H. influenzae* that were starved of hemin. When hemin is bound to PE it thus may serve as a storage pool for *H. influenzae*. To our knowledge this is the first report showing that *H. influenzae* can share hemin via a surface-located outer membrane protein.

Introduction

The Gram-negative *Haemophilus influenzae* is a member of the *Pasteurellaceae* family, and is classified as encapsulated (*H. influenzae* type a to f) and non-typeable *H. influenzae* (NTHi). After introduction of a vaccine against *H. influenzae* type b (Hib) in the 1990s, NTHi are now responsible for the majority of *Haemophilus* infections (Murphy, 2003). NTHi colonizes the mucosa and causes respiratory tract infections such as acute otitis media in children and exacerbations in patients with chronic obstructive pulmonary disease (COPD), but in rare cases also invasive disease, mainly meningitis and sepsis (Murphy et al., 2009; Resman et al., 2011).

H. influenzae has an absolute requirement for heme since it lacks 6 of 7 enzymes in the heme synthetic pathway that consequently leads to an inability to produce protoporphyrin IX (Loeb, 1995). The success of *H. influenzae* colonization thus depends on its ability to acquire protoporphyrin IX or heme from the host (Infante-Rivard and Fernandez, 1993). Since heme is a major source of iron for most bacteria, some species directly extract iron from heme while other transport heme into the cytosol to retrieve iron (Wandersman and Stojiljkovic, 2000). In the human host, iron is present in complex forms bound to high-affinity iron-binding host proteins such as transferrin, lactoferrin, the iron storage protein ferritin, or incorporated into a protoporphyrin ring (Ratledge and Dover, 2000). Free iron is potentially toxic to living cells since it can convert hydrogen peroxide into free radicals that may cause cellular damage. In fact, the free iron concentration is only $\approx 10^{-18}$ M within the human host (Bullen and Ward, 1988). However, freely available iron may occasionally arise during tissue injury, and hence free heme is released from erythrocytes upon intravascular hemolysis and inflammation caused by polymorphonuclear neutrophils (Aruoma et al., 1988; Evans et al., 1994; Resman et al., 2011; Skaar, 2010).

Although it is well known that *H. influenzae* grows on laboratory culture media containing heme as iron and protoporphyrin IX source, all key components necessary for utilization of heme have not yet been identified. Recent studies of heme/iron

* Corresponding author at: Medical Microbiology, Department of Laboratory Medicine Malmö, Lund University, Jan Waldenströms gata 59, SE-205 02 Malmö, Sweden. Tel.: +46 40 338494; fax: +46 40 336234.
E-mail address: kristian.riesbeck@med.lu.se (K. Riesbeck).

http://dx.doi.org/10.1016/j.ijmm.2014.04.015
1438-4221/

acquisition systems in *H. influenzae* have, however, defined several proteins including FbpA (ferric-ion-binding protein A), HbpA (hemoglobin/hemoglobin-haptoglobin binding protein A), SapA (sensitivity to antimicrobial peptides protein A), and finally HxuA (heme–hemopexin binding protein A) (Fournier et al., 2011; Jin et al., 1996, 1999; Khan et al., 2007; Mason et al., 2011). These proteins are located in the periplasm, but HxuA can also be secreted. Lipoprotein P4 has been described as the only outer membrane protein of *H. influenzae* that binds hemin (Reidl and Mekalanos, 1996).

H. influenzae protein E (PE) is a 16 kDa, highly conserved (96.9%–100%), ubiquitous outer membrane lipoprotein that exists in both encapsulated *H. influenzae* and NTHi (Singh et al., 2010). PE was initially described as an adhesin that binds to epithelial cells of different origins including those from COPD patients (Ronander et al., 2009). In addition, PE simultaneously binds to extracellular matrix proteins and plasminogen, interactions that all contribute to bacterial virulence (Barthel et al., 2012; Hallstrom et al., 2009, 2011). We recently crystallized PE and showed that it is a dimer with multiple binding sites for proteins derived from the host (Hallstrom et al., 2011; Singh et al., 2012, 2013). In the present paper, we suggest that *H. influenzae* contains a PE-dependent storage pool of hemin, and this may result in a hemin supply to the *H. influenzae* population when there, for example, is a paucity of hemin in the environment.

Materials and methods

Bacterial strains and reagents

All NTHi strains (NTHi 3655 wild type, NTHi 3655Δ*hpe* and NTHi 3655*lux*) were routinely grown in brain heart infusion (BHI) liquid broth, supplemented with 10 μg/ml nicotinamide adenine dinucleotide (NAD) and 10 μg/ml hemin. NTHi were cultured with shaking at 200 rpm or on chocolate agar plates incubated at 37 °C with 5% CO_2. The NTHi 3655Δ*hpe* was grown in the presence of 4 μg/ml zeomycine and the NTHi 3655*lux* in the presence of 10 μg/ml kanamycin. All strains were grown without antibiotics during co-culture. For hemin starvation, NTHi was grown in BHI medium supplemented with NAD but without hemin. *E. coli* BL21 (DE3) and DH5α were cultured in Luria–Bertani (LB) broth or on LB agar plates at 37 °C in a humid atmosphere containing 5% CO_2. *E. coli* harboring pET26b*hpe* or pET16b*hpe* (Hallstrom et al., 2009; Singh et al., 2013) were grown in LB broth in the presence of 50 μg/ml kanamycin or 100 μg/ml ampicillin, respectively.

Construction of the luminescent NTHi (NTHi 3655lux) strain

The *lux* operon (*lux*ABCDE) from *Photorhabdus luminescens* subsp. laumondii TT01 was kindly provided by Dr. Nick Waterfield (University of Warwick, Coventry, UK) and stably inserted into the genome of NTHi 3655 following a strategy described previously (Fig. S1A) (Unal et al., 2012). The promoter of protein P5 was amplified by PCR using the primers promP5_F and promP5_R (Table S1) and cloned into pKR7.1 (Su et al., 2013) that yielded the plasmid pKR7.3 after digestion by restriction enzymes EcoRV and SalI. The *lux* gene was amplified from the genomic DNA of *P. luminescens* TT01 by using specific primers luxop_F and luxop_R (Table S1). The purified PCR product was inserted into the pKR7.3 vector between restriction sites NheI and BglII to generate the vector pKR7.3*lux*ABCDE. At this stage the functionality of the *lux* operon was assessed by monitoring the chemiluminescence emitted by the *E. coli* clones with the Chemidoc XRS+ system (Biorad). Full *lux* operon along with the P5 promoter was amplified from pKR7.3*lux*ABCDE by using the KS36 and KS37 primer set, and the subsequent PCR product was used to transform the strain NTHi 3655 as described (Poje and Redfield, 2003). Transformants were selected on chocolate agar containing 10 μg/ml kanamycin. The presence of the operon in the resulting clones was verified by PCR (Fig. S1B and S1C).

Hemin-binding to the bacterial surface via PE

NTHi 3655 and NTHi 3655Δ*hpe* were collected from freshly prepared chocolate agar plates and inoculated in BHI medium supplemented with 10 μg/ml NAD only and grown for 8 h. Thereafter, bacteria were collected by centrifugation and resuspended in PBS ($OD_{600\,nm}$ = 0.1). Subsequently, a fraction of this culture (100 μl) was added to 25 ml BHI medium supplemented with hemin and NAD followed by overnight incubation. Bacteria were collected, washed three times in PBS and photographed. For semi-quantitative determination of hemin present in NTHi 3655 and NTHi 3655Δ*hpe*, bacteria were spotted on PVDF membranes by using two-step serial dilutions. Hemin was detected by an enhanced chemiluminescence (ECL) western blot detection kit (Pierce). To define the hemin-binding capacity of PE, we expressed PE on the surface of *E. coli* BL21 using pET16*hpe* as described previously (Singh et al., 2011). *E. coli* expressing PE and control *E. coli* (transformed with the empty vector pET16b) were incubated in PBS with hemin at increasing concentrations (0 μM to 150 μM). After 1 h of incubation at room temperature, *E. coli* were washed twice in PBS to remove the unbound hemin. Bacteria were finally resuspended into PBS and photographed. To assess the importance of available surface bound hemin for bacterial growth, NTHi 3655 and NTHi 3655Δ*hpe* were prepared exactly the same way as described above. After washing three times in PBS, the pellet was finally resuspended in BHI medium ($OD_{600\,nm}$ = 0.1) containing 10 μg/ml NAD in the presence or absence of hemin. Cultures were incubated at 37 °C and shaking at 200 rpm, and bacterial growth was monitored at $OD_{600\,nm}$ every 30 min during 6 h.

Protein purification and preparation of the PE-hemin complex

Protein E was recombinantly expressed in *E. coli* and purified from the soluble fraction or inclusion bodies by using a HisTrap Ni^{++} NTA resin column (GE Healthcare Biosciences) as described previously (Singh et al., 2012, 2013). Hemin (Sigma) was prepared as a 5 mM stock solution in 1 M NaOH, and thereafter diluted 200-fold in Tris-HCl, pH 7.8 containing 100 mM NaCl (TS buffer) and stored at -20 °C. To analyze the hemin bound to PE, purified PE (25 μM) was incubated with hemin at increasing concentrations (0.1–2.5 mM) in a total volume of 20 μl in TS buffer. Samples were incubated for 1 h at RT and analyzed on a 6% native PAGE (Singh and Rohm, 2008). Hemin only (2.5 mM) was also loaded as a control. Gels were run at 80 V using the gel electrophoresis Mini-PROTEAN Tetra System (Bio-Rad). PE and the PE-hemin complex were visualized by Coomassie R250 staining. For PE-hemin complex purification, first recombinant PE and hemin were mixed at a 1:2 molar ratio in TS buffer and incubated overnight at 4 °C to form the complex. The PE-hemin complex was loaded on a gel filtration column (Superdex 200) connected to an ÄKTAprime plus FPLC (GE Healthcare Biosciences) equilibrated with TS buffer, and was separated at a flow rate of 0.5 ml/min. Fractions were collected and analyzed by native PAGE. The integrity of the PE-hemin complex in different fractions was also verified by a UV-visible spectrophotometer Ultrospec 2100 pro (GE Healthcare Bioscience). Fractions containing pure PE-hemin complex were pooled accordingly and concentrated by using 5 kDa MWCO Vivaspin® concentrator (Sartorius). Protein concentration in the PE-hemin complex solution was measured using the BCA kit (Pierce). Hemin bound to PE was quantified at 385 nm by using free hemin as a standard.

UV-visible spectrophotometry and PE-hemin binding analysis

Free hemin generates a characteristic Soret band at 385 nm that shifts towards 415 nm when hemin is bound to a protein. We used this property of hemin to demonstrate the characteristics of hemin binding to PE using a UV-visible spectrophotometer (Vergauwen et al., 2010). Purified PE (15 μM) was incubated with 30 μM hemin in TS buffer for 1 h at room temperature and samples were scanned between 300 nm to 600 nm by using a UV-visible spectrophotometer. The background was corrected by 30 μM hemin (in TS buffer) in the reference cell. Figures were generated by using GraphPad Prism 6 software.

Surface plasmon resonance analysis

The affinity between PE and hemin was analyzed by surface plasmon resonance using a Biacore 2000 (GE Healthcare). Hemin was biotinylated prior to immobilization on a sensor chip. For biotinylation, 1.3 mg hemin was dissolved in 770 μl PBS, pH 7.5. Subsequently, 40 μl Biotin-PEG3 (100 mg/ml) and 190 μl of 1-ethyl-3-(3-dimethylaminopropyl) carbodiimide (EDC) (20 mg/ml) were added to the hemin solution. Hereby hemin was linked to biotin at its carboxy-side chains leaving the central iron atom intact. The labeling reaction was performed for 3 h at room temperature with gentle shaking. Thereafter, the labeled hemin was dialyzed against PBS to remove unbound biotin and finally concentrated to 1 mg/ml by using 5 kDa MWCO Vivaspin® concentrator. The hemin and hemin-biotin binding to PE was verified by using native PAGE. Biotinylated hemin was immobilized on a SA (streptavidin) sensor chip (GE Healthcare). Biotinylated hemin (2 mg/ml) diluted in running buffer (50 mM HEPES, pH 7.8 containing 150 mM NaCl, 2 mM EDTA and 0.005% Tween-20) was injected to achieve 500 resonance units (RU). Adjacent flow cell containing only streptavidin served as a negative control. The binding kinetics was studied for various concentrations of purified PE (0.19–6.0 μM). The signal from the control surface was subtracted. In all experiments, two consecutive injections of 2 M NaCl were used to remove bound ligands during a regeneration step. The BiaEvaluation 3.0 software (Biacore) was used to determine response at steady state for each sensorgram, which was thereafter plotted against PE the concentration. K_d was calculated using a steady state affinity equation.

Analysis of bacterial growth by using the PE-hemin complex as a source of hemin

NTHi 3655 were grown without hemin for 8 h in BHI medium supplemented with 10 μg/ml NAD only. Bacteria were washed three times in PBS and inoculated into fresh BHI ($OD_{600\,nm}$ = 0.1) containing NAD (10 μg/ml). Free hemin or equimolar concentrations of PE-hemin complex were used as an iron source. Growth of bacteria was monitored every 30 min for 6 h by measuring absorbance ($OD_{600\,nm}$) using a cell density meter (Biowave CO8000, Biochrom). These cultures were also grown overnight (18 h) to ensure that most of the hemin was consumed in the culture medium, and to exclude dissociation of the PE-hemin complex. In addition, we incubated the PE-hemin complex in BHI and NAD for 18 h in the absence of NTHi. To purify PE, or the PE-hemin complex, bacteria were spun down, and thereafter supernatants were loaded on a HisTrap Ni^{++}-resin column (GE Healthcare Biosciences). Purified samples were analyzed by a UV-visible spectrophotometer.

Co-culture of luminescent NTHi 3655lux with NTHi 3655 or NTHi 3655Δhpe

NTHi 3655 or NTHi 3655Δ*hpe* were co-cultured with NTHi 3655*lux* to analyze transfer of hemin between the strains. NTHi 3655 and NTHi 3655Δ*hpe* were prepared as described above. In parallel, NTHi 3655*lux* was starved for hemin. For starvation, NTHi 3655*lux* was freshly grown on chocolate agar plates and inoculated in BHI medium containing only NAD (10 μg/ml) for 8 h at 37 °C. The optical densities of all cultures were adjusted in BHI medium, and bacteria at equal numbers were mixed. Each reaction was performed in triplicates (final culture volume 1.3 ml) in a 96-well plate (Uniplate®, Whatman) followed by incubation at 37 °C. One sterile glass bead was added to each well for proper agitation during shaking at 200 rpm. The luminescence was monitored every hour in a 1450 MicroBeta TriLux counter (PerkinElmer).

Statistical analysis

Data were analyzed with the two-way analysis of variance (ANOVA) using the GraphPad Prism 6.0. A P value ≤ 0.05 was considered as statistically significant.

Results

Protein E binds hemin at the surface of Haemophilus influenzae and functions as a reservoir for hemin

It is a well-known fact that *H. influenzae* needs heme for growth and survival in the host (Infante-Rivard and Fernandez, 1993). Based upon the structural data of the PE molecule that appears as a dimer with a pocket (Singh et al., 2013), we screened several ligands including hemin that may possibly interact with PE. Molecular modeling indicated that the binding pocket may accommodate a hemin molecule (Fig. 1).

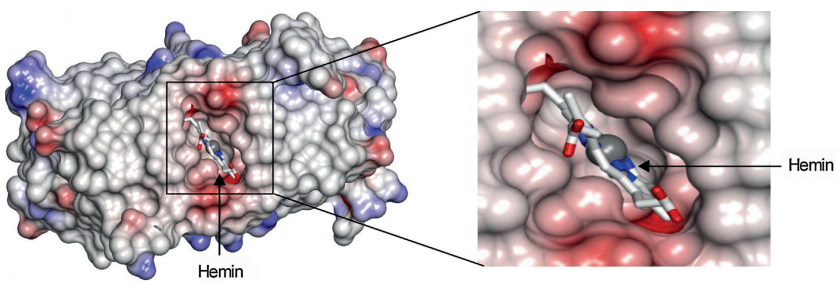

Fig. 1. Putative docking of a hemin molecule in the binding pocket of the PE-dimer. Surface representation of the PE crystal structure (Singh et al., 2012, 2013) with a hypothetical model of the PE-hemin complex. Insert: zoom in projection of a putative hemin-binding pocket in dimeric PE. Docking was performed manually using COOT (Emsley et al., 2010; McNicholas et al., 2011; Potterton et al., 2002). The figures were prepared with Pymol and CCP4MG.

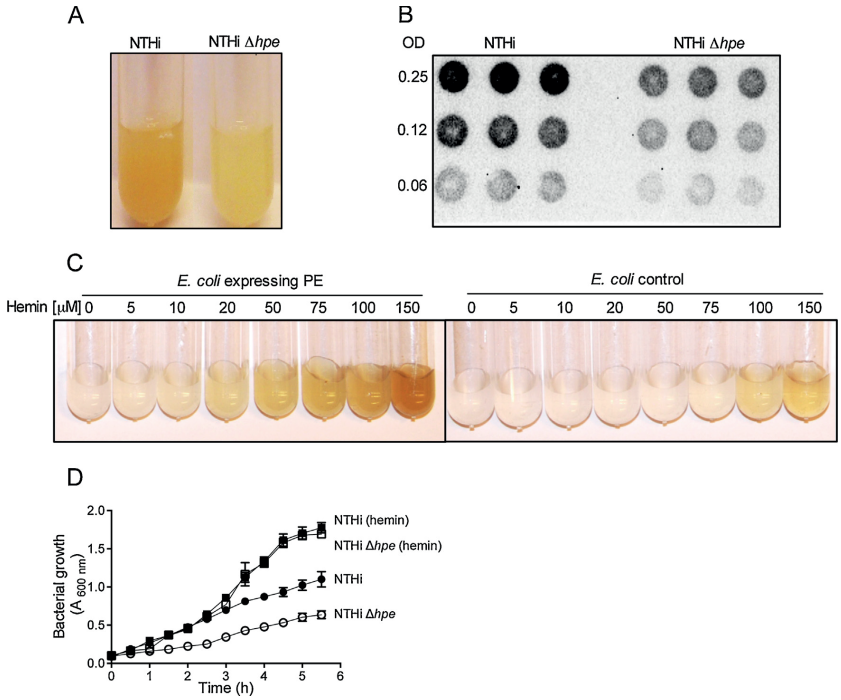

Fig. 2. *Haemophilus influenzae* PE binds hemin at the bacterial surface and utilizes it when needed. (A) Hemin binding to NTHi 3655 and NTHi 3655Δ*hpe*. Bacteria were grown overnight in BHI with hemin and NAD (both at 10 μg/ml). After washing three times in PBS, 5 ml culture ($OD_{600\,nm}$ = 1 corresponding to 10^9 NTHi) of each strain were resuspended in 1 ml PBS. (B) Semi quantitative measurement of PE-dependent hemin-binding on the surface of wild type NTHi 3655 as compared to the PE mutant NTHi 3655Δ*hpe*. Bacteria shown in panel A were serially diluted and spotted on a PVDF filter. ECL was used for detection of hemin on blots. (C) *E. coli* expressing PE at the surface bound hemin. *E. coli* expressing PE and control *E. coli* with an empty vector were incubated at room temperature with increasing concentrations of hemin. After 1 h incubation, bacteria were washed, resuspended in PBS and photographed. (D) Growth of NTHi 3655 and NTHi 3655Δ*hpe* in BHI with NAD in the presence or absence of hemin. Before initiation of the culture for determining a growth curve, NTHi strains were incubated overnight with hemin and NAD followed by three washes in PBS. All experiments were repeated three times. The data in D represent mean values of three independent experiments with error bars indicating standard deviations (SD).

Since PE is a surface-exposed outer membrane protein (Ronander et al., 2009), we questioned if an *hpe* gene mutation would interfere with the hemin-binding capacity of *H. influenzae*. Importantly, we observed a difference in hemin-binding between wild type NTHi 3655 and the PE mutant NTHi 3566Δ*hpe* as visually verified in test tubes (Fig. 2A). Bacteria from cultures shown in Fig. 2A were also blotted on a nitrocellulose membrane and hemin was analyzed by using ECL (Fig. 2B). This semiquantitative determination indicated that more hemin had been acquired by NTHi 3655 in comparison to the PE mutant NTHi 3655Δ*hpe*. To further prove that PE binds hemin, recombinant PE was expressed at the surface of *E. coli*. In agreement with the results obtained with *H. influenzae* (Fig. 2A), addition of hemin to PE-expressing *E. coli*, led to more hemin acquisition in comparison to a control *E. coli* carrying an empty vector (Fig. 2C).

We also analyzed whether hemin bound to PE at the surface of NTHi would influence bacterial growth. The PE-expressing wild type NTHi and the corresponding PE mutant NTHi 3655Δ*hpe* were grown in medium supplemented with hemin overnight. After extensive washing steps to remove unbound hemin, the two NTHi strains were separately incubated in culture medium without hemin. Bacterial growth was thereafter analyzed at the indicated time points (Fig. 2D). Interestingly, the NTHi 3655Δ*hpe* grew slower than NTHi 3655 in the absence of hemin, whereas growth of both strains was comparable in culture medium supplemented with hemin (10 μg/ml) (Fig. 2D). Taken together, our results suggest that PE plays a role as a hemin-binding outer membrane protein of *H. influenzae*, and may work as a storage pool for hemin.

Soluble recombinant H. influenzae PE binds hemin

To examine the direct hemin-binding capacity of PE, recombinant PE and hemin were mixed to form a complex followed by native PAGE. PE without hemin migrated slowly, whereas incubation of PE with increasing hemin concentrations resulted in formation of a PE-heme complex that migrated much faster through the native gel (Fig. 3A). UV-visible spectrophotometry also confirmed a direct interaction between PE and hemin (Fig. 3B). The absorption spectrum of hemin has a characteristic peak in the Soret band region that comprises a wavelength with visible blue light at ≈385 nm. A red shift of the Soret peak occurred with the PE-hemin complex, which was clearly observed at 415 nm (Fig. 3C). This suggested a PE-mediated perturbation of the electronic structure of the hemin iron.

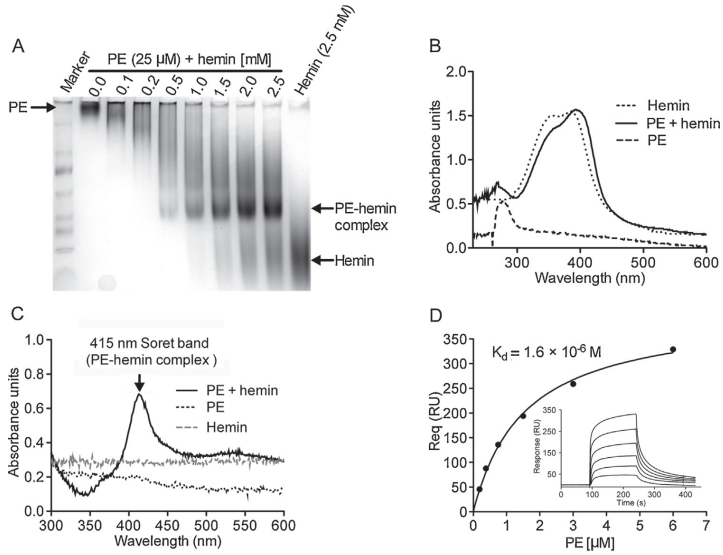

Fig. 3. Protein E of *H. influenzae* is a hemin-binding protein. (A) Native-PAGE gel illustrating binding of hemin to PE. PE (25 μM) was pre-incubated with hemin (0–2.5 mM) and subjected to a native PAGE followed by staining with Coomassie blue R250. The PE-hemin complex migrated faster than only PE. (B) The UV-visible spectra demonstrate the deviation in absorbance spectrum of 30 μM hemin solution when mixed with PE. PE (15 μM) incubated with hemin (30 μM) showed a shift of the peak toward 415 nm. (C) UV-visible spectrum of the PE-hemin complex. Complexes of 15 μM PE with 30 μM hemin was scanned and analyzed. Hemin (30 μM) was used in the reference cell and values presented were adjusted with respect to this background measurement. This spectrum showed that the Soret band for unbound hemin was at 385 nm and shifted to 415 nm upon interaction with PE. (D) Surface plasmon resonance analysis of PE and hemin. Biotinylated hemin was immobilized on a SA sensor chip and PE at increasing concentrations was injected. Sensograms for all PE concentrations (PE at 0.19–6.0 μM) are shown in the inset. The measurements were performed using a Biacore 2000. The response units at saturation were plotted against PE concentrations and fitted using a steady state affinity model and the Biaevaluation software.

The affinity of the hemin interaction with PE was analyzed by surface plasmon resonance (Biacore). Biotinylated hemin was immobilized on a sensor chip followed by injection of PE at increasing concentrations. A steady state affinity model suggested that hemin interacted with PE at $K_d \approx 1.6 \pm 0.27 \times 10^{-6}$ M (Fig. 3D). The surface protein F (PF) (Su et al., 2013) was included as a negative control and did not bind to hemin (data not shown). Taken together, the *H. influenzae* PE has the capacity to attract hemin resulting in a stable complex formation.

H. influenzae captures hemin from a complex consisting of recombinant PE and hemin

To investigate whether hemin bound to recombinant PE can be used by *H. influenzae* and thereby promote bacterial growth, we incubated NTHi 3655 starved of hemin in the presence of the PE-hemin complex or equimolar free hemin. Interestingly, no difference in bacterial growth was observed between cultures supplemented with either the PE-hemin complex or free hemin while in their absence any growth was not observed (Fig. 4A).

To exclude that the PE-hemin complex dissociated during our culture conditions, the PE-hemin complex was incubated for up to 18 h at the same culture conditions but without NTHi. This time point was also chosen to ensure that NTHi had utilized all hemin from the PE-hemin complex. Culture samples were subjected to affinity chromatography using Ni^{++}-NTA resin columns. After elution and quantification, UV-visible spectrophotometry was performed. The integrity of the PE-hemin complex in the absence of NTHi was verified by a shift of the Soret peak toward the wavelength 415 nm (Fig. 4B). In contrast, no PE-hemin complex was detected in cultures with NTHi suggesting that hemin most likely had been consumed by the bacteria. The PE-hemin complex was thus stable and could be used as a hemin source for NTHi.

Hemin loaded on PE at the bacterial surface is donated to H. influenzae starved of hemin

Our experiments with NTHi 3655 and the PE mutant (Fig. 2D) suggested that PE may play a crucial role for the supply of hemin. To further demonstrate the usage of hemin derived from PE, we set up a co-culture with a luminescent NTHi (NTHi 3655*lux*) that was starved of hemin, and NTHi 3655 or NTHi 3655Δ*hpe* that both were cultured in the presence of hemin (Fig. 2A). Interestingly, NTHi 3655*lux* grew better when incubated with NTHi 3655 that carried more hemin at the surface as compared to the PE-deficient NTHi 3655Δ*hpe* (Fig. 5A). Growth of NTHi 3655*lux* in the presence or absence of supplemented hemin was included as a control in a parallel experiment (Fig. 5B). To summarize, our results indicate that hemin is shared between *H. influenzae* during shortage, that is, hemin-carrying NTHi may donate hemin to the co-cultured NTHi population.

Discussion

Iron is an essential element for almost all living organisms. As a catalytic center for redox reactions in many enzymes, iron facilitates numerous cellular processes such as electron transport, peroxide reduction, and nucleotide biosynthesis (Tong and Guo, 2009). As free iron is relatively insoluble and toxic, specific uptake pathways are present in almost all organisms. The iron uptake by

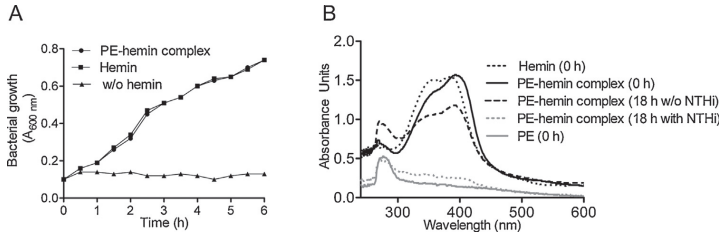

Fig. 4. Hemin is acquired by *H. influenzae* from the PE-hemin complex in solution. (A) Growth of NTHi 3655 in culture medium supplemented with free hemin, or equimolar concentrations (7.6 μM corresponding to 5 μg/ml) of the PE-hemin complex as compared to NTHi incubated in the absence of hemin. NAD was included in all cultures. (B) UV-visible spectrophotometry of samples from the experiment outlined in (A). Hemin was bound to PE as an integrated PE-hemin complex in control cultures that were incubated without NTHi for 18 h. In contrast, hemin was extracted from the PE-hemin complex when incubated for 18 h with NTHi resulting in free PE in the supernatants. This experiment was repeated three times, and one representative experiment is shown here.

Gram negative bacteria is energized by the TonB-ExbB-ExbD system, and iron is imported by ABC transporters. The TonB system of *H. influenzae* is involved in iron uptake mechanisms and is essential for virulence (Jarosik et al., 1995; Morton et al., 2012). Several pathogens also secrete high affinity iron-binding siderophores for iron retrieval from the surrounding tissue (Andrews et al., 2003). *H. influenzae* lacks the enzymes required in the biosynthetic pathway for the porphyrin ring, which is an immediate precursor of heme (Panek and O'Brian, 2002). *H. influenzae* expresses, however, ferrochelatase, which mediates insertion of iron into protoporphyrin IX to produce heme (Loeb, 1995; Panek and O'Brian, 2002). Thus, *H. influenzae* utilizes hemin, hemoglobin, hemoglobin-haptoglobin, heme-hemopexin, transferrin and lactoferrin as iron sources. Since the species cannot grow in the absence of iron or porphyrin, both are indispensable for *H. influenzae* colonization (Gilder and Granick, 1947).

It is now apparent that *H. influenzae* has numerous mechanisms for binding and uptake of heme, irrespectively whether the heme is free or bound to a heme host carrier protein (Cope et al., 2000). However, in contrast to other bacterial species, *H. influenzae* does not produce any siderophores by itself, but can utilize siderophores produced by other microorganisms for iron uptake (Morton et al., 2010). The mechanisms for heme acquisition have not yet been fully elucidated for this bacterial species, but several heme-binding proteins of *Haemophilus* have been studied for their interaction with heme. Most of those are transporters or transport-associated proteins described as hemophores (Whitby et al., 2009). High heme content can be toxic for some pathogens, whereas several pathogens such as *Yersinia pestis*, *Aeromonas salmonicida*, *Shigella flexneri*, *Prevotella* spp., and *Porphyromonas* spp. are known for storing heme at their surface and utilize it for virulence (Anzaldi and Skaar, 2010). *H. influenzae* outer membrane lipoprotein P4 was previously described to play role in hemin uptake and transport (Reidl and Mekalanos, 1996). However, any hemin storage surface protein of *H. influenzae* has until now not been reported. Here we suggest that hemin is not only stored by PE at the bacterial surface but can also be utilized by other NTHi in the population. The hemin storage pool can thus also overcome the nutritional immunity and assist bacteria to survive in conditions related to heme paucity.

The equilibrium dissociation constant (K_d) of the PE-hemin binding affinity was 1.6×10^{-6} M as estimated by surface plasmon resonance. This is one of the highest affinites reported for any membrane protein of *H. influenzae*. Interestingly, the hemin-binding affinity for PE is higher than that of periplasmic heme-binding proteins such as HbpA ($K_d \approx 655 \times 10^{-6}$ M) and SapA ($K_d \approx 56 \times 10^{-6}$ M) (Jin et al., 1996, 1999). However, FbpA binds ferric iron with an affinity that was estimated to $K_d = 2.0 \times 10^{-18}$ M, and FbpA furthermore extracts iron from the human high affinity iron-binding protein transferrin (Khan et al., 2007). Thus, based upon the binding affinity and comparison with other iron acquiring proteins of *H. influenzae*, that is, HbpA, SapA and FbpA, PE has an optimal affinity for hemin to function as a hemin carrier for *H. influenzae*. We hypothesize that PE may attract hemin from the surroundings in the bacterial niche when there is excess hemin available during, for example, tissue destruction linked to infection, smoking-induced damage or inflammation in COPD patients.

In conclusion, this report reveals a unique function attributed to the multifunctional *H. influenzae* PE. The involvement of PE in hemin acquisition was proven by analysis of a NTHi mutant devoid of PE in addition to surface expression of the heterologous host *E.*

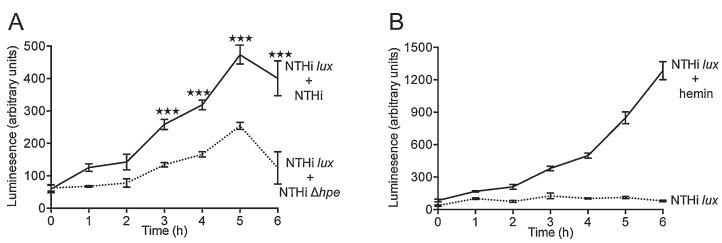

Fig. 5. Hemin bound to PE at the surface of *H. influenzae* is shared with co-cultured NTHi. (A) Growth of NTHi 3655*lux* was significantly promoted by NTHi 3655 as compared to NTHi 3655Δ*hpe* that was devoid of PE. To provide hemin, 10^8 cfu of NTHi 3655 or PE-mutant NTHi 3655Δ*hpe* were added to 10^8 luciferase-producing NTHi 3655*lux*. (B) Growth of NTHi 3655*lux* with or without supplemented hemin. NTHi 3655*lux* was grown in BHI medium containing 10 μg/ml each of hemin and NAD. In (A), NTHi 3655 and the PE-mutant NTHi 3655Δ*hpe* were first grown in BHI supplemented with hemin and NAD (both at 10 μg/ml). After three washings in PBS, the NTHi 3655*lux* was co-cultured with either NTHi or NTHi 3655Δ*hpe* at a ratio of 1:1. Results are shown as luminescence related to growth of NTHi 3655*lux*. The data represent mean values of three independent experiments in triplicates. Error bars indicate SD. Statistical significance of differences was calculated using a two-way ANOVA; $^{***}P \leq 0.001$.

coli. This is to our knowledge the first experimental evidence on distribution of hemin between *H. influenzae* and sheds light upon the mechanisms that are related to nutrient sharing.

Acknowledgements

We thank Dr. Nick Waterfield (University of Warwick, Coventry, UK) for providing us *Photorhabdus luminescens* subsp. laumondii TT01 with the *lux* operon (*lux*ABCDE). This work was supported by grants from the Alfred Österlund, the Anna and Edvin Berger Foundation, the Swedish Medical Research Council (grant number 521-2010-4221 and K2012-66X-14928-09-5, www.vr.se), the Cancer Foundation at the University Hospital in Malmö, the Physiographical Society (Forssman's Foundation), and Skåne County Council's research and development foundation.

Appendix A. Supplementary data

Supplementary data associated with this article can be found, in the online version, at http://dx.doi.org/10.1016/j.ijmm.2014.04.015.

References

Andrews, S.C., Robinson, A.K., Rodriguez-Quinones, F., 2003. Bacterial iron homeostasis. FEMS Microbiol. Rev. 27, 215–237.
Anzaldi, L.L., Skaar, E.P., 2010. Overcoming the heme paradox: heme toxicity and tolerance in bacterial pathogens. Infect. Immun. 78, 4977–4989.
Aruoma, O.I., Bomford, A., Polson, R.J., Halliwell, B., 1988. Nontransferrin-bound iron in plasma from hemochromatosis patients: effect of phlebotomy therapy. Blood 72, 1416–1419.
Barthel, D., Singh, B., Riesbeck, K., Zipfel, P.F., 2012. *Haemophilus influenzae* uses the surface protein E to acquire human plasminogen and to evade innate immunity. J. Immunol. 188, 379–385.
Bullen, J.J., Ward, C.G., 1988. Iron and infection. Br. Med. J. (Clin. Res. Ed.) 296, 1539.
Cope, L.D., Hrkal, Z., Hansen, E.J., 2000. Detection of phase variation in expression of proteins involved in hemoglobin and hemoglobin-haptoglobin binding by nontypeable *Haemophilus influenzae*. Infect. Immun. 68, 4092–4101.
Emsley, P., Lohkamp, B., Scott, W.G., Cowtan, K., 2010. Features and development of Coot. Acta Crystallogr. D Biol. Crystallogr. 66, 486–501.
Evans, P.J., Evans, R.W., Bomford, A., Williams, R., Halliwell, B., 1994. Metal ions catalytic for free radical reactions in the plasma of patients with fulminant hepatic failure. Free Radic. Res. 20, 139–144.
Fournier, C., Smith, A., Delepelaire, P., 2011. Haem release from haemopexin by HxuA allows *Haemophilus influenzae* to escape host nutritional immunity. Mol. Microbiol. 80, 133–148.
Gilder, H., Granick, S., 1947. Studies on the Hemophilus group of organisms; quantitative aspects of growth on various porphin compounds. J. Gen. Physiol. 31, 103–117.
Hallstrom, T., Blom, A.M., Zipfel, P.F., Riesbeck, K., 2009. Nontypeable *Haemophilus influenzae* protein E binds vitronectin and is important for serum resistance. J. Immunol. 183, 2593–2601.
Hallstrom, T., Singh, B., Resman, F., Blom, A.M., Morgelin, M., Riesbeck, K., 2011. *Haemophilus influenzae* protein E binds to the extracellular matrix by concurrently interacting with laminin and vitronectin. J. Infect. Dis. 204, 1065–1074.
Infante-Rivard, C., Fernandez, A., 1993. Otitis media in children: frequency, risk factors, and research avenues. Epidemiol. Rev. 15, 444–465.
Jarosik, G.P., Maciver, I., Hansen, E.J., 1995. Utilization of transferrin-bound iron by *Haemophilus influenzae* requires an intact tonB gene. Infect. Immun. 63, 710–713.
Jin, H., Ren, Z., Pozsgay, J.M., Elkins, C., Whitby, P.W., Morton, D.J., Stull, T.L., 1996. Cloning of a DNA fragment encoding a heme-repressible hemoglobin-binding outer membrane protein from *Haemophilus influenzae*. Infect. Immun. 64, 3134–3141.
Jin, H., Ren, Z., Whitby, P.W., Morton, D.J., Stull, T.L., 1999. Characterization of hgpA, a gene encoding a haemoglobin/haemoglobin-haptoglobin-binding protein of *Haemophilus influenzae*. Microbiology 145 (Pt 4), 905–914.
Khan, A.G., Shouldice, S.R., Kirby, S.D., Yu, R.H., Tari, L.W., Schryvers, A.B., 2007. High-affinity binding by the periplasmic iron-binding protein from *Haemophilus influenzae* is required for acquiring iron from transferrin. Biochem. J. 404, 217–225.
Loeb, M.R., 1995. Ferrochelatase activity and protoporphyrin IX utilization in *Haemophilus influenzae*. J. Bacteriol. 177, 3613–3615.
Mason, K.M., Raffel, F.K., Ray, W.C., Bakaletz, L.O., 2011. Heme utilization by nontypeable *Haemophilus influenzae* is essential and dependent on Sap transporter function. J. Bacteriol. 193, 2527–2535.
McNicholas, S., Potterton, E., Wilson, K.S., Noble, M.E., 2011. Presenting your structures: the CCP4mg molecular-graphics software. Acta. Crystallogr. D Biol. Crystallogr. 67, 386–394.
Morton, D.J., Hempel, R.J., Seale, T.W., Whitby, P.W., Stull, T.L., 2012. A functional tonB gene is required for both virulence and competitive fitness in a chinchilla model of *Haemophilus influenzae* otitis media. BMC Res. Notes 5, 327.
Morton, D.J., Turman, E.J., Hensley, P.D., VanWagoner, T.M., Seale, T.W., Whitby, P.W., Stull, T.L., 2010. Identification of a siderophore utilization locus in nontypeable *Haemophilus influenzae*. BMC Microbiol. 10, 113.
Murphy, T.F., 2003. Respiratory infections caused by non-typeable *Haemophilus influenzae*. Curr. Opin. Infect. Dis. 16, 129–134.
Murphy, T.F., Bakaletz, L.O., Smeesters, P.R., 2009. Microbial interactions in the respiratory tract. Pediatr. Infect. Dis. J. 28, S121–S126.
Panek, H., O'Brian, M.R., 2002. A whole genome view of prokaryotic haem biosynthesis. Microbiology 148, 2273–2282.
Poje, G., Redfield, R.J., 2003. Transformation of *Haemophilus influenzae*. Methods Mol. Med. 71, 57–70.
Potterton, E., McNicholas, S., Krissinel, E., Cowtan, K., Noble, M., 2002. The CCP4 molecular-graphics project. Acta. Crystallogr. D Biol. Crystallogr. 58, 1955–1957.
Ratledge, C., Dover, L.G., 2000. Iron metabolism in pathogenic bacteria. Annu. Rev. Microbiol. 54, 881–941.
Reidl, J., Mekalanos, J.J., 1996. Lipoprotein e(P4) is essential for hemin uptake by *Haemophilus influenzae*. J. Exp. Med. 183, 621–629.
Resman, F., Ristovski, M., Ahl, J., Forsgren, A., Gilsdorf, J.R., Jasir, A., Kaijser, B., Kronvall, G., Riesbeck, K., 2011. Invasive disease caused by *Haemophilus influenzae* in Sweden 1997–2009; evidence of increasing incidence and clinical burden of non-type b strains. Clin. Microbiol. Infect. 17, 1638–1645.
Ronander, E., Brant, M., Eriksson, E., Morgelin, M., Hallgren, O., Westergren-Thorsson, G., Forsgren, A., Riesbeck, K., 2009. Nontypeable *Haemophilus influenzae* adhesin protein E: characterization and biological activity. J. Infect. Dis. 199, 522–531.
Singh, B., Al Jubair, T., Fornvik, K., Thunnissen, M.M., Riesbeck, K., 2012. Crystallization and X-ray diffraction analysis of a novel surface-adhesin protein: protein E from *Haemophilus influenzae*. Acta Crystallogr. Sect. F Struct. Biol. Cryst. Commun. 68, 222–226.
Singh, B., Al-Jubair, T., Morgelin, M., Thunnissen, M.M., Riesbeck, K., 2013. The unique structure of *Haemophilus influenzae* protein E reveals multiple binding sites for host factors. Infect. Immun. 81, 801–814.
Singh, B., Brant, M., Kilian, M., Hallstrom, B., Riesbeck, K., 2010. Protein E of *Haemophilus influenzae* is a ubiquitous highly conserved adhesin. J. Infect. Dis. 201, 414–419.
Singh, B., Jalalvand, F., Morgelin, M., Zipfel, P., Blom, A.M., Riesbeck, K., 2011. *Haemophilus influenzae* protein E recognizes the C-terminal domain of vitronectin and modulates the membrane attack complex. Mol. Microbiol. 81, 80–98.
Singh, B., Rohm, K.H., 2008. A new subfamily of bacterial glutamate/aspartate receptors. Biol. Chem. 389, 33–36.
Skaar, E.P., 2010. The battle for iron between bacterial pathogens and their vertebrate hosts. PLoS Pathog. 6, e1000949.
Su, Y.C., Jalalvand, F., Morgelin, M., Blom, A.M., Singh, B., Riesbeck, K., 2013. *Haemophilus influenzae* acquires vitronectin via the ubiquitous Protein F to subvert host innate immunity. Mol. Microbiol. 87, 1245–1266.
Tong, Y., Guo, M., 2009. Bacterial heme-transport proteins and their heme-coordination modes. Arch. Biochem. Biophys. 481, 1–15.
Unal, C.M., Singh, B., Fleury, C., Singh, K., Chavez de Paz, L., Svensater, G., Riesbeck, K., 2012. QseC controls biofilm formation of non-typeable *Haemophilus influenzae* in addition to an AI-2-dependent mechanism. Int. J. Med. Microbiol. 302, 261–269.
Vergauwen, B., Elegheert, J., Dansercoer, A., Devreese, B., Savvides, S.N., 2010. Glutathione import in *Haemophilus influenzae* Rd is primed by the periplasmic heme-binding protein HbpA. Proc. Natl. Acad. Sci. USA 107, 13270–13275.
Wandersman, C., Stojiljkovic, I., 2000. Bacterial heme sources: the role of heme, hemoprotein receptors and hemophores. Curr. Opin. Microbiol. 3, 215–220.
Whitby, P.W., Seale, T.W., VanWagoner, T.M., Morton, D.J., Stull, T.L., 2009. The iron/heme regulated genes of *Haemophilus influenzae*: comparative transcriptional profiling as a tool to define the species core modulon. BMC Genomics 10, 6.

Appendix A. Supplementary data

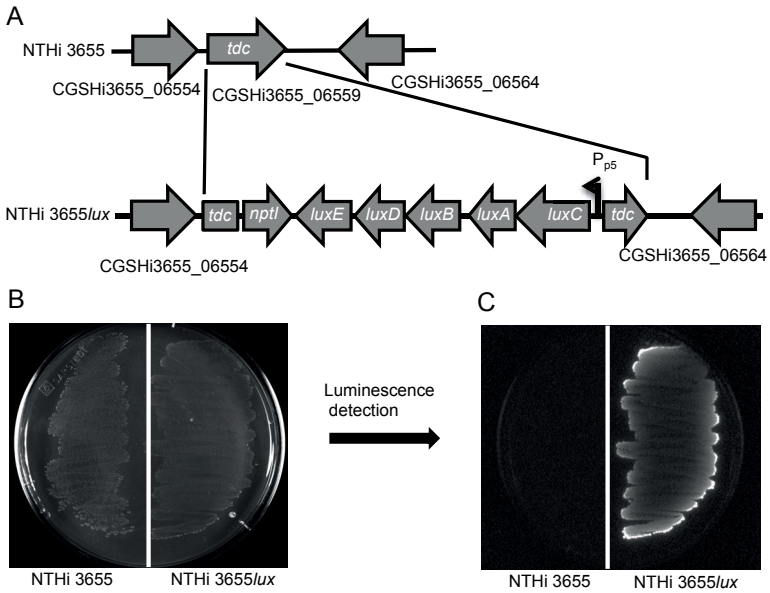

Fig. S1. Insertion of the *P. luminescens lux* operon in the genome of NTHi 3655. (A) Diagram depicting the strategy employed to insert the lux operon (*lux*ABCDE) from luminescens TT01 into NTHi 3655 genome. Genomic insertion was done in the locus CGSHi3655_06559 annotated as threonine dehydratase (*tdc*) in the draft genome of NTHi 3655. (B) NTHi 3655 and NTHi 3655*lux* luminescent clones grown overnight on GCG plates. (C) Luminescence was observed on a chemidoc XRS+ system (Biorad).

Table S1. Primers used for construction of the NTHi 3655*lux* strain

Primer	Sequence (5'-3')	Restriction enzyme
PromP5_F	CGCGATATCTGAAGGTAAAACGGCAGG	EcoRV
PromP5_R	TAACGTCGACAGATCTGGCGCGCCTAGGCTAGCTTTAGTCATCGAATAGTAATAAA	SalI
Luxop_F	AATCTATCGCTAGCTAAAT**AAGGA**CATCTTATGACTAAAAAAATTTCATTCATT	NheI
Luxop_R	CTCTGTCGACAGATCTGGAATCAACTATTAAATGCTT	BglII
KS36	GGCGGATCCTG**ACCGCACTT**AGGGGGATAAAACAAAGG	
KS37	GGCCTCGAG**AAGTGCGGT**CAGGCAAGTCCCTGTTCAAA	

The restriction enzyme sites used for cloning of the inserts are underlined. The ribosome binding site (in Luxop_F) and uptake signal sequences (in KS36 and KS37) are highlighted in bold.

Paper IV

IAI Journals.ASM.org

A Fine-Tuned Interaction between Trimeric Autotransporter *Haemophilus* Surface Fibrils and Vitronectin Leads to Serum Resistance and Adherence to Respiratory Epithelial Cells

Birendra Singh,[a] Yu-Ching Su,[a] Tamim Al-Jubair,[a] Oindrilla Mukherjee,[a] Teresia Hallström,[b] Matthias Mörgelin,[c] Anna M. Blom,[d] Kristian Riesbeck[a]

Medical Microbiology, Department of Laboratory Medicine Malmö, Lund University, Malmö, Sweden[a]; Department of Infection Biology, Leibniz Institute for Natural Product Research and Infection Biology, Hans-Knoell-Institute, Jena, Germany[b]; Section of Clinical and Experimental Infectious Medicine, Department of Clinical Sciences, Lund University, Lund, Sweden[c]; Division of Medical Protein Chemistry, Wallenberg Laboratory, Department of Laboratory Medicine Malmö, Lund University, Skåne University Hospital, Malmö, Sweden[d]

***Haemophilus influenzae* type b (Hib) escapes the host immune system by recruitment of the complement regulator vitronectin, which inhibits the formation of the membrane attack complex (MAC) by inhibiting C5b-C7 complex formation and C9 polymerization. We reported previously that Hib acquires vitronectin at the surface by using *Haemophilus* surface fibrils (Hsf). Here we studied in detail the interaction between Hsf and vitronectin and its role in the inhibition of MAC formation and the invasion of lung epithelial cells. The vitronectin-binding region of Hsf was defined at the N-terminal region comprising Hsf amino acids 429 to 652. Moreover, the Hsf recognition site on vitronectin consisted of the C-terminal amino acids 352 to 374. *H. influenzae* was killed more rapidly in vitronectin-depleted serum than in normal human serum (NHS), and increased MAC deposition was observed at the surface of an Hsf-deficient *H. influenzae* mutant. In parallel, Hsf-expressing *Escherichia coli* selectively acquired vitronectin from serum, resulting in significant inhibition of the MAC. Moreover, when vitronectin was bound to Hsf, increased bacterial adherence and internalization into epithelial cells were observed. Taking our findings together, we have defined a fine-tuned protein-protein interaction between Hsf and vitronectin that may contribute to increased Hib virulence.**

Haemophilus influenzae is a Gram-negative respiratory pathogen. The species is divided into two groups depending on the presence or absence of a polysaccharide capsule. Encapsulated strains are further divided into six different serotypes, a, b, c, d, e, and f, whereas unencapsulated strains are referred to as nontypeable *H. influenzae* (NTHi). The most virulent strain is *H. influenzae* type b (Hib), which causes sepsis, pneumonia, osteomyelitis, epiglottitis, joint infections, and acute meningitis (1, 2). Although the incidence of Hib infections in developed countries has been dramatically reduced since the introduction of the Hib conjugate vaccine in the early 1990s, Hib remains a major infectious agent related to lower respiratory tract infections and causes meningitis in infants and children in many developing countries (3, 4).

The initial step of successful colonization and subsequent infection by *Haemophilus* is bacterial adherence to host tissue, a phenomenon mediated by adhesins. Upon overcoming the mucociliary escalator, bacteria colonize and may damage the epithelial cells and break down tight junctions. Subsequently, *H. influenzae* reaches the basement membrane and the extracellular matrix (ECM) and occasionally penetrates into deeper tissue layers (2, 5–7). In addition to these virulence properties, Hib often breaches the blood-brain barrier and causes inflammation of the meninges of the brain (8). The invasive mechanisms are, however, not fully understood.

Hsf (*Haemophilus* surface fibrils) is a major trimeric autotransporter adhesin initially reported in Hib. Hsf is a protein highly conserved among all typeable strains, with a monomeric size of approximately 243 kDa that builds up a trimer of approximately 750 kDa (9). In unencapsulated strains, a homologue to the Hsf protein, *H. influenzae* adhesin (Hia), can be found. Hia is present only in approximately 25% of clinical NTHi isolates (10) and cannot be found in encapsulated *H. influenzae*. In contrast, the Hia homologue Hsf exists in all typeable strains (11–13). Although Hia has a smaller size of ≈114 kDa (≈342 kDa as a trimer), these two proteins are highly homologous at their N and C termini, with an overall 81% similarity and 72% identity. Both Hia and Hsf are constituted of various repetitive domains, which are also relatively similar in their secondary structures (9, 14).

The survival of Hib in the host is controlled by the acquisition of complement regulators at the surface of the pathogen for effective inhibition of opsonization, phagocytosis, and formation of the membrane attack complex (MAC) (15, 16). A major regulatory component of the MAC is the multifunctional glycoprotein vitronectin (Vn), which is found both in plasma and in the ECM. Vn has an RGD domain in the N terminus that is known to interact with integrins of the host epithelial cells, whereas the C-terminal heparin binding domain (HBD3) has been shown to be used by bacterial pathogens to bind Vn (17–20). Simultaneous interaction of Vn with integrins and bacterial surface proteins has been thought to result in the formation of a bridge between bacteria and

Received 19 December 2013 **Returned for modification** 14 January 2014
Accepted 18 March 2014
Published ahead of print 24 March 2014
Editor: B. A. McCormick
Address correspondence to Kristian Riesbeck, kristian.riesbeck@med.lu.se.
Supplemental material for this article may be found at http://dx.doi.org/10.1128/IAI.01636-13.

doi:10.1128/IAI.01636-13

host cells. This leads to internalization, as exemplified by *Streptococcus pneumoniae* and *Pseudomonas aeruginosa*, resulting in downstream signaling events (21–23). Protein E and protein F of nontypeable *H. influenzae* have been shown to bind Vn and enhance the serum resistance capacity (18, 24). Thus, the Vn-mediated serum resistance of Hib is multifactorial: more than one surface protein is involved in binding to the same complement regulator. In addition, *H. influenzae* also interacts with factor H (FH) and C4b binding protein (C4BP) for protection against complement-mediated killing (15).

We have demonstrated an interaction between Hsf and Vn previously (25). However, this binding was not directly proven to be involved in serum resistance. In the present study, we therefore wanted to define the regions of Vn involved in the bacterial Hsf-Vn interaction and to investigate the role of this interaction in serum resistance and host cell adherence. Our results demonstrate that Vn bound to Hsf at the bacterial surface inhibits the assembly of the MAC, thereby protecting *H. influenzae* from serum-mediated killing. Moreover, Vn bound to Hsf increases the adherence and internalization of bacteria into host cells.

MATERIALS AND METHODS

Bacterial strains and culture conditions. The *H. influenzae* type b strain RM804 and its isogenic *hsf* mutant (25) were grown in liquid brain heart infusion (BHI) medium containing 10 μg ml^{-1} NAD and hemin, or on chocolate agar plates, followed by incubation at 37°C under a humid atmosphere with 5% CO_2. The *hsf* mutant was grown in the presence of 18 μg ml^{-1} kanamycin. *Escherichia coli* DH5α and *E. coli* BL21(DE3) were cultured in Luria-Bertani (LB) broth or on LB agar plates at 37°C. *E. coli* containing pET26b-*hsf* expression vectors was grown in 50 μg ml^{-1} kanamycin, and *E. coli* carrying pET16b-*hsf*$^{4–2413}$ was supplemented with 100 μg ml^{-1} ampicillin, in LB medium. Vitronectin-expressing human embryo kidney (HEK293T) cells were cultured in advanced Dulbecco's modified Eagle medium (DMEM) (Gibco, Invitrogen, Stockholm, Sweden) containing 2 mM L-glutamine, 100 μg ml^{-1} streptomycin, and 100 U ml^{-1} penicillin.

Vector construction, protein expression, and purification. The *hsf* genes were made according to the layout shown in Fig. 2A. Binding domains BD2$^{429–652}$, BD3$^{1103–1338}$, and BD1$^{1792–2022}$ were cloned. In addition to binding domains (BDs), other structural Hsf motifs, called putative domains (PDs), were made: PD2$^{272–375}$, PD3$^{938–1046}$, and PD1$^{1637–1740}$ (see Fig. 2A). Sequence-specific primers were designed for PCR amplification, and forward and reverse primers contained BamHI and HindIII restriction sites, respectively (Table 1). The amplified PCR products were digested and were ligated into the pET26b vector. The sequences of ligated inserts were verified from selected clones by sequencing. Finally the vectors were transformed into *E. coli* BL21(DE3). For surface expression of Hsf, pET16b-*hsf*$^{4–2413}$ and the empty vector pET16b, used as a control, were transformed into fresh *E. coli* BL21(DE3). Single colonies from the LB plates with ampicillin were inoculated into LB medium containing 100 μg ml^{-1} ampicillin and were incubated at 37°C with shaking at 200 rpm. Expression was induced by the addition of 0.2 mM isopropyl-β-D-thiogalactopyranoside (IPTG) at an optical density at 600 nm (OD_{600}) of 0.4 to 0.5, and cultures were grown for the next 15 h at 37°C with shaking at 200 rpm. Expression levels were verified by flow cytometry before any downstream experiment. For purification purposes, *E. coli* BL21(DE3) containing pET26b-*hsf* expression vectors was grown in LB medium with kanamycin at 37°C until the OD_{600} reached 0.8 to 1. Expression of the proteins was induced by the addition of 1 mM IPTG. After 3 h of culture, cells were harvested and were resuspended in a His-tagged protein binding buffer (50 mM Tris-HCl, pH 7.5, containing 50 mM imidazole and 500 mM NaCl). Bacteria were lysed by sonication, and Ni-nitrilotriacetic acid (NTA) affinity purification was performed according to the manufacturer's guidelines (GE Healthcare Biosciences, Uppsala, Sweden). Gel filtration was performed using an analytical gel filtration column (Superdex 200; GE Healthcare Biosciences), connected with an AktaPrime Plus fast protein liquid chromatography (FPLC) system (GE Healthcare Biosciences). The column was equilibrated with phosphate-buffered saline (PBS), and approximately 200 μg of each protein fragment was injected. Separation was achieved at 0.7 ml/min at room temperature (RT). Standard molecular weight markers (Sigma, St. Louis, MO) were used for comparison of molecular weights. Peaks separated by the column were collected as fractions, concentrated by a Centricon concentrator (molecular weight cutoff [MWCO], 5,000), and loaded onto SDS-PAGE gels (see Fig. S3 and S4 in the supplemental material). SDS-PAGE gels were stained with Coomassie blue R-250 (see Fig. S1 and S2 in the supplemental material). Vn constructs were expressed in HEK293T cells, as described elsewhere (18). Protein concentrations were estimated by a NanoDrop spectrophotometer (Thermo Scientific, Wilmington, DE) and were also verified by a bicinchoninic acid (BCA) assay (Pierce, Rockford, IL).

TABLE 1 List of primers used for cloning of recombinant protein

Primer name	Sequence[a]
Hsf_54_F	5′-CTGA*GGATCC*GGAAGATGAAGAGTTAGACCCCGTAGTA CGC-3′
Hsf_2300_R	5′-CTGAC*AAGCTT*GGCAGAAATTTCGCCATTAGCCACAT TGTCAATGA-3′
BD1_For429	5′-CTGA*GGATCC*GAGTTGGAAAGCAAAAGCTGAGGCTGA TACT-3′
BD1_Rev652	5′-CTGAC*AAGCTT*CACACTAACGGTAATCGTATGTTTACCG-3′
BD2_For1103	5′-CTGA*GGATCC*GAGCTGGACGGCAAAAGCCGATAAATAT GCAGAT-3′
BD2_Rev1338	5′-CTGAC*AAGCTT*TGCAACATCAATCGTTACAGTATGTTTTC CGTTGTTATC-3′
BD3_For1792	5′-CTGA*GGATCC*GAGCTGGACGGCAACTGCTGGTAAAG AAG-3′
BD3_Rev2022	5′-CTGAC*AAGCTT*AGCCAATTCAAAGGTAATCACGC GCGTACCG-3′
PD1_For265	5′-CTGA*GGATCC*GACCGAAGTGAAATTCACACCG-3′
PD1_ Rev376	5′-CTGAC*AAGCTT*TTTCGCGTCGTACTTAACAGTGATGCC-3′
PD2_ For932	5′-CTGA*GGATCC*GGACGTTAAAATCGGTGCGAAAACT-3′
PD2_ Rev1047	5′-CTGAC*AAGCTT*ATTTACATCGTATTTGACATTGATGTT GCCATTATC-3′
PD3_For1621	5′-CTGA*GGATCC*GGTTGAAAGTAAAGATAATGGCAAGAG AACC-3′
PD3_Rev1741	5′-CTGAC*AAGCTT*TTTAACATTGTATTTAACAGTAATACTAC CGTCGTTTGC-3′
Hsf608_For	CTGAGGATCCGTCAACCAAAAACGGTACGAAAGAAG AAAGC
Hsf1351_Rev	CTGAC*AAGCTT*ATCTTTTTCAAGACCATCACCAACTTT GGCTTC
Hsf1047_For	CTGA*GGATCCG*AATGTTGGTGACGGCTTGAAGATTGGC
Hsf1751_Rev	CTGAC*AAGCTT*ATCGCCGTCTAGTTTTAAGCCATCAGCCAC
Hsf1755_For	CTGA*GGATCCG*GCAGACACGACCGTACTTACTGTGGCA
Hsf2313_Rev	CTGAC*AAGCTT*GGCATACAACTGACTTCCGTTAATCGCATC GGTGGA
Hsf2315_For	CTGA*GGATCCG*GCAAAAGGGGTAACAAACCTTGCTGGACAA GTG
Hsf2413_Rev	CTGAC*AAGCTT*CTGGTAACCAACACCTGCTGCAACGCC

[a] Underlining and italics indicate restriction sites.

Western blotting. *H. influenzae* RM804, the *E. coli* control, or *E. coli* expressing Hsf at the surface (10^8 cells) was blocked with PBS containing 2.5% bovine serum albumin (BSA) for 1 h at RT. Bacteria were resuspended in PBS containing 2.5% BSA, and different serum dilutions or purified Vn was added. Binding was performed for 1 h at RT. Thereafter, bacteria were washed 3 times with PBS and were resuspended in PBS, and finally SDS-PAGE loading dye was added. In the following step, samples were treated at 95°C for 10 min and were centrifuged at 14,000 × *g* for 10 min. Supernatants were separated on 12% SDS-polyacrylamide gels and were blotted onto polyvinylidene difluoride (PVDF) membranes. The membranes were blocked with PBS containing 5% milk, and specific primary antibodies (AbD Serotec, Düsseldorf, Germany), anti-rabbit FH

antibodies (Calbiochem, San Diego, CA), and anti-rabbit C4BP antibodies (CompTech, Tyler, TX) were added to the membranes in PBS plus 5% milk. After extensive washing, donkey secondary antibodies conjugated with horseradish peroxidase (HRP) were added to the membranes, which were developed with an ECL Western blotting kit (Pierce, Rockford, IL).

Flow cytometry. *E. coli* cells containing pET16b-*hsf*$^{1-2413}$ were prepared according to the method described above. Bacteria (10^6) were resuspended in 100 μl of PBS containing 2.5% BSA and were treated with affinity-purified rabbit polyclonal anti-Hsf or anti-BD antibodies for 1 h at room temperature. After washing, fluorescein isothiocyanate (FITC)-conjugated anti-rabbit polyclonal antibodies (PAb) (Dakopatts) were added, and the mixture was incubated for 1 h at room temperature. *E. coli* harboring an empty vector was used as a control and was stained similarly. Samples were analyzed in a flow cytometer (EPICS XL-MCL; Beckman Coulter). MAC deposition on the surface of *H. influenzae* or Hsf-expressing *E. coli* was analyzed by flow cytometry. Wild-type (WT) RM804 and the Hsf-deficient mutant (RM804 Δ*hsf*) were grown in broth and were washed once in PBS containing 2% BSA (PBS-BSA). Hsf-expressing *E. coli* was grown to an OD_{600} of 0.5, and Hsf expression was induced by 0.2 mM IPTG for 16 h. RM804 and RM804 Δ*hsf* were incubated with 5% normal human serum (NHS), and Hsf-expressing *E. coli* and an *E. coli* control strain were incubated with 1% NHS in GVB++ buffer (CompTech) at 37°C. All bacteria were used at 10^8. Aliquots were removed after 5, 10, 20, and 30 min, and thereafter the bacteria were stained for MAC deposition. Bacteria were washed and were incubated for 30 min with a mouse monoclonal antibody (MAb) against human MAC/C5b-9 (1:100), followed by an Alexa Fluor 647-conjugated anti-mouse PAb (1:200). After washing, binding was analyzed by flow cytometry (with a FACScan LRII flow cytometer; Becton, Dickinson, Mountain View, CA). All bacteria were incubated in PBS-BSA, and primary and secondary antibodies were added separately as negative controls.

TEM. Anti-C9 antibodies were labeled with colloidal gold as described previously (26). Wild-type *H. influenzae* RM804 was grown in BHI for 3 h at 37°C. *E. coli* cells were induced with IPTG to express Hsf, and the expression of the protein at the surface was verified by flow cytometry prior to transmission electron microscopy (TEM). Bacteria were incubated with gold-conjugated antibodies, fixed in PBS containing 4% paraformaldehyde and 0.1% glutaraldehyde, and prepared as described previously (27). TEM was performed as described elsewhere (28), and specimens were examined in a JEOL JEM 1230 transmission electron microscope (JEOL, Peabody, MA) at 60 kV accelerating voltage. The images were recorded with a Gatan MultiScan 791 charge-coupled device (CCD) camera (Gatan, Pleasanton, CA).

Direct binding assay and enzyme-linked immunosorbent assay (ELISA). A direct binding assay was used to detect the binding of ^{125}I-labeled Vn at the surfaces of bacteria. Vn was labeled by the chloramine-T method as described previously (18). Approximately 1×10^8 *H. influenzae* RM804 or *E. coli* bacteria were blocked with PBS–2.5% BSA and were pipetted into microtiter plates. Increased concentrations of ^{125}I-Vn were added to bacteria and were incubated for 1 h at 37°C. For inhibition experiments, cold ligands were added to the samples prior to the addition of ^{125}I-Vn. In the next step, bacteria were washed 3 times with PBS to remove unbound ^{125}I-Vn. Plates were harvested in a 96-well plate harvester (Tomtec, Hamden, CT) and were counted in a liquid scintillation counter (1450 MicroBeta TriLux; PerkinElmer, Waltham, MA).

Purified Hsf fragments (50 nM) were immobilized on PolySorp microtiter plates (Nunc-Immuno; Nunc, Roskilde, Denmark) in Tris-HCl, pH 9.0, for 15 h at 4°C. Plates were washed 3 times with PBS to remove unbound protein and were blocked with PBS–2.5% BSA for 1 h at RT. Vitronectin was added to wells in PBS–2.5% BSA and was incubated for 1 h at RT. For inhibition assays, the wells were supplemented with inhibitor ligands at different concentrations prior to the addition of Vn. Unbound Vn was removed by washing with PBS containing 0.05% Tween 20. Thereafter, the bound Vn was detected by a sheep anti-human Vn PAb and an HRP-conjugated donkey anti-sheep secondary PAb (both from AbD Serotec). The binding of factor H and C4BP to Hsf was also detected by ELISA by using the same protocol and specific antibodies. Finally the plates were developed and were read at 450 nm in a microplate reader (Multiskan Plus; Labsystems, Helsinki, Finland).

Surface plasmon resonance. The interaction between Hsf and Vn was analyzed using surface plasmon resonance (Biacore 2000 system; Biacore, Uppsala, Sweden). Four flow cells of a CM5 sensor chip were activated, each with 20 μl of a mixture of 0.2 M 1-ethyl-3-(3-dimethylaminopropyl) carbodiimide and 0.05 M *N*-hydroxysulfosuccinimide at a flow rate of 10 μl/min, after which Hsf$^{54-2300}$ and BD2 (10 μl/ml in 10 mM sodium acetate buffer, pH 4.0) were injected over separate flow cells. Unreacted groups were blocked with 20 μl of 1 M ethanolamine (pH 8.5). The final immobilization levels were 7,179 resonance units (RU) for Hsf$^{54-2300}$ (244 kDa) and 884 RU for BD1 (25 kDa), and thus, these were immobilized at equimolar ratios. A negative control was prepared by activating and subsequently blocking the surface of flow cell 1. Thereafter, a series of 2-fold dilutions of Vn starting at 200 μg/ml were injected into the flow buffer (50 mM HEPES, pH 7.5, containing 150 mM NaCl, 3 mM EDTA, and 0.005% Tween 20). Vitronectin was injected for 100 s during the association phase at a constant flow rate of 30 μl/min. The sample was injected first over the negative-control surface and then over immobilized ligands. The signal from the control surface was subtracted. The dissociation was followed for 360 s at the same flow rate. In all experiments, 10-μl injections of 2 M NaCl and 100 mM HCl followed by 0.05% SDS were used to remove bound Vn during a regeneration step. The BiaEvaluation software (version 3.0; Biacore) was used for data analysis using a 1:1 Langmuir model of interaction.

Serum killing assay. Approximately 10^5 *H. influenzae* RM804 or *E. coli* bacteria expressing Hsf were resuspended in 100 μl of dextrose-GVB ($DGVB^{++}$) buffer, pH 7.3, containing 140 mM glucose, 0.1% (wt/vol) gelatin, 1 mM $MgCl_2$, 0.15 mM $CaCl_2$, and finally 10% NHS (18, 24). Normal human serum was prepared from 5 different healthy volunteers according to standard guidelines. In parallel, a heat-inactivated serum (HIS) was prepared as a control by inactivation of complement components by heating at 56°C for 30 min. Serum was depleted of Vn, and depleted serum was replenished with new Vn, as described previously (24). *E. coli* expressing Hsf was optimized for serum sensitivity by adding 1 to 10% NHS or HIS at different time intervals. NHS or HIS was added to bacteria resuspended in $DGVB^{++}$, which were then incubated at 37°C. At a particular time, bacteria were plated on chocolate agar. The number of viable bacterial cells was determined by counting CFU after overnight incubation at 37°C.

Membrane attack complex deposition assay. Microtiter plates (F96 MediSorb, Nunc-Immuno module) were coated with Hsf or BSA, each at 5 μg/ml overnight at 4°C. The plates were washed four times with PBS-Tween (PBST) and were blocked for 1 h at RT with PBS containing 2% BSA. After washing, the plates were incubated for 1 h at RT with vitronectin (10 to 50 μg/ml) or FH (10 to 50 μg/ml). Subsequently, the wells were washed and incubated with C5b-6 (1.5 μg/ml) and C7 (1 μg/ml) for 10 min at RT, and thereafter C8 (0.2 μg/ml) and C9 (1 μg/ml) were added, and the mixture was incubated for 30 min at 37°C. MAC deposition was detected with a mouse anti-human C5b-9 MAb and an HRP-conjugated swine anti-mouse PAb. The reaction was developed with 1,2-phenylenediamine dihydrochloride (OPD; DakoCytomation), and absorbance was measured at 492 nm.

***H. influenzae* adherence and invasion assay.** Lung alveolar epithelial cells (A549) were grown in 12-well culture plates in F-12 medium supplemented with 10% fetal calf serum (FCS) and 5 μg/ml gentamicin. Thereafter, 80 to 90% confluent cells were kept overnight in serum-free medium (F-12 medium only), prior to the experiments. *H. influenzae* (10^7 CFU) was added to cells and was incubated at 37°C with gentle shaking (50 rpm). At different time points (1 to 6 h), cells were washed thoroughly, and cells were taken out by treatment with Accutase (Life Technologies, Stockholm, Sweden). Cells were lysed with glass beads and by vortexing. To analyze internalized bacteria, cells were treated with gentamicin (100

μg/ml) for 1 h to kill extracellular bacteria. Finally, different dilutions were made, and solutions were spread on chocolate agar plates. To observe an effect of Vn, cell monolayers were treated with Vn (2 to 4 μg/ml) at 4°C for 2 h, followed by extensive washing (3 times) with PBS. The additional steps were performed as described above.

Confocal microscopy. A549 cells were grown on glass coverslips in F-12 medium supplemented with 10% FCS and 5 μg/ml gentamicin. Confluent cells (90%) were kept in serum-free medium (F-12 medium only) overnight. Bacteria were labeled with FITC (10 μg/ml) in PBS for 30 min at RT, followed by 3 washes to remove unbound FITC. The FITC-conjugated bacteria (10^8) were added to the cells and were incubated for 2 to 8 h at 37°C with gentle shaking. Cell monolayers were treated with 10 μg Vn and were incubated for 2 h at 4°C, prior to the addition of bacteria. Coverslips were washed 3 times in PBS and were fixed by using 4% paraformaldehyde. Finally, coverslips were mounted with Vectashield (Vector Laboratories, United Kingdom) containing 4′,6-diamidino-2-phenylindole (DAPI). Images were taken using a laser scanning microscope (LSM 710; Carl Zeiss, Göttingen, Germany) and were processed using Zen software.

Statistics. One- or two-way analysis of variance (ANOVA) was used to determine the difference between more than two experimental groups when indicated. Differences were considered statistically significant at a P value of ≤ 0.05. Statistical analyses were performed using GraphPad Prism, version 5.0 (GraphPad Software, La Jolla, CA).

RESULTS

***Haemophilus influenzae* type b clinical isolates bind Vn.** To prove that the binding of Vn to Hib strains is a common phenomenon, we analyzed Hib clinical isolates (n, 26) for their Vn-binding capacities. Of 26 Hib isolates, 11 and 10 had high and medium Vn-binding capacities, respectively. *E. coli* DH5α did not bind Vn and was included as a negative control in our assay (Fig. 1A). In parallel, the Vn-binding capacity of RM804 Δ*hsf* (25) was tested and compared to that of the clinical isolates, 19.2% of which had a low Vn-binding capacity similar to that of the RM804 Δ*hsf* mutant (Fig. 1B). We thus defined this group of clinical isolates as low Vn binders. Moreover, when Hsf was expressed at the surface of the heterologous host *E. coli*, significant Vn binding was observed, in contrast to *E. coli* containing an empty vector only (Fig. 1C). Taken together, our data suggested that most of the clinical Hib isolates had the capacity to acquire Vn.

Binding domain 2 of Hsf recognizes vitronectin. To define the Vn-binding region in the Hsf molecule, we expressed full-length $Hsf^{54-2300}$ and the truncated fragments Hsf^{54-608}, $Hsf^{608-1351}$, $Hsf^{1047-1751}$, $Hsf^{1536-2031}$, and $Hsf^{1755-2313}$ (Fig. 2A). On the basis of previously identified epithelial cell binding domains, BD2 ($Hsf^{429-652}$), BD3 ($Hsf^{1103-1338}$), and BD1 ($Hsf^{1792-2022}$) were expressed in *E. coli* (9). In addition to these BDs, we also observed a set of repeats present in putative domain 2 (PD2) ($Hsf^{265-376}$), PD3 ($Hsf^{932-1047}$), and PD1 ($Hsf^{1621-1741}$) that share 65.8 to 80.2% sequence similarity. The function of those repeats is at present unknown, and therefore we named them PDs. Hence, recombinant PD1, PD2, and PD3 were also included in our study (Fig. 2A). The purified proteins were verified for their oligomeric conditions by using gel filtration and subsequent SDS-PAGE of separated protein peaks. All purified proteins were mainly trimers, with minor fractions of higher-molecular-weight oligomers (see Fig. S1 and S2 in the supplemental material). ELISA showed that recombinant Vn^{80-396} bound significantly to $Hsf^{54-2300}$, Hsf^{54-608}, BD2, and $Hsf^{1536-2031}$ (Fig. 2B). Low-level interactions were also observed with the PD2, BD1, and $Hsf^{1047-1751}$ fragments. The remaining fragments (PD3, PD1, BD3, $Hsf^{608-1351}$, and $Hsf^{1047-1751}$) did not interact with Vn. A truncated *Moraxella catarrhalis* IgD binding protein (MID; amino acids [aa] 962 to 1200) was used as a negative control (Fig. 2B). The non-Vn-binding Hsf fragments were excluded from further experiments.

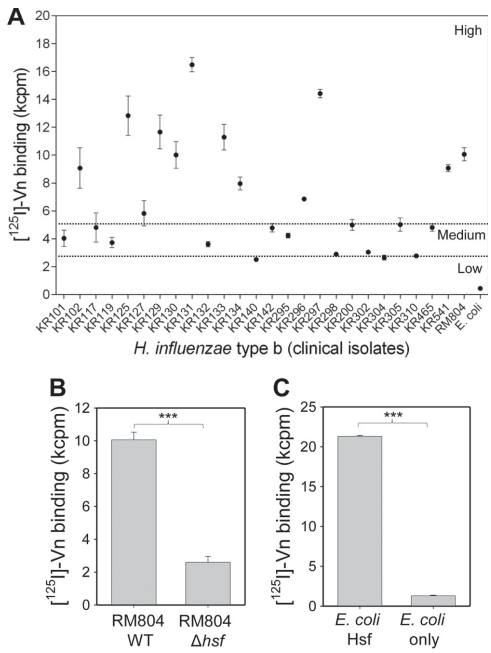

FIG 1 *H. influenzae* type b clinical isolates significantly bind Vn. (A) Direct binding of ^{125}I-labeled Vn to clinical isolates. *E. coli* DH5α was used as a negative control. (B) *H. influenzae* RM804 Δ*hsf* showed a lower level of Vn binding than the Hsf-expressing wild type. (C) *E. coli* expressing Hsf revealed a Vn-binding phenotype.

To confirm the interaction with the Vn-binding Hsf fragments, we also carried out an inhibition assay. Vn^{80-396} in solution was preincubated with increasing concentrations of truncated Hsf fragments (Fig. 2C) prior to addition to the full-length $Hsf^{54-2300}$. The results with recombinant $Hsf^{54-2300}$, BD2, and Hsf^{54-608} showed significant dose-dependent inhibition of Vn^{80-396} binding to $Hsf^{54-2300}$. The remaining proteins (PD2, BD1, $Hsf^{1047-1751}$, and $Hsf^{1536-2031}$), all of which showed only minor binding to Vn (Fig. 2B), did not inhibit the interaction of $Hsf^{54-2300}$ with Vn (Fig. 2C). As expected, heparin inhibited Vn binding to Hsf and was included as a positive control (Fig. 2C). Since PD2 and BD1 were unable to block the interaction, these two domains were excluded as possible binding partners. Furthermore, the C-terminal region of $Hsf^{1536-2031}$ did not inhibit Vn binding to $Hsf^{54-2300}$. Our results clearly suggested that BD2, which is also present in Hsf^{54-608}, was the major Vn-binding region of the Hsf molecule.

The binding affinities of the $Hsf^{54-2300}$ and BD2 interactions were measured using surface plasmon resonance. A CM5 sensor chip was coated with recombinant Hsf, and the binding of several concentrations of Vn^{80-396} was measured in real time. Vn^{80-396}

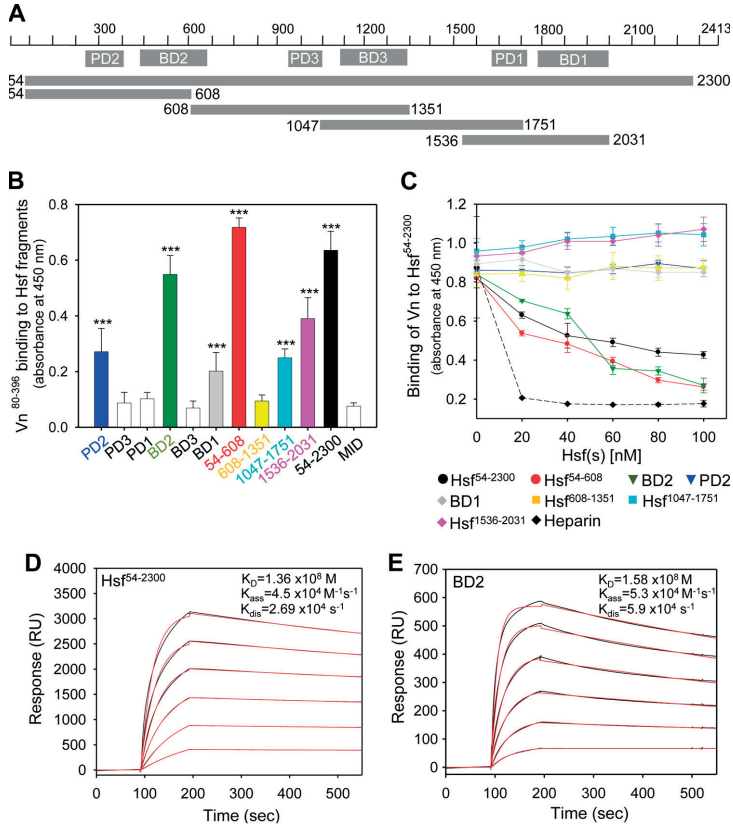

FIG 2 BD2 is the major Vn-binding region of Hsf. (A) Schematic of Hsf showing a plan of the different recombinantly expressed fragments. BD, binding domain; PD, putative domain. (B) An ELISA plate was coated with Hsf fragments (50 nM); Vn^{80-396} (20 nM) was added to each well; the unbound fraction was removed by PBST; and bound Vn was detected with an anti-Vn sheep PAb and an HRP-conjugated anti-sheep donkey PAb. (C) Results obtained by ELISA for inhibition of the interaction of Vn^{80-396} with $Hsf^{54-2300}$. Increasing concentrations of recombinant Hsf fragments were incubated with Vn^{80-396} prior to the addition of Vn to wells coated with $Hsf^{54-2300}$. Heparin was used as a positive control. Statistical analyses for all data in panels B and C were performed by two-way ANOVA. All data are means of results from three independent experiments, and error bars show standard deviations. *, $P \leq 0.05$; **, $P \leq 0.01$; ***, $P \leq 0.001$. (D) Surface plasmon resonance (Biacore) showing the binding of Vn to $Hsf^{54-2300}$ that was immobilized on the chip. (E) $Hsf^{54-2300}$ and BD2 were immobilized, and Vn at increasing concentrations was injected. Vn binding was then analyzed. Sensorgrams (black lines) are shown. The binding curves obtained were analyzed using a 1:1 Langmuir model to obtain kinetic parameters, and the resulting curves are shown in red.

bound $Hsf^{54-2300}$ with an association rate affinity constant (K_{ass}) of 4.5×10^4 1/Ms and a dissociation rate affinity constant (K_{dis}) of 2.69×10^{-4} 1/s, and the calculated equilibrium dissociation constant (K_D) was 1.39×10^{-8} M (Fig. 2D). Similarly, Vn^{80-396} bound BD2 with a K_{ass} of 5.3×10^4 1/Ms and a K_{dis} of 5.9×10^{-4} 1/s, and K_D was estimated at 1.58×10^{-8} M (Fig. 2E). Other fragments did not interact significantly with Vn^{80-396} (data not shown). Our results thus showed that BD2 and full-length Hsf interacted with Vn^{80-396} with the same binding affinity.

Vn amino acids 352 to 374 serve as the Hsf interaction site. We reported previously that *H. influenzae* proteins E (18) and F (24) interact with the heparin binding domain at the C-terminal part of the Vn molecule (HBD3). Here we observed that heparin also blocked the interaction between Hsf and Vn (Fig. 2C). Three different constructs encompassing HBD3 ($Vn^{\Delta 352-362}$, $Vn^{\Delta 362-374}$, and $Vn^{\Delta 352-374}$) were therefore used to analyze binding to Hsf (Fig. 3A). Recombinantly expressed Vn fragments were verified for their purity and oligomeric forms by SDS-PAGE and Western blotting (see Fig. S3 in the supplemental material). Since Vn in serum exists in both monomeric and multimeric forms, we analyzed our purified Vn fragments. These consisted mainly of a multimeric population, as demonstrated in Fig. S3. Some pathogens, e.g., *S. pneumoniae* (22) and *Neisseria meningitidis* (29), preferentially interact with the multimeric form of Vn. We thus tested both

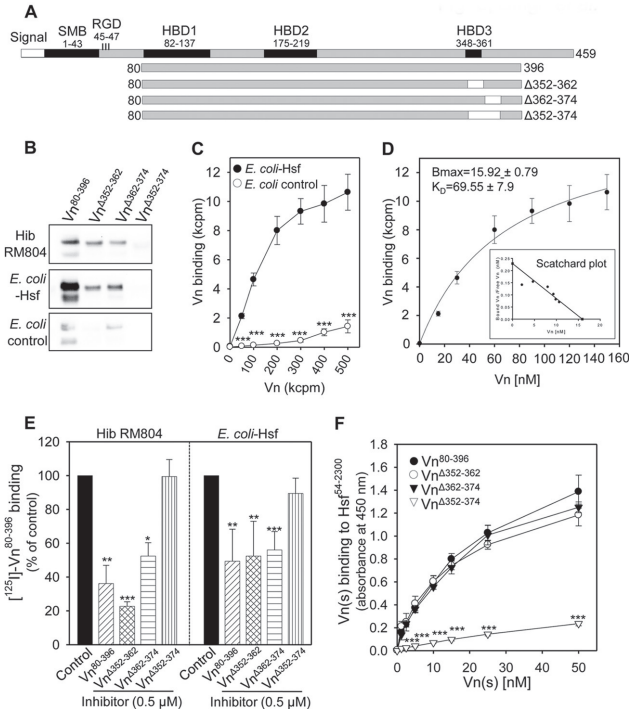

FIG 3 Vitronectin amino acids 352 to 374 bind to the Hsf molecule. (A) Cartoon delineating the Vn molecule and Vn fragments, including the deletion mutants. SMB, somatomedin B; HBD, heparin binding domain; RGD, Arg-Gly-Asp. (B) *H. influenzae* RM804 and Hsf-expressing *E. coli* were incubated with the recombinant protein $Vn^{\Delta 352-362}$, $Vn^{\Delta 362-374}$, or $Vn^{\Delta 352-374}$. Vn bound to bacteria was detected by Western blotting with anti-Vn antibodies. *E. coli* containing an empty pET16b vector was included as a negative control. (C) Direct binding assay demonstrating the interaction of ^{125}I-labeled Vn^{80-396} with Hsf-expressing *E. coli* and the *E. coli* control. Statistical analyses were carried out by one-way ANOVA. (D) Curve fitting of the binding of ^{125}I-labeled Vn^{80-396} to *E. coli* expressing Hsf to calculate B_{max} and K_D values. (Inset) Scatchard plot prepared from the data. (E) Inhibition of binding of ^{125}I-labeled Vn^{80-396} to *H. influenzae* RM804 and Hsf-expressing *E. coli* by cold $Vn^{\Delta 352-362}$, $Vn^{\Delta 362-374}$, and $Vn^{\Delta 352-374}$ (all at 0.5 μM). (F) Binding of $Vn^{\Delta 352-362}$, $Vn^{\Delta 362-374}$, and $Vn^{\Delta 352-374}$ recombinant proteins to $Hsf^{54-2300}$ by ELISA. For panels C, E, and F, two-way ANOVA was used for statistical analyses. All data are means of results from three independent experiments, and error bars indicate standard deviations. *, $P \leq 0.05$; **, $P \leq 0.01$; ***, $P \leq 0.001$.

monomeric and multimeric Vn with $Hsf^{54-2300}$ and found that multimeric Vn had a 15 to 20% higher Hsf-binding capacity (see Fig. S3).

To determine the binding of Vn variants to *H. influenzae* RM804 and Hsf-expressing *E. coli* (see Fig. S4 in the supplemental material), bacteria were incubated with Vn^{80-396}, $Vn^{\Delta 352-362}$, $Vn^{\Delta 362-374}$, or $Vn^{\Delta 352-374}$. The unbound proteins were removed by extensive washing, and fractions bound to Hsf were analyzed by Western blotting. Vn^{80-396}, $Vn^{\Delta 352-362}$, and $Vn^{\Delta 362-374}$ interacted with *H. influenzae* RM804, whereas the deletion of 20 aa in $Vn^{\Delta 352-374}$ completely abolished binding to bacteria (Fig. 3B). The binding of Vn variants was also verified by using a direct binding assay, where Vn^{80-396} was labeled with radioactive iodine. Interestingly, ^{125}I-labeled Vn^{80-396} bound to Hsf-expressing *E. coli* in a dose-dependent manner with a K_D of 69.5×10^{-9} M and a maximum binding (B_{max}) of 15.92×10^{-9} M, whereas the *E. coli* control did not interact with ^{125}I-labeled Vn^{80-396} (Fig. 3C and D). The binding specificity of the Vn variants was verified by a competition assay in the next set of experiments. *H. influenzae* RM804 and Hsf-expressing *E. coli* were incubated with Vn^{80-396}, $Vn^{\Delta 352-362}$, $Vn^{\Delta 362-374}$, and $Vn^{\Delta 352-374}$ before the addition of ^{125}I-labeled Vn^{80-396}. The recombinant Vn^{80-396}, $Vn^{\Delta 352-362}$, and $Vn^{\Delta 362-374}$ significantly blocked the interaction of ^{125}I-Vn^{80-396} with Hib and Hsf-expressing *E. coli* (Fig. 3E). However, the deletion mutant $Vn^{\Delta 352-374}$ did not inhibit the binding of ^{125}I-Vn^{80-396} to bacteria.

Our binding studies of the Hsf-Vn interaction were further confirmed by analyzing protein-protein interactions by ELISA. Microtiter plates were coated with $Hsf^{54-2300}$, and increasing concentrations of Vn^{80-396}, $Vn^{\Delta 352-362}$, $Vn^{\Delta 362-374}$, or $Vn^{\Delta 352-374}$ were added. Bound protein fractions were determined with an anti-Vn PAb. Interestingly, Vn^{80-396}, $Vn^{\Delta 352-362}$, and $Vn^{\Delta 362-374}$ bound $Hsf^{54-2300}$ at levels significantly higher than that of $Vn^{\Delta 352-374}$ (Fig. 3F). In conclusion, our results indicated that the C-terminal region of Vn consisting of amino acids 352 to 374 is necessary for the interaction with *H. influenzae* RM804 and the Hsf molecule.

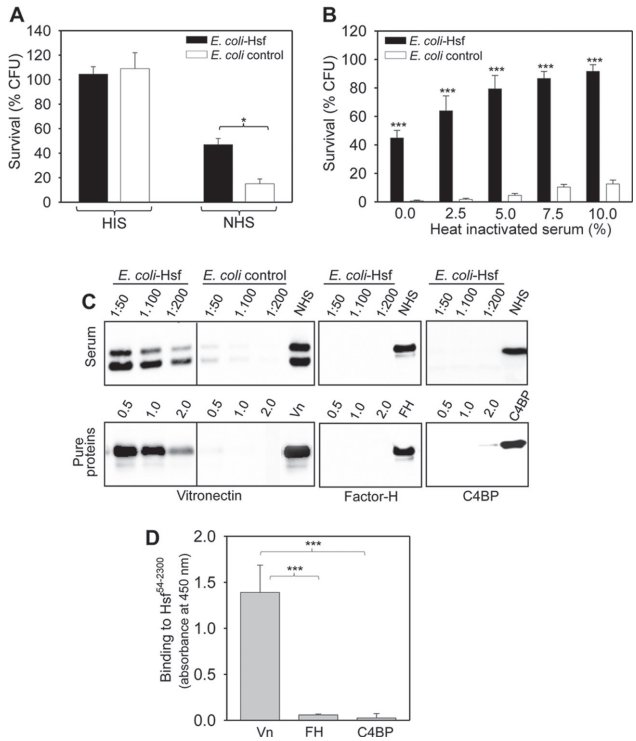

FIG 4 Hsf-expressing *E. coli* selectively interacts with Vn and acquires serum resistance. (A) Hsf expression at the surface of *E. coli* showed a serum-resistant phenotype. Time-dependent serum killing is shown in Fig. S5 in the supplemental material. (B) Hsf-expressing *E. coli* and the isogenic control were incubated with HIS, followed by the addition of 1% NHS. Statistical analysis was performed by one-way ANOVA. The CFU were counted after 10 min of incubation. (C) *E. coli* expressing Hsf was incubated with different dilutions of normal human serum and pure Vn^{80-396}, C4BP, or FH. Bacteria were washed, and bound fractions were detected by Western blotting. This experiment was repeated twice, and the results of one typical blot are shown. (D) Binding of 10 nM Vn, FH, and C4BP to $Hsf^{54-2300}$ as analyzed by ELISA. Statistical analysis was performed by two-way ANOVA. All data are means of results from three independent experiments, and error bars indicate standard deviations. *, $P \leq 0.05$; ***, $P \leq 0.001$.

Hsf acquires Vn from serum and contributes to resistance to serum. We have reported previously that *H. influenzae* RM804 binds Vn and that the isogenic *H. influenzae* RM804 Δ*hsf* mutant binds significantly less Vn (25). Those analyses were performed with purified human Vn from Sigma. In the current study, we used a heterologous *E. coli* system in parallel with *H. influenzae* to prove the fine-tuned Hsf-Vn interaction and furthermore analyzed the role of Vn in resistance to serum. Hsf-expressing *E. coli* (see Fig. S4 in the supplemental material) bound recombinant ^{125}I-labeled Vn^{80-396} in a dose-dependent manner with a K_D of 69.5×10^{-9} M (Fig. 3C and D). Hsf-expressing *E. coli* had a significantly higher level of serum resistance than the *E. coli* control, which harbored an empty plasmid (Fig. 4A; see also Fig. S5A in the supplemental material). In agreement with previously published data (25), we also showed that *H. influenzae* Δ*hsf* had a significantly lower level of serum resistance than the Hsf-expressing wild type (see Fig. S5B in the supplemental material).

To load bacteria with complement-regulatory serum factors, we preincubated Hsf-expressing *E. coli* and the *E. coli* control with various concentrations of human heat-inactivated serum (HIS). This step allowed bacteria to retain the serum proteins at their surfaces without being killed. After washing to remove unbound serum components, bacteria were resuspended in 1% NHS. After 5 min of incubation at 37°C, CFU were determined by plating the bacteria. Hsf-expressing *E. coli* was significantly more serum resistant when pretreated with 2.0 to 10% HIS than control *E. coli* devoid of Hsf, which did not show any increased serum resistance with or without HIS pretreatment (Fig. 4B). Hsf-expressing *E. coli* that was preincubated with HIS (Fig. 4B) was further analyzed by Western blotting for deposition of complement regulators at the surface. Only Vn binding was detected; binding of the complement regulators C4BP and FH was not observed (Fig. 4C). In parallel, purified serum proteins Vn, C4BP, and FH were also tested for interaction with Hsf-expressing *E. coli*. In contrast to wild type *E. coli*, only Hsf-expressing *E. coli* bound Vn (Fig. 4C, lower panel). The Hsf-Vn interaction was also confirmed at the

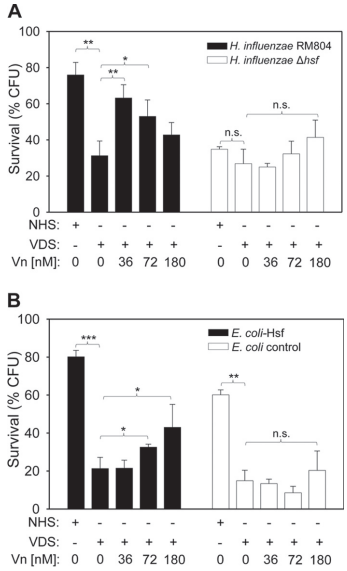

FIG 5 Vn is involved in Hsf-mediated serum resistance. (A) Wild-type *H. influenzae* RM804 and the corresponding mutant *H. influenzae* Δ*hsf* were incubated with normal human serum (NHS) or Vn-depleted serum (VDS). The strains were also incubated for 10 min in 5% Vn-depleted serum supplemented with increasing concentrations of Vn^{20-396}. (B) Hsf-expressing *E. coli* and the negative control were incubated with 1% NHS or Vn-depleted serum for 5 min. In addition, the strains were incubated for 5 min with 1% Vn-depleted serum supplemented with increasing concentrations of Vn^{20-396}. Time-dependent serum killing of the *H. influenzae* and *E. coli* strains is shown in Fig. S5 in the supplemental material. Statistical analyses were performed by two-way ANOVA. All data are means of results from three independent experiments, and error bars show standard deviations. *, $P \leq 0.05$; **, $P \leq 0.01$; ***, $P \leq 0.001$; n.s., not significant.

protein-protein interaction level. When a microtiter plate was coated with $Hsf^{54-2300}$, and 10 nM purified Vn, FH, or C4BP was added, we found that only Vn interacted with Hsf (Fig. 4D). Taken together, our results indicated that a complement-regulatory factor acquired by Hsf-expressing *E. coli* protected bacteria from the bactericidal activity of serum. Importantly, this serum factor was proven to be Vn (Fig. 4C and D).

***H. influenzae* is protected from serum-mediated killing when Vn is available in serum.** To evaluate the role of the Hsf-mediated Vn interaction in the inhibition of the terminal complement pathway, we prepared a Vn-depleted serum (VDS) as described previously (24). When *H. influenzae* RM804 and the corresponding Hsf mutant *H. influenzae* Δ*hsf* were incubated with the VDS, *H. influenzae* RM804 revealed significantly lower (55 to 60%) serum survival than that in NHS (Fig. 5A; see also Fig. S5B in the supplemental material). In contrast, *H. influenzae* Δ*hsf* did not show any significant difference in survival between NHS and VDS (Fig. 5A). To further confirm the role of Vn, we supplemented VDS with Vn^{20-396} (36 to 180 nM) and incubated *H. influenzae* RM804 with this replenished serum. Supplementation of the VDS with Vn (36 or 72 nM) caused a significant increase in the level of serum resistance, while this was not observed with mutant *H. influenzae* Δ*hsf* (Fig. 5A).

In parallel to the experiments with *H. influenzae*, *E. coli* expressing Hsf was also incubated with NHS and VDS. The results obtained at 5 min of incubation showed a lower level of serum resistance in VDS than in NHS (Fig. 5B), whereas no difference was observed in VDS after 5 min (see Fig. S5C in the supplemental material). To confirm the role of Vn, VDS was also supplemented with Vn^{20-396}. Incubation of Hsf-expressing *E. coli* with VDS plus 72 or 180 nM Vn^{20-396} led to significantly higher survival than that of the *E. coli* control or that of Hsf-expressing *E. coli* with VDS only (Fig. 5B). Taken together, our results with Hsf-expressing Hib or *E. coli* clearly indicated that bacteria recruit Vn from NHS and this surface-bound Vn inhibits complement-mediated activity and thus enhances bacterial survival.

Hsf-mediated vitronectin binding results in decreased MAC deposition. To demonstrate that vitronectin bound to Hsf was functionally active, we determined MAC deposition in the presence of vitronectin bound to recombinant Hsf by using purified components of the terminal pathway. The human C3 convertase regulator FH was used in parallel as a negative control. As can be seen in Fig. 6A, the binding of Vn was confirmed by ELISA. Vn or FH was added to wells coated with Hsf, followed by the addition of C5b-6, C7, C8, and C9. MAC deposition was determined by using specific mouse anti-C5b-9 MAbs. Vn (50 μg/ml) inhibited MAC formation by 34% compared to samples without Vn added (Fig. 6C). Addition of 60 to 300 nM (10 to 50 μg/ml) FH showed a minor interaction with Hsf (Fig. 6B). This interaction was not observed when we added 10 nM FH to the Hsf-coated wells (Fig. 4D). In contrast, MAC deposition was not inhibited when FH was added (Fig. 6C). These results clearly showed that Vn bound to Hsf was functionally active and inhibited MAC formation and deposition.

The levels of serum resistance of *H. influenzae* RM804 and the corresponding Hsf-deficient mutant *H. influenzae* RM804 Δ*hsf* were confirmed by measurement of MAC deposition at the bacterial surface. Bacteria were incubated with NHS, followed by analysis of MAC deposition at different time points using specific anti-C5b-9 antibodies and flow cytometry. Significantly lower deposition of MAC was seen on the surface of *H. influenzae* RM804 than on that of the Hsf-deficient mutant (Fig. 6D). In addition, *H. influenzae* RM804 and the Hsf-deficient mutant were also analyzed by TEM after 10 min and 15 min of incubation with NHS. Here, *H. influenzae* RM804 Δ*hsf* showed markedly greater MAC deposition than did the Hsf-expressing wild-type *H. influenzae* strain RM804 (Fig. 6E). We also tested MAC deposition on our *E. coli* strain expressing Hsf and found that Hsf expression at the surface of *E. coli* inhibited MAC deposition (Fig. 6F). Moreover, TEM revealed that a smaller amount of the MAC was deposited on the surface of *E. coli* expressing Hsf than on that of *E. coli* transformed with an empty vector (Fig. 6G). Taken together, our data indicated that Vn bound at the surfaces of bacteria via Hsf was functionally active in inhibiting the MAC and therefore contributed to serum resistance.

The Hsf-dependent interaction with vitronectin increases *H. influenzae* adherence and internalization. Vitronectin contributes to the adherence and internalization of several bacterial species (21). Since it has been shown that Hsf-binding domains (BDs) expressed at the surface of *E. coli* recognize Chang and HeLa cells (9, 30), we compared the adhesion of *H. influenzae* RM804 with

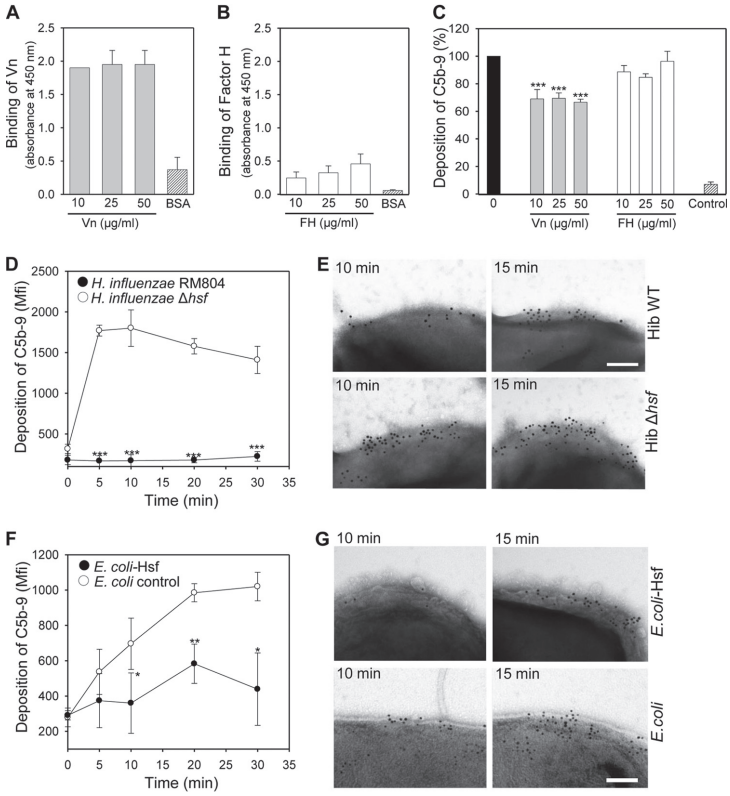

FIG 6 Vn bound to Hsf at the bacterial surface inhibits the assembly of the membrane attack complex. (A and B) Microtiter plates were coated with Hsf, and increasing amounts of Vn (A) or FH (B) were added to the wells. Binding was confirmed by anti-Vn and anti-FH antibodies. (C) The Vn- and FH-coated wells were assayed for MAC deposition by using anti-C5b-9 MAbs. (D) MAC deposition at the surfaces of *H. influenzae* RM804 and the Hsf-deficient mutant at different time points. (E) TEM showing deposition of the MAC at the surfaces of *H. influenzae* RM804 and the Hsf-deficient mutant at 10 and 15 min. (F) Deposition of the MAC at the surfaces of *E. coli* expressing Hsf and the *E. coli* control with an empty pET16b vector. (G) TEM showing deposition of C9 at the surfaces of *H. influenzae* RM804 and the Hsf-deficient mutant at 10 and 15 min. Bars, 100 nm. All experiments (except TEM) were repeated three times. Data in graphs are means of results of three independent experiments, and error bars indicate standard deviations. *, $P \leq 0.05$; **, $P \leq 0.01$; ***, $P \leq 0.001$.

that of a Δ*hsf* mutant. The Hsf-deficient mutant showed dramatically reduced adherence to monolayers of the type II alveolar epithelial cell line A549, as observed by confocal microscopy (Fig. 7A). Epithelial cells infected with WT *H. influenzae* RM804 harbored more intracellular bacteria than cells incubated with the Hsf-deficient mutant. The adherence/internalization capacities of *H. influenzae* RM804 and the corresponding Δ*hsf* mutant were also quantified by estimation of the CFU at different time points. The total number of bacteria associated with A549 cells was significantly higher for the WT strain RM804 than for the Δ*hsf* mutant (Fig. 7B). When the numbers of internalized bacteria were estimated by a gentamicin protection assay, a clear difference in bacterial numbers was observed between cells infected with WT *H. influenzae* RM804 and those infected with the Δ*hsf* mutant (Fig. 7C).

To further investigate whether Vn plays a role in Hsf-mediated adherence to epithelial cells, A549 cells were pretreated with Vn, followed by the addition of bacteria. A higher number of *H. influenzae* RM804 bacteria than of the mutant bacteria devoid of Hsf adhered to cells (Fig. 8A). In contrast to the Δ*hsf* mutant, significantly enhanced adherence/invasion of the WT strain RM804 was observed at increasing concentrations of Vn (2 and 4 μg) (Fig. 8B). A gentamicin protection assay revealed that the number of intracellular WT bacteria was 2-fold-higher than the number of intracellular Δ*hsf* mutant bacteria (Fig. 8C). Taking these findings together, the Hsf-dependent Vn-binding capacity of Hib promoted bacterial adherence to, and invasion of, epithelial cells.

DISCUSSION

Several respiratory pathogens recruit Vn in order to increase their survival in serum and/or to increase adherence to host cells (21). Hallström et al. (2006) reported that Hsf is a Vn-binding protein

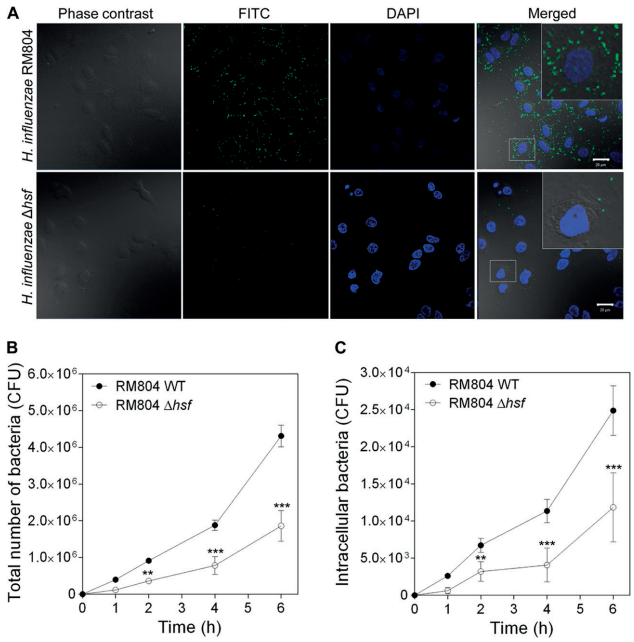

FIG 7 Hsf functions as an adhesin. (A) Confocal microscopy showing the adherence of the WT strain RM804 and a Δ*hsf* mutant. Bacteria were incubated with A549 epithelial cells for 6 h and were imaged thereafter. Bacteria are labeled in green (FITC) and cell nuclei in blue (DAPI). The rightmost panels show merged images. Bars, 20 μM. (B) Measurement of total bacteria associated with A549 cells by counting of CFU. (C) Internalized bacteria after treatment with the extracellularly active drug gentamicin. Each well of the microtiter plate had approximately 3×10^5 to 3.5×10^5 cells, and 1×10^7 CFU was added to each well. Data in graphs are means of results of three independent experiments, and error bars indicate standard deviations. **, $P \leq 0.01$; ***, $P \leq 0.001$.

of Hib and showed that *hsf* deletion mutants were sensitive to the bactericidal effect of serum (25). In the same paper, $Hsf^{608-1351}$ was also reported to bind Vn; that has now been corrected to Hsf^{54-608} (25). Here we further characterized the Hsf-Vn interaction and narrowed down the specific Vn-binding region identified. The results of our protein-protein interaction studies indicate that the BD2 ($Hsf^{429-652}$) serves as the major Vn-binding domain.

We reported previously that *M. catarrhalis* recruits Vn at the surface by using ubiquitous surface protein (Usp) A2 and that the binding region on the Vn molecule is located at $Vn^{312-396}$ (17). Similarly, we also published that *S. pneumoniae* PspC interacts with amino acids 352 to 374 on the Vn molecule (19). Moreover, we showed that nontypeable *H. influenzae* (NTHi) binds to Vn at amino acids 353 to 396 by using its surface adhesin protein E (18). In a very recent study, we identified protein F as another Vn-binding NTHi protein that targets $Vn^{352-374}$ (24). Our earlier studies thus clearly indicate the presence of several bacterial surface proteins of *H. influenzae* that recognize Vn as the same target molecule. Hsf is also known to bind Vn, but where on the Vn molecule Hsf binds was hitherto unknown. In agreement with the previous findings with other pathogens, such as *Moraxella* and pneumococci, our present study shows that Hib Hsf also targets Vn at the region from amino acid 352 to 374.

The structure and function of Hsf are still not very well defined. It has been reported that BD1 and BD2 function as adhesive domains and bind to Chang conjunctival epithelial cells *in vitro*. These binding domains of Hsf have been modeled previously by using binding domains of Hia as a template. The same study showed that mutating D1935 of BD1 to E resulted in the loss of Hsf-dependent interactions with epithelial cells. Homology modeling of BD2 suggested that E569 played a role in the binding pocket. When E569 was mutated to D569, BD2 also showed a markedly increased capacity to adhere to epithelial cells (30). We confirmed that Hsf BD2 has adhesive and Vn-binding properties, supporting previous findings.

Our data support the idea that Hsf functions as an adhesin. It is, however, unclear whether Vn is a direct receptor for Hsf at the surface of the epithelium. In this study, Hsf-deficient mutants exhibited decreased adherence and internalization in the absence of Vn (Fig. 8). In contrast, the presence of Vn revealed enhanced adherence/internalization of *H. influenzae* RM804 (WT) relative to that of the Hsf-deficient mutant (Fig. 8). It has been shown that Hsf BD1 binds to epithelial cells more efficiently than BD2 (30). We speculate that BD1 might be a privileged region that interacts with presently unknown host epithelial surface receptors. In contrast to BD1, BD2 functions as a major Vn-binding region. Upon binding to Hsf BD2, Vn would then function as a bridge molecule

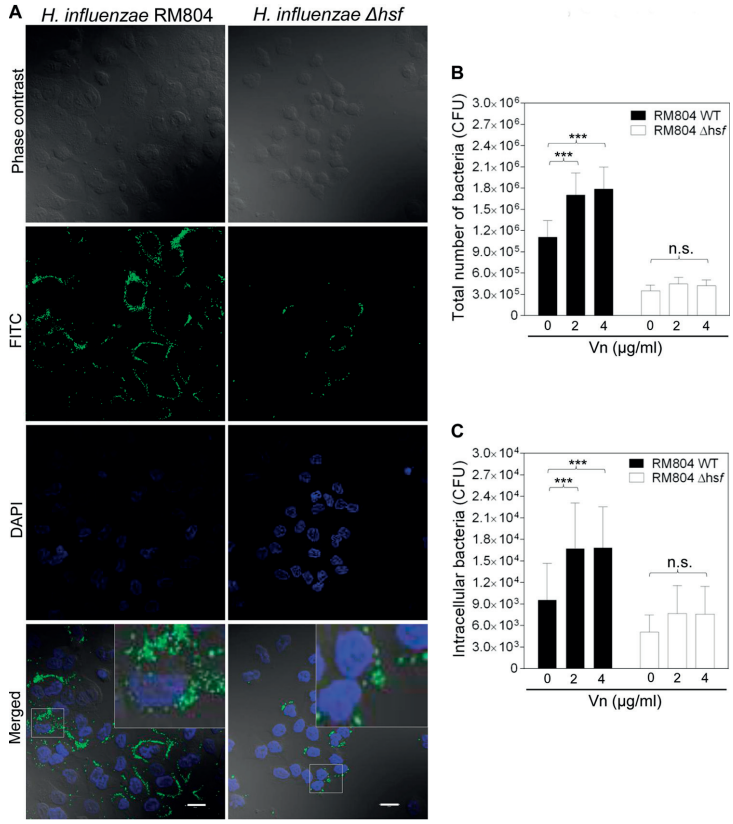

FIG 8 Vitronectin promotes the adherence and internalization of Hib. (A) Confocal microscopy showing increased adherence of *H. influenzae* RM804 (WT) in the presence of Vn. Cell monolayers were treated with 10 μg Vn and afterwards were incubated with FITC-conjugated bacteria for 2 h. Phase-contrast microscopy represents whole-cell images. Bacteria were labeled in green (FITC) and cell nuclei in blue (DAPI). Bars, 20 μM. (B) Bacterial adherence to A549 cells after 2 h in the presence of 2 or 4 μg/ml Vn as measured by counting of CFU. (C) Internalized bacteria were measured by a gentamicin protection assay. Each well of the microtiter plates has approximately 3×10^5 to 3.5×10^5 cells, and 1×10^7 CFU was added to each well. Data in graphs are the means of results of three independent experiments, and error bars indicate standard deviations. ***, $P \leq 0.001$; n.s., not significant.

between bacteria and epithelial cell surface integrins. It is also possible that BD1 may bind directly to receptors on the host epithelium. This may lead to a stronger Hsf-mediated "dual" interaction of *H. influenzae* RM804 with the host cell surface.

It is well known that the complement system is activated via the classical, alternative, and lectin-mediated pathways (31) and is governed, among other regulators, by C4b-binding protein, FH, and Vn. While complement inhibitors such as FH and C4b-binding protein inhibit the alternative pathway and the classical/lectin-mediated pathways, respectively, Vn inhibits the assembly of the membrane binding site of the C5b-7 complex and the polymerization of C9 during the formation of the lytic pore. Thus, Vn would be an effective regulator that would inhibit the terminal lytic pathway regardless of which complement pathway had been activated previously. Our current data indicate that Hsf preferentially bound to Vn and utilized it for the enhancement of resistance against the MAC.

In conclusion, our present study shows that the previously reported Hsf-Vn binding is directly involved in protecting Hib from serum-mediated killing through inhibition of the MAC complex. The results also demonstrate how Hsf might act as an adhesin by binding to Vn, which, in turn, promotes the adherence and internalization of the pathogen. Taking the findings together, our study sheds light on how Hib utilizes the multifunctional host protein Vn for evasion of the immune system and efficient survival in the host.

ACKNOWLEDGMENTS

We report no potential conflicts of interest.

This work was supported by grants from the foundations of Alfred

Österlund, Anna and Edwin Berger, Greta and Johan Kock, Åke Wiberg, and Torsten Söderberg, the Lars Hierta Foundation, the Swedish Medical Research Council (grants 521-2010-4221 and K2012–66X-14928-09-5), the Cancer Foundation at the University Hospital in Malmö, the Physiographical Society (Forssman's Foundation), and the Skåne County Council's research and development foundation.

We thank Alam Kazi Asraful and Marta Brant for excellent technical assistance.

REFERENCES

1. **Morris SK, Moss WJ, Halsey N.** 2008. *Haemophilus influenzae* type b conjugate vaccine use and effectiveness. Lancet Infect. Dis. **8:**435–443. http://dx.doi.org/10.1016/S1473-3099(08)70152-X.
2. **Agrawal A, Murphy TF.** 2011. *Haemophilus influenzae* infections in the *H. influenzae* type b conjugate vaccine era. J. Clin. Microbiol. **49:**3728–3732. http://dx.doi.org/10.1128/JCM.05476-11.
3. **Danovaro-Holliday MC, Garcia S, de Quadros C, Tambini G, Andrus JK.** 2008. Progress in vaccination against *Haemophilus influenzae* type b in the Americas. PLoS Med. **5:**e87. http://dx.doi.org/10.1371/journal.pmed.0050087.
4. **Fitzwater SP, Watt JP, Levine OS, Santosham M.** 2010. *Haemophilus influenzae* type b conjugate vaccines: considerations for vaccination schedules and implications for developing countries. Hum. Vaccin. **6:**810–818. http://dx.doi.org/10.4161/hv.6.10.13017.
5. **Ulanova M, Tsang RS.** 2009. Invasive *Haemophilus influenzae* disease: changing epidemiology and host-parasite interactions in the 21st century. Infect. Genet. Evol. **9:**594–605. http://dx.doi.org/10.1016/j.meegid.2009.03.001.
6. **St. Geme JW, III.** 1996. Molecular determinants of the interaction between *Haemophilus influenzae* and human cells. Am. J. Respir. Crit. Care Med. **154:**S192–S196. http://dx.doi.org/10.1164/ajrccm/154.4_Pt_2.S192.
7. **St. Geme JW, III, Cutter D.** 1996. Influence of pili, fibrils, and capsule on in vitro adherence by *Haemophilus influenzae* type b. Mol. Microbiol. **21:**21–31. http://dx.doi.org/10.1046/j.1365-2958.1996.6241331.x.
8. **Singh B, Fleury C, Jalalvand F, Riesbeck K.** 2012. Human pathogens utilize host extracellular matrix proteins laminin and collagen for adhesion and invasion of the host. FEMS Microbiol. Rev. **36:**1122–1180. http://dx.doi.org/10.1111/j.1574-6976.2012.00340.x.
9. **Cotter SE, Yeo HJ, Juehne T, St. Geme JW, III.** 2005. Architecture and adhesive activity of the *Haemophilus influenzae* Hsf adhesin. J. Bacteriol. **187:**4656–4664. http://dx.doi.org/10.1128/JB.187.13.4656-4664.2005.
10. **St. Geme JW, III, Kumar VV, Cutter D, Barenkamp SJ.** 1998. Prevalence and distribution of the *hmw* and *hia* genes and the HMW and Hia adhesins among genetically diverse strains of nontypeable *Haemophilus influenzae*. Infect. Immun. **66:**364–368.
11. **St. Geme JW, III, Cutter D, Barenkamp SJ.** 1996. Characterization of the genetic locus encoding *Haemophilus influenzae* type b surface fibrils. J. Bacteriol. **178:**6281–6287.
12. **Watson ME, Jr, Nelson KL, Nguyen V, Burnham CA, Clarridge JE, Qin X, Smith AL.** 2013. Adhesin genes and serum resistance in *Haemophilus influenzae* type f isolates. J. Med. Microbiol. **62:**514–524. http://dx.doi.org/10.1099/jmm.0.052175-0.
13. **Rodriguez CA, Avadhanula V, Buscher A, Smith AL, St. Geme JW, III, Adderson EE.** 2003. Prevalence and distribution of adhesins in invasive non-type b encapsulated *Haemophilus influenzae*. Infect. Immun. **71:**1635–1642. http://dx.doi.org/10.1128/IAI.71.4.1635-1642.2003.
14. **Spahich NA, St. Geme JW, III.** 2011. Structure and function of the *Haemophilus influenzae* autotransporters. Front. Cell. Infect. Microbiol. **1:**5. http://dx.doi.org/10.3389/fcimb.2011.00005.
15. **Hallström T, Riesbeck K.** 2010. *Haemophilus influenzae* and the complement system. Trends Microbiol. **18:**258–265. http://dx.doi.org/10.1016/j.tim.2010.03.007.
16. **Winkelstein JA, Moxon ER.** 1992. The role of complement in the host's defense against *Haemophilus influenzae*. J. Infect. Dis. **165**(Suppl 1)**:**S62–S65. http://dx.doi.org/10.1093/infdis/165-Supplement_1-S62.
17. **Singh B, Blom AM, Unal C, Nilson B, Morgelin M, Riesbeck K.** 2010. Vitronectin binds to the head region of *Moraxella catarrhalis* ubiquitous surface protein A2 and confers complement-inhibitory activity. Mol. Microbiol. **75:**1426–1444. http://dx.doi.org/10.1111/j.1365-2958.2010.07066.x.
18. **Singh B, Jalalvand F, Morgelin M, Zipfel P, Blom AM, Riesbeck K.** 2011. *Haemophilus influenzae* protein E recognizes the C-terminal domain of vitronectin and modulates the membrane attack complex. Mol. Microbiol. **81:**80–98. http://dx.doi.org/10.1111/j.1365-2958.2011.07678.x.
19. **Voss S, Hallstrom T, Saleh M, Burchhardt G, Pribyl T, Singh B, Riesbeck K, Zipfel PF, Hammerschmidt S.** 2013. The choline-binding protein PspC of *Streptococcus pneumoniae* interacts with the C-terminal heparin-binding domain of vitronectin. J. Biol. Chem. **288:**15614–15627. http://dx.doi.org/10.1074/jbc.M112.443507.
20. **Singh B, Yu-Ching Su, Riesbeck K.** 2011. Vitronectin in host pathogen interactions and antimicrobial therapeutic applications. Cent. Eur. J. Biol. **6:**973–980. http://dx.doi.org/10.2478/s11535-011-0077-x.
21. **Singh B, Su YC, Riesbeck K.** 2010. Vitronectin in bacterial pathogenesis: a host protein used in complement escape and cellular invasion. Mol. Microbiol. **78:**545–560. http://dx.doi.org/10.1111/j.1365-2958.2010.07373.x.
22. **Bergmann S, Lang A, Rohde M, Agarwal V, Rennemeier C, Grashoff C, Preissner KT, Hammerschmidt S.** 2009. Integrin-linked kinase is required for vitronectin-mediated internalization of *Streptococcus pneumoniae* by host cells. J. Cell Sci. **122:**256–267. http://dx.doi.org/10.1242/jcs.035600.
23. **Leroy-Dudal J, Gagniere H, Cossard E, Carreiras F, Di Martino P.** 2004. Role of αvβ5 integrins and vitronectin in *Pseudomonas aeruginosa* PAK interaction with A549 respiratory cells. Microbes Infect. **6:**875–881. http://dx.doi.org/10.1016/j.micinf.2004.05.004.
24. **Su YC, Jalalvand F, Morgelin M, Blom AM, Singh B, Riesbeck K.** 2013. *Haemophilus influenzae* acquires vitronectin via the ubiquitous protein F to subvert host innate immunity. Mol. Microbiol. **87:**1245–1266. http://dx.doi.org/10.1111/mmi.12164.
25. **Hallström T, Trajkovska E, Forsgren A, Riesbeck K.** 2006. *Haemophilus influenzae* surface fibrils contribute to serum resistance by interacting with vitronectin. J. Immunol. **177:**430–436. (Erratum, 190:4431, 2013). http://dx.doi.org/10.4049/jimmunol.1390012.
26. **Roth J.** 1996. The silver anniversary of gold: 25 years of the colloidal gold marker system for immunocytochemistry and histochemistry. Histochem. Cell Biol. **106:**1–8. http://dx.doi.org/10.1007/BF02473197.
27. **Carlemalm E.** 1990. Lowicryl resins in microbiology. J. Struct. Biol. **104:**189–191. http://dx.doi.org/10.1016/1047-8477(90)90075-N.
28. **Bengtson SH, Eddleston J, Morgelin M, Zuraw BL, Herwald H.** 2008. Regulation of kinin B_2 receptors by bradykinin in human lung cells. Biol. Chem. **389:**1435–1440. http://dx.doi.org/10.1515/BC.2008.159.
29. **Sa E Cunha C, Griffiths NJ, Virji M.** 2010. *Neisseria meningitidis* Opc invasin binds to the sulphated tyrosines of activated vitronectin to attach to and invade human brain endothelial cells. PLoS Pathog. **6:**e1000911. http://dx.doi.org/10.1371/journal.ppat.1000911.
30. **Radin JN, Grass SA, Meng G, Cotter SE, Waksman G, St. Geme JW, III.** 2009. Structural basis for the differential binding affinities of the HsfBD1 and HsfBD2 domains in the *Haemophilus influenzae* Hsf adhesin. J. Bacteriol. **191:**5068–5075. http://dx.doi.org/10.1128/JB.00395-09.
31. **Zipfel PF.** 2009. Complement and immune defense: from innate immunity to human diseases. Immunol. Lett. **126:**1–7. http://dx.doi.org/10.1016/j.imlet.2009.07.005.

Fig. S1, Singh *et al.*

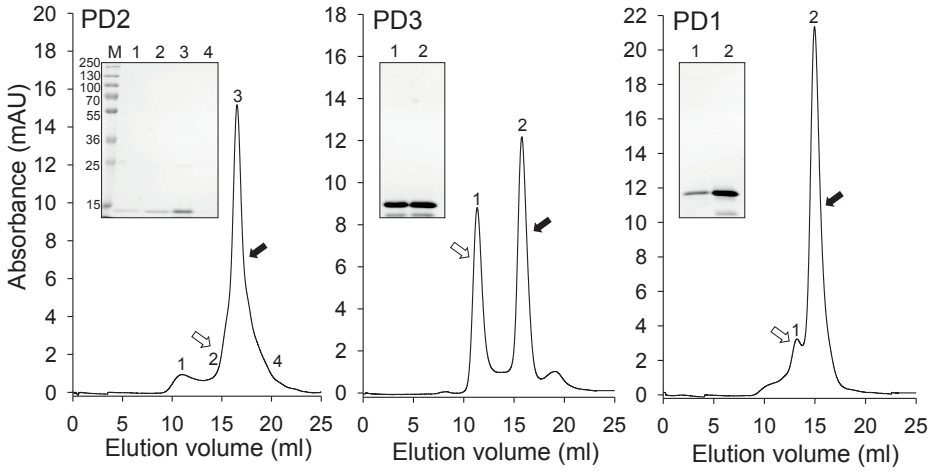

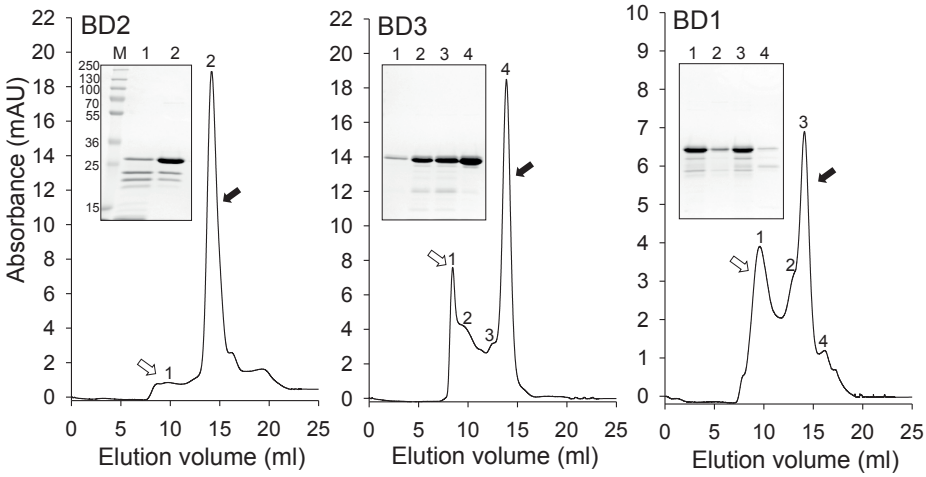

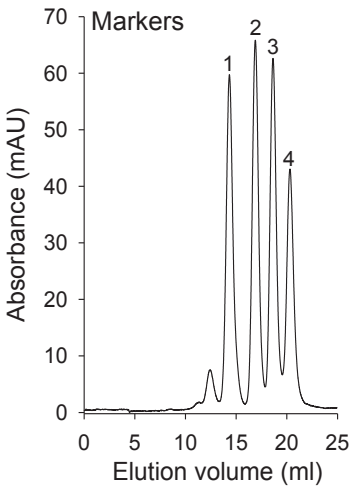

Molecular weight markers

1. Bovine serum albumin (14.3 ml); 66 kDa
2. Carbonic anhydrase (16.8 ml); 29 kDa
3. Cytochrome-c (18.6 ml); 12.4 kDa
4. Aprotinin (20.2 9 ml); 6.5 kDa

Fig. S2, Singh *et al.*

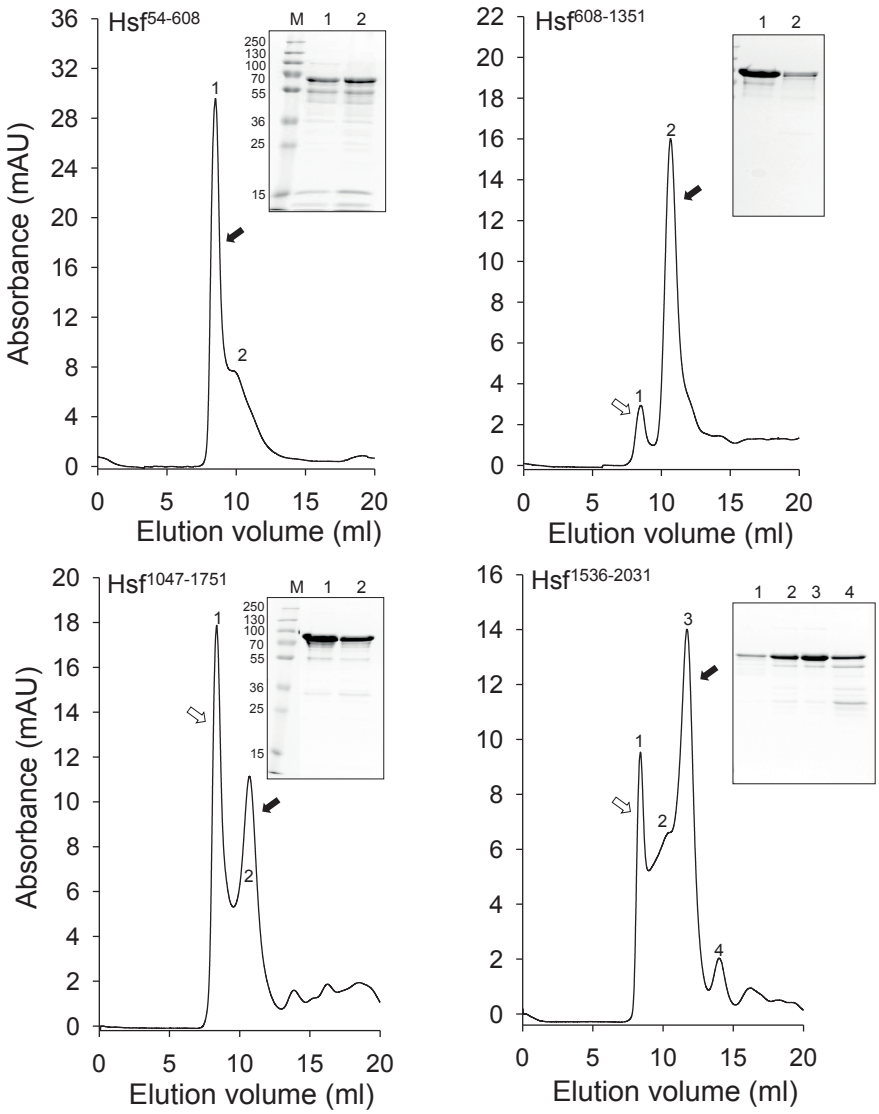

Fig S1-S2 Purification of PDs and BDs and other fragments of Hsf molecule (these proteins were used in figure 1). Approximately 0.5 mg of each protein was injected to Superdex 200 gel filtration column. Peaks collected were separated 12% SDS-PAGE and stained with Coomassie blue R250. Molecular weight of the peaks were calculated by comparing Ve/Vo ratio of the standard peaks. Black arrow represents trimric peak, while white arrow represents higher molecular weight oligomers.

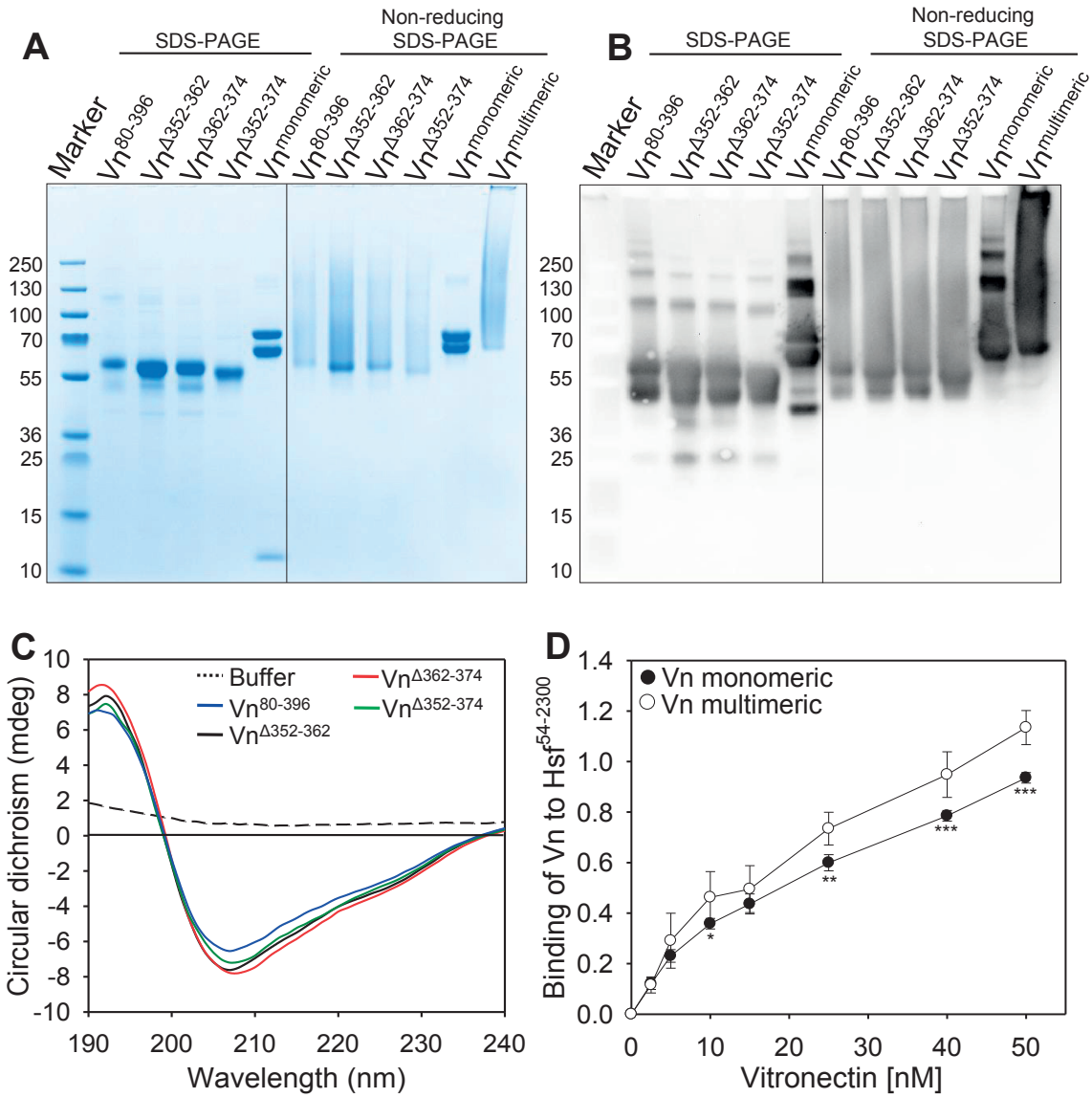

Fig S3 Vn molecules expressed in HEK293T cells and purified with affinity chromatography. Monomeric and multimeric Vn were included from commercial sources. *A*. Vn (3 µg) loaded on SDS-PAGE under denatured conditions and seminative (non-reducing) conditions. Gel was stained with Coomassie blue R250. *B*. SDS-PAGE gel similar to (A), except all proteins 0.1 µg were loaded. The gel was blotted on a nitrocellulose membrane and Vn(s) were detected by using anti-Vn antibodies. *C*. Circular dichroism (CD) spectra showing the folding of $Vn^{80\text{-}396}$, $Vn^{\Delta 352\text{-}362}$, $Vn^{\Delta 362\text{-}374}$ or $Vn^{\Delta 352\text{-}374}$ proteins that were recombinantly expressed in HEK293T cells and purified by affinity chromatography. *D*. Binding of monomeric and multimeric Vn with $Hsf^{54\text{-}2300}$.

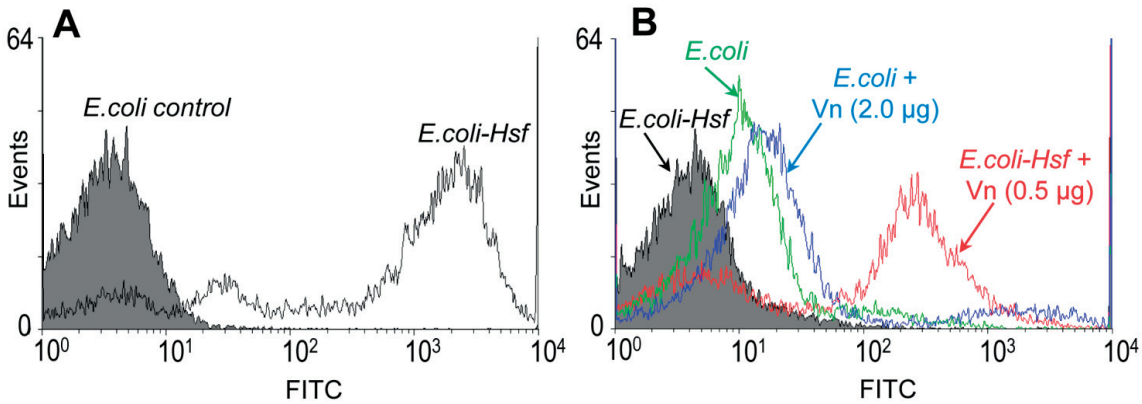

Fig S4 Expression of Hsf in *E. coli* and binding of Vn. A. Flow cytometry profile showing the expression of Hsf in *E. coli*. *E. coli* were transformed with pET16b-Hsf$^{1\text{-}2414}$ and stained with anti-Hsf antibodies produced in rabbit. B. Binding of Vn to *E. coli* control and Hsf expressing *E. coli.*

Fig. S5, Singh *et al.*

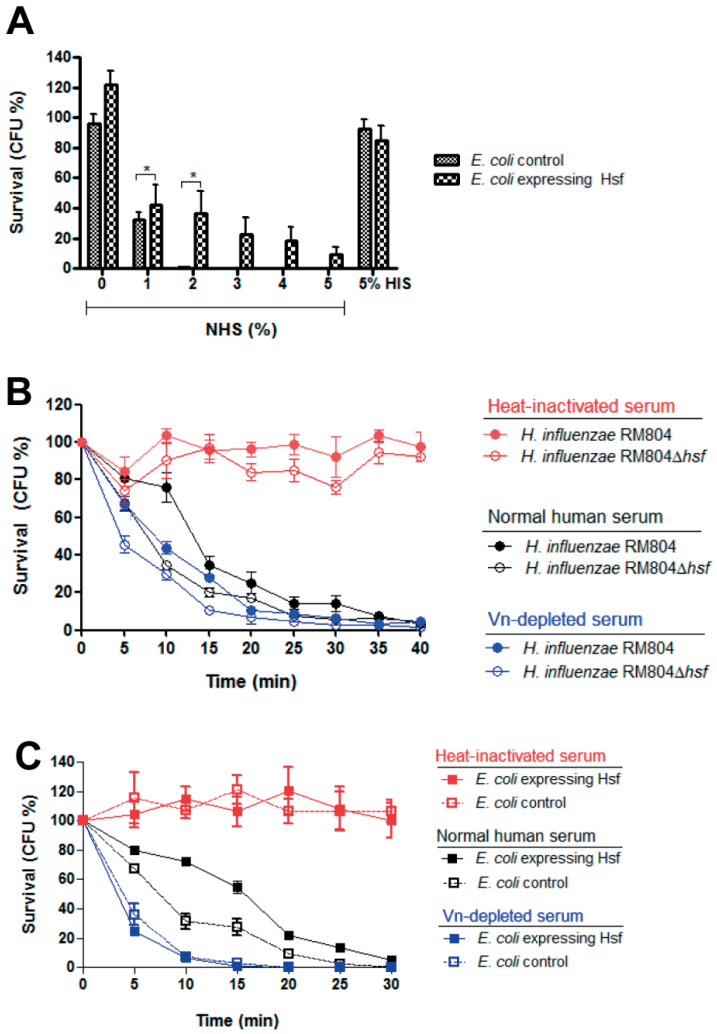

Fig S5 Characterization of serum survival of the Hsf-expressing bacteria. *A*. Survival of *E. coli* expressing Hsf in various percentage of NHS (1-5%) at 5 min. *B*. Survival kinetics of *E. coli* expressing Hsf in 1% of normal human serum (NHS), vitronectin-depleted serum (VDS) and heat-inactivated serum (HIS). *C*. Survival kinetics of wild type *H. influenzae* RM804 and *hsf*-deleted mutant in 5% of NHS, VDS and HIS. All data represent the mean values of three independent experiments and error bars indicate the standard deviations.

Paper V

International Journal of Medical Microbiology 305 (2015) 27–37

Contents lists available at ScienceDirect

International Journal of Medical Microbiology

journal homepage: www.elsevier.com/locate/ijmm

Haemophilus influenzae surface fibril (Hsf) is a unique twisted hairpin-like trimeric autotransporter

Birendra Singh[a], Tamim Al Jubair[a], Matthias Mörgelin[b], Anders Sundin[c], Sara Linse[d], Ulf J. Nilsson[c], Kristian Riesbeck[a,*]

[a] Medical Microbiology, Department of Laboratory Medicine Malmö, Lund University, Jan Waldenströms gata 59, SE-205 02 Malmö, Sweden
[b] Infection Medicine, Department of Clinical Sciences, Lund University, SE-221 84 Lund, Sweden
[c] Centre for Analysis and Synthesis, Department of Chemistry, Lund University, PO Box 124, SE-221 00 Lund, Sweden
[d] Biochemistry and Structural Biology, Lund University, PO Box 124, SE-221 00 Lund, Sweden

ARTICLE INFO

Article history:
Received 7 July 2014
Received in revised form 8 October 2014
Accepted 18 October 2014

Keywords:
Haemophilus influenzae type b
Haemophilus surface fibril
Hib
Hsf

ABSTRACT

The *Haemophilus* surface fibril (Hsf) is an extraordinary large (2413 amino acids) trimeric autotransporter, present in all encapsulated *Haemophilus influenzae*. It contributes to virulence by directly functioning as an adhesin. Furthermore, Hsf recruits the host factor vitronectin thereby inhibiting the host innate immune response resulting in enhanced survival in serum. Here we observed by electron microscopy that Hsf appears as an 100 nm long fibril at the bacterial surface albeit the length is approximately 200 nm according to a bioinformatics based model. To unveil this discrepancy, we denaturated Hsf at the surface of Hib by using guanidine hydrochloride (GuHCl). Partial denaturation induced in the presence of GuHCl unfolded the Hsf molecules, and resulted in an increased length of fibres in comparison to the native trimeric form. Importantly, our findings were also verified by *E. coli* expressing Hsf at its surface. In addition, a set of Hsf-specific peptide antibodies also indicated that the N-terminal of Hsf is located near the C-terminal at the base of the fibril. Taken together, our results demonstrated that Hsf is not a straight molecule but is folded and doubled over. This is the first report that provides the unique structural features of the trimeric autotransporter Hsf.

Introduction

Haemophilus influenzae is a Gram-negative respiratory pathogen that are categorised into encapsulated (serotype a to f) and unencapsulated strains, the later group is designated as non-typeable *H. influenzae* (NTHi). *H. influenzae* type b (Hib) causes pneumonia, osteomyelitis, epiglottitis, sepsis, joint infections, and acute meningitis and is hence considered as the most virulent type (Morris et al., 2008; Agrawal and Murphy, 2011). Even though the incidence of Hib infections in developed countries has been significantly reduced after introduction of the Hib conjugate vaccine in the early 1990s (Danovaro-Holliday et al., 2008), Hib remains a major infectious agent in infants and children in developing countries (Fitzwater et al., 2010). Hib infection starts by attachment of the bacteria to the nasopharyngeal and lung epithelial surfaces resulting in epithelial damage followed by penetration of the underlying tissues mediated by various sophisticated mechanisms (Geme and Cutter, 1995; Geme, 1996; Ulanova and Tsang, 2009; Agrawal and Murphy, 2011). Hib is furthermore able to penetrate the blood-brain barrier and thus causes meningitis (Singh et al., 2012). Survival of Hib in the blood is controlled by acquiring complement regulators to the surface of the pathogen for an effective inhibition of the membrane attack complex (MAC) (Winkelstein and Moxon, 1992; Hallström and Riesbeck, 2010; Singh et al., 2010). However, penetration of this pathogen to deep tissues depends on multiple virulence factors (Agrawal and Murphy, 2011).

Gram-negative pathogens possess a specific group of proteins known as autotransporters, which are translocated to the cell surface by a type V secretion mechanism. Unlike the type I–IV secretory systems that involve multiple proteins, autotransporters are composed of a single protein consisting of an N-terminal signal peptide for secretion, followed by a passenger domain, and a C-terminal translocator (membrane anchoring) domain (Dautin and Bernstein, 2007; Leo et al., 2012). These autotransporters are multifunctional proteins ranging from monomeric to multimeric arrangements (Meng et al., 2011). Recently, the biological role of few autotransporters has been studied in *H. influenzae*. The monomeric autotransporter *Haemophilus* adhesion and

* Corresponding author. Tel.: +46 40 338494; fax: +46 40 336234.
E-mail address: kristian.riesbeck@med.lu.se (K. Riesbeck).

http://dx.doi.org/10.1016/j.ijmm.2014.10.004
1438-4221/

penetration protein (Hap) is involved in bacterial aggregation and adherence to host cells (Meng et al., 2011; Hallström et al., 2011). A trimeric autotransporter adhesin (TAA) known as Hia has also been extensively studied for its functional and structural characteristics (Dautin et al., 2007; Spahich and St Geme, 2011). Hia is only present in approximately 25% of the clinical NTHi isolates (St Geme et al., 1998), and cannot be found in encapsulated *H. influenzae*. In contrast, *Haemophilus* surface fibril (Hsf) is present in all typeable strains (St Geme et al., 1996; Rodriguez et al., 2003; Watson et al., 2013). Notwithstanding homologous, Hia and Hsf are relatively different sizewise; Hia has a size of ≈114 kDa (≈342 kDa as a trimer), whereas Hsf is almost twice in size with a monomer of approximately 243 kDa that builds up a ≈750 kDa trimer (Cotter et al., 2005b). These two TAAs are highly homologous at their N- and C-termini with an overall 81% similarity and 72% identity. Moreover, Hia and Hsf are constituted of various repetitive domains, which in parts have been defined according to their biological functions. For instance, Hia has two functional host epithelial cell binding domains designated BD1 and BD2. Similar binding domains are present in Hsf, but in addition, Hsf has a third binding domain (BD3). The binding domains are similar in their secondary structures. However, a few key amino acids of the binding pocket of the BD3 of Hsf are different as compared to BD1 and BD2, and therefore BD3 appears not to interact with host cells (Danovaro-Holliday et al., 2008; Spahich and St Geme, 2011).

Previously we reported that Hsf recruits Vn and thus inhibits the lytic pathway of the complement system (Hallström et al., 2006). Recently, we studied the Hsf-Vn interaction in detail and found that BD2 of Hsf selectively interacts with the C-terminal end of Vn and thus inhibits MAC formation (Singh et al., 2014). Vn also mediates an increased adherence of Hib to epithelial cells. We proposed that when Vn is bound to BD2 it may function as a bridging molecule between the bacteria and epithelial surface integrins. However, BD1 may directly bind to host epithelium, leading to a stronger Hsf-mediated interaction of Hib with the host cell surface (Singh et al., 2014).

In the present study, we investigated the molecular architecture of Hsf at the bacterial surface. Since the Hsf molecule is an extraordinary large protein and has a repetitive domain structure we modeled this protein by using an *in silico* approach. Our computed model suggested a protein length of approximately 200 nm, whereas the length of Hsf observed by electron microscopy was only 100 nm. Based upon these observations, we analyzed the organisation of Hsf on the bacterial surface by denaturing Hsf using GuHCl in order to unfold the Hsf molecule. In addition, a set of specific anti-Hsf peptide antibodies was included in the analyses to locate the precise regions of the molecule. Our results show that Hsf is not a straight fibre, as reported with several other known bacterial TAAs, but rather consists as a "hairpin-like" twisted molecule.

Material and methods

Bacterial strains and culture conditions

The type b *H. influenzae* RM804 and mutants (Hallström et al., 2006) were grown in brain heart infusion (BHI) liquid medium containing 10 μg ml^{-1} nicotinamide adenine dinucleotide (NAD) and hemin, or on chocolate agar plates. Cultures were incubated at 37 °C in a humid atmosphere containing 5% CO_2. The *hsf* mutant was grown in BHI supplemented with 18 μg ml^{-1} kanamycin. Luria Bertani (LB) broth or on LB agar plates were used to grow *E. coli* DH5α and *E. coli* BL21 (DE3). *E. coli* harboring expression vectors pET26b-*hsf*(s) and pET16b-*hsf*$^{1-2413}$ were grown in 50 μg ml^{-1} kanamycin and 100 μg ml^{-1} ampicillin, respectively.

Bioinformatics and protein modeling

An *in silico* model of Hsf was constructed by using a comparative protein structure modeling on domains with a highly homologous amino acid sequence to that of a known three-dimensional structure determined by X-Ray Diffraction Crystallography. Domains with low homology to known three-dimensional structures was built as a trimeric coiled-coil as described elsewhere (Griffiths et al., 2011). The initial alignment from the BLAST/PSI-BLAST homology search was refined using ClustalW alignment and prime STA alignment combined with manual alignment. From the final alignment, an energy-based homo-multimer model was constructed. The resulting model was evaluated to ensure that hydrophilic amino acids were on the surface and hydrophobic amino acids were buried in the protein interior. If these criteria were not sufficiently met, a new model was constructed after sequence re-alignment. The comparative protein structure modeling was performed using Prime version 3.1, which is part of the Schrödinger Suite 2012 (Prime, version 3.1, Schrödinger, LLC, New York, NY, 2012). In addition, UCSF Chimera 1.6 was used for bookkeeping purposes such as the renumbering of amino acid sequences (Pettersen et al., 2004).

Protein expression and purification

Recombinant DNA plasmids were obtained as described elsewhere (Singh et al., 2014). For surface expression of the Hsf protein, pET16-*hsf*54-2300 (Hallström et al., 2006) was freshly transformed into *E. coli* BL21 (DE3) and plated on LB ampicillin plates. Single colonies were inoculated in 10 ml LB containing 100 μg ml^{-1} ampicillin and incubated at 37 °C at 200 rpm shaking. Expression was induced by addition of 0.2 mM IPTG when $OD_{600\,nm}$ reached to 0.4–0.5. Induced cultures were further incubated at 37 °C with shaking at 200 rpm for the next 15 h. Expression of Hsf at the surface was verified by using anti-PD antibodies in flow cytometry. For purification purposes, *E. coli* BL21(DE3) containing pET26b-*hsf*(s) was grown in LB medium with kanamycin at 37 °C until $OD_{600\,nm}$ reached to 0.8–1. Protein expression was induced by addition of 1 mM IPTG, and protein purification was performed as described elsewhere (Singh and Rohm, 2008). Some Hsf fragments produced inclusion bodies that were purified by using an inclusion body purification protocol (Singh and Rohm, 2008). The purified proteins were dialyzed in PBS and concentrated by using Centricon cartridge (Millipore, Bedford, MA). Purity of the proteins was confirmed by SDS-PAGE and concentrations were estimated by a NanoDrop spectrophotometer (Thermo Scientific, Wilmington, DE) and also verified by a bicinchoninic acid (BCA) assay (Pierce, Rockford, IL).

Production of antibodies

Specific peptides covering the sequence Hsf 153–164, 876–881 (KTRAAS), 1912–1942 were synthesized and conjugated with KLH (Innovagen, Lund, Sweden). For immunization, 500 μl peptides (200 μg) were mixed with 500 μl complete Freunds adjuvant followed by immunization of rabbits. After 4 weeks, the same amount of peptides were injected with aluminium hydroxide as adjuvant. Two boosters were administered after 5 and 6 weeks. Finally, blood was drawn from immunized rabbits and antibodies (Abs) from sera were purified by standard affinity purification protocol (Singh et al., 2013). BD and PD domains were aligned and modeled to identify the conserved surface exposed regions (Fig. 1B–C and Fig. S1). Peptide antibodies against the BD and PD domains were produced in rabbits and purified by affinity purification (Genscript, NJ). Antibodies solutions were concentrated to 1 mg/ml in PBS and stored at −20 °C.

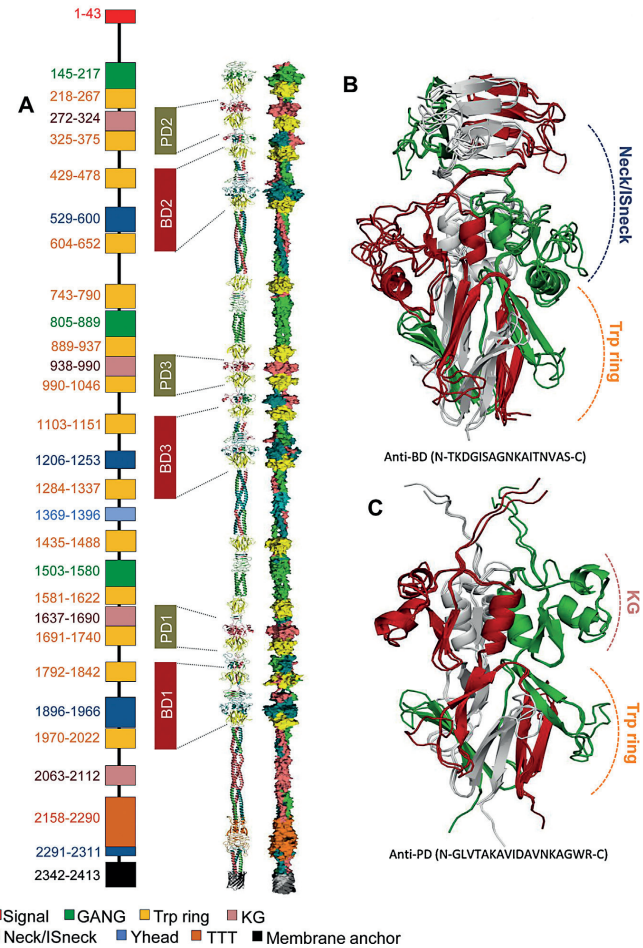

Fig. 1. Modelling of the full length Hsf molecule. (A) Prediction of repetitive motifs in the Hsf molecule by using the domain annotation of trimeric autotransporter adhesins (daTAA) server at Max Planck Institute for Developmental Biology, Tubingen, Germany (http://toolkit.tuebingen.mpg.de/dataa/search). Domains are indicated according to their amino acid numbers, and the BD and PD are named according to the previously described nomenclature (Cotter *et al.*, 2005). (B) A superimposed cartoon model that demonstrates putative domains (3×) present at the regions Hsf 263–376, 938–1050 and 1630–1741 modeled by using template 3emi. (C) Superimposed model that shows binding domains (3x) present at the Hsf regions 500–652, 1173–1338 and 1863–2023 modeled by using template 1s7m. The amino acid regions encompassing PD and BD domains were aligned (Fig. S1), and a conserved surface exposed region was selected for production of peptides that were used for immunization of rabbits. These conserved sequences are shown at the bottom of panels (B and C). PDB templates, 1S7M, 3emi, and 3 emo; Hia of *H. influenzae*, 2qih; UspA1 of *Moraxella catarrhalis*, 3d9x; BadA of *Bartonella henselae*, 3laa; *Burkholderia pseudomallei*. Homology modeling was performed by using different templates available in the PDB data base. The templates are presented as Hsf amino acids (PDB code of template: identity/similarity, gap), 0136–0269 (1s7m: 23/35, 4), 0263–0376 (3emi: 63/73, 12), 377–0481(3emi: 16/31, 5), 0482–0499 (2qih: 22/38, 0), 0500–0652 (1s7m: 54/68, 2), 0653–0742 (2qih: 15/26, 0), 0743–0858 (3d9x: 26/43, 11), 0859–0876 (2qih: 27/44, 0), 0877–0937 (3emi: 22/31, 7), 0938–1050 (3emi: 45/56, 11), 1051–1155 (3emi: 21/33, 4), 1156–1172 (2qih: 23/35, 0), 1173–1338 (1s7m: 47/58, 8), 1339–1433 (2qih: 15/30, 0), 1434–1558 (3d9x: 17/32, 12), 1559–1578 (2qih: 23/33, 0), 1579–1629 (3d9x: 15/33, 3), 1630–1741 (3emi: 71/77, 3), 1742–1862 (3emi: 21/34, 22), 1863–2023 (1s7m: 73/79, 3), 2024–2143 (2qih: 11/23, 0), 2144–2315 (3laa: 15/22, 21), and 2308–2413 (3emo: 100/100, 0).

Western blotting

Purified Hsf fragments (50 ng) were mixed with SDS-PAGE loading dye, incubated at 95 °C for 5 min and centrifuged (14,000 × *g*) for 5 min. Supernatants were loaded on 4–12% Bis-tris gels (NuPAGE; Invitrogen, Carlsbad, CA) and resolved at 80 V until the dye front reached the bottom of gels. Proteins were transferred to a PVDF membrane for 15 h followed by blocking with 5% milk in PBS. Blots were incubated with anti-PD, anti-BD, anti-Hsf$^{153-164}$, anti-Hsf$^{876-881}$, anti-Hsf$^{1912-1942}$ Abs or a combination of Abs as indicated. After 1 h of incubation at RT, blots were washed 4 times in PBS containing 0.05% Tween-20 (PBS-T). Thereafter, secondary anti-rabbit swine polyclonal Abs (Dako, Glostrup, Denmark) were added to the blot in PBS containing 5% milk and incubated for 1 h

at RT. Finally, blots were washed 4 times in PBS-T and developed using an ECL western blotting kit (Pierce, Rockford, IL).

Circular dichroism (CD)

Purified recombinant $Hsf^{54-2300}$ was dialysed against 25 mM phosphate buffer, pH 7.5 containing 100 mM sodium fluoride. Two samples of $Hsf^{54-2300}$ (0.2 mg/ml) were prepared, one in buffer and one in buffer with 6 M GuHCl. Spectra (15×) were recorded for these two samples between 210–250 nm in a Jasco J-815CD spectrophotometer (Jasco, Easton, MD) in a 1 mm quartz cuvette thermostated to 25 °C, and the mean spectrum was plotted. Each spectrum was subtracted from a control spectrum obtained in the absence of protein. The two solutions were mixed in different proportions to prepare a set of solutions containing 0.25–5.75 M GuHCl in steps of 0.25 M. For each these solutions, and the two stock solutions, the ellipticity at 222 nm was recorded during 2 min. The following equation was fitted to the average signal versus GuHCl concentration:

$$y = \frac{y_f^0 + m_f\,[\mathrm{GuHCl}] + \left(y_u^0 + m_u\,[\mathrm{GuHCl}]\right)\exp\left(-1/RT\left(\Delta G^0(\mathrm{H_2O}) - m\,[\mathrm{GuHCl}]\right)\right)}{1 + \exp\left(-1/RT\left(\Delta G^0(\mathrm{H_2O}) - m\,[\mathrm{GuHCl}]\right)\right)} \quad (1)$$

The six fitted parameters are the free energy of unfolding in the absence of denaturant, $\Delta G^o(H_2O)$, and its dependence on denaturant concentration, m, the intercept, y_f^0, and slope, m_f, of the naive state baseline, and the intercept, y_u^0, and slope, m_u, of the unfolded state baseline. The GuHCl concentration at which 50% of the protein molecules are denatured, C_M, is calculated from the fitted parameters as

$$C_M = \frac{\Delta G^o(\mathrm{H_2O})}{m} \quad (2)$$

For presentation, the data are normalized to the apparent fraction folded, F_{app}, according to

$$F_{app} = \frac{y - y_u}{y_f - y_u} \quad (3)$$

Transmission electron microscopy (TEM)

Different Abs were labelled with colloidal gold as described (Roth, 1996). The wild type *H. influenzae* RM804 were grown in BHI for 3 h at 37 °C. *E. coli* were induced with IPTG to express Hsf, and the expression of the protein at the surface was verified by flow cytometry prior to TEM. Bacteria were treated with GuHCl and washed twice in PBS. Thereafter, bacteria were fixed in 2.5% glutaraldehyde, dehydrated and embedded in Epon as described earlier (Oehmcke et al., 2009). For negative staining, bacteria were incubated with 5 nm and 10 nm gold-conjugated antibodies as described, fixed in PBS containing 4% paraformaldehyde and 0.1% glutaraldehyde, and prepared as described (Carlemalm, 1990). TEM was performed as described elsewhere (Bengtson et al., 2008), and specimens were examined in a JEOL JEM 1230 transmission electron microscope (JEOL, Peabody, MA) at 60 kV accelerating voltage. The Images were recorded with a Gatan Multiscan 791 CCD camera (Gatan, Pleasanton, CA). Only particles observed within a distance of 15 nm or less adjacent to the cell surface were counted. This corresponds to the established maximum distance between an IgG and its antigen, or between a protein labeled with gold of this size, and its target.

Results

Hsf is approximately a 200 nm long fibril according to a modelled structure

Autotransporters are very difficult to crystallize, and therefore most structures have been solved in fragments and followed by compilation into full models (Agnew et al., 2011; Hartmann et al., 2012). In order to model the Hsf structure, we first predicted different structural motifs/domains by the daTAA server at Max Planck Institute for developmental Biology, Tubingen, Germany (http://toolkit.tuebingen.mpg.de/dataa/search). Our prediction revealed the presence of an N-terminal signal sequence (1–43 aa) required for protein translocation to the membrane, 14 distinguished Trp-ring domains, 3 GANG domains, 3 Neck/IS-Neck domains, 4 KG motifs, 1 Y head, 1 TTT, and finally a highly conserved membrane anchoring domain (2342–2413 aa) at the C-terminus of Hsf (Fig. 1A). We thereafter modeled various regions of the Hsf molecule by using known templates and finally the full structure was compiled (Fig. 1A).

Previously, on the basis of interactions with Chang conjunctival epithelial cells, three binding domains ($BD2^{529-652}$, $BD3^{1206-1337}$ and $BD1^{1896-2022}$) have been characterized in the Hsf molecule (Cotter et al., 2005b). All binding domains consist of an N-terminal Neck domain and a C-terminal Trp-ring domain "N-Neck: Trp ring-C" (Fig. 1A). The motifs arrangement showed that within the N-terminus of the BDs, an additional Trp ring domain is present and assembled in an "N-Trp ring: Neck: Trp ring-C" triplet arrangement (Fig. 1A). In parallel to Hsf, Hia has a similar N-terminal Trp-ring domain within BD1, whereas it is absent in the BD2. We included these N-terminal Trp-ring domains along with BDs (N-Trp ring: Neck: Trp ring-C) in our study in order to analyze the biological function, that was, Vn binding of these domain triplets. Hence, the domains $BD2^{429-652}$, $BD3^{1103-1338}$, and, $BD1^{1792-2022}$ were expressed and purified (Singh et al., 2014). The alignment of the BDs showed 48.7–54.7% identity and 60.8–61.9% similarity (Fig. S1). The three BDs were modeled against the template 1s7 M and superimposed (Fig. 1B). Importantly, the conserved region of the Neck domains, the peptide sequence N-TKDGISAGNKAITNVAS-C was identified and selected for Ab production (Fig. 1B and Fig. S1).

In addition to BDs, other structural Hsf motifs are organised in a distinguished series that results in three putative domains (PD) without any known biological function, that is, $PD2^{272-375}$, $PD3^{938-1046}$, and $PD1^{1637-1740}$ with 54.1–74.5% identity and 65.8–80.2% sequence similarity, respectively (Fig. S1). The binding domain numbering of Hsf was assigned on the basis of the homology with Hia (Cotter et al., 2005b). Following the previous nomenclature, we named the adjacent PDs with a similar numbering (Fig. 1A). The PDs consist of a KG domain followed by a Trp-ring domain (N-KG: Trp ring-C). A KG domain is also present between amino acids 2063–2112 (Fig. 1A), which has a more variable sequence than the other 3 KG domains.

PDs were aligned for identifying regions with unique amino acids for design of peptides to produce specific Abs that could recognize all three PDs (Fig. S1). The PDs were also modeled against the template (PDB: 3emi) and model structures were superimposed (Fig. 1C). Importantly, the amino acid sequence of the KG domains, N-GLVTAKAVIDAVNKAGWR-C, was conserved, exposed on the surface, and was therefore selected for Ab production. In structural models, highly surface-exposed regions were variable in sequences

of the BD and PD, as compared by aligning the models (Fig. 1B–C and Fig. S1). Therefore, it was almost impossible to select highly surface exposed regions for production of common antibodies that would recognize all three sequences on the fibril at the same time. Hence, we selected the conserved and maximally exposed sequences for designing Abs that would recognize the PDs and BDs in the fibrils (Fig. S1).

The amino acid sequence of the C-terminal membrane anchoring domain and the trimeric coiled coil domain connected to it (2308–2413 aa) completely matched the PDB: 3emo sequence. The PD1, PD2 and PD3 have a high sequence identity with PDB:3emi, whereas the BD1, BD2, and BD3 have high sequence identity with PDB:1s7m. In our models 6 out of 14 Trp-rings predicted by the daTAA server were thus modeled using those templates. The remaining 8 Trp-ring domains present in the Hsf molecule were modelled using templates PDB:1s7m, PDB: 3emi, or PDB: 3d9x, with 15–26% sequence identity, and 30–43% sequence similarity. A domain close to the C-terminal (2144–2315 aa) was constructed from PDB:3laa with low identity, but having a high local similarity. The remaining regions that were not matching with known three-dimensional structures or had low identity/similarity to known templates were constructed as trimeric coiled coils (Griffiths et al., 2011). The trimeric models were first refined with Prime side chain prediction, and strained loops were refined using Prime loop prediction, followed by a constrained Prime energy refinement (imperf minimization). Finally, the 23 domain models were joined to a continuous 0136–2413 aa Hsf-model (Fig. 1A), and the joints were refined with Prime loop prediction and Prime energy refinement. The length of the Hsf-model measured on the symmetry axis was found to be 1675 Å (167.5 nm) from the centroid of the C-alpha of asp136 to the centroid of the C-alpha of gln2371. Nevertheless, this measurement (167.5 nm) did not include the length of 54–135 amino acids of the N-terminal (not modeled) and 2372–2413 amino acids of the C-terminal (membrane anchor). Therefore, we assume that the approximate total length of Hsf (54–2413 amino acids) might reach up to 200 nm.

Partial denaturation suggested a bended and twisted Hsf molecule

We performed TEM to visualise the Hsf molecule on the surface of *H. influenzae* RM804 (Fig. 2A; upper left panel, untreated). At least 50 individual fibrils were measured at the bacterial surface. The mean length of the Hsf^{1-2413} molecule was found to be approximately 100 nm. Theoretically, each Hsf monomer consisted of 2413 amino acids and if monomers trimerize as a straight fibril, the length would be more than 100 nm (Fig. 2A). In support of this, the calculated length of Hsf in our modeled structure was 1675 Å (167.5 nm), *i.e.*, the length of the fibril from Asp136 to Gly2371 (Fig. 1A). The visualized length of the fibre in TEM was less in size than the calculated length of the model. This finding prompted us to in detail investigate this trimeric molecule on the surface of *H. influenzae*. For this purpose, we treated *H. influenzae* RM804 with 0.5–2.5 M guanidine hydrochloride (GuHCl) and visualized the Hsf molecule by using negative staining and TEM. The experiments revealed a stability of the Hsf fibril in up to 1.0 M GuHCl (Fig. 2A). However, bacteria treated with 1.5 M GuHCl showed a partial unwinding of the fibril, whereas the quarternary structure was further open, and more than three fibrils appeared at >2.0 M GuHCl (Fig. 2A). This result clearly indicated that the Hsf molecule at the surface of *H. influenzae* does not consist of three single strands only in the form of a straight fibril.

In parallel, we performed an equilibrium unfolding experiment with recombinant $Hsf^{54-2300}$ in the presence of the denaturing agent GuHCl. Circular dichroism (CD) spectra were recorded in the absence (native protein) and presence of 6 M GuHCl. The large change in signal at 222 nm reflected denaturation of the secondary structure (Fig. 2B). The ellipticity at 222 nm was measured as a function of GuHCl concentration. The data was fitted by equation 1, allowing us to estimate, and presented in Fig. 2C as normalised data (equation 3). C_M, the GuHCl concentration at which 50% of the protein is unfolded is estimated to 2.6 M (Eq. (2)), The denaturation data are in agreement with the TEM data (Fig. 2A). By TEM only folded Hsf is detected up to 1 M GuHCl, which corresponds to the pre-transition baseline (Fig. 2C). To confirm the above observations, we performed embedded sectioning of *H, influenzae* RM804 WT, RM804Δ*hsf*, *E. coli* expressing Hsf, and an *E. coli* control containing an empty vector. Each sample was incubated in PBS or PBS containing 6 M GuHCl, washed twice in PBS and fixed. Bacterial pellets were embedded, and sections were produced in a microtome. Only *H. influenzae* RM804 WT and *E. coli* expressing Hsf showed a layer of Hsf at their surface (Fig. 3A). Interestingly, when RM804 WT and *E. coli* expressing Hsf were treated with 6 M GuHCl for 30 min, the surface proteins appeared as a thick fuzzy layer, approximately with a two-fold increase in thickness in comparison to non-treated bacteria. In contrast, treatment of RM804Δ*hsf* and the *E. coli* control with 6 M GuHCl did not show any Hsf at the surface (Fig. 3B). In the next step, those EM sections were visualized at a higher magnification to observe the fibrils. Hsf was clearly seen at the surface with an approximate length of 100 nm in *H. influenzae* RM804 WT and Hsf-expressing *E. coli* (Fig. 3C). Treatment with 6 M GuHCl revealed an increased fibre length that was more than 100 nm (Fig. 3C, lower panel). Further magnification of the bacterial surface fibrils (*E. coli*-Hsf) showed a clear difference between the length of the fibril in untreated and 6 M GuHCl-treated samples (Fig. 3D). These results thus indicated that Hsf is not a straight fibre. It is bended and two trimeric halves may result in a hairpin-like shape with twisting of each half of the molecule.

Anti-Hsf peptide antibodies are highly specific

Hsf has several repetitive sequence domains as demonstrated by bioinformatics and modeling (Fig. 1A). Some of these sequence motifs in a particular combination serve as functional binding domains. The trimeric organisation of these various domains in a large protein like Hsf (2413 amino acids) has not yet been elucidated or predicted. It was thus interesting to observe how these domains position in the fibril since we suggest that Hsf is a bended and twisted molecule (Fig. 3). The distribution of PDs and BDs were analyzed by using immunogold cryo TEM. Peptide Abs directed against "GLVTAKAVIDAVNKAGWR" (anti-PD Ab), and "TKDGISAGNKAITNVAS" (anti-BD Ab) (Fig. S1), peptide specific anti-$Hsf^{153-164}$, anti-$Hsf^{876-881}$(KTRAAS), and anti-$Hsf^{1912-1942}$ Abs were produced in rabbits. Hsf fragments, BD1–3, PD1–3, Hsf54–608, Hsf608–1351, Hsf1047–1751, Hsf1536–2031, and full length (Hsf54–2300) were tested for Ab cross-reactivity. The anti-$Hsf^{153-164}$ Ab recognized Hsf54–608 and the full length Hsf molecule (Fig. 4A). Blots treated with anti-$Hsf^{153-164}$ + anti-PD Abs recognized all three PDs, but did not react with BDs. Hsf1536–2031 was not recognized by the anti-PD Ab. However, PD1 encompassing amino acids Hsf1637–1740 (*i.e.*, part of the Hsf1536–2031) was easily recognized by anti-PD Abs. This may be due to partial masking of the Ab recognition sequence of Hsf1536–2031 in the blots tested and/or in combination with a low affinity of interaction (Fig. 4A). The anti-$Hsf^{876-881}$Ab crossreacted with Hsf608–1351 and the full-length molecule (Fig. 4B). Incubation of the same blot with anti-$Hsf^{876-881}$ + anti-BD Ab detected all BD domains, and in addition to the other protein fragments. Anti-BD Ab did not cross-react with any of the PD domains (Fig. 4B, Fig. S2). Yet another antibody, anti-$Hsf^{1912-1942}$ Ab detected BD1 (Hsf1536–2031) and full length protein (Fig. 4C). These results suggested that the Abs

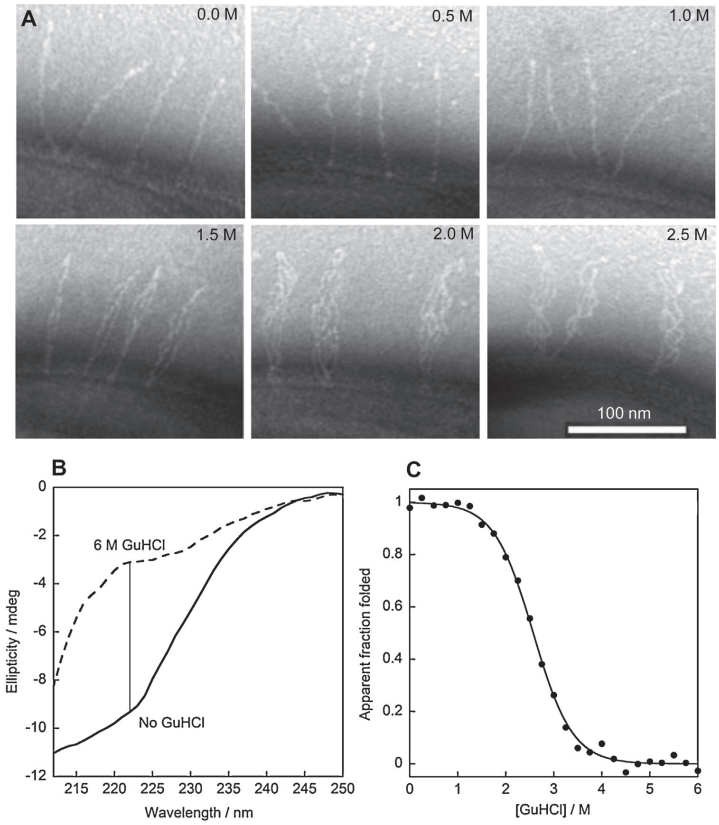

Fig. 2. Hsf is not a straight trimeric autotransporter but a double-folded molecule. (A) *H. influenzae* RM804 expressing Hsf was treated with 0.5 M, 1.0 M, 1.5 M, 2.0 M, and 2.5 M GuHCl as indicated. At high GuHCl concentrations (≥1.5 M) the Hsf molecule opened up and the quarternary structure was abolished. (B) Spectra of folded (no GuHCL) and unfoleded (6 M GuHCl) recombinant Hsf 54–2300 were recorded using CD spectropolarimetry, with the vertical line placed at 222 nm. (C) The normalized ellipticity at 222 nm is plotted against the GuHCl concentration. The solid line shows the fit using equation 1 with the following parameters: $\Delta G^{o}(H_2O) = 16.6$ kJ mol^{-1} and $m = 6.4$ kJ mol^{-2}.

are highly specific for recognizing the corresponding amino acid sequences (Fig. 4D).

Antibody mapping also demonstrated a bending of the Hsf molecule

We used TEM in order to visualize various regions of the Hsf molecules. In the first set of experiments, anti-PD and anti-BD Abs were labeled with 10 nm colloidal gold particles and the other specific Abs were labeled with 5 nm gold particles. Thereafter, *H. influenzae* RM804 WT in parallel with Hsf-expressing *E. coli* were probed with Abs in combination as shown to the left and at the top of Fig. 5A and B. The anti-Hsf$^{153-164}$ Ab recognized the fibril within 10 nm length at the base from the surface. In support of the previous results (Figs. 2A and 3), we here proved that the N-terminal sequence was located close to the base of the fibril, suggesting that the Hsf trimer was a bended molecule. Of notice, the N-terminus in a straight fibril structure should be located at the tip of the fibril (Fig. 1A). As can be seen in Fig. 5A, the anti-Hsf$^{876-881}$ Ab bound to the protein fibril almost near the tip, that is, 80–90 nm from the base. However, probing Hsf with the anti-Hsf$^{1912-1942}$ Ab revealed an interaction at a 35 nm distance from the base of the fibril, and thus verified the C-terminal end near the base (Fig. 5A and B). The relative Ab-binding as revealed by TEM was plotted against the length of the Hsf, and a diagram representing the overall distribution of Abs recognizing the various sequences is shown in Fig. 5C.

To characterize the precise positions of PD and BD domains in the fibril, we probed *H. influenzae* RM804 WT and Hsf-expressing *E. coli* with both anti-PD and anti-BD Abs (10 and 5 nm gold particles, respectively) at a ratio 1:1. The results showed an interaction of the 10 nm gold particles at three distinguished places on the fibril. Similarly, 5 nm gold particles also interacted at three different locations on the fibril (Fig. 6A and B). Several individual fibrils were measured, and the distribution of gold particles in relation to the full length of the fibril was calculated. The results showed that PD2 and BD1 were present at 30–35 nm, BD2 and PD1 at 60–70 nm, and, finally, PD3 and BD2 were located at a 90–95 nm distance from the base of the fibril (Fig. 6C). Taken together, the position of our Abs

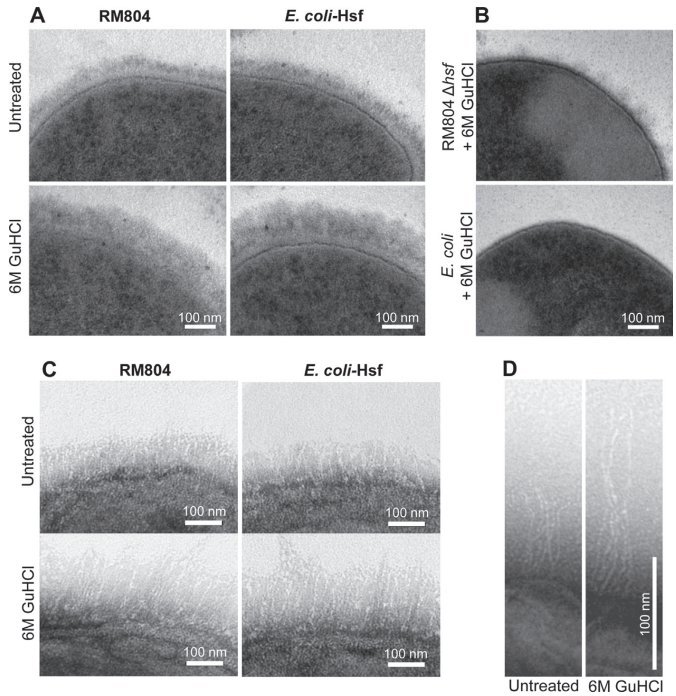

Fig. 3. Unwinding of the Hsf fibril at the bacterial surface by using GuHCl. (A) Hsf appears as a fuzzy layer after GuHCl treatment. *H. influenzae* RM804 WT and *E. coli* expressing Hsf were chosen as untreated, and in another set treated with 6 M GuHCl for 30 min, washed twice in PBS and fixed. Bacterial pellets were embedded in epon and sections were visualised in TEM. (B) Controls including *H. influenzae* RM804Δ*hsf* and *E. coli* containing an empty vector treated with 6 M GuHCl for 30 min. (C) The sections shown in panel A were enlarged in order to observe Hsf at the bacterial surface. (D) *E. coli* expressing Hsf visualized at higher resolution.

suggested approximate parallel distribution of PD and BD on the Hsf molecule, and clearly demonstrated that the fibril is bent back from approximately middle portion of the protein (Fig. 6C).

Discussion

Hsf is an important virulence factor of *H. influenzae* and is present in all encapsulated clinical isolates. Among several known bacterial trimeric autotransporters, Hsf is unique for its structural appearance (Cotter et al., 2005b). It is not a trimeric straight fiber like protein, rather a folded and twisted molecule at the bacterial surface. A prototypical autotransporter such as *Yersinia* adhesin (YadA) and ubiquitous surface proteins (Usp) A1/A2 of *M. catarrhalis* appear as straight "lollipop" like structures consisting of a membrane-anchoring domain, a stalk and finally a head (Nummelin et al., 2004). On the other hand, some of the autotransporters may appear like a fibril, and thus may not be similar to a prototypical TAA (Cotter et al., 2005a). Previously, we noticed a similar double-fold in a large TAA, *i.e., Moraxella catarrhalis* IgD binding protein (MID). In parallel to Hsf, MID is also an extraordinary large protein (Hallström et al., 2008). Interestingly, the Hsf homologue Hia having 70% similarity is present in NTHi, and is only 1000 amino acids in length and not bended and twisted like Hsf (Spahich and St Geme, 2011). Most trimeric autotransporters are straight fibrils regardless of their large sizes. For example, Ishikawa and co-workers reported that the AtaA autotransporter of *Acinetobacter* sp. that is constituted of 3630 amino acids appears like a straight fibril structure (Ishikawa et al., 2014). The BadA protein of *Bartonella henselae* similarly appears as a straight fibril (≈250 nm) that is composed of 3082 amino acids (Muller et al., 2011).

Interestingly, the straight structure of some of the TAAs is dynamically modified once they bind to the host ligands. For example, UspA1 showed a bending after binding to CAECAM-1 and fibronectin (Agnew et al., 2011). Similarly, the *E. coli* autotransporter EibD also bends from a saddle-like structure after binding to its ligand IgG (Leo et al., 2011). This kind of bending has only been observed after interaction with host ligands. On the other hand, the biological significance of bending and twisting of the bacterial autotransporters such as MID and Hsf is currently not understood. The folding might, however, have certain benefits. Firstly, the large Hsf-like fibril (≈200 nM in length) may be very fragile that might easily shear. The winding of two trimeric halves of the fibrils make it stiffer and provide mechanical strength to the fiber. It will be more stable during bacterial mobility and host interaction. Secondly, the trimeric structure of the fibril constitutes functional domains. The double intertwining of the trimeric fibre might generate new intramolecular interactions that may lead to the formation of several new functional domains around the fibril. In Hsf, the core of the repetitive domains is conserved, whereas the surface-exposed regions of these domains are variable as explained in our model (Fig. 1B and C). Thus the conserved core provides a structural stability to the Hsf molecule, while variable surface exposed regions might contribute to different biological functions.

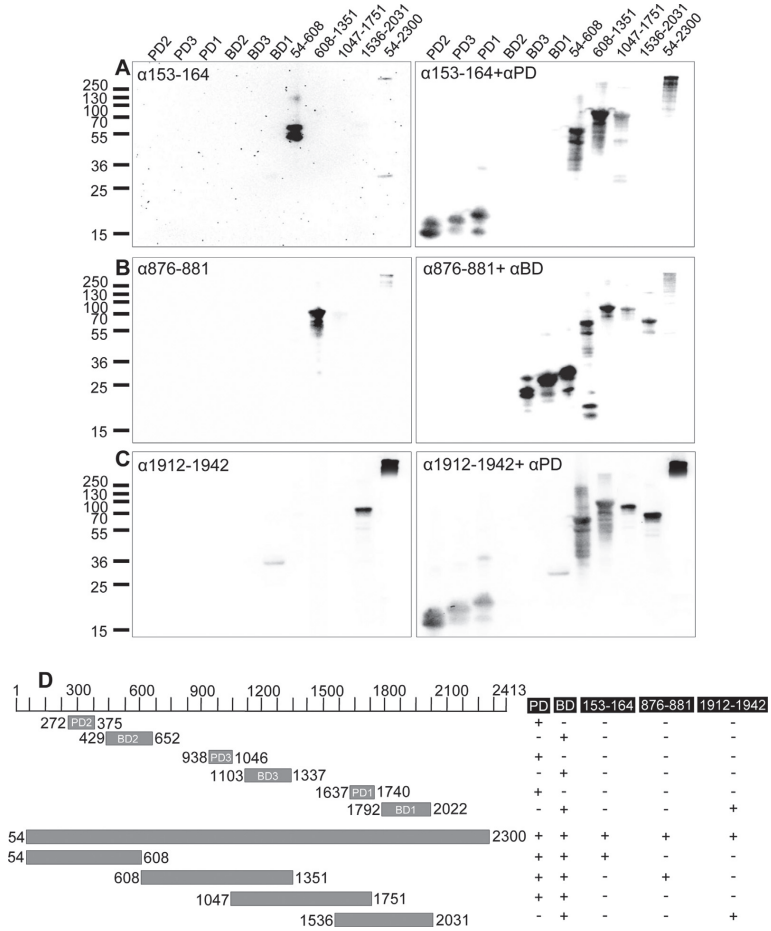

Fig. 4. Quality control of antibodies used in the present study. (A) Western blot that demonstrates the specificity of anti-Hsf$^{153-164}$ pAb (left panel), and cross reactivity of anti-PD antibodies (right panel). The anti-Hsf$^{153-164}$ pAb was added simultaneously with the anti-PD pAb as shown in the right panel. (B) Blots probed with anti-Hsf$^{876-881}$ (left), anti-Hsf$^{876-881}$ and anti-BD pAbs in right. (C) Blots incubated with anti-Hsf$^{876-881}$ (left), anti-Hsf$^{1912-1942}$ and anti-PD pAbs in right. (D) Summary of the results obtained from panels (A–C).

We modeled 136–2413 amino acids of Hsf by using different suitable templates and then finally joined all models together to build the whole fibril (Fig. 1A). The total length of the model was measured from the centroid of the C-alpha of Asp136 to the centroid of the C-alpha of Gln2371 that accounted for 1675 Å (167.5 nm). In this model some important issues have been considered during the comparison of model length with the estimated length in TEM. The Hsf 2372–2413 region is present inside the outer membrane, hence it will not contribute to the visual length at the surface of bacteria during analysis in TEM. Importantly, these membrane-spanning amino acids are not included in the 1675 Å length. In Hsf, the 55–135 aa do not have any suitable crystal structure to be used as a template. Therefore, the 54–135 aa were not included in the model, and these amino acids will definitely contribute to the length of the fibril. In this model, however, only partial structures that have very poor template similarity were modeled as a coiled-coil as described elsewhere (Griffiths et al., 2011). The axial rise for an alpha-helical coiled coil is 1.5 Å per amino acid. The 3emi template (similar to PDs) was found to have an axial rise per amino acid of 0.55 Å. This indicates that Hsf aa 136–2371 is longer than 123 nm even if it is modeled by 3emi template, and less than 335 nm, also if those regions are put as a coiled coil shape. Thus, the approximate visual length of Hsf under natural conditions as revealed by TEM was ≈100 nm, and after complete denaturation this might have a length of ≈200 nm. The modeled Hsf (136–2371 aa) structure is 167 nm that is matching with the length of protein observed in TEM.

Our TEM data showed that bending only does not take place in the Hsf fibre. For instance, in some of the TAAs, interaction of ligands causes a bend in the trimer (Agnew et al., 2011; Leo et al.,

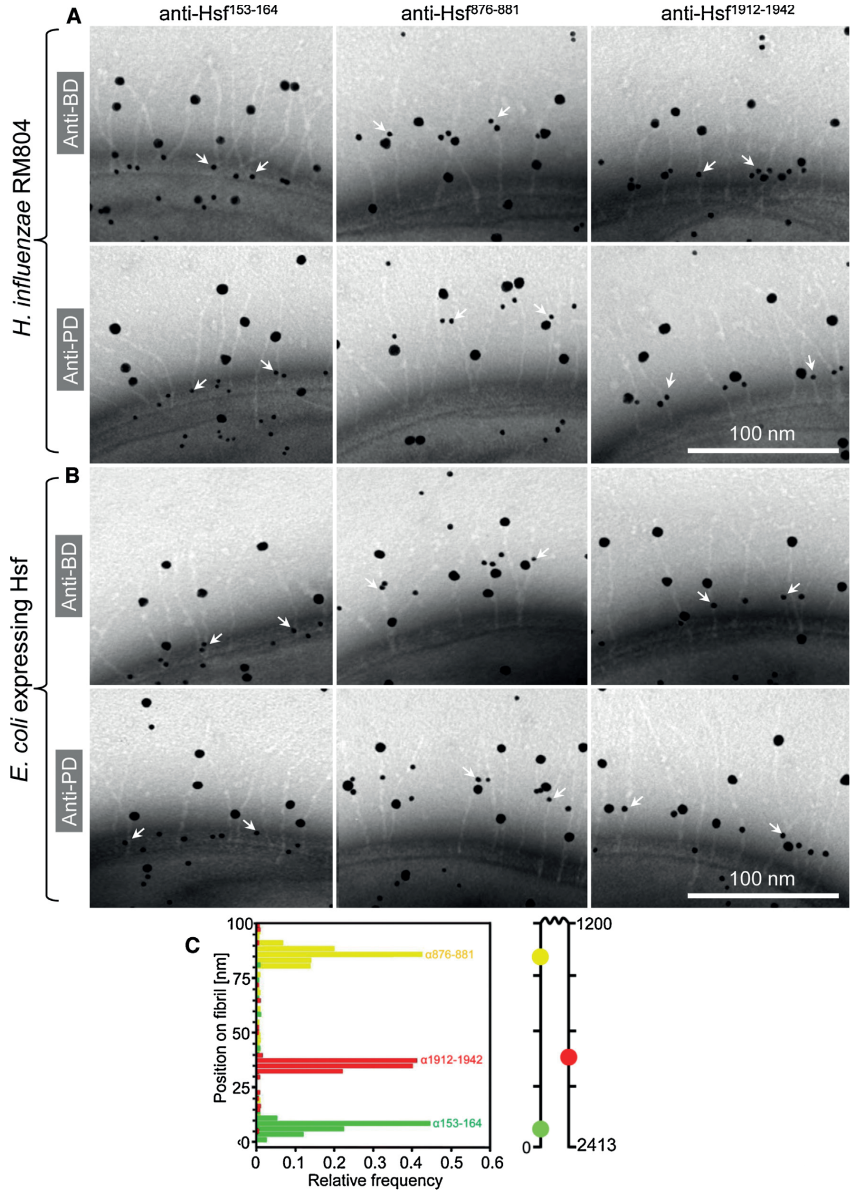

Fig. 5. Mapping of specific amino acid regions of the full length Hsf molecule by anti-BD and anti-PD Abs. (A) The anti-BD and anti-PD pAbs were labelled with gold particles having a size of 10 nm. The other specific pAbs shown at the top of the panels were labelled with 5 nm gold particles. Anti-BD or anti-PD pAb (10 nm) were used to probe *H. influenzae* RM804 with a combination of specific Abs (5 nm). (B) In parallel, a similar strategy as in (A) was used to probe *E. coli* expressing Hsf at its surface. The specificity of the anti-PD and anti-BD pAbs is shown in Fig. S2. (C) The relative frequency of gold particles bound by specific pAbs directed against several fibrils (A and B) were plotted against the length of fibrils. Distribution of specific Abs is schematically presented in a cartoon to the right.

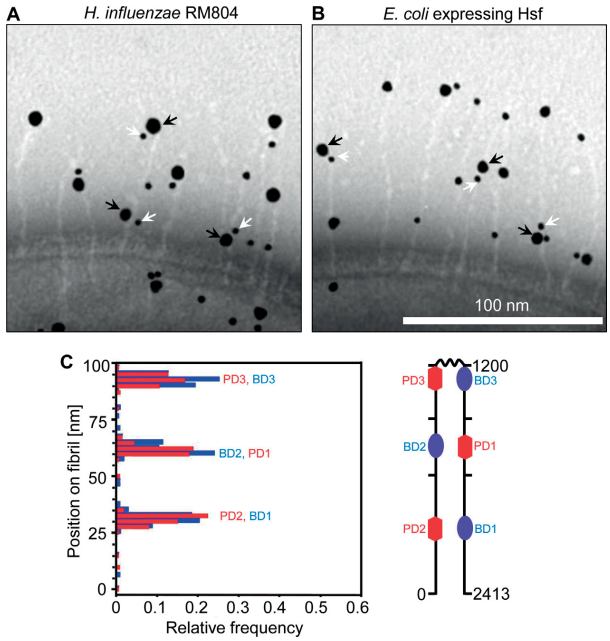

Fig. 6. Hsf PD and BD are parallelly distributed in the double-folded Hsf. (A) The anti-BD and anti-PD pAbs were labeled with 10 nm and 5 nM gold particles, respectively. *H. influenzae* RM804 was probed at a ratio of 1:1. (B) *E. coli* expressing Hsf was also probed with anti-BD (10 nm) and anti-PD (5 nm) pAbs. (C) The distance of the small and large gold particles in several fibrils was measured and their relative frequency was plotted against the length of the fibril. To the right, a cartoon delineates the positions of sequences detected by Abs.

2011). Unlike those proteins, the Hsf fibril is twisted after bending and the bended region may have loose or tight interactions with the first half part of the fibre. Twisting of two trimers is evident from our experiments with bacteria incubated in the presence of GuHCl, and here unwinding of two trimers was observed at high concentrations of GuHCl (Figs. 2 and 3). This intertwining between two halves of the same trimers may thus generate a much more complicated structure.

In the present paper we used protein unfolding and TEM to demonstrate that Hsf is a twisted "hairpin-like" trimeric autotransporter. Our study provides new knowledge on the structural arrangement of the Hsf molecule at the bacterial surface. It will be a challenge to prove the biological significance of this particular folding, and it also remains to study the ultrastructure of this interesting protein to present a full crystal structure model.

Acknowledgements

Potential conflicts of interest: none reported. Financial support: This work was supported by grants from Foundations of Alfred Österlund, Anna and Edwin Berger, Greta and Johan Kock, Åke Wiberg, Torsten Söderberg, Lars Hierta Foundation, O. E. och Edla Johansson, Kungliga Fysiografiska Sällskapet, as well as the Swedish Medical Research Council (grant number 521-2010-4221 and K2012-66X-14928-09-5, www.vr.se), the Cancer Foundation at the University Hospital in Malmö, the Physiographical Society (Forssman's Foundation), nanometer structure consortium at Lund University, and Skåne County Council's Research and Development Foundation.

Appendix A. Supplementary data

Supplementary material related to this article can be found, in the online version, at http://dx.doi.org/10.1016/j.ijmm.2014.10.004.

References

Agnew, C., Borodina, E., Zaccai, N.R., Conners, R., Burton, N.M., Vicary, J.A., Cole, D.K., Antognozzi, M., Virji, M., Brady, R.L., 2011. Correlation of in situ mechanosensitive responses of the *Moraxella catarrhalis* adhesin UspA1 with fibronectin and receptor CEACAM1 binding. Proc. Natl. Acad. Sci. U.S.A. 108, 15174–15178.

Agrawal, A., Murphy, T.F., 2011. *Haemophilus influenzae* infections in the H. influenzae type b conjugate vaccine era. J. Clin. Microbiol. 49, 3728–3732.

Bengtson, S.H., Eddleston, J., Morgelin, M., Zuraw, B.L., Herwald, H., 2008. Regulation of kinin B(2) receptors by bradykinin in human lung cells. Biol. Chem. 389, 1435–1440.

Carlemalm, E., 1990. Lowicryl resins in microbiology. J. Struct. Biol. 104, 189–191.

Cotter, S.E., Surana, N.K., St Geme III, J.W., 2005a. Trimeric autotransporters: a distinct subfamily of autotransporter proteins. Trends Microbiol. 13, 199–205.

Cotter, S.E., Yeo, H.J., Juehne, T., St Geme III, J.W., 2005b. Architecture and adhesive activity of the *Haemophilus influenzae* Hsf adhesin. J. Bacteriol. 187, 4656–4664.

Danovaro-Holliday, M.C., Garcia, S., de Quadros, C., Tambini, G., Andrus, J.K., 2008. Progress in vaccination against *Haemophilus influenzae* type b in the Americas. PLoS Med. 5, e87.

Dautin, N., Barnard, T.J., Anderson, D.E., Bernstein, H.D., 2007. Cleavage of a bacterial autotransporter by an evolutionarily convergent autocatalytic mechanism. EMBO J. 26, 1942–1952.

Dautin, N., Bernstein, H.D., 2007. Protein secretion in gram-negative bacteria via the autotransporter pathway. Annu. Rev. Microbiol. 61, 89–112.

Fitzwater, S.P., Watt, J.P., Levine, O.S., Santosham, M., 2010. *Haemophilus influenzae* type b conjugate vaccines: considerations for vaccination schedules and implications for developing countries. Hum. Vaccin 6, 810–818.

Geme III, J.W., 1996. Molecular determinants of the interaction between *Haemophilus influenzae* and human cells. Am. J. Respir. Crit. Care Med. 154, S192–S196.

Geme III, J.W., Cutter, D., 1995. Evidence that surface fibrils expressed by *Haemophilus influenzae* type b promote attachment to human epithelial cells. Mol. Microbiol. 15, 77–85.

Griffiths, N.J., Hill, D.J., Borodina, E., Sessions, R.B., Devos, N.I., Feron, C.M., Poolman, J.T., Virji, M., 2011. Meningococcal surface fibril (Msf) binds to activated vitronectin and inhibits the terminal complement pathway to increase serum resistance. Mol. Microbiol. 82, 1129–1149.

Hallström, T., Muller, S.A., Morgelin, M., Mollenkvist, A., Forsgren, A., Riesbeck, K., 2008. The *Moraxella* IgD-binding protein MID/Hag is an oligomeric autotransporter. Microb. Infect. 10, 374–381.

Hallström, T., Riesbeck, K., 2010. *Haemophilus influenzae* and the complement system. Trends Microbiol. 18, 258–265.

Hallström, T., Trajkovska, E., Forsgren, A., Riesbeck, K., 2006. *Haemophilus influenzae* surface fibrils contribute to serum resistance by interacting with vitronectin. J. Immunol. 177, 430–436.

Hallström, T., Singh, B., Resman, F., Blom, A.M., Mörgelin, M., Riesbeck, K., 2011. *Haemophilus influenzae* protein E binds to the extracellular matrix by concurrently interacting with laminin and vitronectin. J. Infect. Dis. 204 (7), 1065–1074.

Hartmann, M.D., Grin, I., Dunin-Horkawicz, S., Deiss, S., Linke, D., Lupas, A.N., Hernandez Alvarez, B., 2012. Complete fiber structures of complex trimeric autotransporter adhesins conserved in enterobacteria. Proc. Natl. Acad. Sci. U.S.A. 109, 20907–20912.

Ishikawa, M., Shigemori, K., Hori, K., 2014. Application of the adhesive bacterionanofiber AtaA to a novel microbial immobilization method for the production of indigo as a model chemical. Biotechnol. Bioeng. 111, 16–24.

Leo, J.C., Grin, I., Linke, D., 2012. Type V secretion: mechanism(s) of autotransport through the bacterial outer membrane. Philos. Trans. R. Soc. London, Ser. B: Biol. Sci. 367, 1088–1101.

Leo, J.C., Lyskowski, A., Hattula, K., Hartmann, M.D., Schwarz, H., Butcher, S.J., Linke, D., Lupas, A.N., Goldman, A., 2011. The structure of *E. coli* IgG-binding protein D suggests a general model for bending and binding in trimeric autotransporter adhesins. Structure 19, 1021–1030.

Meng, G., Spahich, N., Kenjale, R., Waksman, G., St Geme III, J.W., 2011. Crystal structure of the *Haemophilus influenzae* Hap adhesin reveals an intercellular oligomerization mechanism for bacterial aggregation. EMBO J. 30, 3864–3874.

Morris, S.K., Moss, W.J., Halsey, N., 2008. *Haemophilus influenzae* type b conjugate vaccine use and effectiveness. Lancet Infect. Dis. 8, 435–443.

Muller, N.F., Kaiser, P.O., Linke, D., Schwarz, H., Riess, T., Schafer, A., Eble, J.A., Kempf, V.A., 2011. Trimeric autotransporter adhesin-dependent adherence of *Bartonella henselae*. Bartonella quintana, and Yersinia enterocolitica to matrix components and endothelial cells under static and dynamic flow conditions. Infect. Immun. 79, 2544–2553.

Nummelin, H., Merckel, M.C., Leo, J.C., Lankinen, H., Skurnik, M., Goldman, A., 2004. The *Yersinia adhesin* YadA collagen-binding domain structure is a novel left-handed parallel beta-roll. EMBO J. 23, 701–711.

Oehmcke, S., Morgelin, M., Herwald, H., 2009. Activation of the human contact system on neutrophil extracellular traps. J. Innate. Immun. 1, 225–230.

Pettersen, E.F., Goddard, T.D., Huang, C.C., Couch, G.S., Greenblatt, D.M., Meng, E.C., Ferrin, T.E., 2004. UCSF Chimera—a visualization system for exploratory research and analysis. J. Comput. Chem. 25, 1605–1612.

Rodriguez, C.A., Avadhanula, V., Buscher, A., Smith, A.L., St Geme III, J.W., Adderson, E.E., 2003. Prevalence and distribution of adhesins in invasive non-type b encapsulated *Haemophilus influenzae*. Infect. Immun. 71, 1635–1642.

Roth, J., 1996. The silver anniversary of gold: 25 years of the colloidal gold marker system for immunocytochemistry and histochemistry. Histochem. Cell Biol. 106, 1–8.

Singh, B., Al-Jubair, T., Morgelin, M., Thunnissen, M.M., Riesbeck, K., 2013. The unique structure of *Haemophilus influenzae* protein E reveals multiple binding sites for host factors. Infect. Immun. 81, 801–814.

Singh, B., Su, Y.C., Riesbeck, K., 2010. Vitronectin in bacterial pathogenesis: a host protein used in complement escape and cellular invasion. Mol. Microbiol. 78, 545–560.

Singh, B., Fleury, C., Jalalvand, F., Riesbeck, K., 2012. Human pathogens utilize host extracellular matrix proteins laminin and collagen for adhesion and invasion of the host. FEMS Microbiol. Rev. 36, 1122–1180.

Singh, B., Rohm, K.H., 2008. Characterization of a *Pseudomonas putida* ABC transporter (AatJMQP) required for acidic amino acid uptake: biochemical properties and regulation by the Aau two-component system. Microbiology 154, 797–809.

Singh, B., Su, Y.C., Al-Jubair, T., Mukherjee, O., Hallstrom, T., Morgelin, M., Blom, A.M., Riesbeck, K., 2014. A fine-tuned interaction between the trimeric autotransporter *Haemophilus* surface fibrils and vitronectin leads to serum resistance and adherence to respiratory epithelial cells. Infect. Immun. 82, 2378–2389.

Spahich, N.A., St Geme III, J.W., 2011. Structure and function of the *Haemophilus influenzae* autotransporters. Front. Cell Infect. Microbiol. 1, 5.

St Geme III, J.W., Cutter, D., Barenkamp, S.J., 1996. Characterization of the genetic locus encoding *Haemophilus influenzae* type b surface fibrils. J. Bacteriol. 178, 6281–6287.

St Geme III, J.W., Kumar, V.V., Cutter, D., Barenkamp, S.J., 1998. Prevalence and distribution of the hmw and hia genes and the HMW and Hia adhesins among genetically diverse strains of nontypeable *Haemophilus influenzae*. Infect. Immun. 66, 364–368.

Ulanova, M., Tsang, R.S., 2009. Invasive *Haemophilus influenzae* disease: changing epidemiology and host-parasite interactions in the 21st century. Infect. Genet. Evol. 9, 594–605.

Watson Jr., M.E., Nelson, K.L., Nguyen, V., Burnham, C.A., Clarridge, J.E., Qin, X., Smith, A.L., 2013. Adhesin genes and serum resistance in *Haemophilus influenzae* type f isolates. J. Med. Microbiol. 62, 514–524.

Winkelstein, J.A., Moxon, E.R., 1992. The role of complement in the host's defense against *Haemophilus influenzae*. J. Infect. Dis. 165 (Suppl. 1), S62–S65.

Fig. S1, Singh *et al.*

Fig S1 Alignment of Hsf PD and BD protein sequences and identification of conserved sequences for design of peptides (black background) that were used for immunization of rabbits.

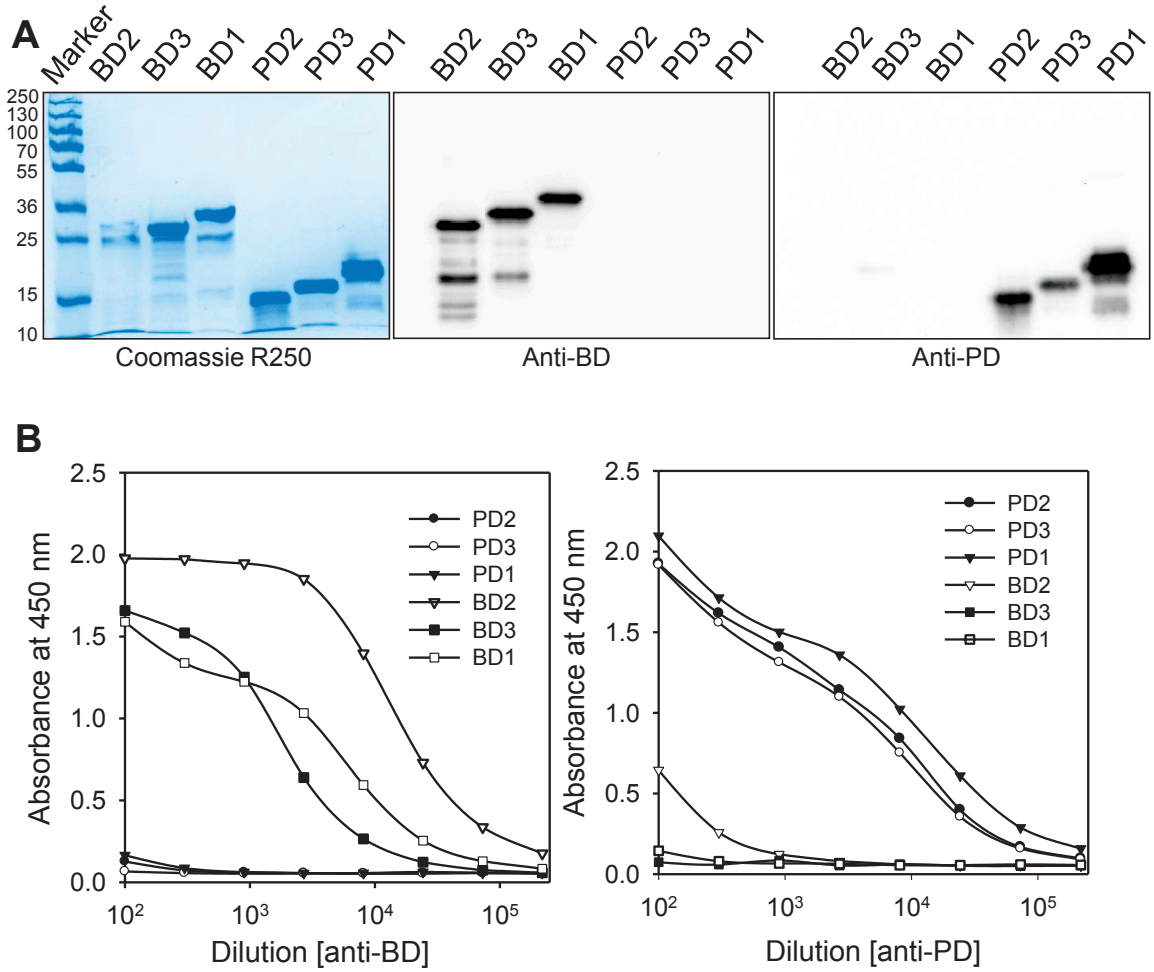

Fig S2 Specificity of anti-BD and anti-PD Abs. *A*. Left panel shows purified recombinant BD and PD proteins. Proteins (5 μg) were separated in a 12% SDS-PAGE and stained with Coomassie blue R250. Middle and right panels indicate blots probed with anti-BD and anti-PD Abs, respectively. Fifty ng of each protein was loaded on gels. *B*. ELISA that demonstrates the specificity of anti-BD and anti-PD Abs. All recombinant proteins (50 nM) were coated on ELISA plates and different dilutions of Abs were used.

Paper VI

Haemophilus influenzae Type f Hijacks Vitronectin Using Protein H To Resist Host Innate Immunity and Adhere to Pulmonary Epithelial Cells

Tamim Al-Jubair,* Oindrilla Mukherjee,* Sharon Oosterhuis,* Birendra Singh,* Yu-Ching Su,* Christophe Fleury,* Anna M. Blom,† Susanna Törnroth-Horsefield,‡ and Kristian Riesbeck*

The incidence of invasive *Haemophilus influenzae* type b (Hib) disease has significantly decreased since the introduction of an efficient vaccine against Hib. However, in contrast to Hib, infections caused by *H. influenzae* serotype f (Hif) are emerging. We recently did a whole genome sequencing of an invasive Hif isolate, and reported that Hif interacts with factor H by expressing protein H (PH). In this study, upon screening with various human complement regulators, we revealed that PH is also a receptor for vitronectin (Vn), an abundant plasma protein that regulates the terminal pathway of the human complement system in addition to being a component of the extracellular matrix. Bacterial Vn binding was significantly reduced when the *lph* gene encoding PH was deleted in an invasive Hif isolate. The dissociation constant (K_D) of the interaction between recombinant PH and Vn was 2.2 μM, as revealed by Biolayer interferometry. We found that PH has different regions for simultaneous interaction with both Vn and factor H, and that it recognized the C-terminal part of Vn (aa 352–362). Importantly, PH-dependent Vn binding resulted in better survival of the wild-type Hif or PH-expressing *Escherichia coli* when exposed to human serum. Finally, we observed that PH mediated an increased bacterial adherence to alveolar epithelial cells in the presence of Vn. In conclusion, our study reveals that PH most likely plays an important role in Hif pathogenesis by increasing serum resistance and adhesion to the airways. *The Journal of Immunology*, 2015, 195: 5688–5695.

Haemophilus influenzae is a Gram-negative bacterial species classified as typeable (encapsulated) or nontypeable *H. influenzae* (NTHi) based upon the presence or absence of a polysaccharide capsule. Typeable isolates are further subdivided into six serotypes designated a–f, depending on the capsular polysaccharide composition and antigenicity. *H. influenzae* type b (Hib) has been the most significant serotype causing invasive disease, for example, meningitis, epiglottitis, septicaemia, and osteomyelitis (1–3). Since the introduction of a vaccine against Hib, the incidence of invasive Hib disease has significantly decreased. In contrast, the number of cases with invasive disease caused by non-Hib, that is, NTHi and *H. influenzae* serotype f (Hif), seems to increase, suggesting a serotype replacement phenomenon (4–6).

The successful colonization and subsequent infection of *H. influenzae* depend on its ability to adhere to the host tissue promoted by adhesins at the bacterial surface. After these initial steps, bacteria occasionally disrupt the epithelium and penetrate into deeper tissue layers after passing through the basement membrane and extracellular matrix (ECM) (7, 8). Encapsulated *H. influenzae* may also breach the blood-brain barrier and cause meningitis (9, 10).

Upon contact with the host, bacteria encounter the complement system, the first line of defense and an important component of the innate immunity. Importantly, many bacterial species acquire complement regulatory factors, including factor H (FH), C4b-binding protein (C4BP), or vitronectin (Vn), on their surface for effective inhibition of phagocytosis and formation of the membrane attack complex (MAC) (11–13). The complement regulator Vn is an abundant plasma protein at a concentration of 250–450 μg/ml, which corresponds to 3–6 μM (14), but also builds up the ECM. It efficiently inhibits the terminal pathway of the complement system by preventing MAC formation at the bacterial surface (12, 15). Recent studies indicate that the interaction between *H. influenzae* surface proteins and Vn results in an inhibition of the bactericidal effect of serum, thus increased survival. We reported recently that protein E (PE) and protein F (PF) of NTHi (16, 17) and *Haemophilus* surface fibrils of Hib (9) all have the capacity to recruit Vn to the bacterial surface. PE and PF are ubiquitously expressed multifunctional proteins found in both capsulated and noncapsulated *H. influenzae* (18) (Y.-C. Su, personal communication). Importantly, the Vn-binding proteins also function as adhesins for *H. influenzae* mediating bacterial adherence to several

*Clinical Microbiology, Department of Translational Medicine, Lund University, SE-205 02 Malmö, Sweden; †Protein Chemistry, Department of Translational Medicine, Lund University, SE-205 02 Malmö, Sweden; and ‡Department of Biochemistry and Structural Biology, Lund University, SE-221 00 Lund, Sweden

ORCIDs: 0000-0001-6954-5293 (T.A.-J.); 0000-0002-3531-091X (S.O.); 0000-0002-7246-1442 (B.S.); 0000-0003-3398-6294 (Y.-C.S.); 0000-0002-1348-1734 (A.M.B.); 0000-0002-9435-8243 (S.T.-H.).

Received for publication May 27, 2015. Accepted for publication October 6, 2015.

This work was supported by grants from the Alfred Österlund Foundation, the Anna and Edwin Berger Foundation, and the Greta and Johan Kock Foundation; the Swedish Medical Research Council (Grant K2015-57X-03163-43-4, http://www.vr.se); the Physiographical Society (Forssman's Foundation); and the Skåne County Council's Research and Development Foundation.

Address correspondence and reprint requests to Prof. Kristian Riesbeck, Clinical Microbiology, Department of Translational Medicine, Lund University, Jan Waldenströms Gata 59, SE-205 02 Malmö, Sweden. E-mail address: kristian.riesbeck@med.lu.se

The online version of this article contains supplemental material.

Abbreviations used in this article: C4BP, C4b-binding protein; ECM, extracellular matrix; FH, factor H; HBD, heparin-binding domain; Hib, *Haemophilus influenzae* type b; Hif, *Haemophilus influenzae* serotype f; LB, Luria–Bertani; MAC, membrane attack complex; NHS, normal human serum; NTHi, nontypeable *Haemophilus influenzae*; pAb, polyclonal Ab; PE, protein E; PF, protein F; PH, protein H; VDS, Vn-depleted human serum; Vn, vitronectin.

www.jimmunol.org/cgi/doi/10.4049/jimmunol.1501197

human pulmonary cell lines (17–20). In fact, *Haemophilus* surface fibrils also contribute to an increased bacterial binding to integrins by utilizing Vn as a bridging molecule (9).

We have recently defined a unique 35-kDa FH-binding protein designated protein H (PH), which is expressed mainly in Hib and Hif (21). The goal of this study was to further examine the role of Hif PH in interactions with the human host. We found that PH has a strong affinity for Vn that significantly contributes to an increased survival of Hif against complement-mediated killing and also increased adhesion to type II alveolar epithelial cells.

Materials and Methods

Bacteria, eukaryotic cells, and culture conditions

The *H. influenzae* type f strain Hif M10 and its isogenic *lph* mutant Hif M10Δ*lph* (21) were grown in liquid brain heart infusion medium containing 10 μg ml^{-1} NAD and hemin, or on chocolate agar plates, followed by incubation at 37°C in a humid atmosphere with 5% CO_2. The *lph* mutant was grown in the presence of 10 μg ml^{-1} kanamycin. *Escherichia coli* DH5α and BL21 (DE3) were cultured in Luria-Bertani (LB) broth or on LB agar plates at 37°C. *E. coli* containing pET26b-*lph* or pET16b-*lph* expression vectors was grown in LB medium supplemented with 50 μg ml^{-1} kanamycin or 100 μg ml^{-1} ampicillin, respectively. Vn-expressing human embryo kidney (HEK293T) cells were cultured in advanced DMEM (Life Technologies, Invitrogen, Stockholm, Sweden) containing 2 mM L-glutamine, 100 μg ml^{-1} streptomycin, and 100 U ml^{-1} penicillin.

Expression and purification of recombinant proteins

Cloning procedures were as described in detail previously (21). Briefly, the gene encoding the FH-binding protein (*lph*) in Hif was amplified by PCR excluding the 63 initial nucleotides encoding for the signal peptide. The genes were cloned into pET26b and pET16b vectors for recombinant protein purification and surface expression on *E. coli* BL21, respectively. Expression was induced by the addition of 0.2 mM isopropyl-β-D-1-thiogalactopyranoside at an OD at 600 nm (OD_{600}) of 0.5, and cultures were grown for the next 16 h at 37°C with shaking at 200 rpm. Expression levels were verified by flow cytometry using specific anti-PH polyclonal Ab (pAb) (21) before downstream experiments. For purification purposes, *E. coli* BL21 (DE3) containing pET26b-*lph* was grown in LB medium with kanamycin at 37°C until OD_{600} reached 0.8 to 1. Expression of the proteins was induced by the addition of 1 mM isopropyl-β-D-1-thiogalactopyranoside. After 3 h of culture, cells were harvested and resuspended in a His-tag protein-binding buffer (50 mM Tris-HCl [pH 7.5] containing 50 mM imidazole and 500 mM NaCl). Bacteria were lysed by sonication, and Ni-nitrilotriacetic acid affinity purification was performed, according to the manufacturer's guidelines (GE Healthcare Biosciences, Uppsala, Sweden). After elution, proteins were dialyzed against PBS (pH 7.5). The protein samples were concentrated by a Centricon concentrator (m.w. cutoff 5000) and loaded onto SDS-PAGE gels that were stained with Coomassie blue R-250. Vn constructs were expressed in HEK293T cells, as described elsewhere (15). Protein concentrations were estimated by a NanoDrop spectrophotometer (Thermo Scientific, Wilmington, DE) and were also verified by a bicinchoninic acid assay (Pierce, Rockford, IL).

Flow cytometry

PH expression at the bacterial surface was detected by flow cytometry. Hif from midlog phase cultures or PH-expressing *E. coli* BL21 (DE3) transformants induced overnight were resuspended in PBS containing 1% BSA (blocking buffer) and adjusted to 10^9 CFU ml^{-1}. Aliquots containing 5×10^6 CFU were incubated with affinity-purified rabbit anti-PH pAb for 1 h at room temperature, washed, and centrifuged. Thereafter, bacterial suspensions were incubated with FITC-conjugated swine anti-rabbit pAb (Dako, Copenhagen, Denmark) for 30 min. For ligand binding at the bacterial surface, Hif and *E. coli* BL21 (DE3) expressing PH were incubated with 250 nM Vn for 1 h at room temperature. *E. coli* harboring empty vector was used as a control and stained similarly. After washing, bound ligands were detected using sheep anti-human Vn pAb (dilution 1:100), followed by FITC-conjugated donkey anti-sheep pAb (dilution 1:100) (both from AbD Serotec,

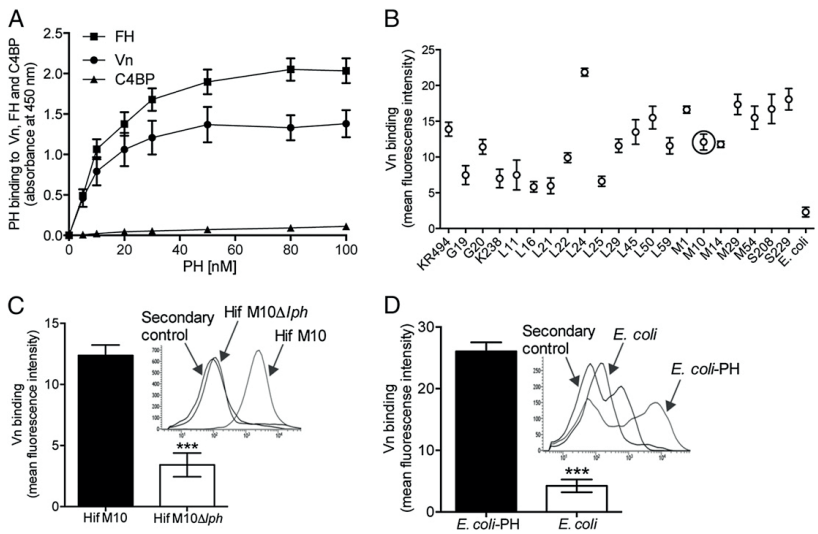

FIGURE 1. *H. influenzae* serotype f binds Vn via surface expression of PH. (**A**) PH interacts with Vn and FH in a dose-dependent manner. Microtiter plates were coated with equal molar (50 nM) of Vn, FH, and C4BP and incubated with increasing concentrations (5–100 nM) of purified His-tag PH. Bound PH was detected by HRP-conjugated anti-His pAb. PH only bound to FH and Vn, but not to C4BP. (**B**) Vn binding in clinical isolates of *H. influenzae* type f as analyzed by flow cytometry. Equal numbers of bacteria (5×10^6 CFU) of each isolate were incubated with 250 nM plasma Vn, and bound ligand was detected with sheep anti-Vn pAb and FITC-conjugated donkey anti-sheep pAb. Data are presented as the mean fluorescence intensity (mfi) after subtracting the background. *E. coli* was used as a negative control. Circled data indicates mfi of the strain M10 used in current study. (**C** and **D**) Vn binding by Hif M10 (C) and *E. coli* expressing PH (D) as analyzed by flow cytometry. Small insert in each panel shows a representative flow cytometry histogram of bacteria binding to 250 nM Vn. (C) Hif M10Δ*lph* lacking the protein H exhibited reduced Vn binding compared with the wild type. (D) *E. coli* expressing PH revealed a Vn-binding phenotype. In contrast, control *E. coli* transformed with the empty vector pET-16b bound less Vn. Mean values of three separate experiments with triplicates are shown, and error bars indicate SDs. In (C) and (D), differences in Vn binding between Hif wild type and mutant or *E. coli*-PH and control *E. coli* were calculated by Student *t* test. $***p \leq 0.001$.

Oxford, U.K.). All bacterial samples were incubated in PBS-BSA, and primary and secondary Abs were added separately as negative controls. Bacteria were washed with PBS-BSA before analysis on a FACS Canto (BD Biosciences, Franklin Lakes, NJ) using the software Diva 6.1.1.

ELISA

Interactions between PH and Vn, FH, or C4BP were analyzed by ELISA. Ligands, recombinant purified PH, or other bacterial proteins PE (20, 22) and UHP_09011 (17) (50 nM) were immobilized overnight on Polysorb microtitre plates (Nunc-Immuno; Nunc, Roskilde, Denmark) in Tris-HCl (pH 9.0) for 15 h at 4°C. After washing, His-tagged PH or Vn fragments as outlined in Fig. 3A were added to each well at the indicated concentrations, followed by incubation for 1 h at room temperature. Thereafter, bound recombinant Vn and PH were detected by HRP-conjugated anti-His tag pAb (Abcam, Cambridge, UK). In a multiligand simultaneous binding assay, PH-coated wells were incubated for 1 h with 15 nM ligand (Vn or FH) in addition to different concentrations of FH or Vn (2.5–50 nM), respectively. In the inhibition assay with heparin, an equal molar concentration of Vn (20 nM) was preincubated with increasing concentrations of heparin (0.05–0.2 μM) or type B bovine skin gelatin (Sigma-Aldrich, St. Louis, MO), and then the mixtures were added to the PH-coated wells. Unbound ligands (Vn or FH) were removed by washing with PBS containing 0.05% Tween 20. Thereafter, bound Vn and FH were detected by primary sheep anti-human Vn pAb or mouse anti-human FH mAb, followed by HRP-conjugated donkey anti-sheep and rabbit anti-mouse secondary pAbs (all were obtained from AbD Serotec). ELISAs were developed with 20 mM tetramethylbenzidine and 0.1 M potassium citrate. Finally, the reactions were stopped with 1 M H_2SO_4. Signals were read at OD_{450}. All experiments were performed three times in triplicates.

Affinity measurements of the PH–Vn interaction

Kinetic analyses were performed by Biolayer interferometry using a forteBio OctetRed96 platform (Pall, Menlo Park, CA). Recombinant $Vn^{80–396}$ was immobilized on AR2G sensors (Pall) by amino coupling. The analyte (recombinant PH) was serially diluted in running buffer (PBS) ranging from 0 to 4 μM. The experiments were conducted at 30°C. Data analysis was performed using the forteBio Data Analysis software 8.1 (Pall). Curves were fitted with 1:1 binding kinetics, and affinity (K_D) was calculated.

Serum bactericidal assay

Normal human serum (NHS) and Vn-depleted serum (VDS) were prepared, as previously described (16). The NHS used in the current study was reactive against Hif, as revealed by Western blotting (data not shown). VDS was replenished with new Vn, as described previously (17). In parallel, heat-inactivated serum was prepared by inactivation at 56°C for 30 min. Susceptibility of Hif and *E. coli* BL21(DE3) to complement-mediated killing was tested, as described (21). The optimal concentrations of serum and time points used were as previously described (16, 17, 21), and were empirically determined for Hif (5% NHS and 15 min) and *E. coli* BL21 (DE3) (1% NHS and 10 min). We optimized our experiments and used 5% of NHS at 15 min, as this percentage of NHS caused killing of the PH mutant (Hif M10Δ*lph*), and yet exerted the serum-resistant phenotype of the wild-type Hif M10. Serum resistance was considered as ≥50% bacterial survival in 5% NHS (23). Aliquots of 1.5×10^3 CFU in 100 μl $DGVB^{2+}$ (2.5 mM veronal buffer [pH 7.3], 2.5% glucose, 2 mM $MgCl_2$, 0.15 mM $CaCl_2$, and 0.1% gelatin) were added with appropriate dilutions of serum and incubated at 37°C at the indicated time points with gentle shaking. At 0 min (T_0 sample) and indicated times (T_t sample), aliquots of 10 μl reaction mixtures were plated on chocolate agar for Hif or LB agar containing ampicillin for PH-expressing *E. coli* and incubated at 37°C. Percentage of bacterial killing was calculated as (CFU at T_t)/(CFU at T_0) × 100. Three individual experiments, each performed in triplicates, were done. Control experiments with heat-inactivated NHS were also performed, as described above.

Bacterial binding to immobilized Vn on glass slides

Adherence of bacteria to immobilized Vn was studied by coating 5 μg Vn on glass slides (Menzel-Gläser; Thermo Scientific, Wilmington, DE). Bacteria

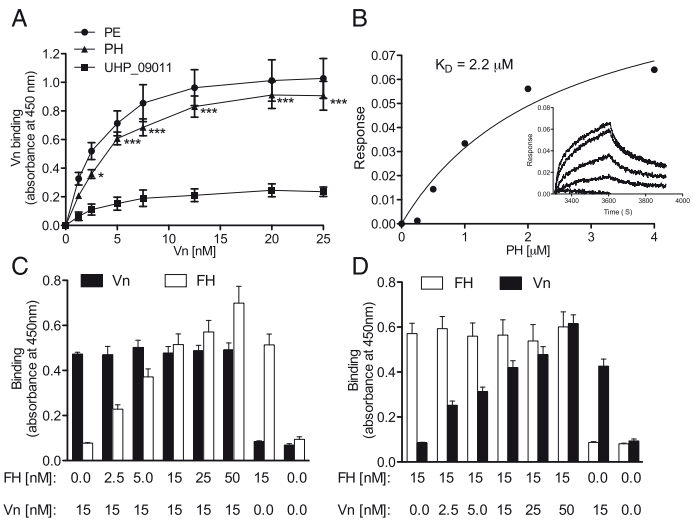

FIGURE 2. PH binds Vn at high affinity. (**A**) ELISA analysis of Vn binding by PH in comparison with PE from NTHi. A non-Vn–binding *Haemophilus* protein, UHP_09011, was included as a negative control. Equal molar concentrations (50 nM) of all purified recombinant proteins were immobilized separately in microtiter plates, followed by incubation with increasing amount (1.25–25 nM) of plasma Vn. Bound Vn was detected with sheep anti-Vn pAb and HRP-conjugated donkey anti-sheep pAb. Mean values of three separate experiments were plotted to generate the curves, and error bars indicate SD. (**B**) Kinetic analysis of the PH–Vn interaction as analyzed by Biolayer interferometry (Octet Red96). Recombinant $Vn^{80–396}$ was immobilized on AR2G sensors, and bindings by PH were analyzed at different concentrations (0.25–4 μM). Binding affinity (K_D) was calculated by fitting the curves with 1:1 binding kinetics. (**C** and **D**) Vn and FH concurrently bind to PH as analyzed by ELISA. PH (50 nM) was coated in microtiter plates and incubated with Vn or FH in the presence of increasing concentrations (2.5–50 nM) of either FH (C) or Vn (D). Interaction of Vn (15 nM) to immobilized PH was not influenced by FH (C), and binding of FH (15 nM) to immobilized PH was not disrupted by Vn (D). Bound ligands were detected using ligand-specific primary and secondary Abs. Mean values of three separate experiments were plotted. Error bars indicate SDs. In (A), PE was used as a positive control. Differences in Vn binding between PH and UHP_09011 were calculated by a two-way ANOVA. $*p \leq 0.05$, $***p \leq 0.001$.

were grown in broth until midlog phase (OD_{600} = 0.5) and incubated on Vn-coated glass slides for 1 h at 37°C. Unbound bacteria were washed away with PBS, followed by Gram-staining and analysis in an Olympus IX73 microscope at 100× amplification.

H. influenzae *adherence assay*

Type II lung alveolar epithelial cells (A549) were maintained in F12 medium containing 10% FCS supplemented with 5 μg/ml gentamicin. Cells were routinely subcultured every 2–3 d. A modified adherence assay from that one described previously (9) was used. Briefly, cells were cultured in 24-well plates till confluency. Prior to the experiment, cells were kept in serum-free medium (F12 medium only) overnight. To observe an effect of Vn, cell monolayers were treated with Vn (10 μg/ml) at 4°C for 1 h, followed by three washes with PBS. Cells were incubated with bacteria at MOI 100 for the indicated time points in F12 medium at 37°C. Cells were washed thoroughly postinfection, harvested by treatment with Accutase (Life Technologies), and then lysed with glass beads and vortexing. Serial dilutions were plated to calculate CFU.

Statistical analyses

Student *t* tests were used to compare two experimental groups, and one- or two-way ANOVA tests were included for comparison of differences between more than two groups as indicated. Differences were considered statistically significant at $p \leq 0.05$. Statistical analyses were performed using Graph-Pad Prism version 5.0 (GraphPad Software, La Jolla, CA).

Results

H. influenzae *serotype f acquires Vn by protein H*

To investigate whether Hif PH-dependent serum resistance also involves other complement regulators than FH (21), we compared binding of PH to Vn, C4BP, or FH in ELISA. Interestingly, PH bound both FH and Vn, but did not interact with C4BP (Fig. 1A). In addition, we found that PH binding to Vn was equal with and without a His tag attached to recombinant PH (Supplemental Fig. 1). In the light of the emergence of Hif invasive disease (4, 6), we examined Hif blood and cerebrospinal fluid isolates (n = 21) (24) for Vn binding by flow cytometry (Fig. 1B). All clinical strains significantly bound Vn as compared with the negative control *E. coli.*

To in detail analyze the role of PH for Vn binding, we deleted the *lph* gene in Hif M10. The resulting Hif M10Δ*lph* mutant bound significantly less Vn in comparison with the wild type, as revealed by flow cytometry (Fig. 1C). We also recombinantly expressed PH at the surface of the heterologous host *E. coli*. This experimental system made it possible to evaluate the specificity of PH and to exclude other surface proteins interfering

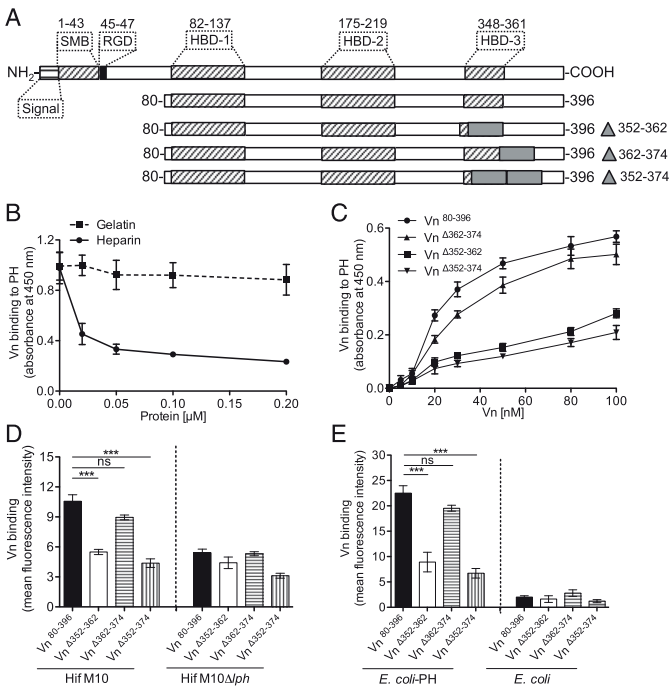

FIGURE 3. Amino acids 352–362 at the C terminus of Vn are involved in the binding to PH. (**A**) Illustration of the full-length Vn molecule and truncated fragments. (**B**) Inhibition of the PH–Vn interaction by heparin as analyzed by ELISA. We used gelatin (type B from bovine skin) that did not interact with Vn and PH (data not shown) as a negative control. Increasing concentrations of heparin (0.05–0.2 μM) and gelatin were preincubated individually with $Vn^{80–396}$ (20 nM). Thereafter, heparin–Vn and gelatin–Vn mixtures were added to the microtiter wells coated with recombinant PH (100 nM). (**C**) PH binding to different fragments of Vn as found by ELISA. PH coated on microtiter plates were incubated with increasing concentrations (5–100 nM) of recombinant $Vn^{80–396}$, $Vn^{\Delta352–362}$, $Vn^{\Delta362–374}$, or $Vn^{\Delta352–374}$. Bound Vn fragments were detected with anti-Vn pAb. (**D**) Binding of Vn fragments by Hif M10 and the corresponding PH-deletion mutant as measured by flow cytometry. Data are shown in mean fluorescence intensity. Deletion of amino acid residue 352–362 at the C terminus of Vn significantly reduces its binding to PH on the bacterial surface when compared with full-length $Vn^{80–396}$. Hif M10 Δ*lph* showed low binding to all Vn fragments. (**E**) Flow cytometry analysis of *E. coli* expressing PH and control *E. coli* binding to Vn fragments. PH-expressing *E. coli* has reduced binding to Vn fragments lacking the residue 352–362 compared with the full-length $Vn^{80–396}$. Data represent the mean of three independent experiments performed in duplicates. Statistical analyses were carried out by one-way ANOVA, and error bars indicate SDs. $*p \leq 0.05$, $***p \leq 0.001$. ns, not significant; RGD, Arg-Gly-Asp; SMB, somatomedin B.

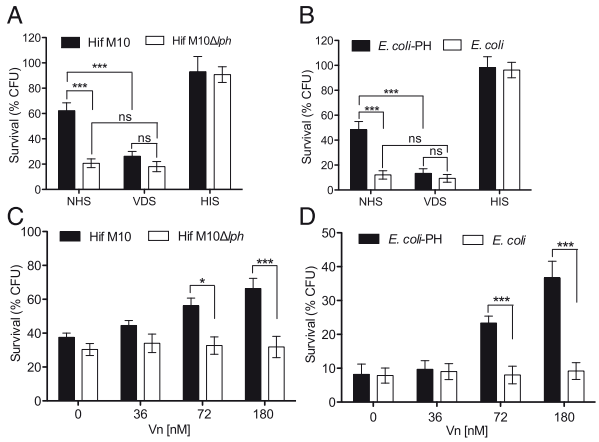

FIGURE 4. PH confers serum resistance to Hif and PH-expressing *E. coli* via recruitment of plasma Vn. (**A**) Wild-type *H. influenzae* Hif M10 and Hif M10Δ*lph* mutant were incubated for 15 min in 5% of NHS, VDS, or heat-inactivated serum (HIS). Wild-type Hif was sensitive to complement killing in VDS compared with NHS, whereas the Hif isogenic mutant was equally sensitive in both NHS and VDS. (**B**) PH-expressing *E. coli* is more serum sensitive in 1% of VDS compared with NHS after 10 min of incubation. (**C**) Serum resistance of Hif and the *lph*-deletion mutant in 5% VDS that was supplemented with increasing concentrations of Vn (36–180 nM). (**D**) Serum resistance of PH-expressing *E. coli* and the control *E. coli* after incubation with 1% of VDS supplemented with increasing concentrations of Vn. We used heat-inactivated NHS as a negative control of complement-mediated killing. Statistical analyses were performed by a two-way ANOVA. All data are the means of results from three independent experiments performed in triplicates, and error bars show SDs. $*p \leq 0.05$, $***p \leq 0.001$. ns, not significant.

with Vn. A significant Vn-binding population was observed when PH-expressing *E. coli* were incubated with Vn (Fig. 1D). In conclusion, a series of invasive Hif isolates bound soluble Vn at their surface, and, when PH was removed from the model isolate Hif M10, a significantly decreased Vn binding was observed.

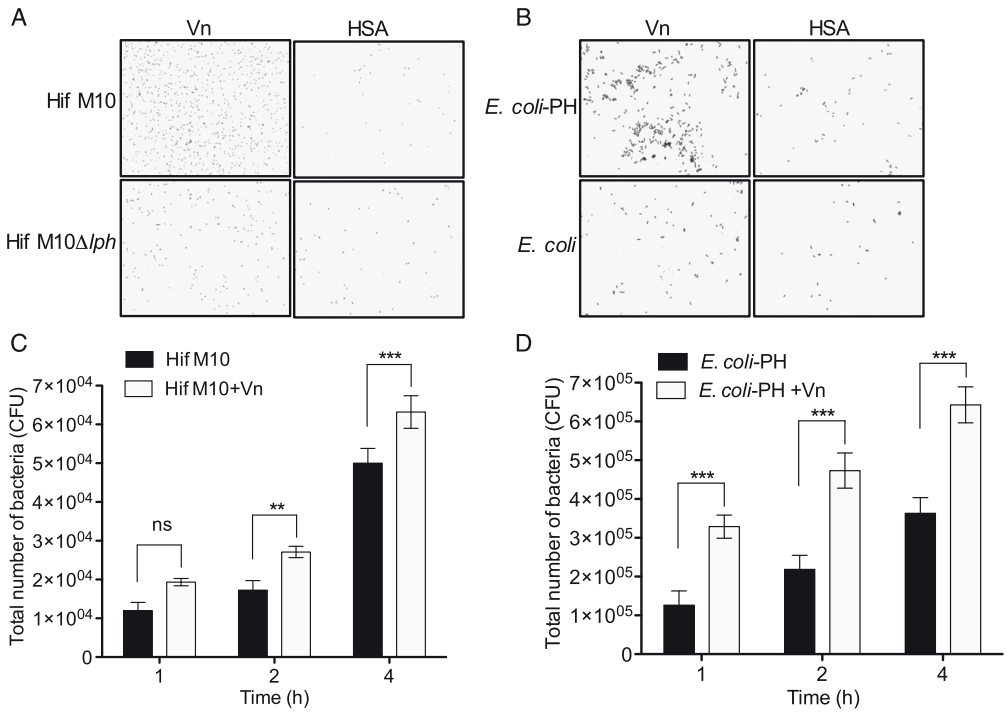

FIGURE 5. The PH-dependent Vn interaction mediates bacterial adherence to Vn-coated glass surface and pulmonary epithelial cells. (**A** and **B**) Adherence of Hif (A) and *E. coli*-PH (B) to Vn-coated glass slides. Representative images of three independent experiments are shown. Bacterial adherence was visualized by light microscopy after a standard Gram staining. (**C** and **D**) Adherence of Hif M10 (C) and PH-expressing *E. coli* (D) to A549 cells at three different time points (1 h, 2 h, 4 h) in the presence or absence of 10 μg/ml additional Vn as measured by counting CFU. The PH-deficient Hif M10 Δ*lph* and the control *E. coli* did not show any differences in adhesive capacity when incubated with epithelial cells in the presence or absence of exogenously added Vn (data not shown). In (C) and (D), ~2×10^5 cells/well and 2×10^7 CFU bacteria were added to each well. Data in graphs are the means of results of three independent experiments performed in triplicates, and error bars indicate SDs. $**p \leq 0.01$, $***p \leq 0.001$. ns, not significant.

PH has a high affinity for Vn and simultaneously interacts with both FH and Vn

To ascertain the Vn-binding property of PH, we analyzed the protein–protein interaction by ELISA. *H. influenzae* PE and UPH_09011 were included for comparison as positive and negative controls, respectively (16, 17, 22). Recombinant proteins were coated in microtiter plates, followed by addition of Vn at increasing concentrations. A dose-dependent binding of Vn to PH was observed (Fig. 2A). PH had a similar binding profile as *H. influenzae* PE and significantly bound Vn in comparison with the negative control protein (UPH_09011). Further evaluation of the binding kinetics was performed by Biolayer interferometry with Vn immobilized on the sensors. The interaction with Vn was analyzed with PH at increasing concentrations (0.25–4 μM). We observed a dose-dependent binding, and the dissociation constant (K_D) was calculated to 2.2 ± 0.12 μM (Fig. 2B).

Because PH has been shown to interact with FH (21), one of the regulators of the alternative pathway of complement activation, we wanted to define whether FH and Vn could simultaneously interact with PH. In a multiligand-binding assay, PH was immobilized in microtiter plates and incubated with either 15 nM Vn (Fig. 2C) or FH (Fig. 2D) in the presence of increasing concentrations of FH or Vn (2.5–50 nM), respectively. Coincubation of FH and Vn did not affect the binding of each other to the immobilized PH. Interestingly, although PH is a relatively small molecule (35 kDa), FH and Vn concurrently bound to PH, as judged by ELISA. We further confirmed the concurrent interaction by an inhibition assay, which revealed that Vn and FH bound to separate regions on the PH molecule (Supplemental Fig. 2). Thus, these experiments proved that PH comprised regions that simultaneously interacted with the two complement regulators Vn and FH.

PH recognizes the C-terminal region of Vn by interacting with amino acids $Vn^{352–362}$

Vn consists of three heparin-binding domains (HBDs) that are located upstream of the RGD sequence, a motif that binds to integrins (25) (Fig. 3A). To analyze whether HBDs were involved in the PH-dependent Vn binding, we preincubated Vn with heparin. As can be seen in Fig. 3B, heparin significantly blocked the interaction between Vn and PH, whereas the control protein, type B bovine gelatin, from skin did not block that interaction. Previous studies with other bacterial species (26, 27) suggested that bacterial proteins interact with the third HBD at the C-terminal part of the Vn molecule. To further pinpoint the binding site for PH on the Vn molecule, three different truncated fragments of Vn molecules encompassing deletions in HBD3 ($Vn^{\Delta 352–362}$, $Vn^{\Delta 362–374}$, and $Vn^{\Delta 352–374}$) (Fig. 3A) were included in our analysis. Interestingly, $Vn^{80–396}$ or $Vn^{\Delta 362–374}$ readily bound to PH, whereas $Vn^{\Delta 352–362}$ and $Vn^{\Delta 352–374}$ did not bind, suggesting that 10 aa within the sequence $Vn^{352–362}$ comprised the minimal PH binding site on the Vn molecule (Fig. 3C).

To further examine the importance of the deletion in $Vn^{\Delta 352–362}$, a set of experiments was also done with whole bacteria. Hif M10 and PH-expressing *E. coli* were used for flow cytometry analysis with the different Vn fragments. For comparison, we also included the mutant Hif M10Δ*lph* that was devoid of PH in addition to control *E. coli*. Hif M10 (Fig. 3D) and *E. coli* expressing PH at the surface (Fig. 3E) significantly bound Vn as compared with the controls Hif M10Δ*lph* and *E. coli*. In agreement with the results obtained by ELISA, flow cytometry experiments with intact bacteria also showed similar binding pattern with the different Vn fragments, and thus further confirmed that PH bound Vn at aa 352–362 within the HBD3 located at the C-terminal domain of Vn.

H. influenzae *type f is protected from complement-mediated killing by Vn bound to PH*

To evaluate the importance of PH when bacteria were exposed to NHS, we incubated the PH-expressing Hif M10 and the corresponding mutant Hif M10Δ*lph* with pooled NHS obtained from healthy donors. As shown in Fig. 4A, the Hif M10 wild-type expressing PH survived significantly better ($p \leq 0.001$) in NHS as compared with the mutant counterpart. When Vn was depleted (VDS), Hif M10 was, however, significantly more susceptible to killing as compared with incubation with NHS, indicating the importance of Vn acquisition for Hif serum survival. In contrast, mutant Hif M10Δ*lph* was sensitive to the bactericidal effect of both NHS and VDS. In parallel, the PH-expressing *E. coli* was more resistant to NHS as compared with control *E. coli* (Fig. 4B), and *E. coli*-PH did not survive in the absence of Vn (VDS).

To further define the role of the Vn–PH interaction in Hif serum resistance, we supplemented the VDS with $Vn^{20–396}$ at increasing concentrations, followed by incubation with *H. influenzae* or *E. coli*. Addition of Vn at 72 or 180 nM to VDS resulted in a significantly increased survival of Hif M10 (Fig. 4C) and

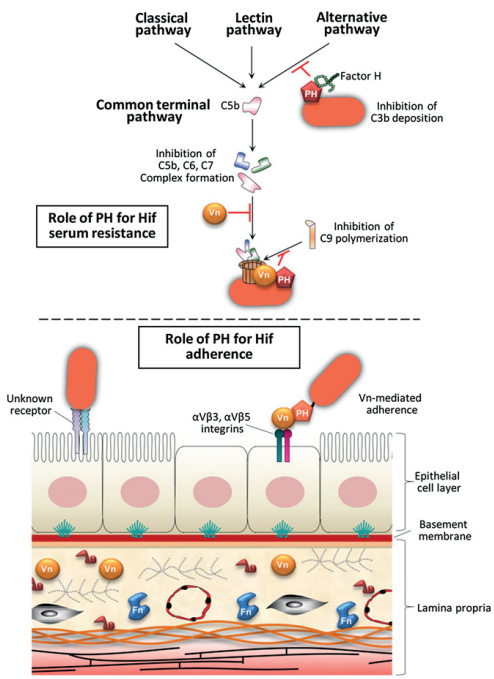

FIGURE 6. Cartoon summarizing the functional roles of PH during host colonization. PH interacts with human FH (21) and inhibits the activation of the alternative complement pathway. Vn interaction with PH suppresses the common terminal pathway of MAC by selectively inhibiting C5b–C6–C7 complex formation and C9 polymerization. We have demonstrated that PH simultaneously interacts with Vn and FH. Thus, both of these factors effectively function in favor of bacteria. Vn can be found and deposited at the apical surface of the airway epithelial cells by plasma exudation. Surface-bound Vn also mediates binding to integrins on host epithelial cells, and thus Vn functions as a bridging molecule between Hif and epithelial cells that consequently leads to increased adherence to the airway mucosa.

PH-expressing *E. coli* (Fig. 4D). Taken together, our results suggested that Hif recruits Vn from NHS by using PH to inhibit the MAC formation at the terminal lytic step. The Vn acquisition leads to a decreased complement-mediated bactericidal activity and thus enhanced bacterial survival.

PH-dependent Vn acquisition promotes adherence of Hif to epithelial cells

Vn is an abundant plasma protein, but is also an important component of the ECM together with several other host proteins (28). To evaluate the role of PH in adherence to immobilized Vn, we incubated both Hif M10 and the isogenic *lph* mutant with Vn coated on glass slides. In contrast to the wild-type Hif M10, Hif M10Δ*lph* that was devoid of PH adhered less efficiently to the Vn-coated glass slides (Fig. 5A). This observation was further supported by a significantly increased adherence of PH-expressing *E. coli* compared with the control *E. coli* (Fig. 5B).

Recent studies have shown that several bacteria, including Hib, interact with Vn via surface proteins contributing to adherence to respiratory epithelial cells (9, 26). To examine the role of PH on Hif adherence to type II alveolar epithelial cells, Hif M10 was incubated with Vn and added to the epithelial cells. We found that Hif adhered more efficiently when exogenous Vn was provided (Fig. 5C). To validate that the increased bacterial adherence was indeed caused by PH interacting with Vn, and not by any other Vn-binding protein or the Hif capsule, we also analyzed adherence by PH-expressing *E. coli* with or without Vn. Consistent with the results obtained with PH-expressing Hif, *E. coli*-PH also had an increased adherence in the presence of Vn (Fig. 5D). In conclusion, Hif PH interacts with both immobilized and soluble Vn, facilitating bacterial adherence to the ECM as well as epithelial cells (Fig. 6).

Discussion

Many pathogenic bacteria can recruit complement regulatory factors such as C4BP, FH, and Vn, thus enabling them to survive the bactericidal effect of serum (12). Hijacking Vn is one of many powerful strategies to evade the host innate immune system in addition to facilitating colonization and subsequent infection (25, 29). *H. influenzae* serotype f is an increasingly important cause of invasive disease (4–6, 30). However, there is less information regarding virulence mechanisms related to this serotype. In this work, we explored the role of Hif PH (21) in serum resistance and adhesion via the acquisition of abundant plasma and cellular Vn.

In conjunction to the clonal distribution of serotype f (31), we showed that all invasive Hif isolates (n = 21) (24) exhibit a Vn-binding capacity in comparison with the control *E. coli* (Fig. 1B). Interestingly, despite the fact that all the clinical strains tested had almost similar PH expression levels (Supplemental Fig. 3), we observed different capacities among the isolates to attract Vn (Fig. 1B). We previously reported that *H. influenzae* concurrently expresses PE (15), PF (17, 24), and P4 (24, 32) to interact with Vn. Despite the fact that we observed that PH was expressed in all clinical isolates, it is plausible that other Vn-binding proteins may play a role in expression level or surface exposure due to the presence of a capsule in Hif. This might explain the absence of correlation between PH expression and the Vn-binding phenotypes. We compared the Vn binding of PH with the well-defined NTHi outer membrane protein PE (15), and found that PH interacted with Vn as efficiently as PE (Fig. 2A). The K_D of the PH–Vn interaction was 2.2 μM (Fig. 2B), and was similar to the K_D for PE (0.4 μM) despite the fact that different methods were used (16). It thus seems that PH derived from Hif might play an equally important role as PE does in NTHi, that is, as a high-affinity Vn-binding receptor.

Vn inhibits MAC assembly by blocking the membrane binding site of the C5b–C7 complex and prevents polymerization of C9 (15, 25). The multifunctional Vn molecule is an effective regulator that inhibits the terminal lytic pathway regardless of which complement pathway that is activated. Deposition of Vn on the Hif surface might thus prevent lytic pore formation. Our current report clearly shows that Vn in NHS and supplementation of Vn to VDS caused a significant increase in the level of Hif serum resistance via the PH–Vn interaction (Fig. 4). We further demonstrated that PH simultaneously binds FH and Vn (Fig. 2C, 2D). However, most likely the interaction between PH and FH plays a minor role as compared with binding of Vn because the later complement regulator interferes with the terminal pathway and hence inhibits MAC formation.

In parallel with previous findings on other bacterial pathogens, including *Moraxella catarrhalis*, pneumococci, Hib, and NTHi (9, 15, 17, 26, 27), PH also specifically bound to the C-terminal of Vn (aa 352–362) (Fig. 3). As has been reported for other microbes (25), Hif also targeted the C-terminal HBD3 via PH, leaving the RGD-containing binding site available on the Vn molecule. We found that the presence of Vn resulted in an increased Hif adherence to glass slides as well as to epithelial cells (Fig. 5). Because the RGD motif is located at the N-terminal end, and consequently in most cases is freely available, bacterial binding to integrins, especially $\alpha_v\beta_3$, on host cells is facilitated. Hence, a cross-link between bacteria and epithelial cells can occur (25). The binding of integrins to RGD motifs is evolutionarily conserved, but, when host proteins are bound to the bacterial surface, RGD sequences need to be available at the surface of the protein to cross-link integrins (33). In accordance with what has been shown with other pathogens, we also demonstrated that the PH-dependent Vn interaction resulted in an increased bacterial adherence to epithelial cells (Fig. 5C, 5D). However, when we compared the adhesive capacity, with or without additional Vn added to the epithelial cells for Hif M10Δ*lph* and *E. coli* with empty vector, no difference in adherence was observed (data not shown). Thus, PH is not an adhesin per se, because it cannot support Hif adherence to epithelial cells by itself, but merely facilitates adhesion by interacting with Vn and using it as a bridging molecule to epithelial integrins. Our recent report on Hib (9) and another study on *Pseudomonas aeruginosa* (34) show that the interaction between Vn and integrins considerably increases bacterial adherence and invasion of epithelial cells. Intriguingly, several bacterial species use this strategy for evasion of the host defense system. The gastrointestinal pathogens *Yersinia enterocolitica* and *Helicobacter pylori* as well as the urethral *Neisseria gonorrheae* all interact indirectly with integrins by molecular bridges consisting of host proteins included in the ECM or plasma (35).

In the host lung tissue, cellular Vn molecules derived from the ECM are usually targeted and anchored by integrin receptors (i.e., $\alpha_v\beta_3$ and $\alpha_5\beta_1$) at the basolateral side of epithelial cells (25, 34). In addition, plasma exudation also results in Vn exposure on the apical side of the epithelial cells (36). Because Vn is present in both serum and the ECM, opportunistic acquisition of Vn at the Hif surface mediated by PH facilitates bacteria to inhibit MAC formation and promote adhesion to epithelial cells, as outlined in Fig. 6.

In conclusion, our study sheds light upon how Hif utilizes the multifunctional host protein Vn for evasion of the innate immunity and invasion of the host. More studies are required to fully delineate virulence factors related to Hif that might explain why there is an increased incidence of invasive Hif disease in the human population.

Acknowledgments

We thank the Clinical Microbiology Laboratory at Labmedicin Skåne for providing clinical isolates.

Disclosures

The authors have no financial conflicts of interest.

References

1. Singh, B., T. A. Jubair, M. Mörgelin, A. Sundin, S. Linse, U. J. Nilsson, and K. Riesbeck. 2015. *Haemophilus influenzae* surface fibril (Hsf) is a unique twisted hairpin-like trimeric autotransporter. *Int. J. Med. Microbiol.* 305: 27–37.
2. Tudor-Williams, G., J. Frankland, D. Isaacs, R. T. Mayon-White, J. A. MacFarlane, M. P. Slack, E. Anderson, D. G. Rees, and E. R. Moxon. 1989. *Haemophilus influenzae* type b disease in the Oxford region. *Arch. Dis. Child.* 64: 517–519.
3. Murphy, T. V., D. M. Granoff, L. M. Pierson, P. Pastor, K. E. White, J. F. Clements, and M. T. Osterholm. 1992. Invasive *Haemophilus influenzae* type b disease in children less than 5 years of age in Minnesota and in Dallas County, Texas, 1983-1984. *J. Infect. Dis.* 165(Suppl. 1): S7–S10.
4. Hoshino, T., Y. Hachisu, T. Kikuchi, S. Tokutake, H. Okui, S. Kutsuna, C. Fukasawa, K. Murayama, A. Oohara, H. Shimizu, et al. 2015. Analysis of *Haemophilus influenzae* serotype f isolated from three Japanese children with invasive *H. influenzae* infection. *J. Med. Microbiol.* 64: 355–358.
5. Ladhani, S. N., S. Collins, A. Vickers, D. J. Litt, C. Crawford, M. E. Ramsay, and M. P. Slack. 2012. Invasive *Haemophilus influenzae* serotype e and f disease, England and Wales. *Emerg. Infect. Dis.* 18: 725–732.
6. Resman, F., T. Svensjö, C. Ünal, J. Cronqvist, H. Brorson, I. Odenholt, and K. Riesbeck. 2011. Necrotizing myositis and septic shock caused by *Haemophilus influenzae* type f in a previously healthy man diagnosed with an IgG3 and a mannose-binding lectin deficiency. *Scand. J. Infect. Dis.* 43: 972–976.
7. Ulanova, M., and R. S. Tsang. 2009. Invasive *Haemophilus influenzae* disease: changing epidemiology and host-parasite interactions in the 21st century. *Infect. Genet. Evol.* 9: 594–605.
8. Jalalvand, F., and K. Riesbeck. 2014. *Haemophilus influenzae*: recent advances in the understanding of molecular pathogenesis and polymicrobial infections. *Curr. Opin. Infect. Dis.* 27: 268–274.
9. Singh, B., Y. C. Su, T. Al-Jubair, O. Mukherjee, T. Hallström, M. Mörgelin, A. M. Blom, and K. Riesbeck. 2014. A fine-tuned interaction between trimeric autotransporter *haemophilus* surface fibrils and vitronectin leads to serum resistance and adherence to respiratory epithelial cells. *Infect. Immun.* 82: 2378–2389.
10. Ronit, A., R. M. Berg, H. Bruunsgaard, and R. R. Plovsing. 2013. *Haemophilus influenzae* type f meningitis in a previously healthy boy. *BMJ Case Rep.* 2013: pii: bcr2013008854.
11. Winkelstein, J. A., and E. R. Moxon. 1992. The role of complement in the host's defense against *Haemophilus influenzae*. *J. Infect. Dis.* 165(Suppl. 1): S62–S65.
12. Blom, A. M., T. Hallström, and K. Riesbeck. 2009. Complement evasion strategies of pathogens-acquisition of inhibitors and beyond. *Mol. Immunol.* 46: 2808–2817.
13. Blom, A. M., and S. Ram. 2008. Contribution of interactions between complement inhibitor C4b-binding protein and pathogens to their ability to establish infection with particular emphasis on *Neisseria gonorrhoeae*. *Vaccine* 26(Suppl. 8): I49–I55.
14. Barnes, D. W., and J. Silnutzer. 1983. Isolation of human serum spreading factor. *J. Biol. Chem.* 258: 12548–12552.
15. Singh, B., F. Jalalvand, M. Mörgelin, P. Zipfel, A. M. Blom, and K. Riesbeck. 2011. *Haemophilus influenzae* protein E recognizes the C-terminal domain of vitronectin and modulates the membrane attack complex. *Mol. Microbiol.* 81: 80–98.
16. Hallström, T., A. M. Blom, P. F. Zipfel, and K. Riesbeck. 2009. Nontypeable *Haemophilus influenzae* protein E binds vitronectin and is important for serum resistance. *J. Immunol.* 183: 2593–2601.
17. Su, Y. C., F. Jalalvand, M. Mörgelin, A. M. Blom, B. Singh, and K. Riesbeck. 2013. *Haemophilus influenzae* acquires vitronectin via the ubiquitous protein F to subvert host innate immunity. *Mol. Microbiol.* 87: 1245–1266.
18. Singh, B., M. Brant, M. Kilian, B. Hallström, and K. Riesbeck. 2010. Protein E of *Haemophilus influenzae* is a ubiquitous highly conserved adhesin. *J. Infect. Dis.* 201: 414–419.
19. Jalalvand, F., Y. C. Su, M. Mörgelin, M. Brant, O. Hallgren, G. Westergren-Thorsson, B. Singh, and K. Riesbeck. 2013. *Haemophilus influenzae* protein F mediates binding to laminin and human pulmonary epithelial cells. *J. Infect. Dis.* 207: 803–813.
20. Singh, B., T. Al-Jubair, M. Mörgelin, M. M. Thunnissen, and K. Riesbeck. 2013. The unique structure of *Haemophilus influenzae* protein E reveals multiple binding sites for host factors. *Infect. Immun.* 81: 801–814.
21. Fleury, C., Y. C. Su, T. Hallström, L. Sandblad, P. F. Zipfel, and K. Riesbeck. 2014. Identification of a *Haemophilus influenzae* factor H-binding lipoprotein involved in serum resistance. *J. Immunol.* 192: 5913–5923.
22. Al Jubair, T., B. Singh, C. Fleury, A. M. Blom, M. Mörgelin, M. M. Thunnissen, and K. Riesbeck. 2014. *Haemophilus influenzae* stores and distributes hemin by using protein E. *Int. J. Med. Microbiol.* 304: 662–668.
23. Su, Y. C., B. M. Hallström, S. Bernhard, B. Singh, and K. Riesbeck. 2013. Impact of sequence diversity in the *Moraxella catarrhalis* UspA2/UspA2H head domain on vitronectin binding and antigenic variation. *Microbes Infect.* 15: 375–387.
24. Su, Y. C., F. Resman, F. Hörhold, and K. Riesbeck. 2014. Comparative genomic analysis reveals distinct genotypic features of the emerging pathogen *Haemophilus influenzae* type f. *BMC Genomics* 15: 38.
25. Singh, B., Y. C. Su, and K. Riesbeck. 2010. Vitronectin in bacterial pathogenesis: a host protein used in complement escape and cellular invasion. *Mol. Microbiol.* 78: 545–560.
26. Singh, B., A. M. Blom, C. Unal, B. Nilson, M. Mörgelin, and K. Riesbeck. 2010. Vitronectin binds to the head region of *Moraxella catarrhalis* ubiquitous surface protein A2 and confers complement-inhibitory activity. *Mol. Microbiol.* 75: 1426–1444.
27. Voss, S., T. Hallström, M. Saleh, G. Burchhardt, T. Pribyl, B. Singh, K. Riesbeck, P. F. Zipfel, and S. Hammerschmidt. 2013. The choline-binding protein PspC of *Streptococcus pneumoniae* interacts with the C-terminal heparin-binding domain of vitronectin. *J. Biol. Chem.* 288: 15614–15627.
28. Schvartz, I., D. Seger, and S. Shaltiel. 1999. Vitronectin. *Int. J. Biochem. Cell Biol.* 31: 539–544.
29. Hallström, T., and K. Riesbeck. 2010. *Haemophilus influenzae* and the complement system. *Trends Microbiol.* 18: 258–265.
30. Puig, C., I. Grau, S. Marti, F. Tubau, L. Calatayud, R. Pallares, J. Liñares, and C. Ardanuy. 2014. Clinical and molecular epidemiology of *haemophilus influenzae* causing invasive disease in adult patients. *PLoS One* 9: e112711.
31. Resman, F., M. Ristovski, J. Ahl, A. Forsgren, J. R. Gilsdorf, A. Jasir, B. Kaijser, G. Kronvall, and K. Riesbeck. 2011. Invasive disease caused by *Haemophilus influenzae* in Sweden 1997-2009; evidence of increasing incidence and clinical burden of non-type b strains. *Clin. Microbiol. Infect.* 17: 1638–1645.
32. Su, Y. C., O. Mukherjee, B. Singh, O. Hallgren, G. Westergren-Thorsson, D. Hood, and K. Riesbeck. 2015. *Haemophilus influenzae* P4 interacts with extracellular matrix proteins promoting adhesion and serum resistance. *J. Infect. Dis.* DOI: 10.1093/infdis/jiv374.
33. Ruoslahti, E. 1996. RGD and other recognition sequences for integrins. *Annu. Rev. Cell Dev. Biol.* 12: 697–715.
34. Leroy-Dudal, J., H. Gagnière, E. Cossard, F. Carreiras, and P. Di Martino. 2004. Role of alphavbeta5 integrins and vitronectin in *Pseudomonas aeruginosa* PAK interaction with A549 respiratory cells. *Microbes Infect.* 6: 875–881.
35. Buommino, E., M. Di Domenico, I. Paoletti, A. Fusco, V. De Gregorio, V. Cozza, A. Rizzo, M. A. Tufano, and G. Donnarumma. 2014. Alpha(v)beta5 integrins mediates *Pseudomonas* fluorescens interaction with A549 cells. *Front. Biosci.* 19: 408–415.
36. Persson, C. G. 1991. Plasma exudation in the airways: mechanisms and function. *Eur. Respir. J.* 4: 1268–1274.

Supplemental Data

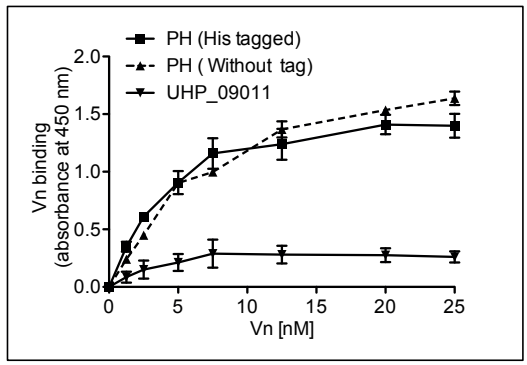

FIGURE S1. ELISA of Vn binding by His-tagged PH in comparison with PH without a His-tag. Equal molar concentrations (50 nM) of purified recombinant proteins were immobilized in microtiter plates, followed by incubation with increasing concentrations (1.25-25 nM) of Vn. Bound Vn was detected with sheep anti-Vn pAb and a secondary HRP-conjugated donkey anti-sheep pAb.

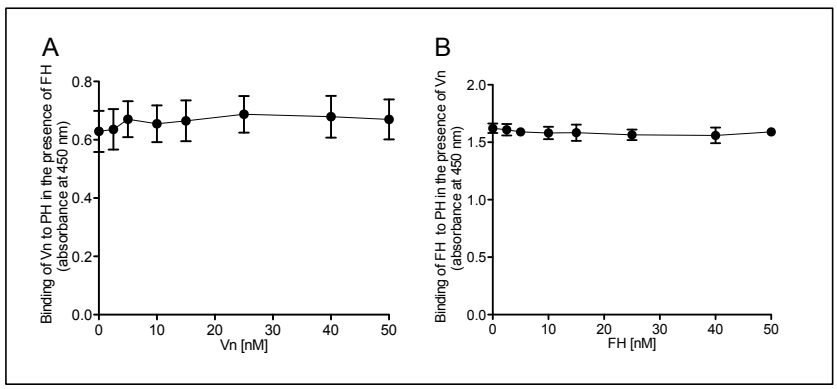

FIGURE S2. Vn and FH bind to separate regions on PH as analysed by ELISA. **A.** Binding of Vn (15 nM) to immobilized PH was not inhibited by FH. **B.** Binding of FH (25 nM) to immobilized PH was not inhibited by Vn. PH (50 nM) was coated in microtiter plates and pre-incubated with increasing concentrations (2.5-50 nM) of either FH (A) or Vn (B)**.** Unbound ligands (Vn or FH) were removed by washing. Thereafter, bound Vn and FH were detected by primary sheep anti-human Vn pAb or mouse anti-human FH mAb followed by HRP-conjugated donkey anti-sheep and rabbit anti-mouse secondary pAbs (all were obtained from AbD Serotec, Oxford, UK).

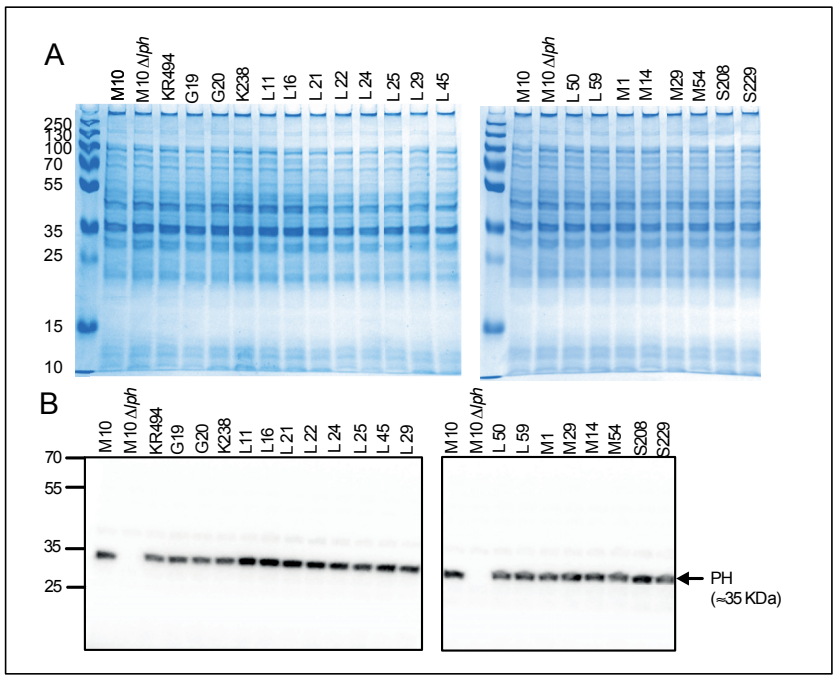

FIGURE S3. All clinical strains showed similar levels of protein H (PH) expression as analysed by SDS-PAGE and Western blot. **A.** SDS-PAGE of whole cell lysates. **B.** Detection of PH by Western blotting as a ~35 kDa single band (indicated by an arrow) in all Hif strains. Total cell lysates from equal number of bacteria (1×10^7 CFU per lane) were denatured at 95°C for 5 min in loading buffer (50 mM Tris-HCl, 2% SDS, 10% glycerol, and 100 mM DTT, pH 6.8) and separated on an SDS-PAGE using a Mini Protean II system (Bio-Rad, Hercules, CA) at 110 V. Thereafter, proteins were transferred to a polyvinylidene difluoride membrane (Immobilon; Millipore, Billerica, MA) at 16 V for 16 h. For detection of PH, membranes were incubated with the primary Ab (rabbit anti-Hif polyclonal Ab) followed by HRP-conjugated swine anti-rabbit IgG pAb (DakoCytomation, Glostrup, Denmark) and enhanced luminescence detection substrate (ECL; Pierce, Rockford, IL). Signals from antibody-antigen complex were visualized on a Chemidoc XRS+ system (Bio-Rad).